Ph.D 13097

The topography and flow of the Antarctic ice sheet

Neil Forbes McIntyre

UNIVERSITY
LIBRARY
CAMBRIDGE

A dissertation submitted for the degree of

Doctor of Philosophy in the University of Cambridge

St. John's College
Cambridge

November 1983

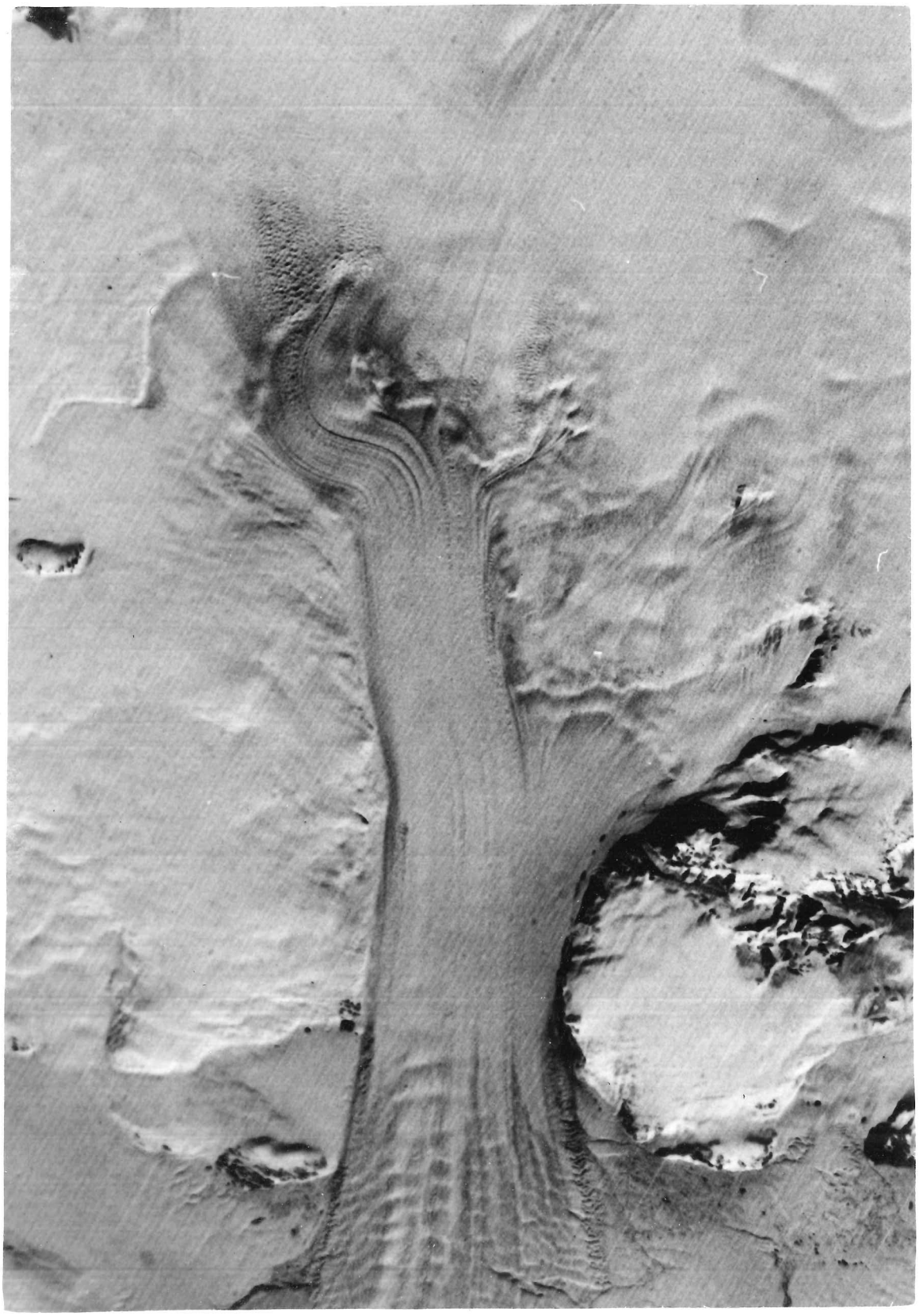

Frontispiece: Extract from Landsat image of David Glacier and Drygalski Ice Tongue, Victoria Land, Antarctica. Image width is approximately 60 km. Path 65, row 114. E-1543-20305.

Preface

The work described in this thesis was carried out at the Scott Polar Research Institute between October 1980 and November 1983 under the careful guidance and direction of Dr. G.deQ. Robin, to whom I am indebted. I am also grateful for discussions with, and the advice of, many colleagues, including Dr. D.J. Drewry, Dr. C.S. Neal, Dr. E.J. Jankowski, Dr. D.H.M. Millar, M.R. Gorman and J.A. Dowdeswell. Dr. C.W.M. Swithinbank of the British Antarctic Survey and Dr. R.S. Williams of the U.S. Geological Survey have been most helpful by enabling me access to their collections of and experience with Landsat imagery. A.P.R. Cooper guided me through the twists and turns of computing and the Sea Ice Group at the Scott Polar Research Institute allowed me to use its suite of Fast Fourier Transform programs. I would like to thank all of the above and, in particular, Dr. E.G.M. Kristensen whose example and friendship have proved a great inspiration.

I thank the Natural Environment Research Council which has supported me with a maintenance grant during the period of research. I am also grateful to all at the Scott Polar Research Institute and especially to Dr. G.deQ. Robin, Dr. T.E. Armstrong and Prof. E.R. Oxburgh, successive directors of the Institute, for the provision of such excellent facilities and a stimulating work place.

With the exceptions of section 4.6, the modelling for which was done with A.P.R. Cooper, and section 6.2, which is based on work previously published by Cooper, McIntyre and Robin (1982), the analysis and interpretation in this thesis is the result of my own work. I also declare that this dissertation does not exceed the regulations on length and that it has not been submitted for a degree at any other university.

Summary

A combination of altimetry and imagery from aircraft and satellite has been used to investigate the form and topography of the Antarctic ice sheet and to relate these to the physical processes of ice flow and basal conditions. Topographic roughness typically increases towards the thin ice of coastal regions as surface undulation wavelengths decrease and amplitudes increase. Temperature and velocity variations also have significant effects. The coastal zone is punctuated by embayments of severe topography immediately inland of outlet glaciers. This topographic variability has been summarized in a statistical model for the purposes of simulating satellite radar altimeter waveforms.

Consideration of the relationship between bedrock and surface profiles has shown that ice temperature is a major influence on the response of the surface to bedrock irregularities. Regional subglacial water layers may also have an important effect on surface topography. A re-analysis of models of longitudinal stress gradients suggests that crystal fabrics favouring faster flow develop with distance from ice divides and that the relative depth of the zone of maximum shear fluctuates in response to topographic and glaciological constraints. Driving stress patterns have been associated with characteristic glaciological regimes and have suggested a qualitative difference between outlet glaciers and ice streams.

The transition to high velocity flow in outlet glaciers has been shown to be triggered abruptly in response to subglacial fjord heads. The dependence of fast flow on subglacial topography indicates a significant stabilizing effect on discharge from ice sheets and suggests that surge behaviour is unlikely within existing ice sheet outlets. The onset of basal sliding at the head of subglacial fjords suggests a mechanism for the production of overdeepened fjords and steep headwalls through concentrated erosion. This may help in the reconstruction of the dynamics of former ice sheets. Some West Antarctic ice streams do not exhibit this rapid transition in behaviour.

Table of contents

List of figures

List of tables

List of acronyms

ARDS: Airborne Research Data System.

EGIG: Expeditions Glaciologique International au Groenland.

IAGP: International Antarctic Glaciological Project.

IGY: International Geophysical Year.

MSS: Multispectral Scanner.

NSF: National Science Foundation.

RMS: Root mean square.

RBV: Return beam vidicon.

SPRI: Scott Polar Research Institute.

TM: Thematic Mapper.

TUD: Technical University of Denmark.

List of symbols

$\dot{a}$	accumulation rate
b	amplitude of bedrock undulation
c	acceleration
d	distance
e	base of natural logarithms
f	form factor
g	gravitational acceleration
j	element of distribution
k	constant
m	constant
m_3	coefficient of skewness
m_4	coefficient of kurtosis
n	flow law exponent
p	perimeter
s	amplitude of surface undulation
s_i	amplitude of surface undulation i
t	time
u	velocity
u_b	basal velocity
u_o	initial velocity
x	down-glacier coordinate axis
x_{off}	random offset in x dimension
y	cross-glacier coordinate axis
y_{off}	random offset in y dimension
z	vertical coordinate axis, ice thickness
A	constant in flow law (temperature dependent)
A'	constant
A_f	angle of D_{max} relative to flow direction
A_r	area
A_x	amplitude of cross-flow sinusoid at distance x
D_{max}	maximum diameter
F	filter function (Hutter and others, 1981)
2G	longitudinal stress term (Budd, 1970)
G_s	grid spacing
H	satellite/terrain range
L	half-width of ice sheet
N	sample size
P_a	pressure altitude
P_x	x/L
P_y	y/W_y
R_a	radar altitude
S_e	surface elevation
T	variable basal shear stress (Budd, 1970)
W_y	wavelength of cross-flow sinusoid
Z	maximum ice thickness
α	surface slope
γ	inclination of ice mass

$\dot{\epsilon}$	effective strain rate
$\dot{\epsilon}_x$	longitudinal strain rate
λ	wavelength of undulation
λ_c	critical wavelength
λ_i	wavelength of undulation i
μ	mean value of distribution
ρ	density of ice
σ	effective stress
σ_{sd}	standard deviation of distribution
σ_x	longitudinal stress
$\overline{\sigma}'_x$	longitudinal stress deviator averaged over ice thickness
τ	effective shear stress
τ_b	basal shear stress, τ_{xz}
τ_o	yield stress
ψ	damping factor
ω	$2\pi/\lambda$
Ψ	damping function
Ψ_m	minimum value of damping function
η	viscosity of ice

CHAPTER 1

THE ANTARCTIC ICE SHEET

1.1 Introduction

The shape of an ice mass is the product of the physical processes operating on and within it. Knowledge of the form of an ice sheet is therefore a key to explaining its dynamics; information on slopes can, for instance, be used for the derivation of important parameters and as an input to modelling. This link between form and process has often been identified as a fruitful avenue for research, in particular, with regard to the Antarctic ice sheet about which knowledge is notably incomplete. During the last half century the surface form of the Antarctic ice sheet has been increasingly widely studied both through observation and theory. Early exploration was followed from 1948 by a rapidly progressing theoretical basis for glaciology which soon became more advanced than information obtained from observations. More recently, the balance has been adjusted, if not over-balanced, by the introduction of remote sensing as a means of data collection.

1.2 Observations of the Antarctic ice sheet

Although the presence of a cold southern continent, Terra Australis, was suspected during the 15th century, it was not until the expeditions of Captain Robert Scott, Ernest Shackleton and Roald Amundsen in the first decade of this century that reports on both large and small scale features of the inland ice sheet were made. Twenty years later the pioneering flights of Rear Admiral Richard Byrd and Lincoln Ellsworth marked the beginning of an era of increasingly intense observation of the ice mass. Exploratory ventures continued throughout the 1930s and 1940s as many

UNIVERSITY
LIBRARY
CAMBRIDGE

national governments showed an increasing awareness of, and interest in, the importance of the continent. Operation 'Highjump' (1946-47), sponsored by the US Navy and at that time the largest operation to visit the Antarctic, had among its specific aims aerial photography and reconnaissance. While much of the 3.9 M km^2 covered by photographs was of coastal areas, sorties were made to the interiors of Marie Byrd Land, the Ross Ice Shelf and to the polar plateau (see figure 1.1, which shows place names used in this thesis. Figure 1.2 shows the location of all figures).

The Norwegian-British-Swedish Antarctic Expedition (1949-1952) to western Dronning Maud Land was one of the first of a series of overland traverses, a method of survey which was to be used throughout the continent in the 1950s (figure 1.3.A). The expedition was also notable in that, unlike most of its predecessors, specific scientific enquiry was given priority over general geographical observation. Nevertheless, an extensive survey of the ice sheet surface and subglacial topography inland of Maudheim did result (Robin, 1958; Swithinbank, 1959). The International Geophysical Year (IGY) in 1957-1958 saw a burst of activity with 12 nations participating in an extensive Antarctic programme of meteorological, oceanographic, glaciological, magnetic and physical observation and experiment. Although its principal objectives were to contribute to global knowledge (Dater, 1975), delineation of the geographic features of the continent and the ice sheet was also much enhanced (for instance, Lister, 1959; Blaiklock and others, 1966). Oversnow traverses continued during the 1960s (figure 1.3.B), covering extensive areas of both East and West Antarctica. The USA and USSR were the main sponsors but the UK, France, Australia, Japan, Belgium, New Zealand, South Africa and Argentina also participated. As on previous traverses, barometric and gravity profiling and seismic shooting were the principal geophysical survey tools employed (Bentley, 1964).

Although a small number of surface traverses were made during the 1970s (figure 1.3.C), the introduction of airborne radio echo sounding enabled the ice sheet to be surveyed with a speed and accuracy which could not be achieved by earlier methods. The first extensive profiling was undertaken

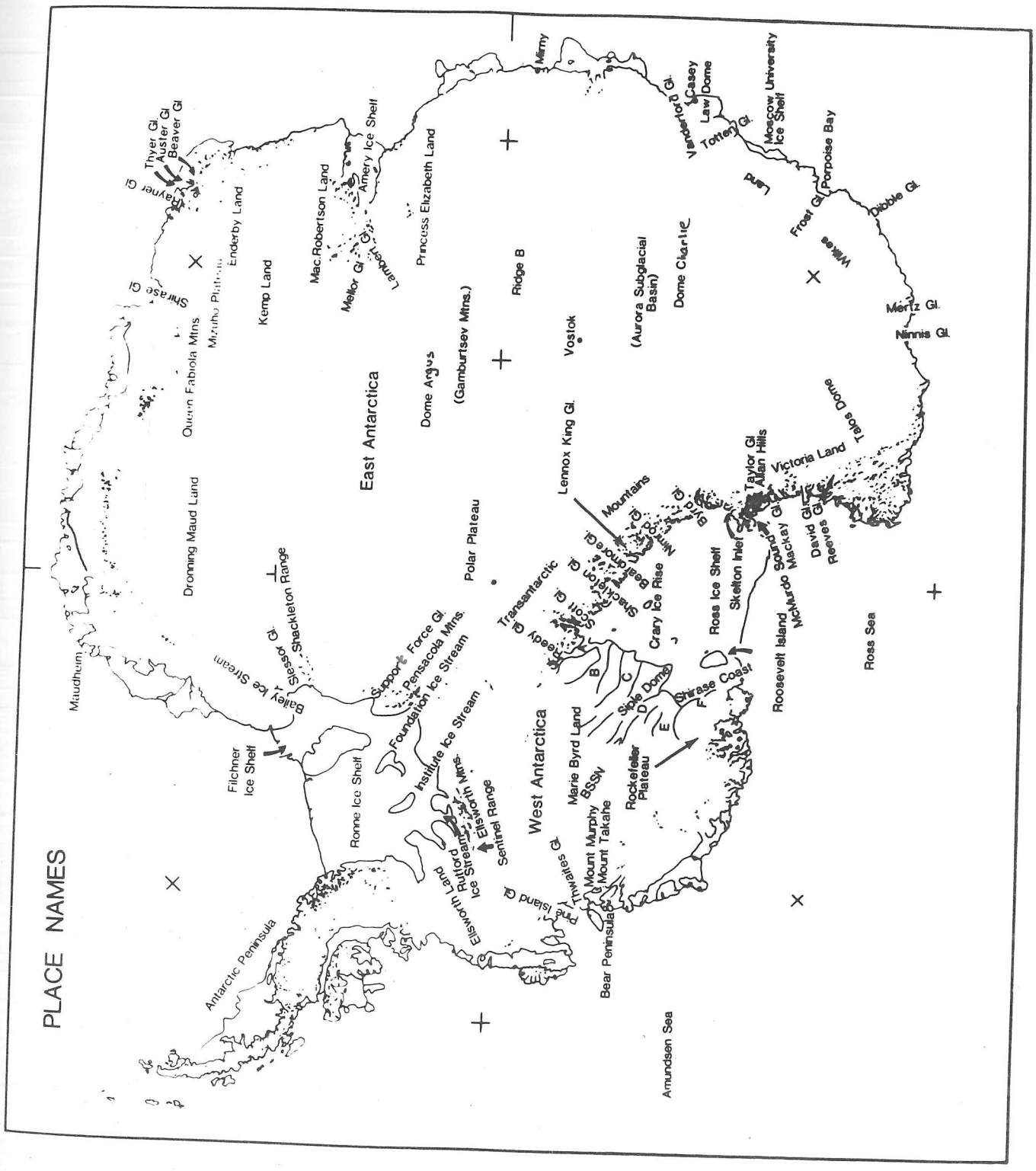

Figure 1.1: The location of Antarctic place names used in this thesis. Bracketed names indicate subglacial features. BSSN: Byrd Station Strain Network; A to F are ice streams in Marie Byrd Land.

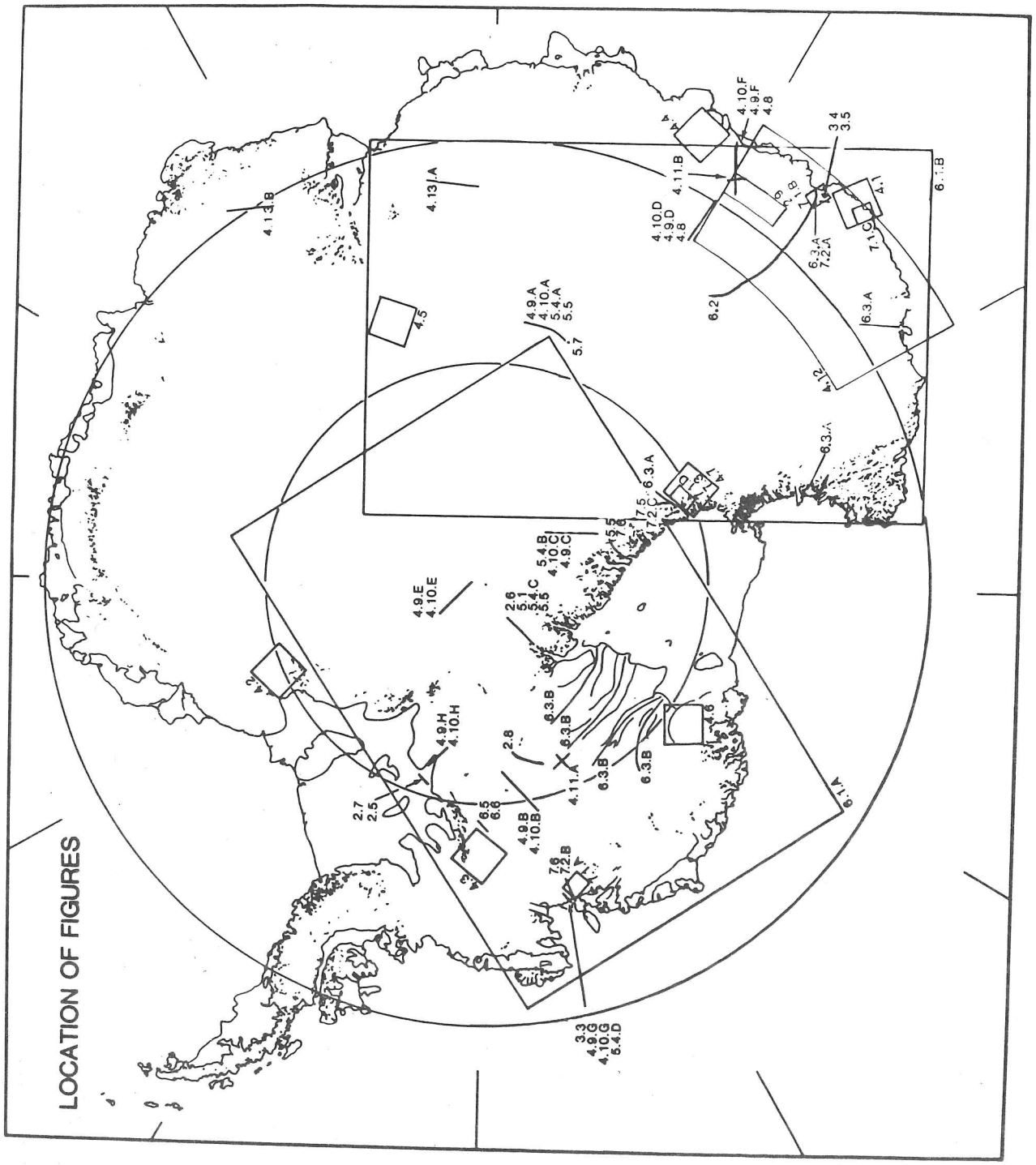

Figure 1.2: The location of figures in this thesis.

in 1967-68 by a joint programme involving the Scott Polar Research Institute, Cambridge and the National Science Foundation of the USA (Robin and others, 1970). This project was developed and expanded, and continued for a further five seasons until 1978-79 by which time approximately 50% of the Antarctic continent had been covered by a grid of 50 to 100 km. Other national programmes operated during the 1970s and sizeable contributions were made by the USA, USSR, Japan, Australia, South Africa, Belgium and UK (British Antarctic Survey). By the end of the decade, all of the major features of the ice sheet were known and considerable portions could be described in detail (for instance, Drewry, 1983a; Drewry and Robin, 1983).

Today, the use of satellites for the observation and study of the Antarctic offers many advantages over conventional airborne remote sensing, just as the latter had done with respect to oversnow traverses ten years previously. The ability to monitor extensive areas with a variety of sensors and to relay the data swiftly to dispersed locations has been demonstrated by the satellites which have already been put into service. Perhaps the best known of these is the Landsat series of which there have so far been four (section 2.3). Although their orbits only reach to 81°S, the whole continent up to that latitude (11.441 M km^2) may be covered with 519 multispectral scanner images (Williams and others, 1983). The list of other satellite-based projects being planned or under development is impressive (Duchossois and Plevin, 1981). The advantages of this scale of survey, when allied with the increasing accuracies and resolutions now available, point the way in which many important observations of the Antarctic ice sheet will be made in the future.

1.3 The geometry of the Antarctic ice sheet

A theoretical approach provides valuable insights to the form of ice masses and hence to their behaviour. In this section, we shall consider three models for the regional shape of an ice sheet before comparing them with observations and noting the deviations. The coordinate system used is

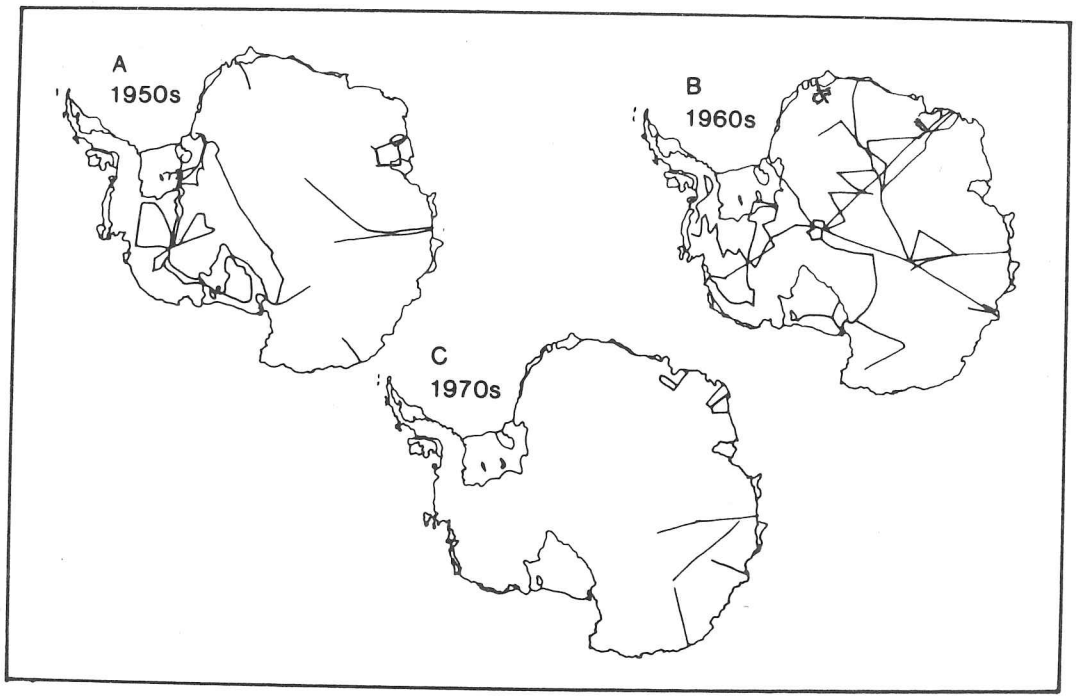

Figure 1.3: Overland traverses carried out in the Antarctic during the 1950s (A), 1960s (B) and 1970s (C).

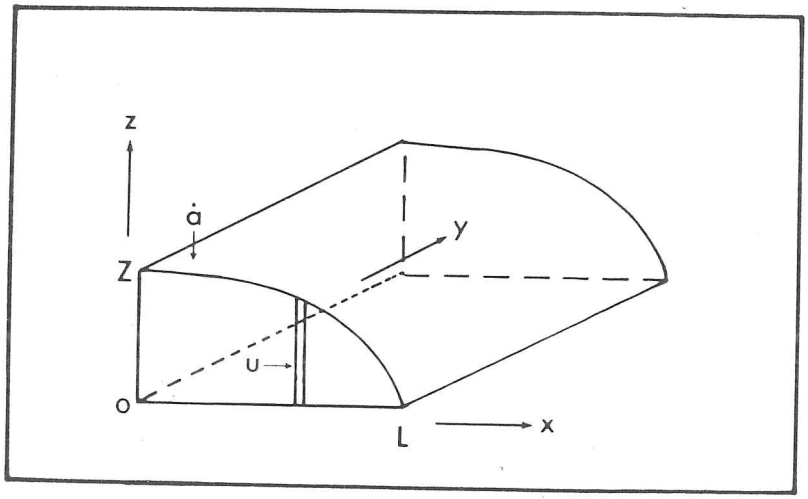

Figure 1.4: The coordinate system used in this thesis showing maximum height (Z) and half-width (L) of the ice sheet, accumulation rate (ȧ) and mean velocity of an ice column (u).

given in figure 1.4.

1.3.1 Models of the form of ice sheets

Assuming an ice sheet in steady state and resting on a flat bed, Orowan (1949) considered ice as a perfectly plastic material with a single yield stress τ_o = 100 kPa. For equilibrium to be maintained, the total horizontal force on OZ (that is, the integral of the hydrostatic pressure) must equal the yield stress on the bed which is everywhere equal to the basal shear stress, τ_b. Thus,

$$\frac{1}{2} \rho g z^2 = \tau_b L \qquad [1.1]$$

and hence, the surface profile may be described by

$$(z/Z)^2 + x/L = 1 \qquad [1.2]$$

where ρ is the density of ice and g is the gravitational acceleration.

Nye (1957) replaced the assumption of perfect plasticity with a more realistic flow law for ice, thereby allowing for variations in temperature and shear stress. Assuming that all surface velocity is due to sliding at the bed (that is, that du/dz is constant and that the longitudinal strain rate, $\dot{\epsilon}_x = 0$), Weertman's (1957) expression for the sliding of a glacier can be used; thus

$$u_b = A' \tau_b^m \qquad [1.3]$$

where A' and m are constants. Finding the solution for the expression produced by combining equation [1.3] with that for basal shear stress

$$\tau_b = \rho g z \sin \alpha \qquad [1.4]$$

where $\alpha = -dz/dx$, the surface slope, gives

$$(z/Z)^{2.5} + (x/L)^{1.5} = 1. \qquad [1.5]$$

This assumes a steady state ice sheet on a flat bed and that m = 2.

A further analysis was that of Vialov (1958) who, for an ice sheet frozen to its bed, began with the flow law for polycrystalline ice derived from laboratory studies (Glen, 1955)

$$\dot{\epsilon} = A \tau^n \qquad [1.6]$$

where A and n are constants, $\dot{\epsilon}$ is the effective strain rate and τ is the effective shear stress. Assuming that the shear stress is very much greater than all other stress deviators and hence that all motion is through internal deformation, by setting n = 3, we obtain

$$(z/Z)^{2.7} + (x/L)^{1.3} = 1. \qquad [1.7]$$

1.3.2 Observations of the form of the Antarctic ice sheet

Observations have shown that equations [1.2], [1.5] and [1.7] can provide reasonable approximations of the surface profile of parts of the Antarctic ice sheet, thus indicating that its overall shape is, to a large degree, dependent on the plastic properties of ice. Drewry (1983a), taking τ_b = 50 kPa, compared equation [1.2] with profiles inland from the Support Force and Slessor Glaciers and Bailey Ice Stream (figure 1.5.A). The fit gives a satisfactory first approximation. However, vertical deviations of 300 to 500 m in the lowermost 200 to 400 km of each profile indicate a break-down in the model's assumptions.

Equation [1.3] predicts that τ_b is proportional to the sliding velocity, u_b. The dependence of motion on internal deformation assumed by equation [1.7] suggests that, if longitudinal stress gradients have been effectively smoothed out, τ_b will be proportional to some power of u/z (Budd and Radok, 1971), a ratio which is proportional to the mean shear strain rate through the ice thickness. Whether motion is dependent on basal sliding or internal deformation may be tested by considering the

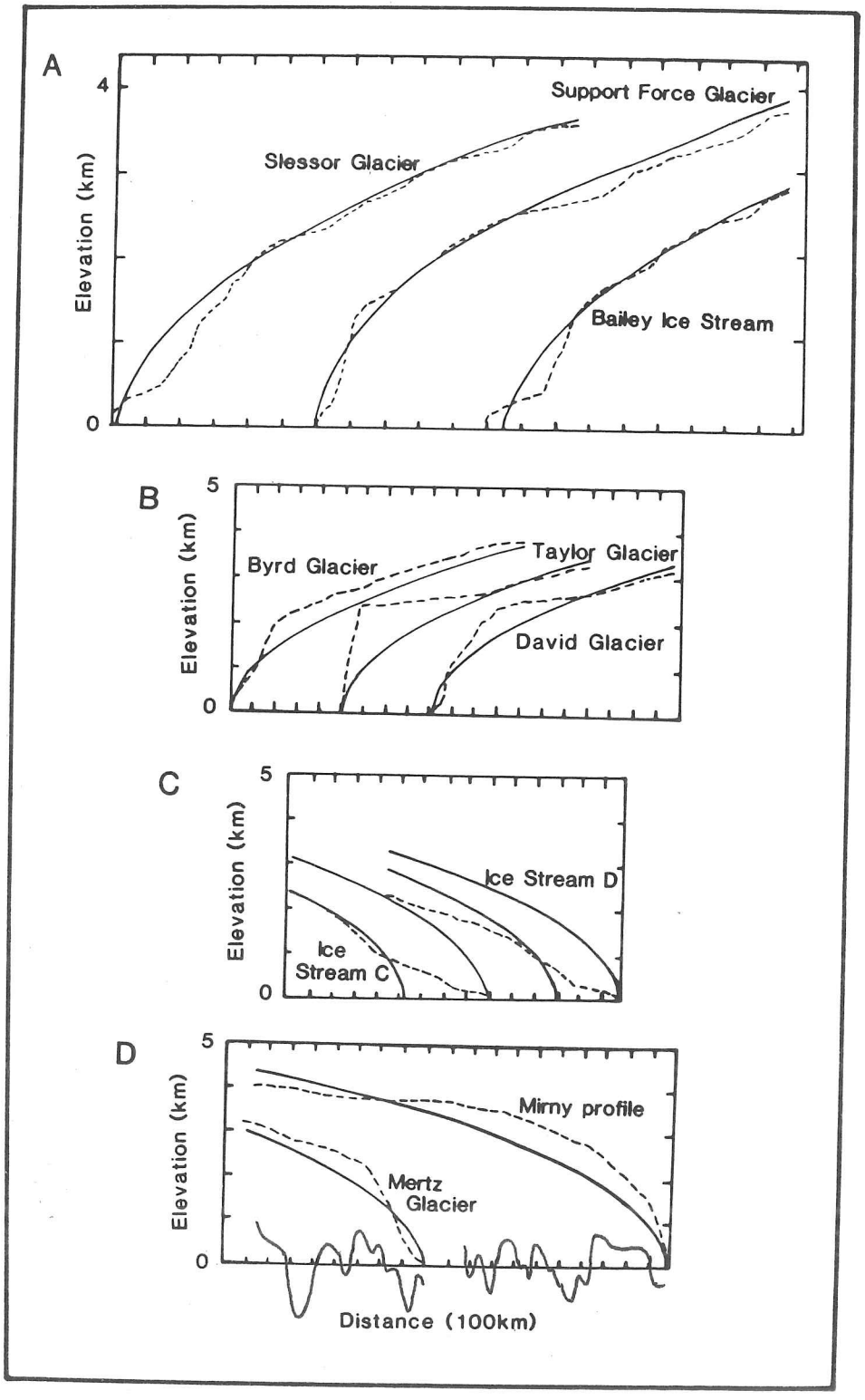

Figure 1.5: Comparison of measured ice sheet profiles (dashed lines) with the form specified by equation (1.2) (solid lines). A: flowlines leading to major ice sheet outlets; B: flowlines leading to glaciers passing through fringing mountains; C: flowlines leading to West Antarctic ice streams; D: flowlines over regions with irregular bedrock. (Redrawn from Drewry, 1983a). Bedrock profiles shown in D.

relationship between the above variables. Data from Wilkes Land (Cooper, McIntyre and Robin, 1982), Law Dome (Budd, 1969) and East Antarctica inland of Casey (Budd and Young, 1979) show that τ_b is more closely related to u/z than u, indicating that the major part of surface motion is due to shear within the ice mass and not to sliding. This supports the use of equation [1.7] rather than [1.5] when modelling the Antarctic ice sheet on a regional scale.

Figure 1.6 shows an isometric view of the ice sheet on a 50 km square grid excluding areas of exposed rock. Although areas approximating the form given by equation [1.7] can be identified, particularly in East Antarctica, the overall shape is very much more irregular and complex. The terrain is dominated in coastal areas by major promontaries and indentations, the latter being associated with fast flowing ice streams which drain the coastal region. In the catchment areas for the Ross and Ronne and Filchner Ice Shelves in West Antarctica, the low slopes of these amphitheatre-like embayments coalesce, producing concave seaward margins to the convex profiles inland. Several steady state models alternative to those above have been advanced to account for such regional variability. For example, Weertman (1963) considered an ice sheet bordered by mountains and drained by outlet glaciers. Byrd, David and Taylor Glaciers (figure 1.5.B) illustrate the locally significant deviations that may be expected to occur. Similarly, the presence of water at the bed of the ice mass may lead to a substantial reduction of the basal shear stress and hence surface gradient (Weertman, 1966); the low slopes of Ice Streams C and D draining into the Ross Ice Shelf (figure 1.5.C) have been attributed to this (Rose, 1978). Rough bedrock, such as that found in the Antarctic Peninsula, will also cause deviations from such simple profiles, especially near the ice sheet margin where the ice is thin (figure 1.5.D).

1.3.3 Observations of the topography of the Antarctic ice sheet

Deviations from theoretically derived profiles have also been shown to occur on scales of a few tens of kilometres (Bentley, 1964), as can be seen in figures 1.5 and 1.6. A thorough search of the literature was undertaken

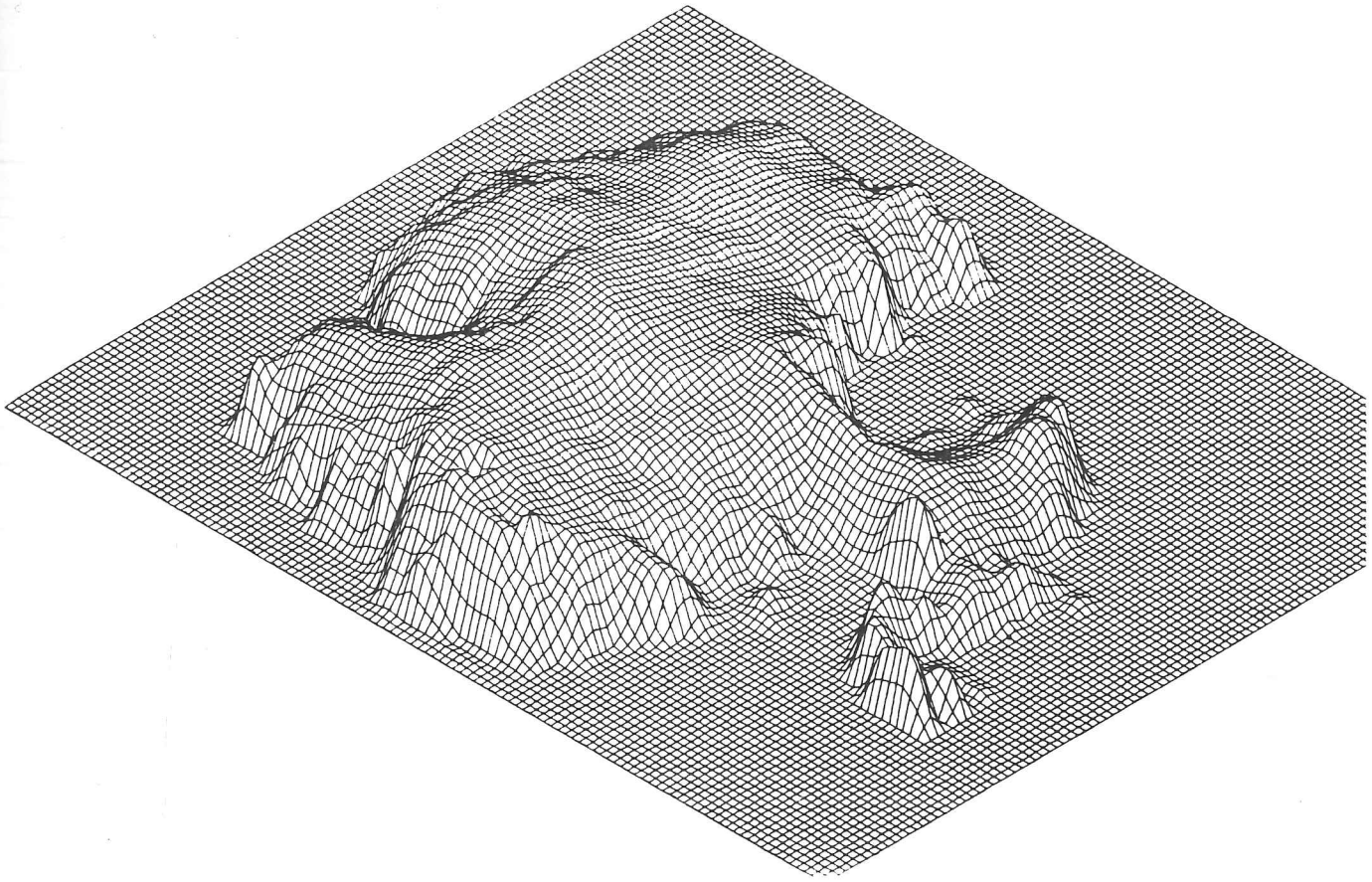

Figure 1.6: Isometric view of the Antarctic ice sheet on a 50 km square grid excluding areas of exposed rock.

to collect all previous observations and measurements of such features. The results are summarized in figure 1.7 in terms of wavelength and peak-to-trough amplitude. Where these were not explicitly mentioned in the text, values were extracted from surface profiles whenever possible.

The range in the dimensions of undulations (figure 1.7) is undoubtedly great; for instance, within a distance of 100 km near the head of Ice Stream A (shown as A in figure 1.1), reported wavelengths vary between 10 and 65 km. There is less variability in terms of amplitude but this may reflect the subjectivity of recording. The ratio of wavelength to amplitude is generally very variable and does not have a regular distribution. The magnitude of wavelengths in the polar plateau appears markedly greater than in other parts of the ice sheet. Although significant variations are apparent, the data are insufficient to draw conclusions regarding classifications or patterns. Traverse data on their own are too isolated and infrequent to be used as a basis for statistical analyses.

The structure of undulations in the ice sheet surface has been attributed to the processes of ice flow (Robin, 1967; Collins, 1968; Budd, 1971), to drifting snow (Bader, 1961), to aeolian scouring of the ice surface (Whillans, 1975) and to various combinations of these. For instance, accumulation rates are influenced by topographic variations and masking of the real ice profile is not always uniform (Black and Budd, 1964; Gow and Rowland, 1965; Young and others, in press). To distinguish between these causes is not always possible, particularly when remote sensing forms the main component of one's data and ground truth is lacking. Perhaps one of the more reliable methods of differentiation is scale, since depositional snow features are most likely to be in the range of tens to hundreds of metres (Yokoyama, 1978). Products of the dynamics of the ice sheet may involve features one to four orders of magnitude greater than this, that is, between 1 and 100 km. Although an immediate distinction is not always possible, we intend in this thesis to refer primarily to ice flow features.

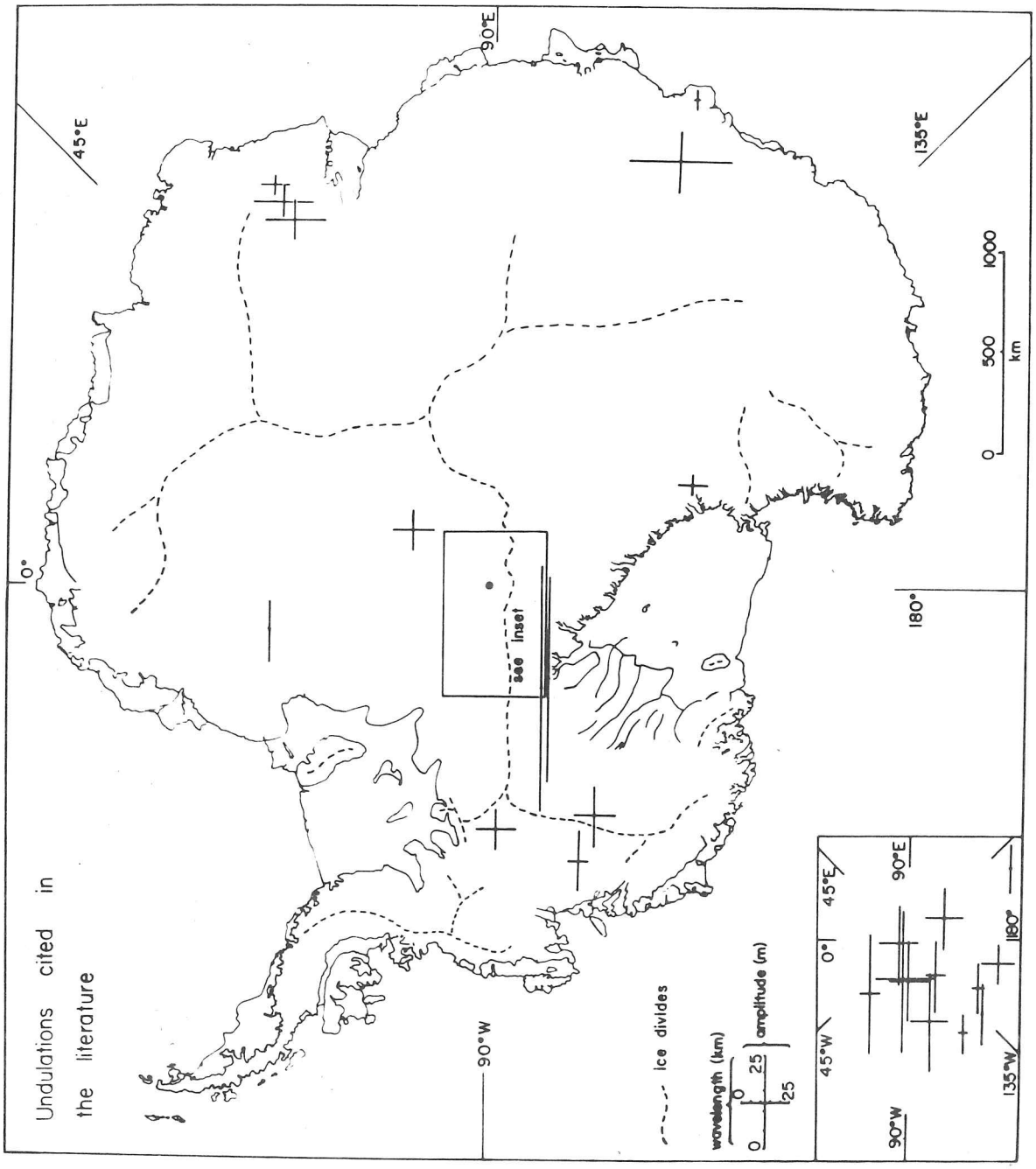

Figure 1.7: Dimensions of surface undulations (wavelengths and peak-to-trough amplitudes) reported in the literature, largely from observations made during overland traverses.

1.4 Causes of topographic variability

The variability evident in the surface of the Antarctic ice sheet is clearly dependent on the manner in which the ice flows over subglacial topography. The relation between bedrock and ice surface terrain has been widely demonstrated; bedrock irregularities cause damped undulations in the ice sheet surface (for example, Robin, 1958; Budd, 1966). Along flowlines, ice surface slopes have been found to be related to bedrock topography such that maximum slopes occur in phase with the thinnest ice (Budd, 1969; Beitzel, 1970).

1.4.1 Basal and longitudinal stresses

Although strictly only applying to two dimensional analysis, the theory of ice flow over bedrock undulations (Robin, 1967; Budd, 1970) explains, to a degree, the relation between measured surface and bedrock profiles. A certain amount of variability may be expected due to the three dimensional character of the bedrock and the ice flow. Robin (1967) explained surface slope fluctuations in terms of variations in the longitudinal stress, σ_x, which are produced by ice flow over bedrock irregularities. These can be found from the flow law and values of $\dot{\epsilon}_x$, in this case derived from

$$\dot{\epsilon}_x = (\dot{a} - u \frac{dz}{dx}) / z \qquad [1.8]$$

where $\dot{a}$ is the accumulation rate and u is the mean forward velocity. He then suggested that the dominant terms, after some approximations, are

$$\alpha = \frac{\tau_b}{\rho g z} - \frac{1}{\rho g} \frac{d\bar{\sigma}'}{dx} \qquad [1.9]$$

where $\bar{\sigma}_x'$ is the longitudinal stress deviator averaged over the ice thickness. Although assuming that $\dot{\epsilon}_x$ does not vary with depth, that deformation is in plane strain, that there is no sliding and that the ice sheet is in steady state, Robin (1967) found qualitative agreement with measured surface slopes down a flowline in north-west Greenland; Beitzel (1970) confirmed this with Antarctic data.

Budd (1969, 1970) included in his theory a locally varying τ_b. Thus,

$$\alpha = \frac{(\tau_b - 2G + T)}{\rho g z} \qquad [1.10]$$

where 2G is the longitudinal stress as determined by Robin (1967) and

$$T = \int_0^z \int_0^z \frac{d^2 \tau_{xz}}{dx^2} dz\, dz. \qquad [1.11]$$

He also postulated, on the basis of observations from Law Dome, that for distances greater than 20 times the ice thickness, the effects of σ_x would be negligible. Cooper, McIntyre and Robin (1982) suggested that averaging on a larger scale is necessary and this has been confirmed empirically in Wilkes Land (Young and others, in press).

1.4.2 Bedrock topography and ice thickness

The extent to which surface features reflect bedrock undulations is a function of ice thickness relative to the wavelength of subglacial irregularities, the mean forward velocity and mean viscosity of the ice column (Budd, 1969). This relationship has been defined by a damping factor (Budd, 1970). Three dimensional bedrock protuberances will be slightly more damped than the two dimensional theory suggests. Results from Dronning Maud Land (Beitzel, 1970) and Law Dome (Budd and Carter, 1971) supported the prediction that, for a given ice thickness, there is a characteristic wavelength for which damping is at a minimum. Thus, bedrock wavelengths 3.3 times the ice thickness are preferentially transmitted to the ice sheet surface although it is not clear why ice sheets behave in this way (Paterson, 1981, p167). Dominant wavelengths are therefore longest in the thicker ice which is typically found towards ice divides. However, more recent analyses (Hutter and others, 1981; Whillans and Johnsen, 1983) indicate that there is no preferred wavelength and that the response of the ice sheet surface increases with bedrock undulation wavelength. These also suggest that the transfer of bedrock-induced stresses will be seriously affected by mean inclination, velocity, viscosity and variations in sliding and basal shear.

1.4.3 Ice velocity and viscosity

Effects of the velocity and viscosity of ice are likely to vary less rapidly over given distances than those of bedrock roughness and ice thickness. Regionally, surface velocities increase with distance from ice divides and so damping will decrease towards the ice sheet periphery. In marginal areas, however, significant variations are more likely as ice is channelled through ice streams and outlet glaciers (Drewry and Robin, 1983). Velocity differences between domes and the ice streams in Marie Byrd Land may reach orders of magnitude (Rose, 1978) with consequent effects on ice undulation amplitudes. Young and others (in press) have shown that surface velocity differences on the scale of the undulations themselves are small.

Ice viscosity may be closely related to altitude through its dependence on temperature. Although the damping factor is inversely dependent on the mean viscosity through the ice column (section 5.2), surface temperatures in central East Antarctica (down to -55 ^{o}C) suggest that the ice will behave very much as a rigid body which inhibits the transmission of bedrock-induced strains to the ice sheet surface. Towards the margins, where the temperature may be 30 C^{o} higher and hence viscosities very much lower, the damping of bedrock irregularities will be significantly different. This is a result of the strong temperature dependence of the constant A in the flow law for ice (Glen, 1955).

1.5 Aims of this thesis

This thesis aims to investigate details of the surface morphology of the Antarctic ice sheet so as to infer basal conditions and characteristics of ice flow. This approach enables theories relating to these physical processes to be tested through comparisons with current data.

Sources of data are introduced in the second chapter; these consist largely of aircraft altimetry, radio echo soundings and both altimetry and imagery collected by satellite. They are discussed in terms of coverage,

accuracy and applicability to the study of the Antarctic ice sheet. In chapter 3, consideration is given to the understanding of these data sources since not all may be interpreted unambiguously. Comparisons are made between imagery and altimetry from aircraft and satellite so as to assess their relative merits. Chapter 4 brings these sources together in a description of the ice sheet's surface topography. Qualitative description and several quantitative methods are applied and the interpretation is summarized in a new statistical model of the ice sheet surface. In the fifth chapter, factors producing variations in the form and topography of the ice sheet are considered; relationships between the ice sheet's form and parameters which were discussed in section 1.4 are tested where data permit. In chapter 6, driving and longitudinal stresses and the extent to which they affect ice sheet topography are analysed. The manner in which ice flows through outlet glaciers and ice streams is considered in chapter 7 in terms of flow regime, stability of the ice sheet and landform development.

Discussions of the form and flow of the Antarctic ice sheet raise many unanswered questions which are of considerable importance to the study of ice masses. Among the questions addressed in this thesis are:

- how useful for the glaciologist are the various means currently available of observing ice sheets?

- what is the topographic variability of the Antarctic ice sheet?

- what can be deduced about basal conditions and ice dynamics from inspection of the form and topography of the Antarctic ice sheet?

- how well is existing theory relating the form and flow of ice sheets supported by current data?

- how, and to what extent, do ice streams and outlet glaciers control the discharge of ice from, and hence stability of, the Antarctic ice sheet?

UNIVERSITY
LIBRARY
CAMBRIDGE

CHAPTER 2

SOURCES OF DATA

2.1 Radio echo sounding

2.1.1 Antarctic coverage

One of the most successful survey techniques to be employed in the polar regions has been radio echo sounding. Despite uncertainties about exact field conditions, an early system was developed at the Scott Polar Research Institute and since the early 1960s, there has been considerable interest in its application to ice masses (Evans, 1963). The principal advantages of this technique over other forms of geophysical survey, such as seismic traverses, include the continuous recording of the ice thickness profile, the speed of survey and the coverage of large and remote regions.

The technique was tested in long range flights over a wide variety of ice terrain in the Antarctic during the 1967-68 austral summer and led to a joint programme in 1969-70 by the National Science Foundation (NSF) and the Scott Polar Research Institute (SPRI) (Robin and others, 1970). After the 1971-72 season in East Antarctica, the Technical University of Denmark (TUD) joined the programme and a 50 km grid was flown over Marie Byrd Land and much of the Ross Ice Shelf in 1974-75 (Robin and others, 1977). Two further seasons in 1977-78 and 1978-79 enabled this grid to be extended over the greater part of West Antarctica and gaps in the East Antarctic coverage to be covered (Drewry and Meldrum, 1978; Drewry and others, 1980). At present, approximately 50% of the Antarctic ice sheet (6.8 M km^2) has been covered by radio echo sounding with systems operating at frequencies of 60 and 300 MHz on a grid of 50 to 100 km (figure 2.1).

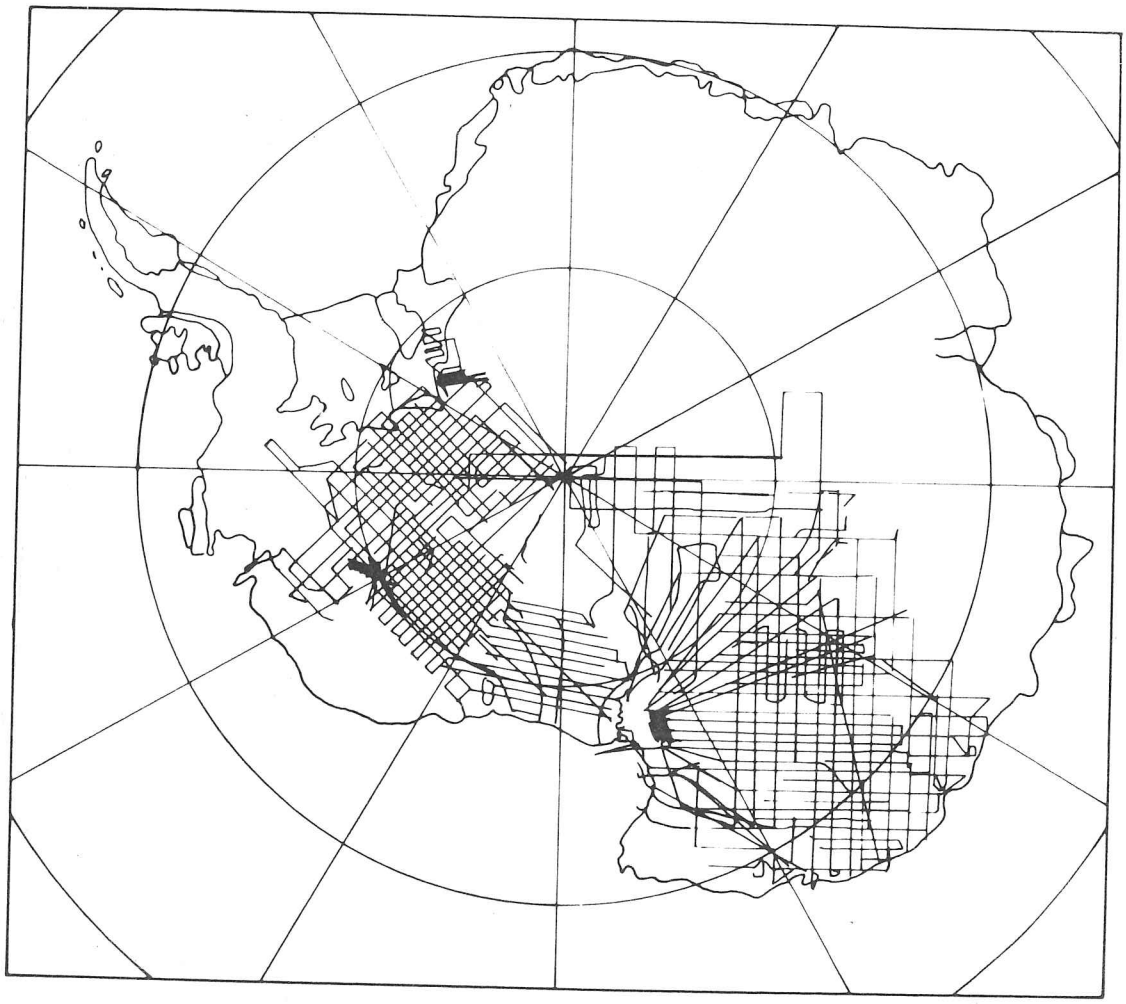

Figure 2.1: Flight lines of radio echo sounding missions undertaken since 1971 by the joint NSF-SPRI-TUD programme.

2.1.2 Methods of recording

Several methods of recording the radio echoes were used (figure 2.2). The most effective presentation for large scale survey is given by the Z-mode of a recording oscilloscope, which records on 35 mm film a continuous intensity-modulated record of the differentiated return, namely a function of delay time against flying time (a 'Z-scope'). In the last two seasons, this was supplemented by a Honeywell fibre-optic oscillograph which produced a paper output of the 60 MHz Z-scope within minutes of recording (Drewry and Meldrum, 1978). It was of higher resolution than the film and allowed an immediate check that the system was recording satisfactorily. 'A-scope' displays (received power against delay time) were also recorded on 35 mm film during all seasons and on 8 mm cine film for very short, high speed bursts in 1974-75 and 1977-78. A third means of recording used from the 1974-75 season onwards was echo-strength measurement (ESM) which gives a continuous record of any echo (for instance, bedrock) that is followed by a recording gate (Neal, 1976).

2.1.3 Data processing

The bedrock profile digitized from the Z-scope film is a convoluted representation of the true subglacial surface (Harrison, 1972; summary in Drewry, 1973, p52). Discrete bedrock reflectors generate hyperbolae on the film. Over rough topography, hyperbolae from peaks may obscure returns from intervening valleys and so give the impression of a much smoother surface than that actually possessed by the bedrock. Harrison developed a computer program to migrate these complicated patterns by removing hyperbolae and correcting slopes while leaving peaks and level surfaces unchanged. Migration was not used for the general processing of SPRI flights during broad scale surveys (Rose, 1978) but for the detailed study of specific flight sections in this thesis, re-digitized at fine intervals (roughly 100 m), an adapted version of Harrison's program has been used.

Data collected throughout the NSF-SPRI-TUD radio echo sounding programme has been analysed at the Scott Polar Research Institute (Drewry, 1973; Rose, 1978; Steed, 1980; Jankowski, 1981; Millar, 1981b). The present

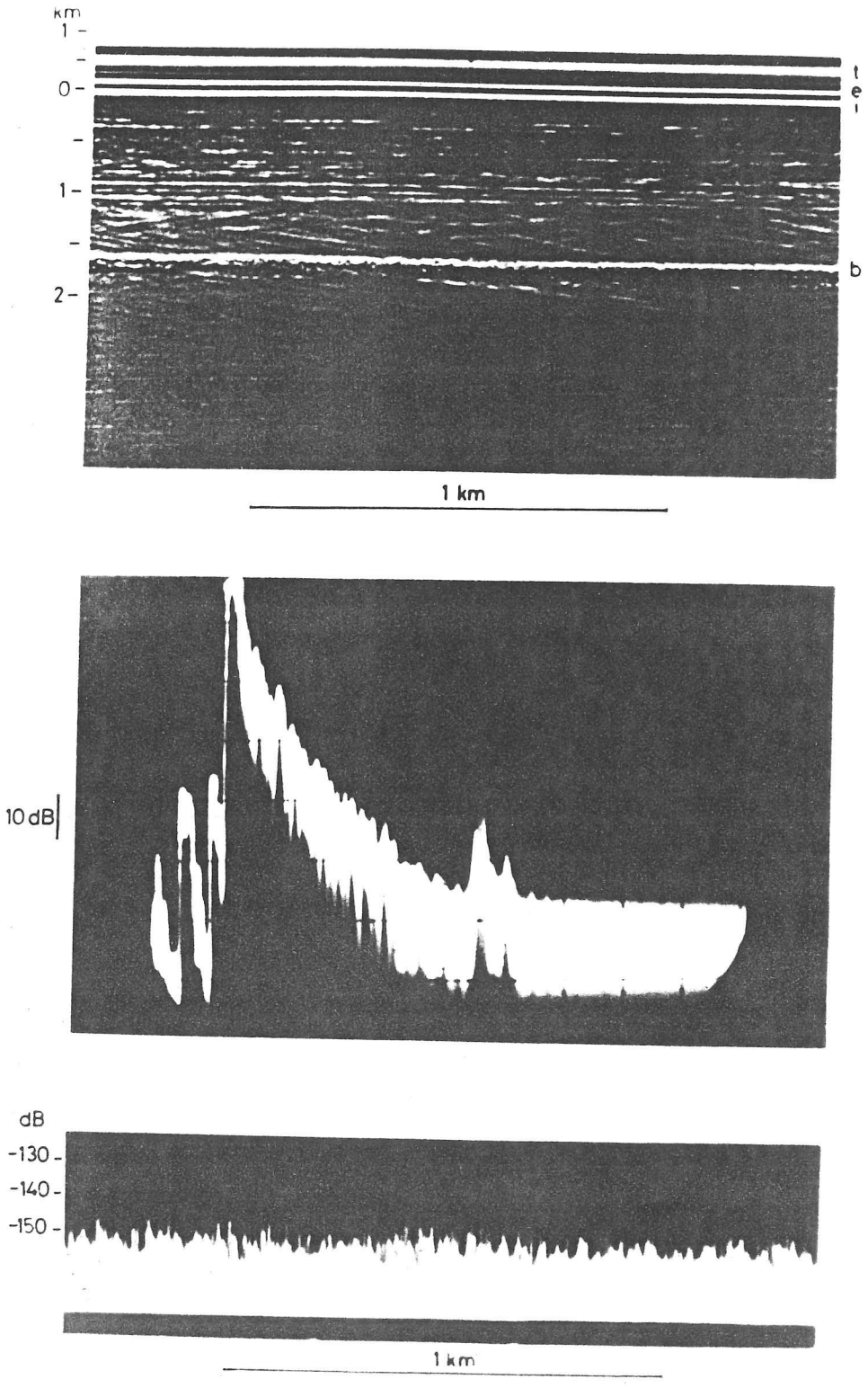

Figure 2.2: Methods of recording radio echo sounding data. A: a 60 MHz Z-scope, a function of ice thickness against flying time. Transmitter pulse (t), surface (i) and bedrock (b) echoes are shown. Internal layering can also be seen. B: an A-scope showing received power against delay time. C: echo strength measurements (ESM) showing the echo strength as a function of time.

author was responsible for the reduction of data for two flights from the 1977-78 season. Similar techniques were used throughout the data reduction as indicated in figure 2.3. Individual surface and bedrock elevation maps have been produced for various parts of the Antarctic (Rose, 1978; Steed, 1980; Jankowski, 1981) while all of the radio echo sounding data is summarized in a series of maps of the major glaciological and geophysical parameters (Drewry, 1983a).

2.2 Aircraft altimetry

2.2.1 Introduction

The Airborne Research Data System (ARDS) was used throughout the 1977-78 and 1978-79 radio echo sounding flights as the primary means of logging navigation data (Drewry and Meldrum, 1978). The ARDS is capable of recording up to 100 channels of 6 digit data eight times per second but, at most, 38 of these were used (table 2.1). The rate of recording was reduced from 8 to 4 scans per second during the 1978-79 season so that data from a whole flight could be stored on a single magnetic tape, thus avoiding the loss of about 15 minutes of data while tapes were being changed. Given an aircraft ground speed of 100 m s^{-1}, the parameters were recorded at spatial intervals of 12.5 m or 25 m; this is considerably more detailed than that required by the resolution of airborne radio echo sounding.

2.2.2 Derived surface elevations

As part of the standard navigation equipment carried by the aircraft, the ARDS made simultaneous recordings of terrain clearance and aircraft pressure altitude, thereby enabling the determination of surface elevations along the flight lines (figure 2.4). Thus,

$$S_e = P_a - R_a \qquad [2.1]$$

where S_e is the surface elevation of the ice sheet, P_a is the pressure

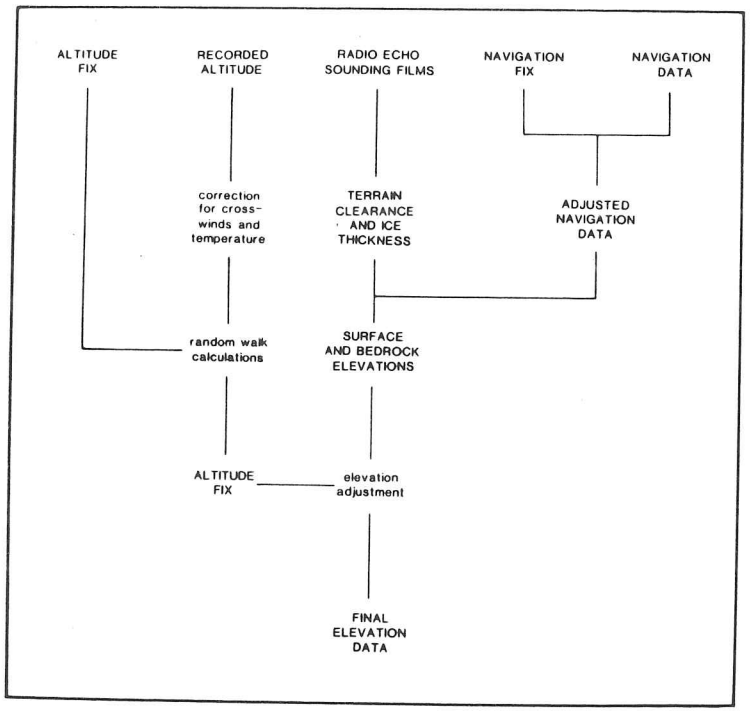

Figure 2.3: A scheme of the processing undertaken for all radio echo sounding data collected during the NSF-SPRI-TUD Antarctic programme. Only 1974-75 data were corrected for wind speed and temperature variations.

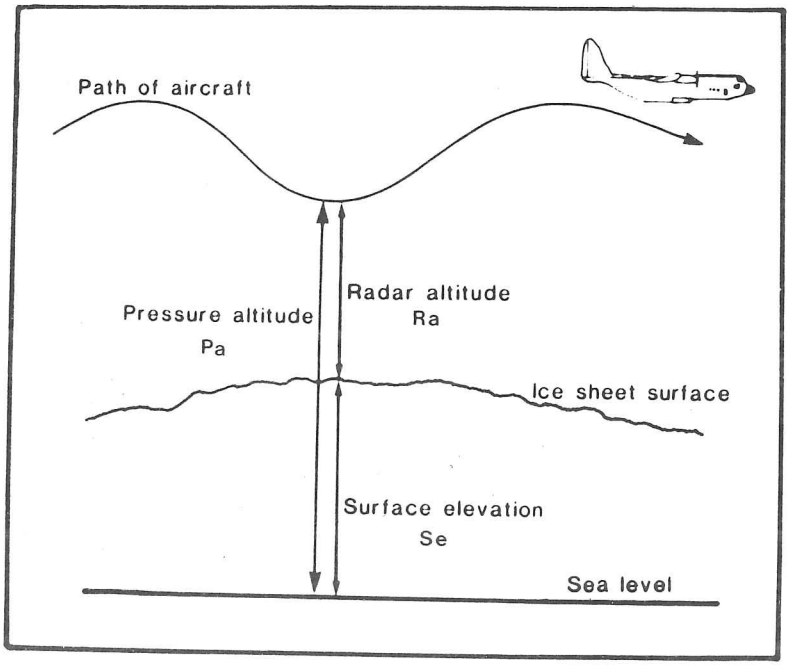

Figure 2.4: Measurements involved in the derivation of the surface elevation of the ice sheet.

Table 2.1: Parameters recorded by the Airborne Research Data System.

Channel	Parameter	Source	Unit
00	Blank	Manual entry	
01	Identification	Manual entry	
02	Date	Manual entry	
03	Time	ARDS clock	Hr. Min. Sec.
04	Quadrant/latitude	LTN 51 INS	Deg. 0.1 min.
05	Longitude	LTN 51 INS	Deg. 0.1 min.
06	Absolute altitude	APN 194 radar alt.	1 ft.
07	Spare	Manual entry	
08	Pressure altitude	Garrett pressure transducer	1 ft.
09	Spare	Manual entry	
10	Angle of attack	Rosemount transducer	0.01 MB
11	Angle of side slip	Rosemount transducer	0.01 MB
12	Drift angle/ true heading	LTN 51 INS	1 deg. 1 deg.
13	Heading/ true air speed	C12 compass 1 A/A 24G9 TAS	1 deg. 1 kt.
14	Heading/ true air speed	C12 compass 2 A/A 24G9 TAS	1 deg. 1 kt.
15	Track angle/ ground speed	LTN 51 INS	1 deg. 1 kt.
16	Drift angle/ ground speed	APN 147 Doppler radar	1 deg. 1 kt.
17	Spare	Manual entry	
18	Static air pressure	Garrett pressure transducer	0.001 inches mercury
19	Wind direction/speed	LTN 51 INS	1 deg./ 1 kt.
20	Static air pressure	Garrett pressure transducer	0.01 MB
21	Differential pressure	Rosemount transducer	0.01 MB
22	Total temperature	Rosemount transducer	0.01 ^{o}C
23	Dew point	1011 Dew Point	0.1 ^{o}C
24	Free air temperature	HP2801 quartz thermom.	0.01 ^{o}C
25*	Ambient air	Nuclei counter	
26*	DE air	Nuclei counter	
27*	DED air	Nuclei counter	
28*	Ozone concentration		
29*	Water vapour	303 Moisture monitor	
30*	Cabin pressure altit.	Rosemount transducer	1 ft.
31	CBD	Radio echo clock	15 secs.
32	Radio echo flight no.	Manual entry	
33	Blank		
34*	Scalar magnetometer		1 gamma
35*	X vector magnetom.		1000 gamma
36*	Y vector magnetom.		1000 gamma
37*	Z vector magnetom.		1000 gamma

* 1978-79 flights only.

altitude of the aircraft derived from the Garrett pressure transducer and R_a is the terrain clearance of the aircraft as measured by the radar altimeter. An example of the records and derived surface elevation is shown in figure 2.5. The technique has been used previously, for instance, in central Marie Byrd Land (Behrendt and others, 1962) and at the southern end of the Antarctic Peninsula and northern Ellsworth Land (Swithinbank and others, 1976). With an estimated 65% of the 1977-78 and 1978-79 flights within the radar altimeter's upper operational limit of 1524 m (5000 ft), these data represent 55 000 km of detailed ice sheet profiling at a high density. This will form the basis of much of the ensuing description and analysis of the Antarctic ice sheet's surface morphology.

2.2.3 Accuracy and errors

Surface elevations derived from the aircraft's altimeters are estimated to have a relative accuracy of 2 m. Terrain encountered over ice shelves and during and immediately after take-off was considered to be the smoothest which the aircraft would pass over; radar altimeter records would therefore contain minimal contributions from the ice surface topography. The high frequency component in such cases was typically less than 2 m in amplitude.

The determination of absolute altitudes by barometric methods is dependent on the temporal and spatial stability of pressure surfaces, variations of which are associated with weather systems. Measurements of such surfaces suggest vertical variations of up to 200 m over distances of 200 km (Smith, 1980). To avoid the somewhat minor corrections (Rose, 1978) to allow for this, flight sections from which altimetry data were taken were kept comparatively short (mostly less than 200 km) and usually were used to calculate only relative surface elevations.

Altimetric calculations of the ice sheet surface are dependent on either the relative stability of the aircraft or a knowledge of its motion; inaccuracies may be introduced in several ways. First, random errors are produced by the system noise of the radar altimeter and the pressure transducer. Inspection of these signals (figure 2.5) shows high

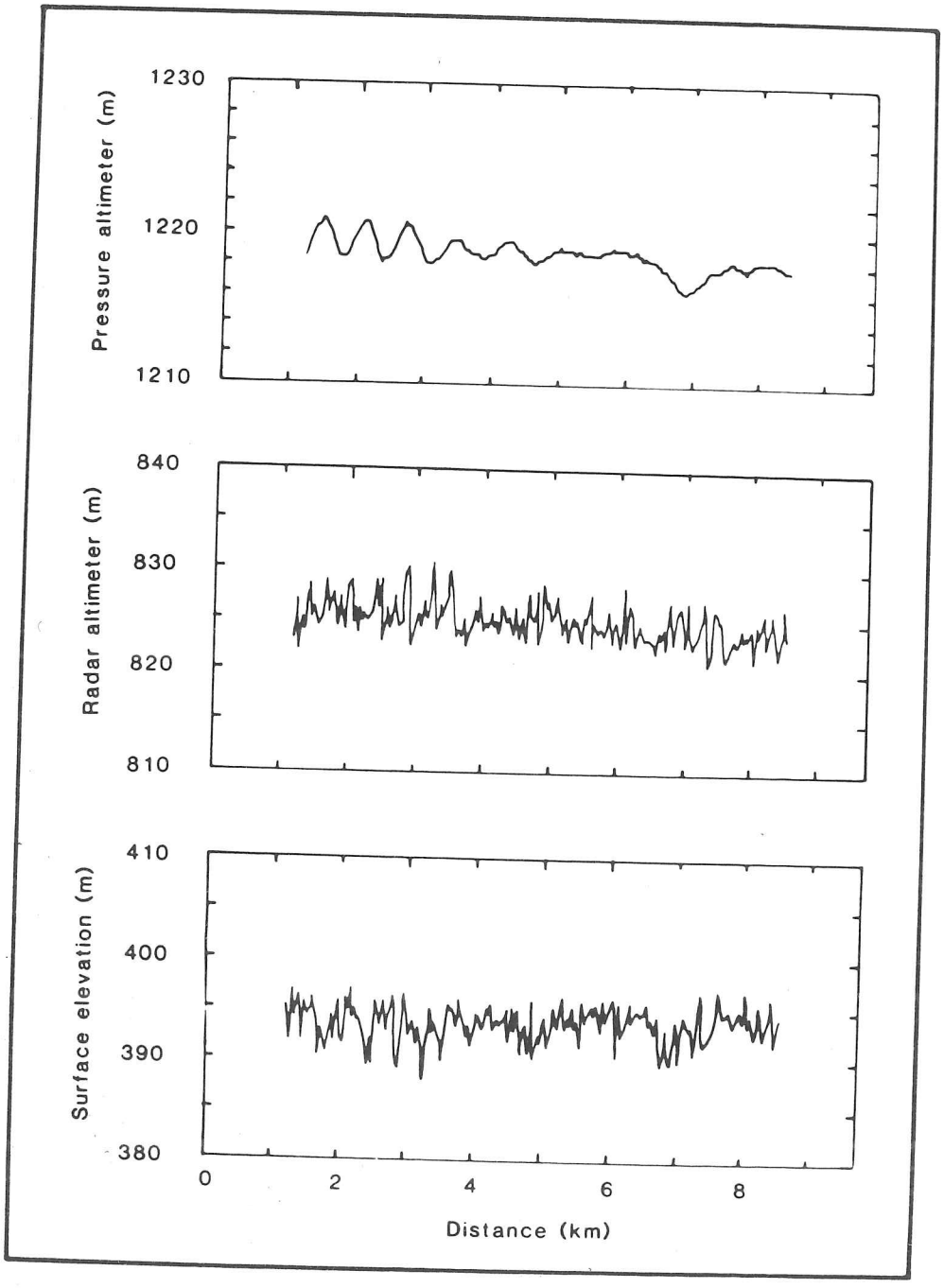

Figure 2.5: Examples of records of pressure altitude, radar altitude and the derived surface profile across the Ronne Ice Shelf downstream from Institute Ice Stream.

frequency oscillations typically with amplitudes of 4 and 3 m and wavelengths of 0.1 and 0.5 km respectively. Using

$$d = u_o t + \tfrac{1}{2} c t^2 \qquad [2.2]$$

where d is distance, u_o is initial velocity, t is time and c is acceleration, it can be shown that these high frequency variations are equivalent to vertical accelerations of roughly 32 to 42 m s^{-2} for the radar altimeter and 2.5 to 3.2 m s^{-2} for the pressure altimeter. Given that the flight of the aircraft was not markedly turbulent (C.S. Neal, personal communication), these high frequency components with accelerations of approximately 3.3 to 4.3 and 0.25 to 0.32 times that of gravity must be attributed to factors other than aircraft motion. This is confirmed by a derived surface profile down a flowline to Reedy Glacier (figure 2.6), which suggests that much of the high frequency component is due to the scattered return signal from sastrugi and other small-scale accumulation features. The amplitude of these high frequency variations decreases abruptly at the point of the increase in the regional surface slope which is due to subglacial terrain. This is the response in sastrugus size which would be expected as one moves into a region of steeper slopes and hence stronger katabatic winds (Ball, 1960) which maintain considerable quantities of snow in motion and inhibit deposition.

Second, aircraft oscillate in all dimensions while in flight and in a manner described as a 'Dutch Roll'. Consultation with aircraft manufacturers [1] has suggested that transport aircraft, such as the Hercules C130s used for the Antarctic radio echo sounding, oscillate with a period of 15 to 50 s, but typically 20 to 30 s. The maximum peak-to-trough amplitude (normally constrained by customer demand) is roughly 8 m. Since the pressure altimeter signal will reflect aircraft motion and system noise while the radar altimeter will have the added component of variations in surface topography, the porpoising of the aircraft should be

---

[1] Smith's Industries of Basingstoke and Cheltenham and Marshall's of Cambridge.

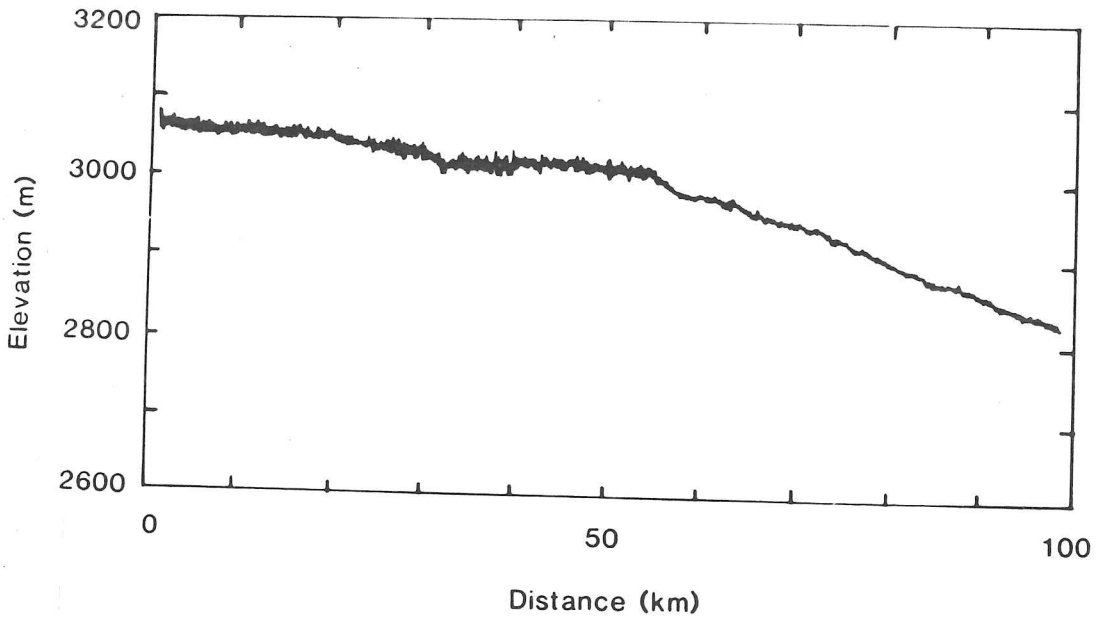

Figure 2.6: The surface profile derived from aircraft altimetry down a flowline to Reedy Glacier, showing the change in the amplitude of the high frequency component in association with the change in regional gradient. This is taken to indicate the inhibition of snow deposition and the supression of sastrugi by very strong katabatic winds (Endo and Fujiwara, 1973) and hence that the signal is largely due to real ice surface features than system noise.

compensated in the calculation of surface elevation (equation [2.1]). This is illustrated by consideration of power spectra for the two altimetry records and the surface elevation (figure 2.7) which were produced by the application of a Fast Fourier Transform (discussed in section 4.3.2) to data from the Ronne Ice Shelf. This area was chosen as a likely approximation to a level surface. The deviations of up to 30 m seen in both the altimeter profiles are absent in the surface profile where only long wavelength, low amplitude deviations occur. The spectra give details of the removal of wavelengths of 10 km and less. The rms deviations for the radar and pressure altitude surfaces are 4.1 and 3.9 m respectively but that of the surface profile is only 1.7 m. The remaining small variability of the surface profile has greater wavelengths than those reported in the literature for ice shelves (Robin, 1958; Zumberge and Swithinbank, 1962). However, the proximity to Institute Ice Stream (which is likely to cause substantial disruption to the surface) and the relative regularity of the derived surface as compared with the two altimetry profiles indicate that the variability of the surface is due to real topographic features rather than aircraft motion.

Third, occasional instabilities in one or both of the altimeters may affect ice sheet profiling. Figure 2.8 shows pressure altimeter, radar altimeter and surface elevation profiles over the West Antarctic ice divide. The derived surface profile contains a number of 'troughs' which are unlikely features given the glaciological conditions close to an ice divide of deep ice, low temperatures and hence rigid ice, very low velocities and therefore small strain rates. If these features are not real (and no evidence for them can be found by inspection of the raw radio echo sounding data, at either 60 or 300 MHz), the error must be the product of one or both of the aircraft's altimeters. The absence of these features in the radar altimeter record, as well as the greater sensitivity of the radar altimeter and hence the very much greater proportional error that these features represent (4.0% for the radar altimeter but only 0.5% for the pressure altimeter), indicate that they probably emanate from a fault in the pressure transducer. Such features can indeed be seen in the pressure altimeter signal at the point at which these troughs occur in the

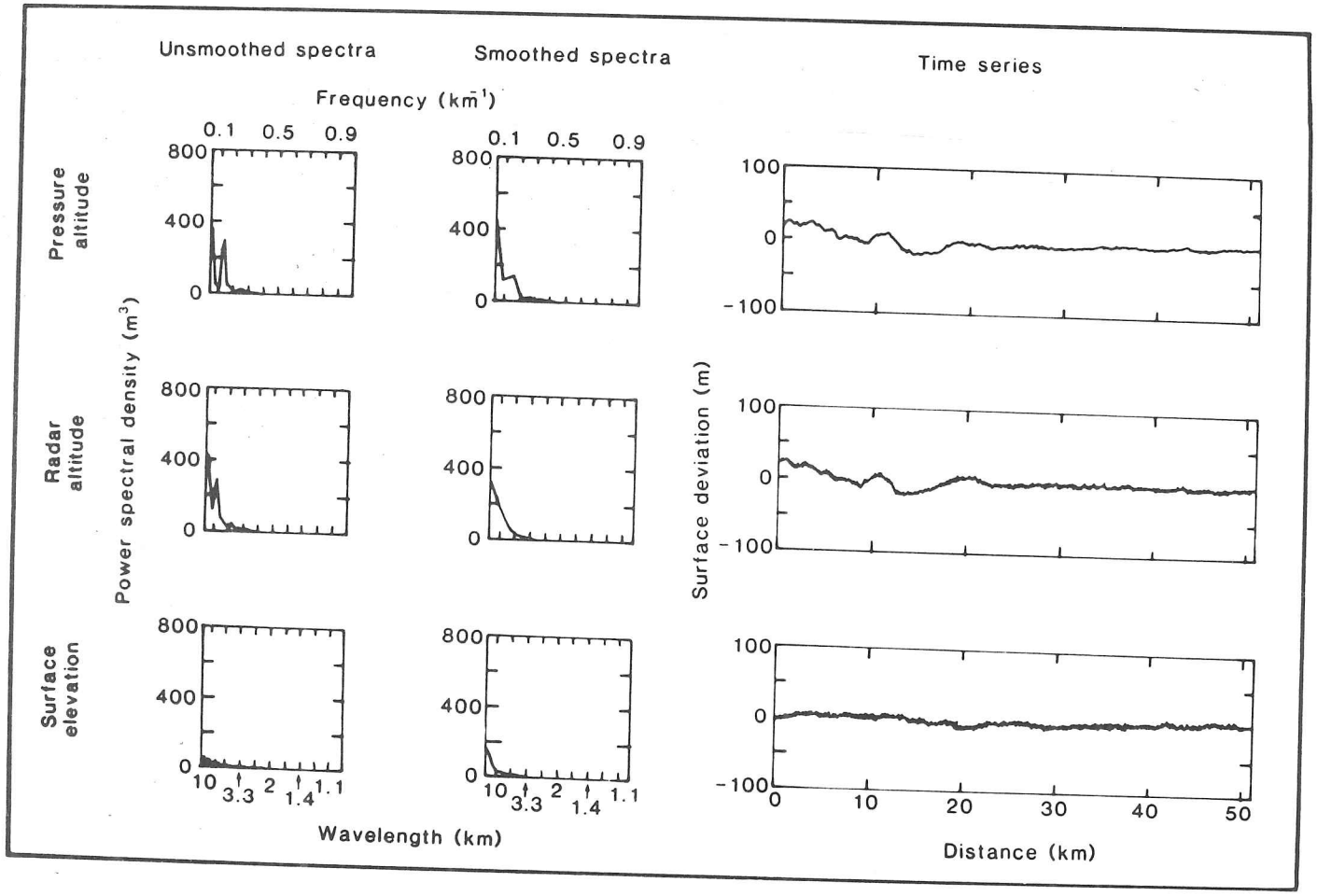

Figure 2.7: Unsmoothed and smoothed spectra of altimetry data across the Ronne Ice Shelf. Pressure altitude, radar altitude and surface elevations are shown. The spectra of the surface profile contain very much less energy than those of the two altimetry signals indicating that the motion of the aircraft has been subtracted during the derivation of the surface.

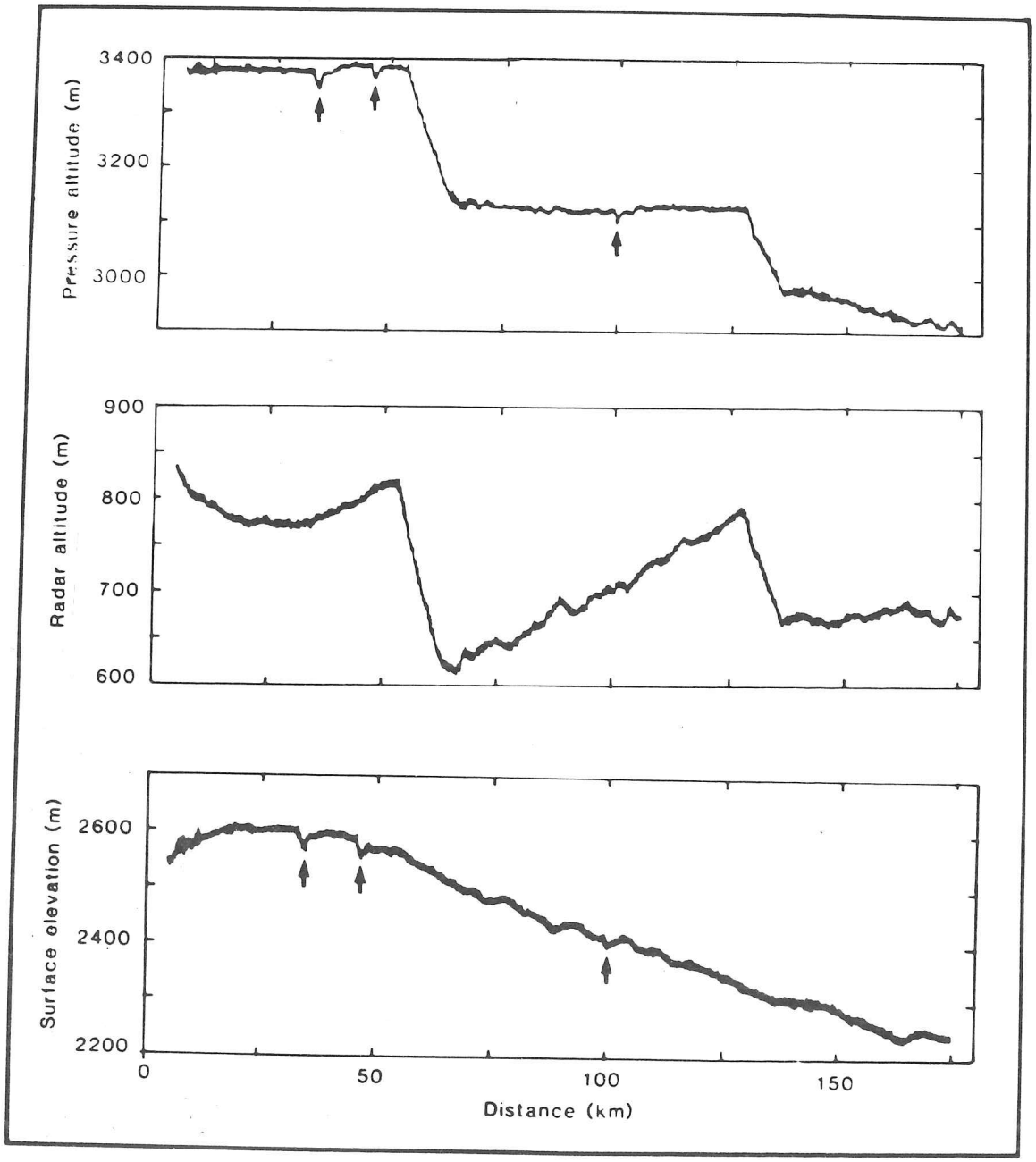

Figure 2.8: Records of pressure altitude, radar altitude and surface profile across the West Antarctic ice divide showing the large-scale irregularities (arrowed)in the surface profile which derive from the pressure altitude signal.

surface profile (figure 2.8).

An atmospheric or meteorological source for the irregularities (which would probably have registered in both altimeters) was rejected on the basis of an examination of wind direction and velocities measured by the ARDS (channel 19, table 2.1). The data, which come from a straight flight path with no banking or turning of the aircraft, indicate that wind velocity varied in a regular fashion between 3.6 and 5.7 m s^{-1} while wind heading was always in the range 275° to 304°. These records, measured to 0.5 m s^{-1} and 1° eight times per second, would be quite sufficient to show any atmospheric disturbance large enough to generate the errors illustrated in figure 2.8. The question of whether such system errors occur in regions of very rough topography, and hence remain obscured, should be borne in mind. With a mean amplitude of 46 m, a mean wavelength of 3.5 km and notable asymmetry, such that downslope gradients are a factor of three less than upslope ones, these troughs are markedly uncharacteristic of undulations in both the pressure altitude and surface elevation profiles, even during the significant changes in aircraft altitude (figure 2.8). It is taken that their distinctiveness will enable their identification and avoidance. However, they are obviously a limiting condition for the altimetric record which necessitates great caution in the selection of data.

As a result of variations in altitude and wind speed and direction, the aircraft's ground speed tends to vary to such an extent that significant errors would be introduced to altimetric profiling if the horizontal dimension was not controlled. The mean ground speed during sections for which the altimetry data were used was 116 m s^{-1} with a standard deviation of 10.6 m s^{-1}. This necessitated the use of a linear interpolation program to produce data at regular intervals; 50 m was thought to be sufficiently detailed for most of the present purposes.

2.3 Landsat

The first Earth Resources Technology Satellite (ERTS 1, but later named Landsat 1) was launched in July 1972. It was put into a near polar, sun-synchronous orbit which reached latitudes of 81°. Complete global coverage was achieved every 18 days but, because of the overlap of images (14% between successive images on a track) and the convergence of orbits at high latitudes (up to more than 85%), the polar regions were covered more frequently. In January 1975, Landsat 2 was put into the same orbit, thereby providing global coverage every 9 days until the retirement of its predecessor from service in January 1978.

The main operational sensor used in Landsat 1 and 2 was a multi-spectral scanner (MSS) which recorded in four bands, named four to seven (table 2.2). The energy in different radiation bands is determined by the physical properties of the reflecting surface. Thus images from band 7 tend to show water bodies more clearly than those in band 4 but, since water absorbs infrared radiation, there is less penetration below the surface. The effects of cloud tend to be at a minimum at longer wavelengths and the delineation of glacial features, termini and coastlines is easier.

Landsat 3 (launched in March 1978) also used an MSS but with an added thermal band. A line-scan problem limited its ability to transmit MSS signals to the ground and it became largely a recorder of return beam vidicon (RBV) data (table 2.2). However, of the 1437 scenes of the Antarctic acquired by July 1982, all but 11 are saturated by extreme light levels and so are unusable (R.S. Williams, personal communication).

The most interesting new development of Landsat 4, launched in July 1982, is the Thematic Mapper (Duchossois and Plevin, 1981). This is a new design of scanning radiometer which has three more bands and better spectral and spatial resolution than the MSSs flown in previous Landsat missions (table 2.2). An up-dated MSS was included in the sensor package to provide continuity with previous missions. Landsat-4 will transmit data through the Tracking and Data Relay Satellite system and so eliminate the need to rely on tape recorders (one of the parts of previous missions most

Table 2.2: Operational characteristics of Landsat sensors.

Sensor	Spectral bandwidth (μm)	Pixel size (m)
MSS band 4*	0.50 - 0.60	80
MSS band 5*	0.60 - 0.70	80
MSS band 6*	0.70 - 0.80	80
MSS band 7*	0.80 - 1.10	80
MSS band 8**	10.40 -12.60	240
RBV	0.55 - 0.72	40
TM band 1	0.45 - 0.52	30
TM band 2	0.52 - 0.60	30
TM band 3	0.63 - 0.69	30
TM band 4	0.76 - 0.90	30
TM band 5	1.55 - 1.75	30
TM band 7	2.10 - 2.35	30
TM band 6	10.40 -12.50	120

* Landsats 1, 2 and 3.

** Landsat 3 only.

Source: Landsat Data Users' Handbook (1979) and Duchossois and Plevin (1981).

prone to failure). This is necessary when data from regions outside a 1600 km radius of receiving stations are required. However, since no receiving stations at present cover the continent and since Landsats 2 and 3 had been removed from service by September 1983, no Antarctic images can be received until this tracking system is in operation.

Landsat images offer several advantages over other methods available for observing ice masses (Krimmel and Meier, 1975). For example, very subtle but large features, often lost in the process of contructing mosaics of aerial photographs, can be seen on one frame. Further, Landsat images, particularly at high latitudes, are often taken at low sun angles, that is, when regional topographic features are accentuated to a great extent. The accuracy, resolution and repeat coverage of images are very important when considering the dynamic behaviour of ice masses and the near global coverage of the system has obvious advantages. The processing of images by digital techniques and the interpretation of surface features will be considered in sections 3.2 and 3.3.

2.4 The potential of satellite altimetry

2.4.1 Radar altimetry from Seasat

Despite first being mooted in the 1960s (Robin, 1966), the idea of mapping by satellite altimetry has not borne fruit until recently. Even now, the mapping of ice sheets (specifically, that of the Antarctic) has emerged as a by-product of missions flown with the objective of collecting oceanographic data. Even though Seasat's orbit was only to a latitude of 72°, a sufficient proportion of its 400 hours of measurement in 1978 was over ice masses to allow an assessment of the radar altimeter's performance over glacial topography (Brenner and Martin, 1982; Arnold, 1982; Rapley and others, 1983).

Accuracy of the radar altimeter was limited by a number of problems largely related to the topography of the ice. Thus, because of the geometry of the altimeter beam, satellite-terrain ranges obtained over sloping surfaces come from a point displaced upslope from the normal to the

satellite. This amounted to a vertical error of nearly 80 m for a slope of 1.4%. When undulations were present on the surface (chapter 4; Zwally and others, 1981) the bias did not remain constant; the indicated surface was smoother, distorted and above the average surface (section 3.4). The error is dependent on the wavelength and amplitude of the undulations and the magnitude of the mean regional slope (Brenner and others, 1983) and is further complicated by cross-track slopes.

A more fundamental problem was caused by the tracking loop of the altimeter. Each range observation was actually a prediction from the previous two; at each up-date of the tracker which occurred 20 times a second, a range error was computed and used in the prediction of the next range. If the rate at which the slope changed was greater than that which the tracking loop could follow, a loss of track resulted (Martin and others, 1983). The performance of Seasat's altimeter was thus nearly ideal over water, where the dynamic lag resulted in errors significantly less than 10 cm, but it was only successful in tracking the ice sheet in areas where the regional slope was less than about 2%. Consequently, retracking software had to be employed to categorize each waveform, perform the appropriate functional fit and compute the retracked range (Martin and others, 1983). This was thought to remove most of the offset between input and output profiles (section 3.4).

A final difficulty in tracking experienced by Seasat seems to have arisen because, at some undulation wavelengths and amplitudes, the ice sheet surface may have been disruptive to the tracker. There are likely to be areas where the surface has radii of curvature comparable to that of the pulse which has a 22 km beam-limited footprint with a sagitta of 80 m. Given the high orbital velocity of the satellite (6.62 km s^{-1}), there was probably a rapid focussing and defocussing which caused variations in echo strength, pulse shape and leading edge slope. It has been suggested that loss of lock, when slopes were apparently within limits, may have been due to this effect (Robin and others, 1983).

Despite these difficulties, the final accuracy of absolute elevations was anticipated to be approximately 2 m or better over the smooth or near-

horizontal portions of the ice sheet and approximately 15 m over steeply-sloping and undulating regions (Zwally and others, 1983), even though the expected slopes were under-estimates of those experienced (chapter 4). A comparison of elevations from geoceiver stations and from Seasat in Wilkes Land (figure 2.9) shows that agreement can be within the ± 4 m accuracy of the geoceivers (R.L. Brooks, written personal communication) but this may be the result of the considerable local variability which is evident from adjacent elevations. The relative and absolute accuracy of Seasat's altimeter is discussed further in section 3.4.

2.4.2 Laser altimetry

Although ice sheet can be successfully mapped using a satellite radar altimeter (Brooks and others, 1978; Zwally and others, 1983), a number of inadequacies have been identified, many of which may be attributed to the instrument's geometric limitations, accuracy and resolution. A satellite laser altimeter system would obviate many of these difficulties and enable very high-resolution mapping of polar ice sheet topography (Zwally and others, 1981). One of its principal advantages would be a beam-limited footprint of about 70 m, although this would require simultaneous measurement of beam-pointing angle to an accuracy of 10 seconds of arc (Bufton and others, 1981). This choice was based primarily on the desire to average small-scale roughness while retaining a precise footprint with which to measure surface slopes. The laser data would define surface topography to a high accuracy (a performance better than 10 cm rms is thought to be possible over the ice sheet (Zwally and others, 1981)), remove the surface-slope ambiguity of radar data and provide altimetry in regions where the surface slopes are too great for radar operation. Glaciologically, such data would be significant in that they would provide detailed maps of surface elevation enabling better delineation of features such as flowlines, ice streams and grounding lines. Analysis of the returned pulse shape would yield information on topography within the laser footprint (Zwally and others, 1981). The implementation of such a system, although undoubtedly of enormous potential value, is some way off.

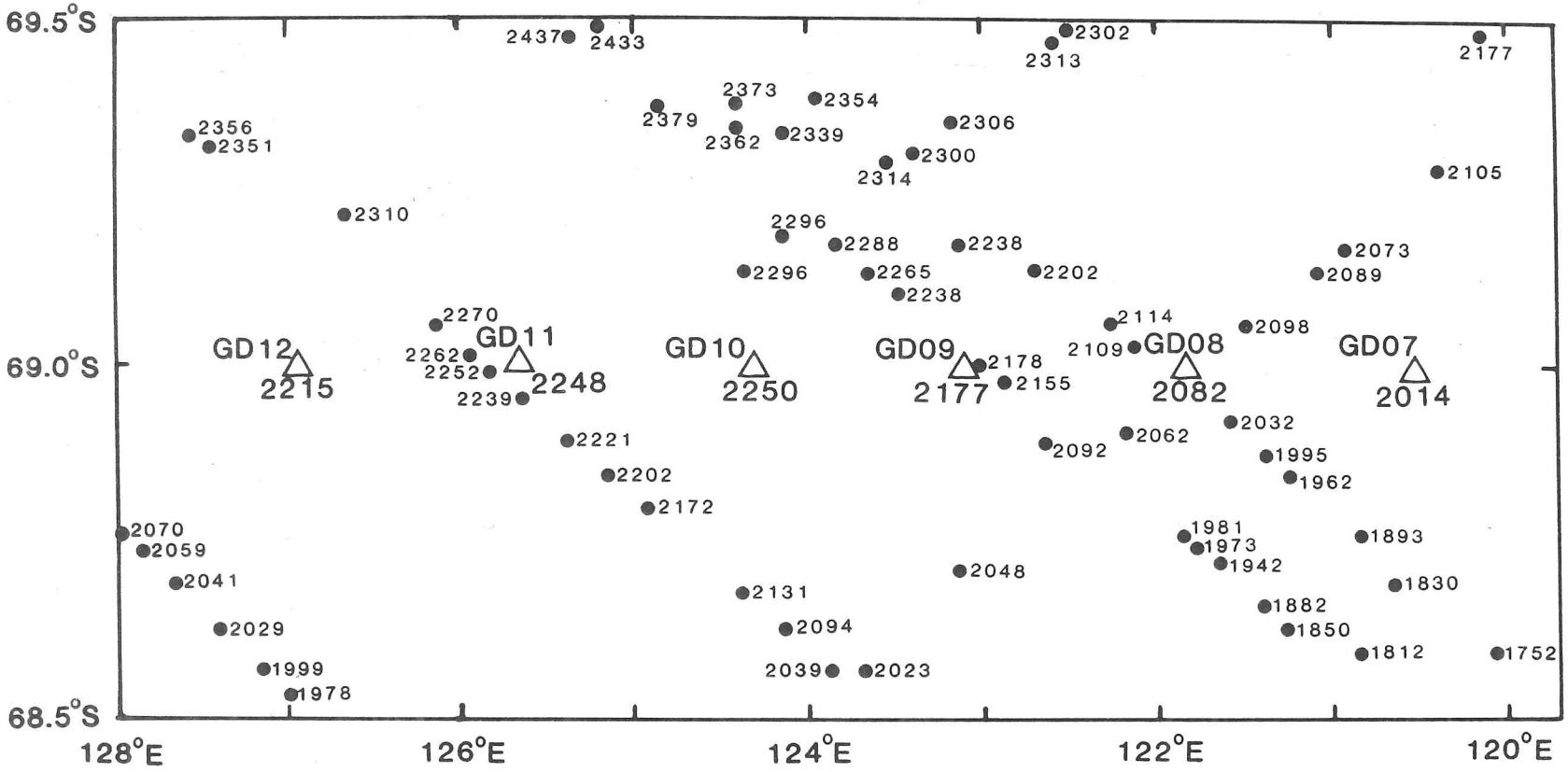

Figure 2.9: A comparison of surface elevations from geoceiver stations and Seasat altimetry in Wilkes Land. (Redrawn from R. Brooks, documented personal communication, 1982.)

CHAPTER 3

INTERPRETATION AND COMPARISON OF DATA SOURCES

3.1 Introduction

The sources introduced in the previous chapter present many different aspects of the ice sheet and its topography. Other than the most basic distinction between altimetric and imaging systems which generate digital and analogue data, the sources may be contrasted in terms of their resolution and accuracy, the extent to which data are averaged, their density and repetition of coverage, and the two-dimensional plane into which they compress the real surface.

Each data collection system thus acts as a filter to the real ice sheet, abstracting the topographic or other elements identified by its mode of operation. It is necessary and important to consider the exact information content of each source so that invalid comparisons and deductions may be avoided. This chapter considers the information content of Landsat imagery and of Seasat and aircraft altimetry. It also tests the interpretation of these sources by verifying the features identified through comparison with other data and assesses the relative accuracy and strength of each in terms of the present study.

3.2 Digital processing of Landsat MSS data

3.2.1 Introduction

The study of snow and ice masses presents a number of difficulties which test the operation of the Landsat's MSS, RBV and TM sensors at extreme levels. Most of the Antarctic ice sheet, for instance, has very low slope and relief in relation to the sun angle, particularly uniform

surface properties and high albedos. The lack of contrast and exceptionally high reflectivities often make the differentiation of surface features difficult and result in the saturation of sensors by extreme energy levels. Partial compensation may be achieved through numerical manipulation of data so as to enhance features of interest (Williams and others, 1979).

It was intended in this section to use data from an Antarctic Landsat MSS image encompassing a variety of flow regimes, surface topographies and ice types to investigate the possibilities for digital enhancement and analysis. Although the process of purchasing a computer compatible tape (CCT) was initiated some time ago, it has recently become apparent that many of the early Landsat tapes of polar regions (and most Antarctic tapes date from before 1976) 'have now deteriorated to the point that only the film archive remains for scientific use' (Washburn and Bentley, 1983, p117). This difficulty was further compounded because NASA plans in the near future to discontinue storage of pre-December 1976 Landsat CCTs (R.S. Williams, personal communication). In view of these problems, two tapes have been used which cover the outlet of Jakobshavn Glacier, West Greenland and were already available at the National Remote Sensing Centre at the Royal Aircraft Establishment, Farnborough. This was felt to be a suitable substitute since the high velocity and discharge of this outlet make it similar to many Antarctic glaciological situations. Digital processing was peformed on a GEMS image display system, originally developed by the Computer Aided Design Centre, Cambridge to deal with Landsat MSS data. In the next section, we illustrate some of the processes available which can be used to increase the amount of information readily derived from raw data tapes. In section 3.2.3, we consider the potential for extracting real reflectance values which may be related directly to other sources.

3.2.2 Enhancement of features

One of the principal purposes of digital processing of Landsat data is to enhance features so that they may be displayed in a more expressive,

interpretable form. This is a particularly necessary task in the case of ice masses which are often poorly portrayed by photographic products of raw data because of the lack of contrast.

One of the most useful facilities commonly available in image processing systems is the contrast stretch function. This expands the grey scale range of pixel values so that they are displayed over a fuller scale of grey values and increases the interpreter's ability to discriminate radiometric detail. Figures 3.1 shows four band 7 extracts from a spring scene (11th April 1982) of Jakobshavn Glacier which illustrates the effects of applying three different types of stretch. A two-part linear contrast stretch (figure 3.1.B) results in the mean value of the input distribution being centred at mid-grey (level 127) in the output and then a uniform expansion of the rest of the data to fit the total range of 256 grey scales. Although this considerably enhances the detail of the inland ice (cf. raw data - figure 3.1.A), it has the disadvantage similar to that of a simple linear stretch in which as many display levels are assigned to the rarely occurring image values as to the frequently occurring ones. The result is that detail is 'washed out' and lost in the region of crevassing, bare ice and streaming flow. A Gaussian stretch (figure 3.1.C) obviates this difficulty by assigning grey levels such that the output histogram is normally distributed. This enables us to retain detail across the inland ice sheet at the same time as exaggerating tonal differences in the high-contrast region of the outlet glacier. Further types of contrast stretch are available on the GEMS system, including a number of manual operations which allow one to choose the enhancement most appropriate for the sun angle, topography and ice type.

Although conditions across ice sheets typically show only gradual spatial changes, there are many instances of abrupt transitions, such as crevasse zones, which can readily be identified on Landsat MSS data. By emphasizing such features, an apparent increase in spatial resolution is produced. This correction is achieved by doubling the deviation of a pixel value from its surrounding average. Figure 3.1.D shows the effects of edge enhancing figure 3.1.A with average grey-levels calculated over boxes

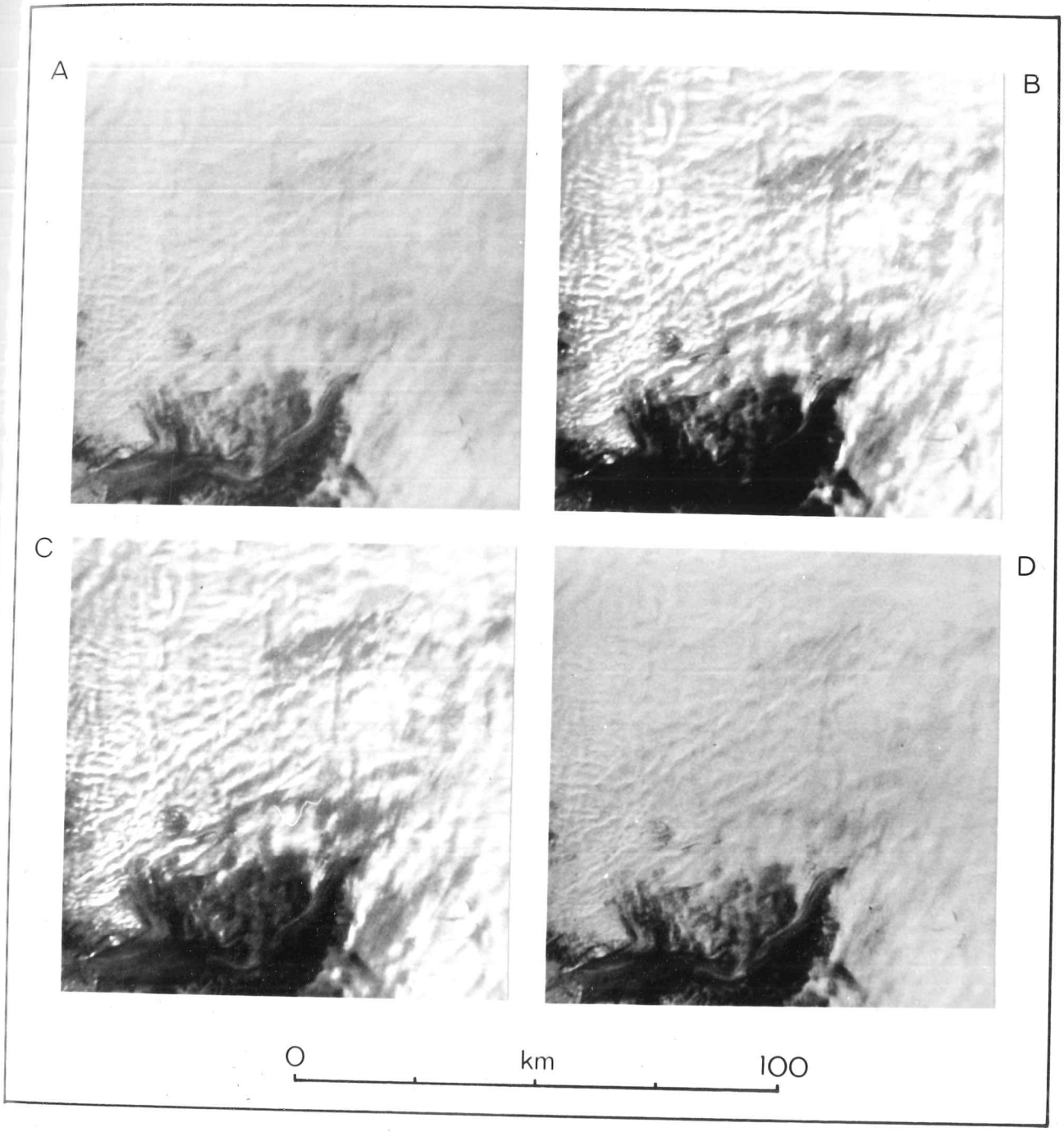

Figure 3.1 Extracts from a band 7 Landsat image of the ice sheet margin inland of Jakobshavn Glacier (69°N 50°W) showing some effects of digital enhancement. Extracts have been sampled every third pixel horizontally and every second pixel vertically to encompass a variety of types of terrain. A, untreated extract. B, two-part linear stretch. C, auto-Gaussian stretch. D, edge enhancement. Sun angle is 29°. Path 11, row 11.

three pixels square. Although both extracts are only samples of the original data (every sixth pixel has been sampled), the crevassed areas and flowlines of the glacier are more sharply resolved after edge-enhancement.

The separate wavebands in which MSS data are recorded may be utilized to accentuate spectral contrasts. Since the energy in each band is determined by different surface properties, contrasts between them may be exaggerated by taking the ratio of a pixel value in one band to that in another. A particularly useful aspect of such ratio techniques is that they help negate factors influencing radiometry and sensor data which act equally in all wavelengths of analysis (Lillesand and Kiefer, 1979). This includes, for instance, differential illumination of the surface due to topographic variability. This approach may prove useful in the analysis of ice types and, for example, the continuing search for areas of blue ice (Williams and others, 1983) and meteorites. Although of great scope and potential, such techniques must be used with caution. In the absence of detailed ground truth and knowledge of surface properties which affect particular wavelengths, the interpretation of resulting imagery may be an ambiguous process. The ease of manipulation is such that the exact cause of the results of complex processing, which may be significantly divorced from the original data, must be considered with great care.

A variety of other functions available on the GEMS system perform filtering, arithmetic and mathematical operations and classificatory procedures. Many are most useful for specific investigations and enable great flexibility in image enhancement which can partly compensate for the effects of high sun angles. However, it is not possible to correct for saturation of the sensors which occurs when received energy exceeds the levels appropriate to the aperture sizes. This problem is most severe where contrast is low, for instance, in the low regional and local slopes in the interior of ice sheets and in summer, when sun angles are relatively high. The sensors may be unable to resolve detail at the extreme of the radiometric spectrum. This problem is not uncommon and presents a severe restriction for several of the numerical processes outlined above since

three pixels square. Although both extracts are only samples of the original data (every sixth pixel has been sampled), the crevassed areas and flowlines of the glacier are more sharply resolved after edge-enhancement.

The separate wavebands in which MSS data are recorded may be utilized to accentuate spectral contrasts. Since the energy in each band is determined by different surface properties, contrasts between them may be exaggerated by taking the ratio of a pixel value in one band to that in another. A particularly useful aspect of such ratio techniques is that they help negate factors influencing radiometry and sensor data which act equally in all wavelengths of analysis (Lillesand and Kiefer, 1979). This includes, for instance, differential illumination of the surface due to topographic variability. This approach may prove useful in the analysis of ice types and, for example, the continuing search for areas of blue ice (Williams and others, 1983) and meteorites. Although of great scope and potential, such techniques must be used with caution. In the absence of detailed ground truth and knowledge of surface properties which affect particular wavelengths, the interpretation of resulting imagery may be an ambiguous process. The ease of manipulation is such that the exact cause of the results of complex processing, which may be significantly divorced from the original data, must be considered with great care.

A variety of other functions available on the GEMS system perform filtering, arithmetic and mathematical operations and classificatory procedures. Many are most useful for specific investigations and enable great flexibility in image enhancement which can partly compensate for the effects of high sun angles. However, it is not possible to correct for saturation of the sensors which occurs when received energy exceeds the levels appropriate to the aperture sizes. This problem is most severe where contrast is low, for instance, in the low regional and local slopes in the interior of ice sheets and in summer, when sun angles are relatively high. The sensors may be unable to resolve detail at the extreme of the radiometric spectrum. This problem is not uncommon and presents a severe restriction for several of the numerical processes outlined above since

significant proportions of images contain no information in some bands. Figure 3.2 shows an enhanced and stretched summer scene (11th August 1981) of Jakobshavn Glacier area with a sun angle of 35°; regional slopes are of the order of 2% and, in view of the very high velocities (over 7 km a^{-1}) attained downstream (Hughes, 1983), this is probably one of the most irregular and steeply sloping parts of the Greenland ice sheet. However, bands 4, 5 and 6 become saturated within an average of 74, 21 and 37 km of the ice sheet margin respectively. On this basis, and given the very much lower slopes and gentler topography of the Antarctic ice sheet, it is possible that of the order of 60% of this southern ice sheet north of 81°S contains no information in these bands. This limitation is severe and must be corrected for in the design of future satellite imaging systems if the sensing of snow and ice covered terrain is to be developed as a primary objective of remote sensing missions.

3.2.3 Derivation of real values

Although Landsat images are often analysed using the pixel values on a CCT, these numbers do not represent real physical values. Comparison of such values from different times or locations is unsatisfactory and may result in substantial errors because of the variability and, at times, substantial pre-processing of data which is carried out to provide standard products for the remote sensing community (Landsat Data Users' Handbook, 1979; Verdin, 1983). To ensure comparability, grey levels should be converted to dimensioned equivalents such as reflectance or radiance (Robinove, 1982). This should enable direct comparison with other sources and would allow greater certainty in the identification of surfaces such as snow and ice types and it could be used as an input to important glacio-climatic modelling. Such analysis has not been possible in the present case for the reasons listed below, the main one being the lack of suitable raw data which has not been pre-processed or corrected geometrically.

The conversion of pixel values to dimensioned equivalents requires knowledge of several variables. The sun angle and calibration of sensors at a given time are documented variables and can be accounted for without

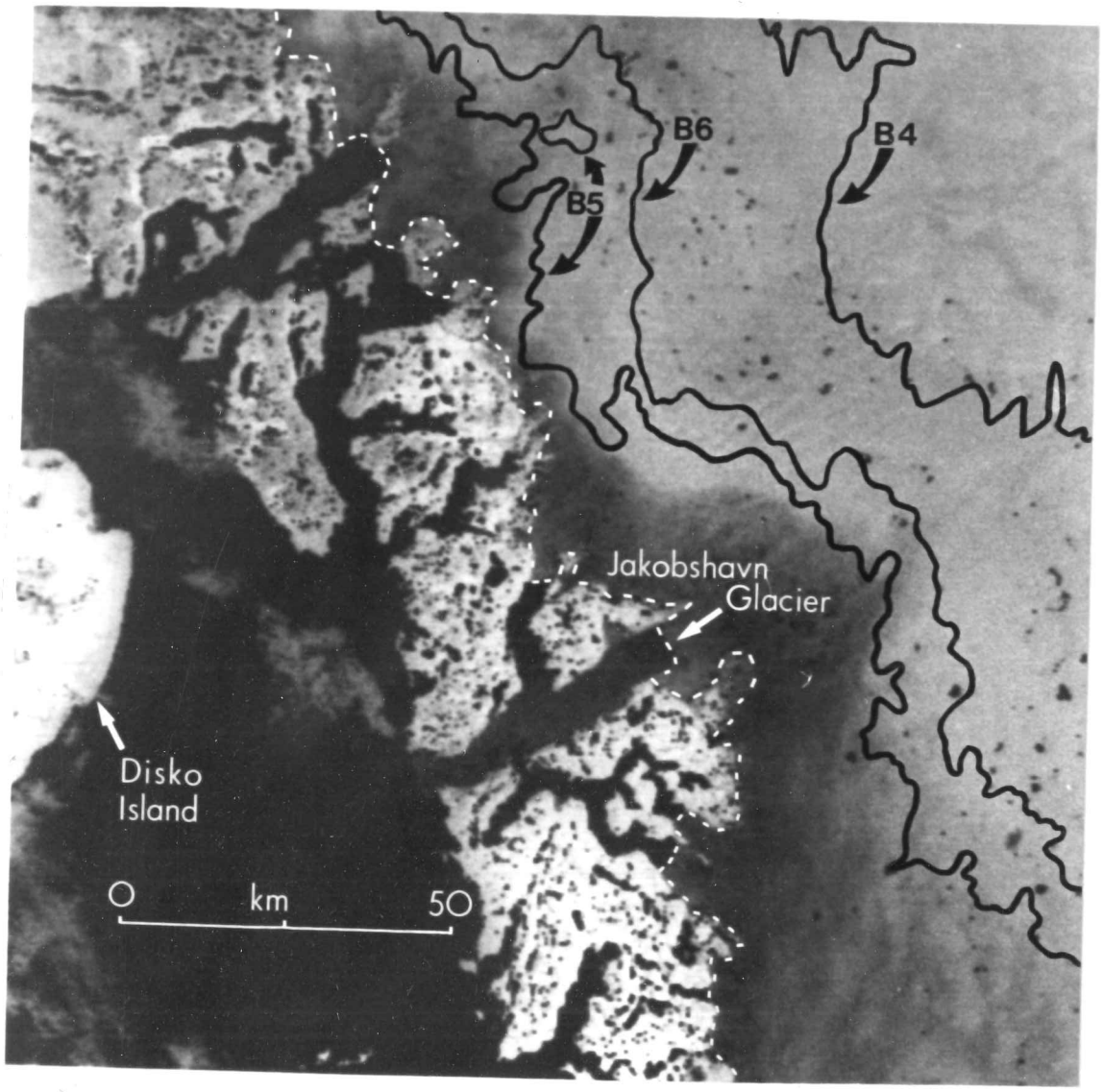

Figure 3.2 Landsat image (band 7) of Jakobshavn Glacier (69°N 50°W) and surrounding region showing the distance from the ice sheet margin (dashed white line) at which bands 4, 5 and 6 become saturated. Sun angle is 35°. Path 11, row 11.

difficulty. Atmospheric effects can, however, have a significant impact through the scattering and absorption of energy. Variations are due to temperature, humidity and pressure differences and, although algorithms for these corrections are now well developed, they may be only locally applicable (Robinson, 1983). The geometric manner in which surface reflect energy is also an important consideration (Warren, 1982). This is primarily a function of surface roughness in relation to the wavelength of the incident energy; most surfaces are neither perfectly specular nor diffuse reflectors and assumptions about their reflective properties may not be valid.

A further requirement for the calculation of reflectances and radiances is that raw Landsat data are used. Many CCTs are automatically subjected to geometric and radiometric corrections before delivery to customers. During the former, uncorrected imagery is re-sampled to produce an image consistent with a particular map projection (Landsat Data Users' Handbook, 1979). The algorithm used computes a new radiance for each pixel from the 16 surrounding the location in question (Verdin, 1983). Radiometric corrections typically involve stretching and filtering to standardize and enhance the data which further corrupts the source. Clearly, such alterations will invalidate any attempt to generate absolute values of reflectance or radiance and, in general, corrected Landsat MSS data are to be avoided when undertaking quantitative analyses with the imagery.

A principal aim of this type of analysis is to define spectral response patterns for various surfaces and so enable automatic identification of snow and ice types, for instance, as would be found along a transect through an ablation area. Although many surface features manifest distinctive spectral reflectances, experience has shown that these are neither absolute nor unique and that some features of interest cannot be spectrally separated (Hoffer, 1978; Lillesand and Kiefer, 1979). Thus, to utilize remote sensing data effectively, one must fully understand the spectral characteristics of the feature under investigation in any given application and the factors that influence these characteristics.

3.3 Comparison of Landsat with other sources

3.3.1 Introduction

For over a decade, Landsat imagery has enabled the rapid and accurate viewing of the Antarctic ice sheet; however, unambiguous interpretation of all the features recorded, particularly when only photographic products are available, has not always been possible. For instance, although apparent ridges can be seen on ice rises around the Antarctic Peninsula (Martin, 1976), abrupt changes in slope have not been confirmed by surface levelling (Martin and Sanderson, 1980). In this section, comparison is made between features identified on Landsat MSS data and by aircraft altimetry and radio echo sounding, the latter two being used as substitute 'ground truth' to aid interpretation of the former. The high frequency of the radar altimeter (4.3 GHz) ensured that penetration below the surface was negligible and hence that the topographic profile was generated with only small errors (section 3.4).

3.3.2 Surface undulations

Examination of apparent undulations in the ice sheet surface seen on Landsat imagery from many parts of the Antarctic raises the possibility that they are, at least in part, due to factors such as albedo differences caused by non-uniform accumulation rather than topographic variability (section 1.3). Indeed, it has been demonstrated that the presence of undulations affects the manner of snow deposition; the resulting small-scale variations in firn density, crystal structure and albedo may contribute to the apparent topography seen on the images.

Figure 3.3.A shows a Landsat image of Thwaites Glacier with the ground track of an ARDS profile. Because of the uncertainties of the Landsat graticule (Swithinbank and Lane, 1977), the positioning of the flight path was achieved by mosaicing five Landsat images which included sufficient outcrops, nunataks (Mount Murphy, Mount Takahe and Bear Peninsula) and identifiable features for fixing the position of the region of interest. Clearly, errors in the inertial navigation system (Drewry and

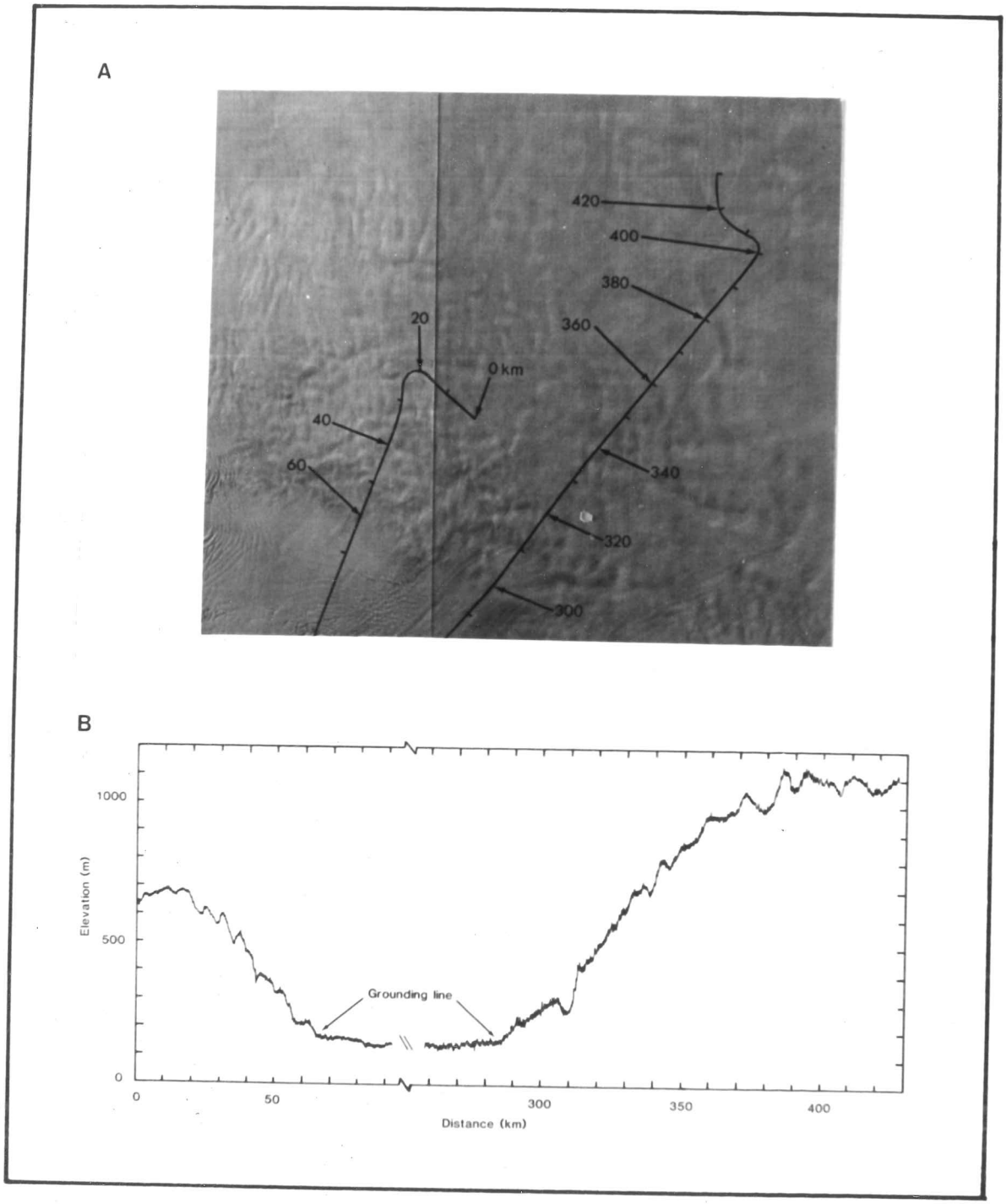

Figure 3.3 Comparison of Landsat and ARDS in the region of Thwaites Glacier. Distances in B correspond to those along the flight track in A.

others, 1982) must also be accounted for, but it will be seen from the correlation of physical features on the two sources that the fixing is probably accurate to within 1 km.

The main difficulty involved in matching these two data sources is identification of common features for comparison. The technique used here is to relate the crests of undulations seen on Landsat and the derived surface profile (figure 3.3.B) to distance along the radio echo sounding flight tracks. The tops of undulations were chosen for comparison since the maximum rate of change of slope in a position exposed to solar illumination produces the most rapid transition of grey levels and hence is usually the most easily identifiable part of an undulation. Exact delimitation of surface inflections is not always possible since only slight tonal changes will occur when a flight crosses the change in slope on the flank of an undulation. Table 3.1 presents the relative positions of undulation crests identified from Landsat and the altimetry in the region of Thwaites Glacier.

The matching of features is particularly good inland. Twelve of the 16 crest positions seen in both sources agree to within 1 km, the fit being best in regions of high relief (for instance, at 383 km). Other than near the grounding line of Thwaites Glacier itself, only two of the crests seen on Landsat appear to have no correspondence to the surface profile. Such agreement is supported by analyses from other parts of the Antarctic; an ARDS profile passing from an outlying nunatak of the Ellsworth Mountains (enabling very accurate fixing of the flight) to the apparently almost stagnant ice immediately to the south showed a virtually featureless, level surface. The corresponding Landsat image, even with a solar elevation of 17^{o}, showed no discernible surface features. These correlations clearly confirm that, in the areas studied, the dimples seen on Landsat images of the ice sheet correspond to undulations in the real surface.

Table 3.1: Relative position of undulation crests on Landsat imagery and aircraft altimetric profiles. Distances refer to the flight track shown in figure 3.3.

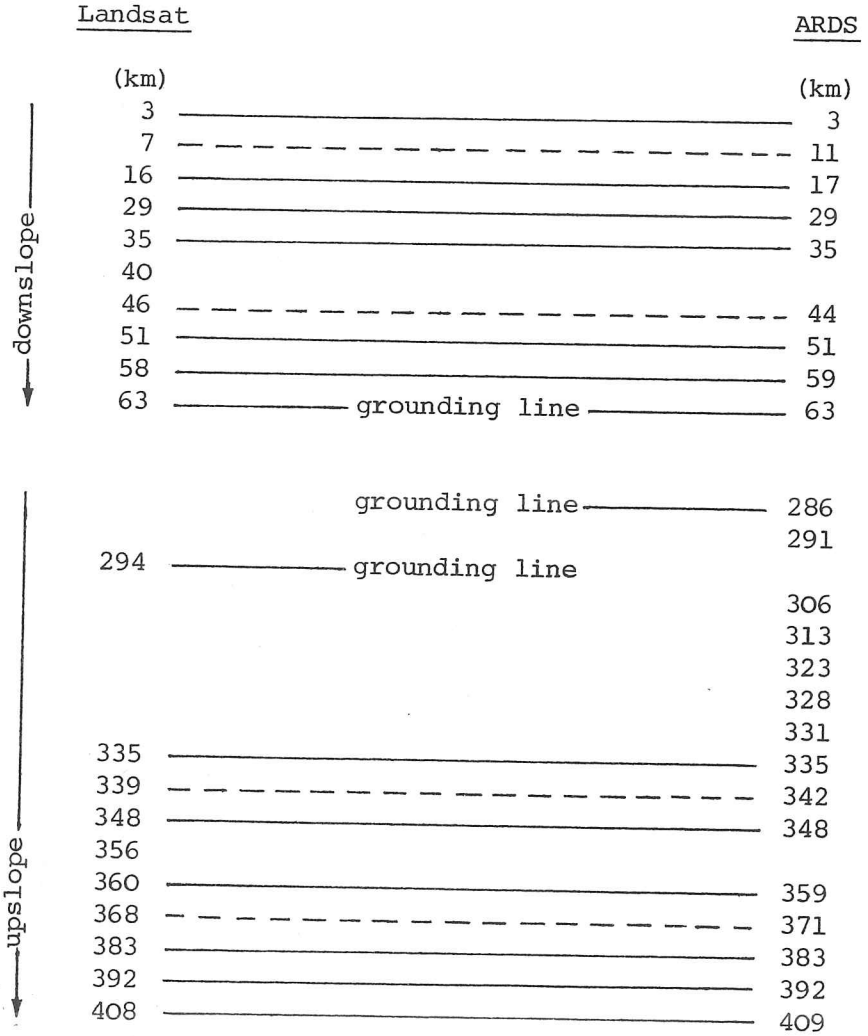

3.3.3 Grounding lines

Another fruitful comparison to be made between aircraft altimetry and Landsat data is the position of the ice sheet grounding line which divides the sloping surface of grounded ice from an almost horizontal surface generally assumed to be afloat. It is seldom possible to identify this feature very accurately, particularly within an ice stream where the ice is likely to undergo a very gradual transition from being grounded to floating (Stephenson and Doake, 1982); this may be better termed a grounding zone (Hughes, 1977). The difference between grounding lines within ice streams and elsewhere as seen from Landsat is well illustrated in figure 3.3.A. As the flight crosses the coast 30 km east of Thwaites Glacier, the grounding line may be accurately positioned by the change in morphology (Crabtree and Doake, 1982). A similar technique was used by Swithinbank (1977) to provide navigational fixing where radio echo sounding flights intersected features which were clearly identifiable on satellite imagery. There is close agreement with the altimetry data (figure 3.3.B and table 3.1) where the transition was identified on the basis of a break in slope and a transition to more subdued relief, both of which suggest decoupling of the ice from its bedrock. Confirmation of this comes from the occurrence of hyperbolae on radio echo sounding records which indicate the presence of bottom crevasses and from comparisons of surface elevation and ice thickness which can be used to define where the ice is in hydrostatic equilibrium. However, the agreement is very much poorer within Thwaites Glacier itself. Although from the surface profile the grounding line appears to be at 286 km (and this is again confirmed by bottom crevasses), it may not be identified with any degree of precision on the Landsat image. There is a very diffuse zone about 15 km across which has been identified from radio echo sounding records as heavily crevassed ice and which represents the transition from floating to grounded ice. The precise delimitation of the grounding line within ice streams and outlet glaciers is very difficult. This is in agreement with the inter-fingering of grounded and floating ice thought to occur in Rutford (Stephenson and Doake, 1982) and in other West Antarctic ice streams (Hughes, 1977).

Ice streams and flowlines, described in section 4.2, have been identified in many parts of the Antarctic from Landsat imagery (Hughes, 1977; Colvill, 1977; Rose, 1978; Crabtree and Doake, 1980, 1982; Allison, 1979). Crevasse trains, marking the boundaries of fast-flowing outlets, have been shown to produce clear lineations on Landsat imagery which enable easy identification of flow directions. The seaward portions of many glaciers and ice streams, however, do not display such distinct features; instead, they have markedly blurred, indefinite zones often with slight linear traces which are notably different from the undulations typical of much of the coastal zone. Thwaites Glacier (figure 3.3.A) displays an amorphous area of this sort in its lowermost 30 km and many other small glaciers illustrate this feature. Comparisons with radio echo sounding Z-scopes show these areas to be heavily crevassed and thus, although the individual features may not be identified (cf. figures 4.7 and 4.9), their zones of occurrence may often be distinguished.

3.4 Comparison of aircraft amd Seasat altimetry

3.4.1 Introduction

The data generated during the brief life-time of Seasat are undoubtedly of great value in that they provide coverage of many parts of the Antarctic ice sheet which, at best, were previously mapped by results of limited coverage and accuracy (Zwally and others, 1983). Subsequent processing of the data (Martin and others, 1983; Brenner and others, 1983) has been shown to enhance its quality and consistency but few assessments have been made of the altimetry in comparison with other high resolution systems. The close coincidence of altimetry from aircraft and satellite in the coastal part of Wilkes Land has enabled us to test the accuracy and resolution of each system. However, a number of corrections must be made to the navigation and elevations of both sources before direct comparison may be made.

3.4.2 Navigational and altitudinal corrections

Across the eastern part of Frost Glacier's drainage basin, 70 km from Porpoise Bay, segments of two ground tracks of these altimeters diverge at 3.6° and, over a distance of 45 km, have a mean lateral separation of 4.1 km. The navigational accuracy of the ARDS is probably considerably better than the maximum error of 2.5 km (Drewry and others, 1982) because of the proximity of the coast with its identifiable features. Allowance must be made for the slope-induced error in the Seasat navigation which results from the altimeter tracking the nearest, rather than the sub-satellite, point (Brenner and others, 1983). For small angles, this can be approximated as

$$\Delta H = \frac{H\alpha^2}{2} \qquad [3.1]$$

where α is the surface slope in radians and H is the satellite-terrain range. The maximum regional slope is 1.07% at 80° to the direction of the track (Drewry, 1983a), giving a vertical slope-induced error of 45.5 m and horizontal displacement of 4.26 km. Thus, Seasat was sensing terrain upslope of its stated position and hence closer to the ARDS ground track. With this correction, the profiles intersect after a distance of 24 km and the mean lateral displacement is less than 1.0 km. The radar altimeter ground track will fall directly within Seasat's 1.6 km diameter pulse-limited footprint for 85% of its path.

The derived ARDS surface is liable to vertical errors because of its dependence on barometric profiling (section 2.2). This was corrected by pinning the ends of the profile to points whose altitudes were known with greater accuracy and adjusting intermediate elevations accordingly. The profile passed over open sea water 94 km downslope and intersected the 1971-1972 NSF-SPRI radio echo sounding grid 101 km in the other direction. This was flown at constant pressure altitudes to enable accurate vertical positioning and crossing-point errors over much of East Antarctica were minimized by random walk and least squares techniques. Probable errors in the grid are thought to be less than 30 m (Drewry, 1975). Fixing the

profile to these two points involved a maximum adjustment of 22 m at the upslope end of the profile. The validity of the ARDS terrain clearances is supported by ranges measured from A-scope records of the radio echo sounding 300 MHz radar which had a footprint 550 m in diameter. They agree closely with the results from the radar altimeter (figure 3.5.A) and are a useful check on the irregularity of the terrain shown by the ARDS.

Satellite-terrain ranges derived from raw Seasat data are produced by on-board tracking of the leading edge of the waveform reflected from the ice surface. As a result of the unresponsive nature of the tracker to rapid changes in surface slope angle and because of frequent difficulties in defining the mid-point of the leading edge when waveforms become irregular (Rapley and others, 1983), the raw data must be retracked to give corrected waveforms (Martin and others, 1983). In the present case, this was done manually by calculating the number of range gates (each corresponding to about 46.8 cm) between the altimeter's tracking point and the actual leading edge, if it could be identified. Only two of the 63 waveforms did not require retracking; a further 6 were adjusted by two gates or less. Corrections applied varied between -6.08 m and +14.04 m, the latter representing the maximum displacement of 30 range gates. Figure 3.4 shows two groups of 16 consecutive pulses for which serious ambiguities occur. Many have gently sloping leading edges which indicate variability about the mean terrain elevation and an inclined reflecting surface. Waveforms 3, 5, 22, 23 and 24 illustrate the difficulty involved in defining the mid-point of the leading edge. Several of the returned pulses also display multiple peaks which either represent distinct reflecting surfaces simultaneously observed but horizontally displaced or are a product of the averaging process used to construct waveforms. Instances of this are shown by pulses 27, 28, 31 and 32. There are clearly many ambiguities involved in retracking waveforms and the use of even quite sophisticated software to perform this automatically is liable to result in many errors.

Further vertical corrections have to be made to Seasat data to account for slope-induced errors which result from regional and local gradients at

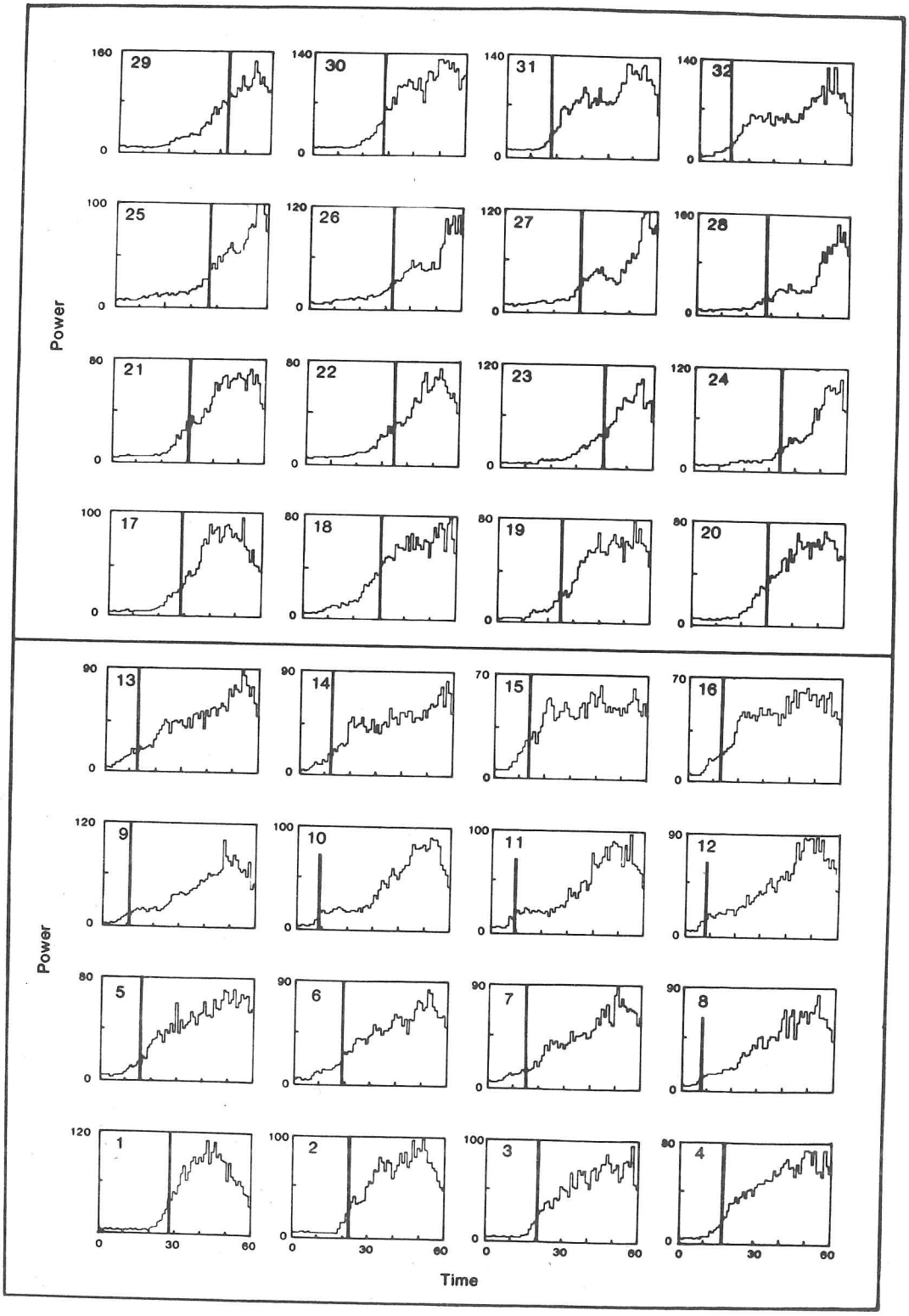

Figure 3.4: Raw Seasat waveforms from 32 locations along a profile in Wilkes Land, the surface profile from which is shown in figure 3.5. They occur in two separate groups of 16 consecutive measurements spaced at intervals of 662 m. Heavy vertical bars represent the manual retracking corrections to the leading edge calculated by the on-board tracker.

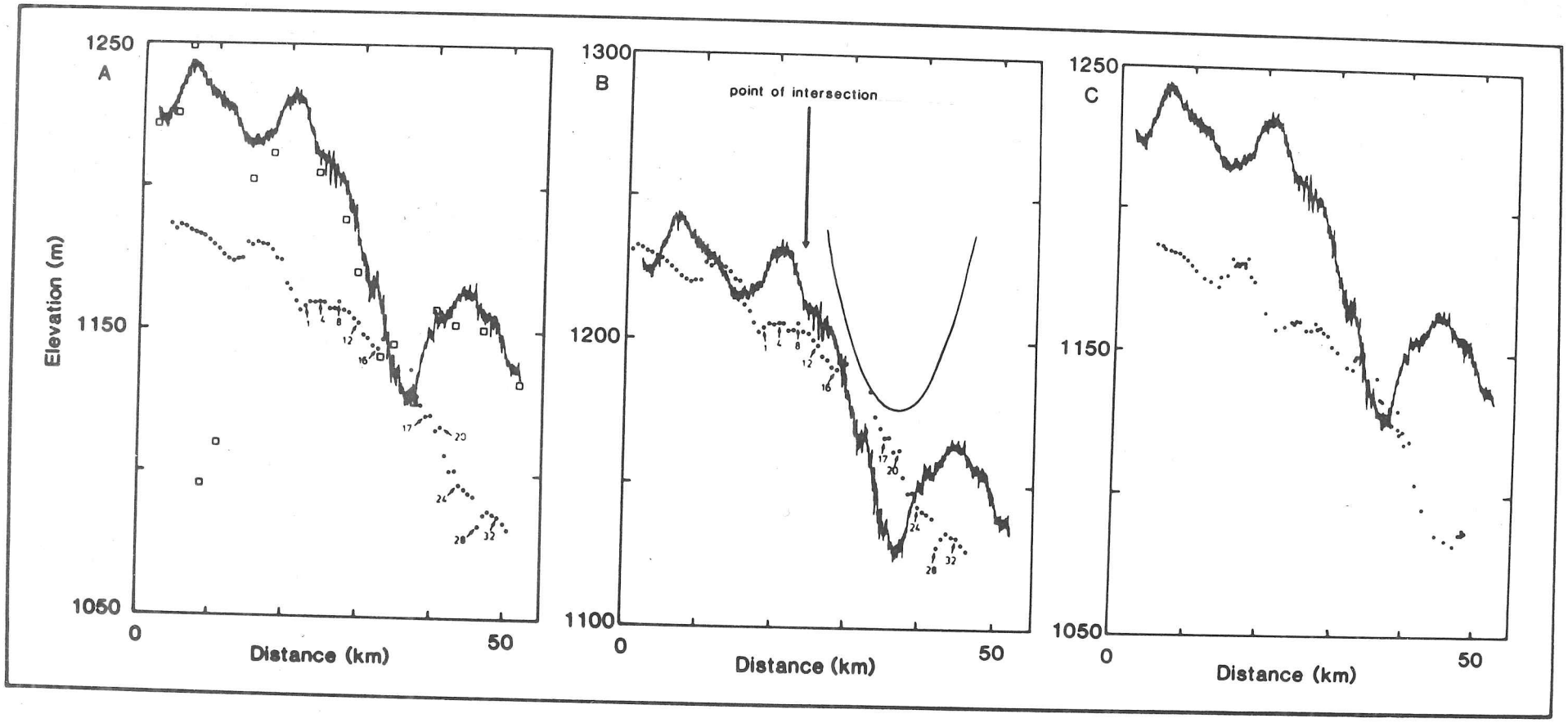

Figure 3.5: Comparison of Seasat and ARDS elevations (dots and continuous profile respectively) over a distance of 45 km in coastal Wilkes Land. All Seasat elevations have been retracked, as shown in the two groups of 16 numbered points which correspond to those shown in figure 3.4. A: Seasat elevations uncorrected for slope-induced errors. Also shown are elevations derived from measurements of terrain clearances from radio echo sounding A-scopes (squares). B: Seasat elevations corrected for the regional cross-track slope-induced error; the horizontal displacement causes the profiles to intersect at the point indicated. Also shown is the form of the pulse waveform. C: Seasat elevations corrected for local (5-point) along-track slope-induced errors.

various angles to the flight track. As with radio echo sounding (section 2.1), reflections from peaks obscure those from intervening valleys if the terrain is of greater curvature than the transmitted pulse. The apparent surface will be smoother and above the real terrain; the tops of undulations will be broadened and some deep troughs may be missed altogether (Brenner and others, 1983). Where the direction of maximum slope is along the flight path, equation [3.1] may be used to calculated corrections. An iterative scheme which converges to the corrected solution over about four steps can be employed (Brenner and others, 1983). Since local slopes may be several times the regional gradients (chapter 4), corrections for slope-induced errors should be calculated over about 5 points (just over 2.5 km). However, maximum local slopes are very seldom in line with the satellite's ground track, particularly in areas of complex, anisotropic topography as occurs towards the margins of ice sheets. In such cases, a detailed knowledge of local slope variations in three dimensions is necessary for the true profile to be calculated. This is clearly not possible in most parts of the ice sheet; Seasat tracks are typically separated by 20 to 50 km and often there are no other sources which provide such information. This is a complex problem which is further discussed below in relation to the present example.

3.4.3 Comparisons

Ice sheet elevations from Seasat and ARDS altimetry may be compared in terms of absolute and relative values. Figure 3.5 shows three attempts at comparison on the basis of different corrections. All Seasat data shown have been retracked as discussed above and as shown in figure 3.4. The general trend in the surface and the range in elevations is demonstrated by both profiles but there are significant differences at many levels. With no corrections for slope-induced errors (figure 3.5.A), there is substantial disagreement between the profiles in terms of absolute elevations and the detection of surface features. Vertical offsets are, in places, in excess of 60 m but this may be partly due to the mean horizontal displacement of 4.1 km. By correcting for the regional cross-track slope of 1.07% (figure 3.5.B), which is over 4 times the gradient along the ground

track, vertical differences fall within the range of expected errors of the radio echo sounding grid (that is, 30 m) except for between 32 and 38 km where the profiles disagree by nearly 35 m. Agreement of elevation and the form of the surface is best where the profiles are thought to intersect at 24 km. The correspondence cannot be said to be close, however.

Correlation between the two surfaces on the local scale is very poor. The ARDS profile shows three major crests centred at 5, 21 and 45 km with wavelengths of 8, 11 and 17 km and amplitudes of 20, 15 and 40 m respectively. Although the retracked Seasat profile corrected for regional slopes (figure 3.5.B) suggests minor undulation crests in phase with the latter two, it is directly out of phase with the ARDS crest at 5 km and misses the largest trough at 37 km altogether. This is an unexpected result given the shape of the Seasat wavefront (figure 3.5.B) which should penetrate most of the observed features in the ARDS profile and give strong returns from the valley bottoms. The inconsistency is furthered by consideration of the power of returned pulses. Those above the valley in the surface at 37 km (waveforms 18 to 21 in figure 3.4) have maximum power values which are only 60% of those corresponding to the undulation crest at 45 km (waveforms 29 and 30). The reverse is to be expected intuitively.

Such errors must be explained in terms of offsets induced by local rather than regional slopes, the former being often 4 or 5 times steeper. The relocation of Seasat elevations on the basis of slope-induced errors calculated from five consecutive points (figure 3.5.C) shows comparatively little difference from the uncorrected data (figure 3.5.A). Horizontal displacements do not exceed 2.2 km and vertical corrections are typically 5 to 10 m. Clearly, to explain the substantial differences between the two profiles, we must consider local slope variation in three dimensions. The regional cross-track slope is four times that along the profile, but we have no information on adjacent local gradients. Although of poor quality due to low sun angles, Landsat imagery of this area shows a number of anisotropic features with long axes approximately parallel to the ground tracks. We may therefore envisage that the derived Seasat elevations are significantly influenced by lateral features which fall within the 1.6 km

pulse-limited footprint. This would explain the inability of the wavefront to penetrate valleys in the ice sheet surface of apparently greater dimensions. It may also account for the inconsistency between surface features and the power of the returned pulses.

Although much of the Antarctic ice sheet has surface terrain considerably less irregular than that shown in figure 3.5, such topography is characteristic of 28% of the continental ice (section 4.5) and a high proportion of the area covered by satellites, such as Seasat, in inclined polar orbits. It also covers the areas of most active ice flow and hence those which are most interesting glaciologically. The inability of Seasat's radar altimeter to detect surface detail on the scale shown by ARDS profiling is a product of the geometry and size of the footprint and represents a severe limitation inherent in the mapping of ice sheets by this method (Rapley and others, 1983). This may restrict some of the uses of Seasat data and results such as the map of Wilkes Land in figure 4.12 must be seen as a severely averaged product. This may, however, be advantageous in some instances. For example, with this data source the calculation of surface elevation changes, as is necessary for mass balance considerations, need not be so dependent on the ability of navigational positioning to precisely re-locate ground tracks.

3.5 Summary

Digital processing enables considerably more detail to be extracted from Landsat CCTs than photographic MSS data. Commonly available image processing functions may be used to enhance and exaggerate ice sheet features, such as undulations and flowlines, which are normally of low contrast and relief and hence not clearly represented. Spectral response patterns of snow, firn and ice types may be derived but unambiguous interpretation is not always possible without ground truth. This could be clarified by converting all MSS data to absolute values of reflectance or radiance but this requires data not subjected to standard pre-processing and involves assumptions about atmospheric and ice surface variables.

Comparison of features seen on Landsat with altimetric profiles in the region of Thwaites Glacier has confirmed that the dimples seen on photographic MSS data are, in almost all cases, real topographic features. The correspondence is best in areas of high relief. The marked topographic change on Landsat imagery in coastal areas can be confirmed as the grounding line by surface profiles which show a distinct change in slope. This is less clear within ice streams where crevassing blurs image resolution and the topographic change is less abrupt.

Overlapping profiles of Seasat and aircraft altimetry in Wilkes Land require significant horizontal and vertical corrections before comparison between them is possible. All but two Seasat pulses out of a sample of 63 required slope-induced error correction of up to 14 m to compensate for the unresponsive on-board tracker. Allowing for regional cross-track slope induced errors gives approximate vertical coincidence of the profiles. Maximum local slopes must be accounted for, however, and where these are not directly along the flight track, the iterative scheme breaks down because of insufficient data. Even when the profiles intersect, comparison of the results shows that Seasat profiles are very greatly averaged results. Phase differences in the profiles and variable returned power suggest that significant effects are produced by lateral features on the ice sheet surface.

CHAPTER 4

THE TOPOGRAPHY OF THE ANTARCTIC ICE SHEET

4.1 Introduction

In this chapter, we combine evidence from Landsat imagery and aircraft and Seasat altimetry to discuss the form and topography of the Antarctic ice sheet. Topographic patterns are identified, exceptions are noted and the distribution of terrain types is mapped. These variations in terrain are then summarized in a statistical model which has been used as a basis for the simulation of satellite radar altimeter waveforms.

4.2 Results from Landsat

4.2.1 Introduction

A common problem in interpreting Landsat images is the extent to which it is possible to extract numerical results without resorting to the processing of digital data which requires a very much more sophisticated and costly analysis (section 3.2). Landsat has been used extensively for descriptive work and mapping (for instance, Swithinbank and others, 1976; Swithinbank and Lane, 1977) but studies which extract quantified results from them are rare. The quantitative results presented in section 4.2.2 have been produced by digitizing MSS images at a scale of 1:1 million. The main errors involved are from the interpretation of features on the image (section 3.3). Repeat measurement has indicated an areal digitizing accuracy of $\pm 2\%$. The features identified include undulations, ice streams and crevasses.

4.2.2 Undulations

Some of the most distinctive features on Landsat images of the ice sheet surface are undulations which have a wide distribution and great variety of size. Given a constant solar elevation, they are most apparent in the thin ice of coastal regions and, in particular, around the heads of outlet glaciers and ice streams where velocities increase with the convergence of ice flow. For instance, inland of Dibble Glacier (figure 4.1), there is an embayment of irregular topography which contrasts with that inland and to either side. These undulations are of the order of a few kilometres in diameter but are irregular and form a complex topography. In places, their presence is enhanced by areas of bare ice resulting from wind action, such as those along the eastern flank of Dibble Glacier and other parts of the coastal zone. Towards the thicker ice at the divide (inland of Slessor Glacier - figure 4.2) undulations are present but are notably larger, more widely spaced and less easily distinguishable. The variability of sizes and orientations is less but, in the thin, slow-moving ice near the outcrops of the Shackleton Range, the undulations are smaller and more angular.

Asymmetrical undulations are apparent in the thinner, faster flowing ice of coastal areas. For instance, immediately west of the Sentinel Range of the Ellsworth Mountains (figure 4.3), there is a series of elongate steps normal to the direction of ice flow which appear to reflect the form of subglacial ridges. Similarly, on the margins of Law Dome in Wilkes Land (figure 4.4), very small undulations, typically less than 2 km in diameter, are interspersed with linear troughs of variable orientations. Despite very low velocities and mean annual temperatures, marked undulations can also be seen in the region of the subglacial Gamburtsev Mountains (figure 4.5) where ice is less than 1000 m thick. This image also displays areas of bare ice which may be identified as such by comparison with Landsat images of the 'blue ice' fields of the Queen Fabiola Mountains and Allan Hills (Williams and others, 1983).

The presence of substantial areas of bare ice 500 km from the Amery Ice Shelf is of great significance for the mass balance of Lambert Glacier.

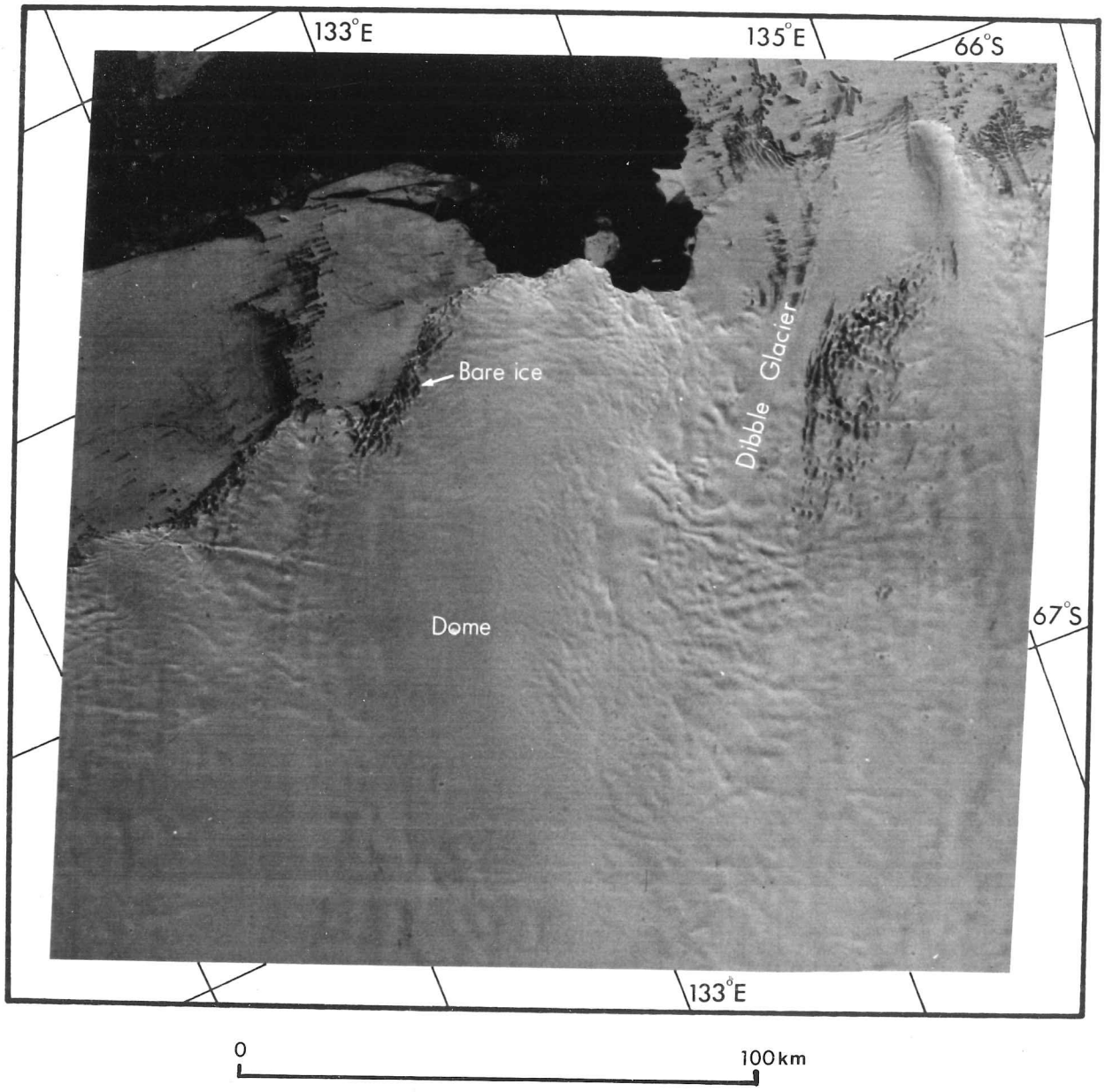

Figure 4.1 Landsat image of Dibble Glacier and coastal Wilkes Land. Sun angle is 21°. Path 95, row 107. E-1447-23214.

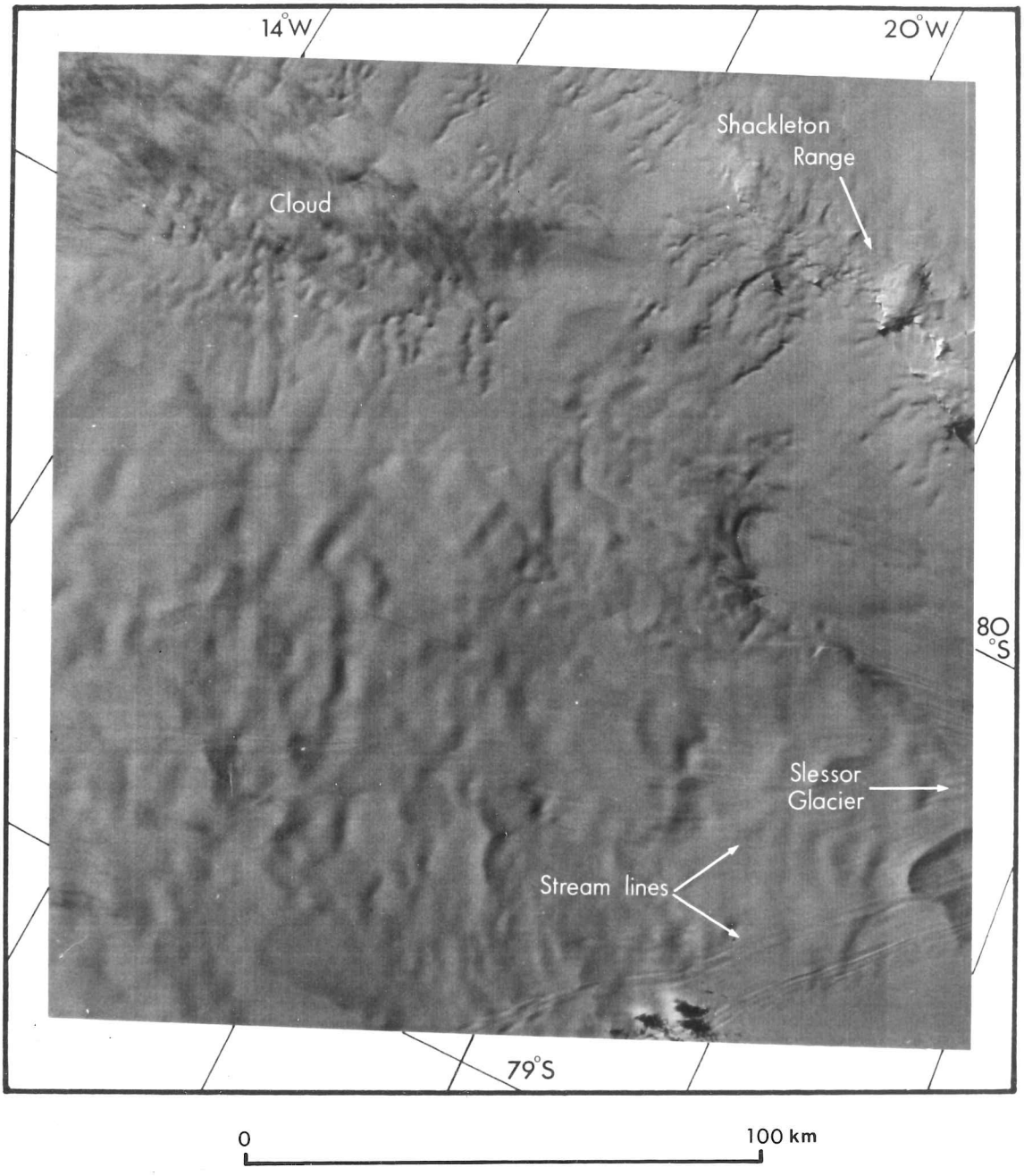

Figure 4.2 Landsat image showing features of the ice sheet surface 50 km inland from Slessor Glacier. Sun angle is 18°. Path 170, row 119. E-1487-06363.

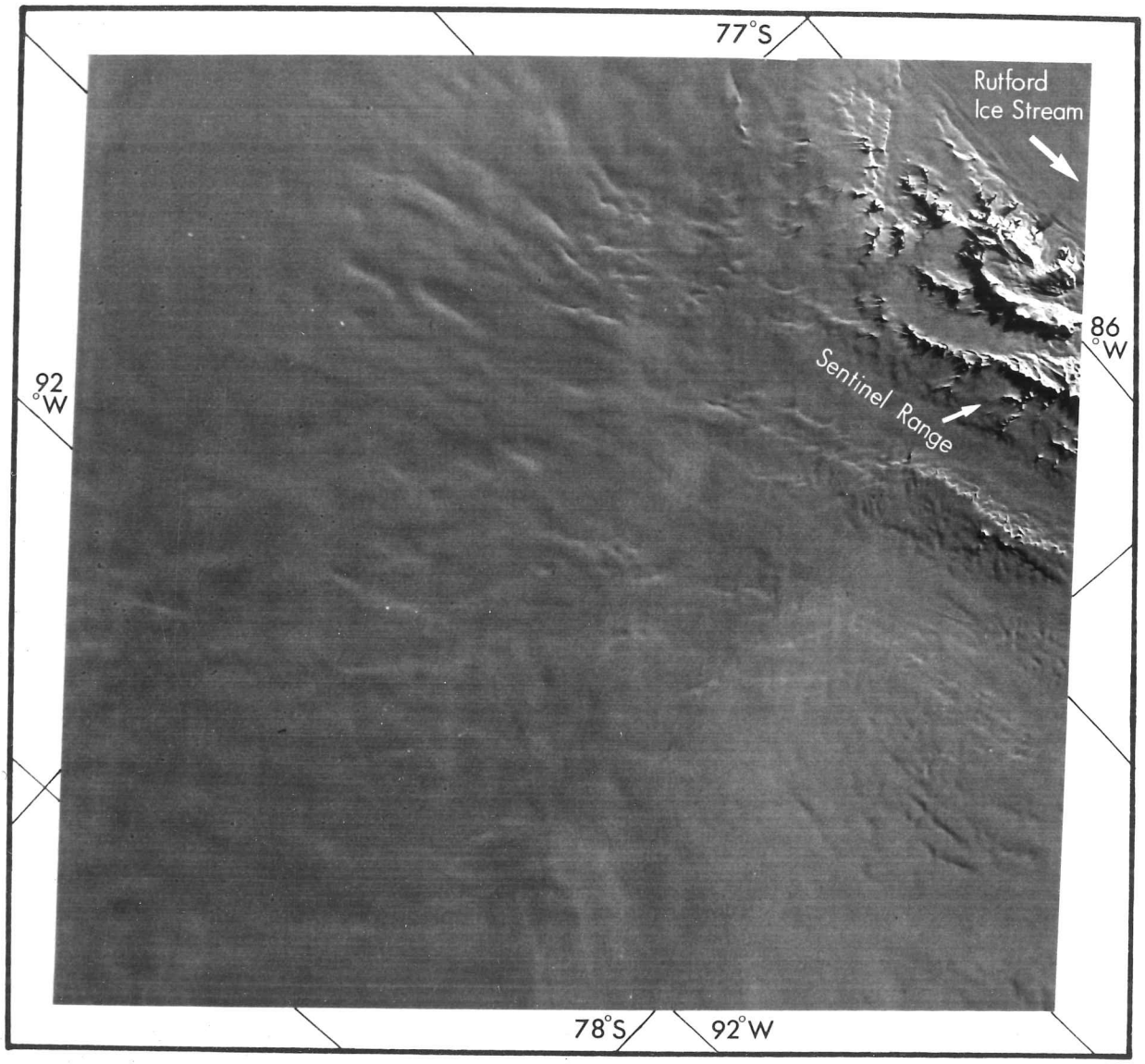

Figure 4.3 Landsat image showing features of the ice sheet surface near the Sentinel Range of the Ellsworth Mountains. Sun angle is 14°. Path 233, row 116. E-1568-12344.

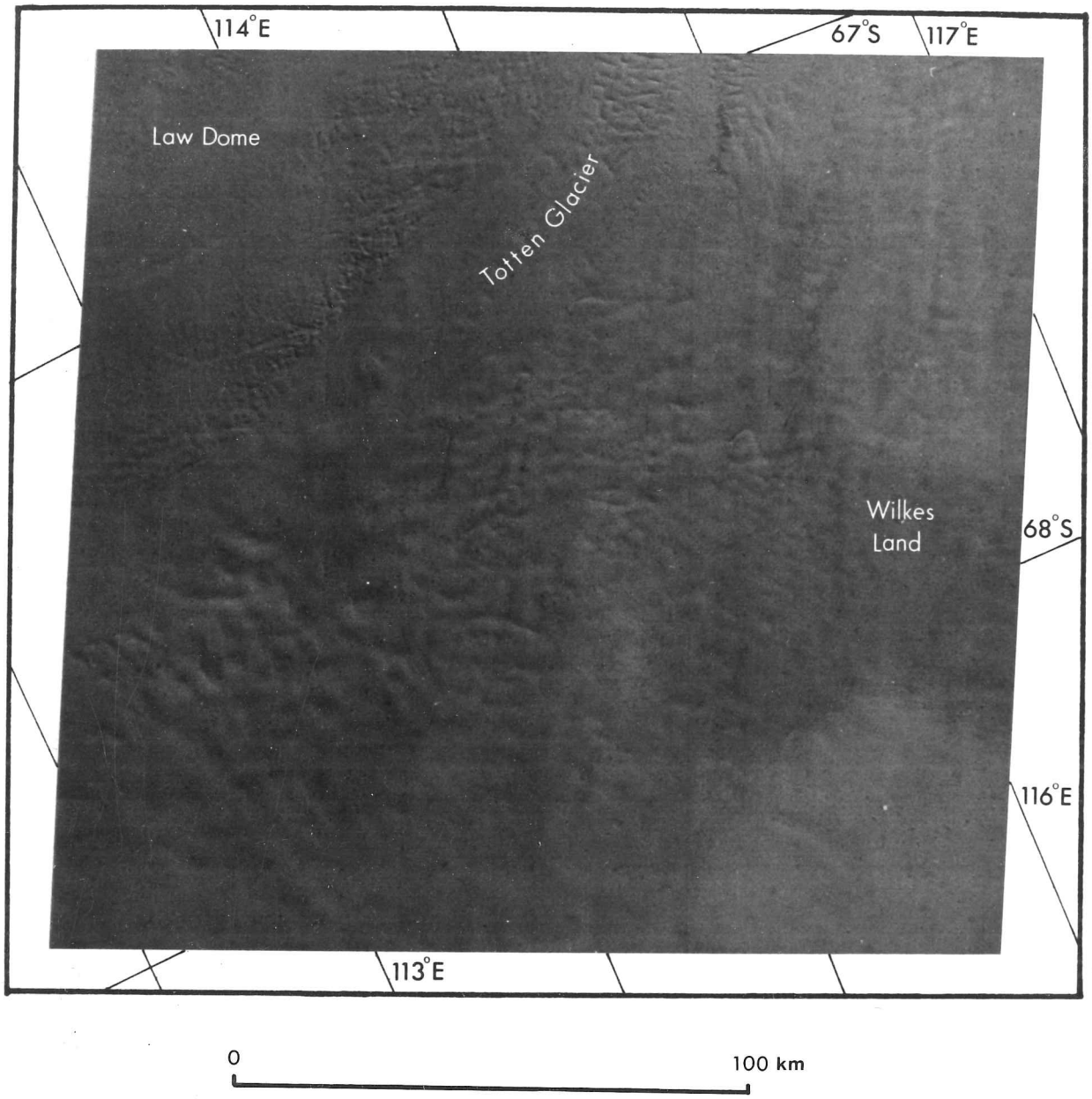

Figure 4.4 Landsat image of the margin of Law Dome, Totten Glacier and coastal Wilkes Land. Sun angle is 24°. Path 107, row 108. E-1460-00303.

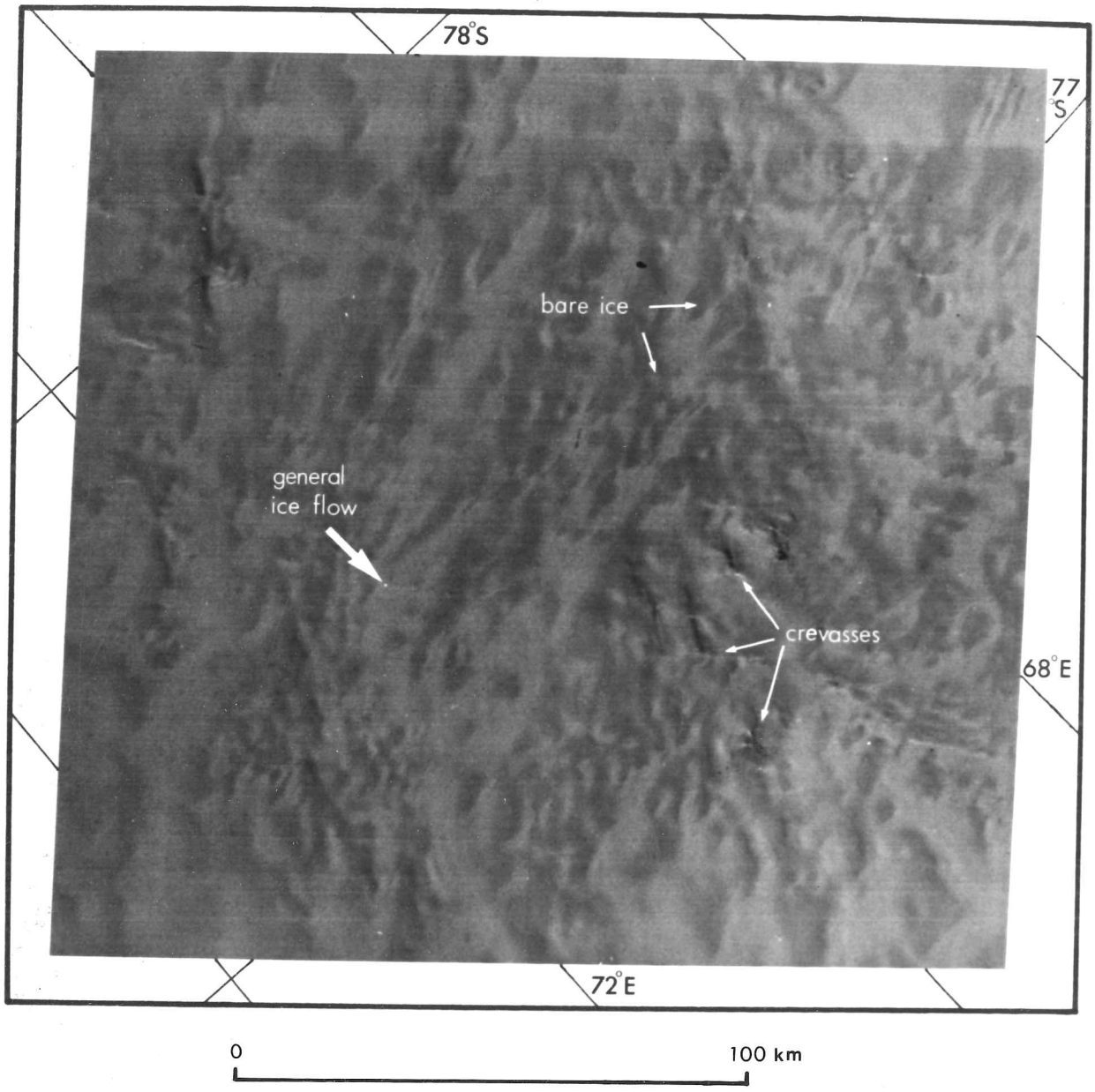

Figure 4.5 Landsat image of central East Antarctica showing marked undulations associated with the subglacial Gamburtsev Mountains. Also shown are areas of bare ice (darker tones) and crevasse trains. Sun angle is 19°. Path 122, row 116. E-1475-12595.

Previous studies (Mellor, 1959, 1964; Giovinetto, 1964, 1970; Budd and others, 1967) have indicated positive budgets. Allison (1979) found that only half of the ice accumulating in the interior drainage basin was discharging into the glacier and interpreted a mean rate of surface increase of +0.03 m a^{-1} of water for the interior drainage basin as indicating a post-surge build-up. Relying on sparse data largely from oversnow traverses at the margin of the drainage basin, Allison based his calculations on conservative accumulation values; however, several sources suggest the Lambert Glacier region is one of exceptionally low accumulation (Robin, 1983).

Zwally and Gloersen (1977) interpreted passive microwave radiation data as indicating exceptionally low accumulation for the whole basin. Fujii and Kusunoki (1982) reported 54 kg m^{-2} a^{-1} lost by sublimation at Mizuho Station. The exceptionally steep slopes in the Lambert basin mean that it will also be subject to strong katabatic winds (Ball, 1960) and hence that sublimation, comparable to that reported further west, may also substantially reduce the net accumulation. The presence of bare ice over 6% of the basin (calculated from a mosaic of Landsat images, one of which is shown in figure 4.5) where average slopes are particularly steep (typically 0.45% over 50 km sections) confirm that, at least locally, there is likely to be a negative mass balance. Combining these data has enabled up-dating of accumulation maps for the region (Bull, 1971; Kotlyakov and others, 1974; Allison, 1979). Revision of the delimitation of Lambert Glacier's drainage basin from the most recent maps (Drewry, 1983a) showed the area to be 875,300 $\pm$ 90,000 km^2; this is 20% less than the 1.09 M km^2 estimated by Allison. Re-calculation of the budget using the revised accumulation and areal data (table 4.1) gives a value of +8 Gt a^{-1} for the interior basin and +20 Gt a^{-1} for the whole Lambert Glacier-Amery Ice Shelf system (McIntyre, in preparation) compared with Allison's values of +30 and +42 Gt a^{-1} respectively. This is equivalent to a mean rate of surface increase of +0.009 m a^{-1} of water for the interior drainage basin. Although still positive mass balances, these values are very much lower and the estimated errors for the interior drainage basin (-0.006 and +0.025 m a^{-1} of water) fall below zero. The possibility of Lambert Glacier

Table 4.1: Re-calculation of the mass balance of Lambert Glacier on the basis of the revised accumulation pattern and area (McIntyre, in preparation). Values in brackets below each component are the equivalent values of Allison (1979).

	Interior drainage basin	Lambert Glacier system	Total drainage basin
Inflow (Gt a^{-1})	-	+30	-
	(-)	(+30)	(-)
Gain in basin (Gt a^{-1})	+38	-7	+31
	(+60)	(-7)	(+53)
Outflow (Gt a^{-1})	30	11	11
	(30)	(11)	(11)
Budget (Gt a^{-1})	+8	+12	+20
	(+30)	(+12)	(+42)
Budget limits (Gt a^{-1})	-5, +22	-4.5, +28	+8, +32
	(+3, +79)	(-4.5, +28)	(+9, +89)
Area (km^2)	875 000	62 000	937 000
	(1 090 000)	(62 000)	(1 152 000)
Mean annual surface-level change (m water a^{-1})	+0.009	+0.19	+0.021
	(+0.03)	(+0.19)	(+0.04)
Surface change limits (m water a^{-1})	-0.006,+0.025	-0.07,+0.45	+0.009,+0.034
	(+0.003,+0.07)	(-0.07,+0.45)	(+0.01,+0.08)

being in a post-surge build-up is therefore, although not refuted, much reduced.

Observations of trends in undulation size across the ice sheet are supported by measurements from sample areas. Table 4.2 presents statistics from ten parts of the Antarctic. The division into coastal, mid ice sheet and central ice sheet splits the surface types into three broadly coherent classes of increasing ice thickness. Variations in the mean and standard deviation of maximum diameter and area testify to the tendency for small undulation wavelengths to be damped out in the thicker, colder ice near centres of outflow. The form factor, defined by

$$f = (4 \pi A_r) / p^2 \qquad [4.1]$$

where A_r is the area and p is the perimeter, will equal one for a circle and have lower values for less regular shapes. With two exceptions, all the samples indicate that undulations are virtually isotropic, the slight departures of form factors from unity being attributable to illumination from one angle and uncertainty of the exact identification of the features. The orientation of maximum diameters bears no relation to flow direction. The regularity of dimensions is taken to indicate that as ice flows over a peak it produces similar stress gradients in both longitudinal and transverse directions to ice flow. The controlling factor is the presence of positive or negative stress gradients and unambiguous deductions about the details of subglacial relief under such thick ice are not possible.

In areas of thin ice, however, the form and alignment of subglacial topography is often revealed. The anisotropic undulations at the head of Dibble Glacier (figure 4.1) indicate bedrock ridges normal to the flow direction. Resulting from longitudinal and transverse stress gradients, they indicate relatively substantial but irregular basal relief which is only partly damped by the effects of ice thickness, velocity and viscosity.

Undulations in coastal parts of the Antarctic have far from uniform distributions. The zones of undulations grouped around outlet glaciers are

Table 4.2: Dimensions of surface undulations derived from the quantification of Landsat imagery. D_{max} is the maximum diameter of an undulation and A_f is the angle D_{max} makes to the flow direction in a clockwise rotation. The form factor is defined by equation (4.1) and N is the number of undulations measured in each sample.

Region	Area (km^2)		D_{max} (km)		A_f (degree)		Form factor		N
	μ	σ_{sd}	μ	σ_{sd}	μ	σ_{sd}	μ	σ_{sd}	
Coastal									
Dibble Glacier	10.2	5.8	4.5	1.6	104	18	0.70	0.12	41
Thwaites Glacier	12.7	4.7	4.5	1.0	174	29	0.90	0.05	35
Moscow University Ice Shelf	12.2	5.3	4.5	1.2	181	35	0.90	0.08	50
Mid ice sheet									
Upper Totten Glacier	30.4	14.7	7.4	2.6	165	48	0.80	0.10	23
Inland of Moscow Univ. Ice Shelf	20.3	7.7	5.7	1.5	184	48	0.90	0.06	50
Ice Stream E	36.7	14.0	7.3	1.0	134	24	0.90	0.08	25
Upper Slessor Glacier	41.6	18.3	7.3	1.7	131	41	0.90	0.07	31
Ellsworth Mountains	39.3	14.3	7.6	1.9	130	24	0.90	0.04	20
Central ice sheet									
Byrd Land	58.5	20.5	9.0	1.9	127	48	0.90	0.04	17
Inland of Slessor Glac.	69.3	27.9	10.9	2.9	111	28	0.90	0.09	18

separated by seemingly domed areas on which surface features are smaller or notably absent. Dibble Glacier (figure 4.1) is flanked by two such zones; the larger one, to the west of the outlet, displays a rapid transition from a featureless centre to small surface irregularities bordering the glacier which seem to have fairly small amplitudes. This change in topography occurs over 20 km and distinguishes a glaciologically stagnant dome, with low ice velocities and possibly low basal temperatures, from more active outlets. The ice sheet margin is punctuated in this manner by numerous ice domes and outlet glaciers (Shumskiy, 1970), the latter accounting for the major discharge of inland ice (Hughes, 1972; Morgan and others, 1982; Drewry and Robin, 1983).

4.2.3 Ice streams and crevasses

Ice streams can be distinguished from intervening domes and undulating areas by features such as the dark, linear 'blurs and streaks' identified as bands of open crevasses (Rose, 1978). The boundary of Ice Stream E with Rockefeller Plateau (figure 4.6) is thus clearly visible and Ice Stream F (Hughes, 1973) can also be seen. Similar features, although much narrower, are found inland of many outlet glaciers; figure 4.2 shows a series of converging lineations running towards Slessor Glacier, which is 50 km downstream. The adjoining images show there to be multiple converging linear features which form a braiding pattern extending 450 km inland from Slessor Glacier's grounding line. The width of individual bands is typically almost constant as they pass through undulating terrain; the one entering figure 4.2 halfway along the bottom of the image is between 3 and 5 km wide for its entire length of over 150 km. Allison (1979) has identified such features inland of Lambert Glacier as fast moving ice streams and this appears to be a likely explanation in the present case. Pine Island, Totten, David, Frost and Shirase Glaciers have similar features feeding their outlets. The margins of these streams are usually very distinct (Swithinbank, 1977) such as that of Ice Stream E (figure 4.6), suggesting proportionately little lateral input of ice. However, Ice Stream F is typical of some, in that it displays curved traces through the margins which indicate peripheral feeding of the ice stream.

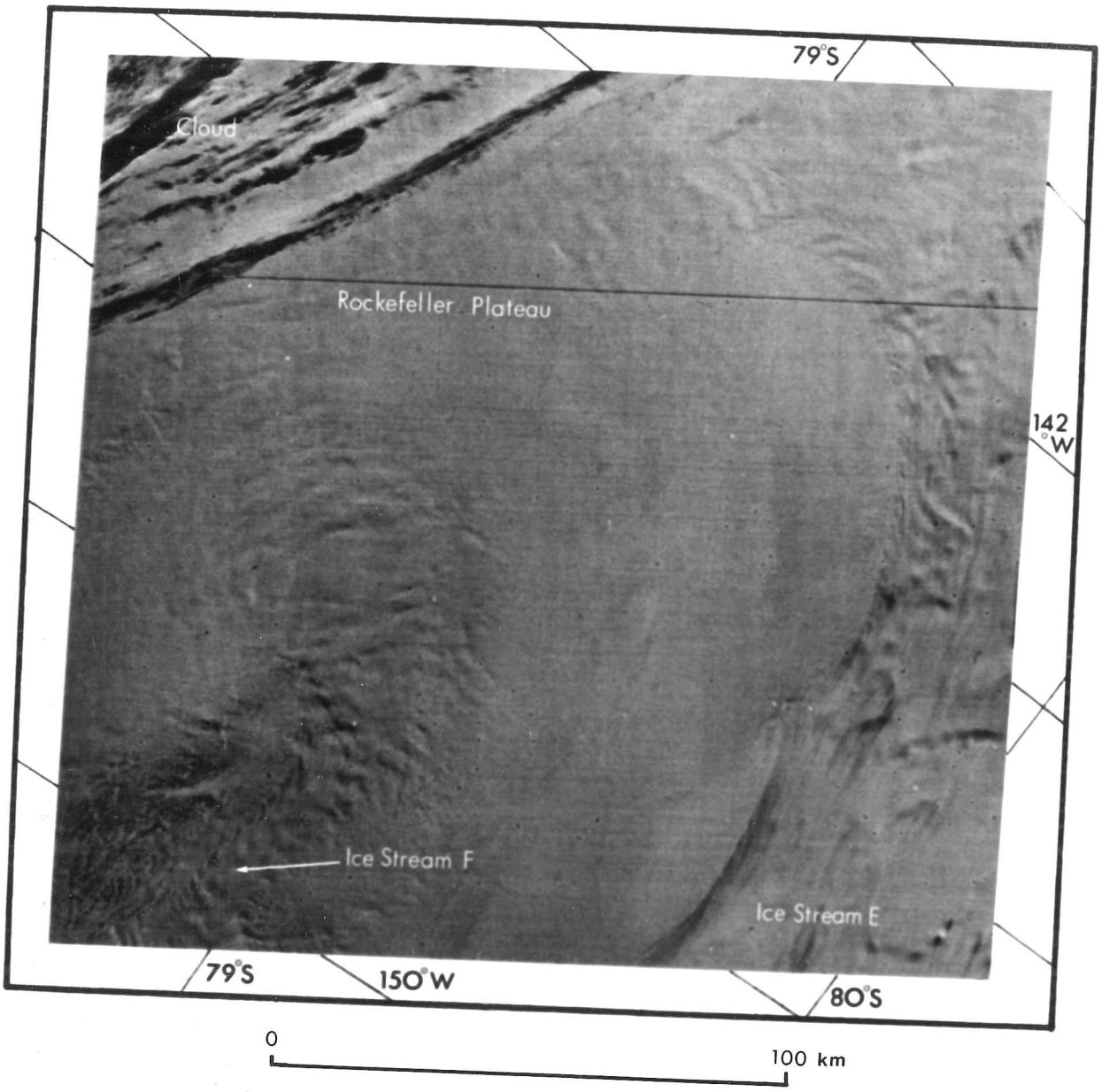

Figure 4.6 Landsat image of northern Marie Byrd Land showing the margin of Ice Stream E, Ice Stream F and the Rockefeller Plateau. Clouds obscure the upper left hand corner of the image. Sun angle is 20°. Path 3, row 119. E-1491-15352.

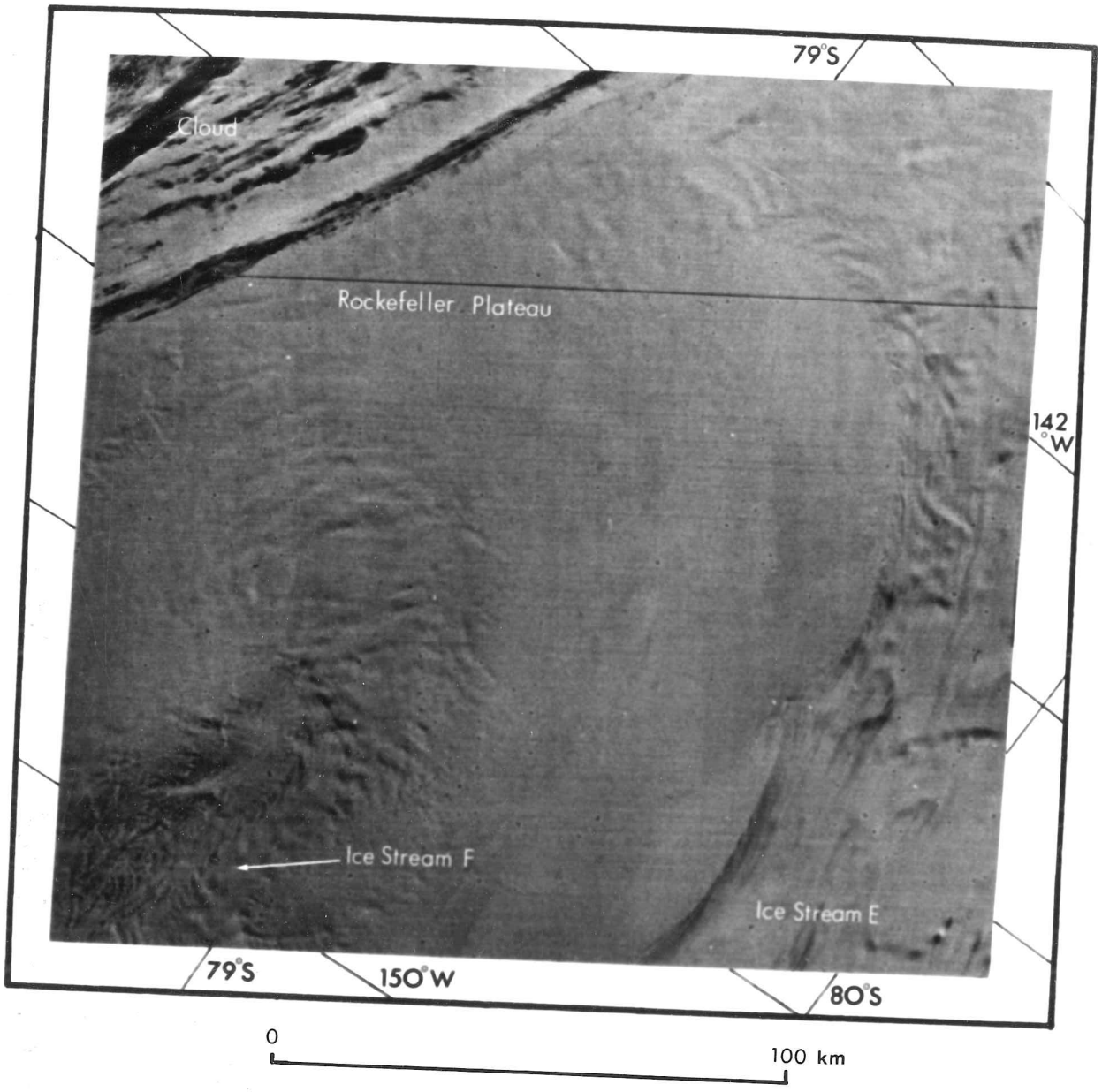

Figure 4.6 Landsat image of northern Marie Byrd Land showing the margin of Ice Stream E, Ice Stream F and the Rockefeller Plateau. Clouds obscure the upper left hand corner of the image. Sun angle is 20°. Path 3, row 119. E-1491-15352.

Few of the largest ice streams display this feature.

The wider streams, such as Ice Stream E and Pine Island Glacier, have undulations within their boundaries (figure 4.6, right hand side of the image). Their density decreases towards the coast, indicating that they are probably areas of local grounding (Crabtree and Doake, 1980).

Byrd Glacier is at the very limit of Landsat coverage and so it is not possible to say whether ice streams penetrate far inland from where it transects the Transantarctic Mountains. It does, however, display a series of widely radiating crevasse lines reaching at least 70 km from the mountains (figure 4.7), a feature which none of the other outlets appear to have. In this particular example, individual crevasses may be clearly identified as contributing to the dark linear features.

Crevasses have been noted on several Landsat images, typically near the coast, in association with ice streams or outlet glaciers and at their boundaries with intervening stagnant areas where lateral shearing occurs. Rifts and chasms can be seen where glaciers are afloat, for instance, where Totten Glacier flows along the subglacial trench around the eastern margin of Law Dome (figure 4.4). Rather more unexpectedly, crevasses can be seen in the interior of the East Antarctic ice sheet (figure 4.5) where marked undulations and bare ice were noted in association with the subglacial Gamburtsev Mountains. At least three trains of crevasses can be seen and, although they do not seem to be associated with any form of ice stream, they are oriented in the estimated flow direction. The length of individual crevasses is up to about 1 km and the trains are approximately 5 km long.

4.3 Results from aircraft altimetry

4.3.1 Introduction

This section describes the techniques used to analyse the altimetric profiles of the ice sheet surface collected during radio echo sounding

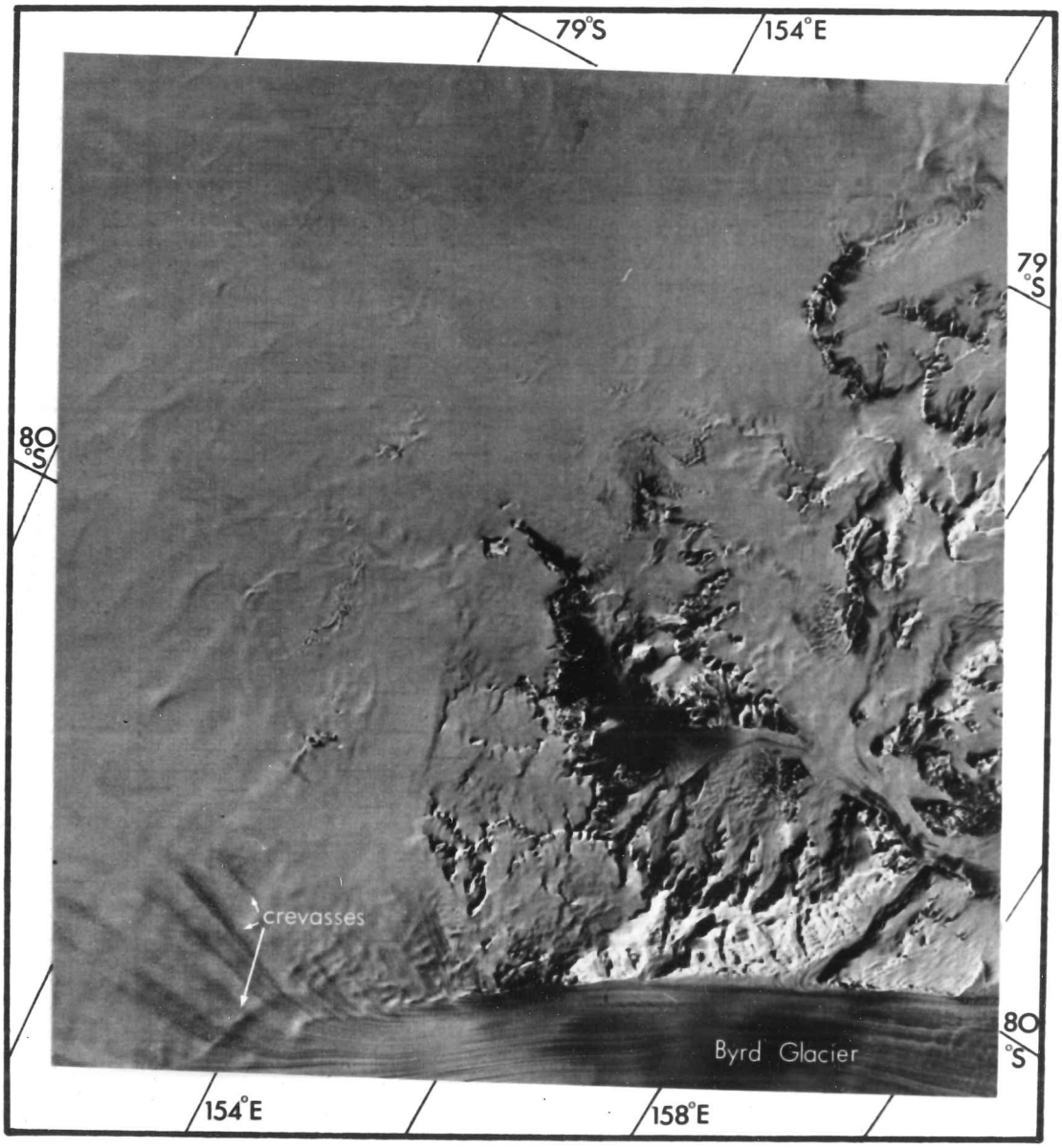

Figure 4.7 Landsat image of the western half of Byrd Glacier where it transects the Transantarctic Mountains. Distinct bands of crevasses can be seen. Sun angle is 19°. Path 49, row 119. E-1492-19080.

0 100 km

missions (section 2.2) and discusses the topographic patterns which were noted. Both lowpass and bandpass digital filters (Hamming, 1977) have been used in the following analysis. A 500 m lower limit on wavelength was selected to remove features such as snow dunes, sastrugi and system noise. A cutoff of 50 km was chosen as an upper bandpass limit on the basis of wavelengths identified in the data. Given that the question of the symmetry of ice sheet features was seen as one of the products of the following analysis, comparability of results was achieved by restricting the profiles to those either down or normal to flowlines, as deduced from surface contours (Drewry, 1983a).

4.3.2 Descriptive techniques

A description of ice sheet terrain can be attempted by calculating gradients from the altimetric profiles and considering the statistical properties of their distribution. Slope segments 1 km long were derived by fitting a least squares linear regression to the data. The first four moments of the distribution were calculated, the latter two (namely, skewness and kurtosis) having standardized forms. The coefficient of skewness (m_3) is defined by

$$m_3 = \frac{\sum(j - \mu)^3}{\sigma_{sd}^3} \qquad [4.2]$$

and the coefficient of kurtosis (m_4) is defined by

$$m_4 = \frac{\sum(j - \mu)^4}{\sigma_{sd}^4} - 3 \qquad [4.3]$$

where j is an element of a distribution, μ is the mean of the distribution and σ_{sd} is the standard deviation. A Gaussian distribution will therefore have $m_3 = m_4 = 0$.

Spectral analysis enables both horizontal and vertical components of a topographic profile to be considered simultaneously by examination of its frequency content (Rozema, 1968). One of the more important restrictions is that samples are statistically homogeneous. As shown below, the

transition of slopes from the Gaussian distribution with distance across the ice sheet is very gradual in comparison with sample lengths and so stationarity is not a problem. It is also necessary to avoid contamination of the series' true power by large scale trends. A bandpass filter with cutoffs of 500 m and 50 km was therefore applied to all data before analysis. The length of surface profiles is an important consideration for spectral analysis. For results to be comparable, the maximum lengths of appropriate data were restricted by the coincidence of the flight grid and flow directions. Therefore, no profiles much greater than 200 km were available. However, to obtain meaningful results from spectral analysis, the sample length should be no less than five times the maximum detectable wavelength. The minimum frequency limit imposed on spectra was thus 0.25×10^{-4} cycles m^{-1}, which is equivalent to a wavelength of 40 km. These difficulties severely constrained the altimetric data available for spectral analysis. A technique which has been used to facilitate the accurate delimitation of frequencies is zero-padding (Henry and Graefe, 1971). The finest spacing at which independent spectral estimates may be formed is equal to the reciprocal of the record length. By adding a null record to the sample, the spectral resolution may be significantly increased and standardized. Samples were therefore extended by zero-padding so that they contained 8192 data points, thereby giving a frequency resolution of 2.44×10^{-6} cycles m^{-1}.

4.3.3 Topographic patterns

Let us begin by considering the variations of ice sheet morphology which occur down a flowline between an ice divide and the ice sheet margin. Figure 4.8 shows a section from Dome C to the Wilkes Land coast at 120°E; surface and bedrock profiles (from aircraft altimetry and radio echo sounding, respectively) are shown with five spectra produced by applying a Fast Fourier Transform to sections of the former. Regional ice thicknesses decrease in a generally uniform manner and ice velocities and temperatures may be assumed to increase fairly regularly with distance from the ice divide. The spectra provide details of the increasing topographic roughness with distance from the ice divide, a trend which can also be seen

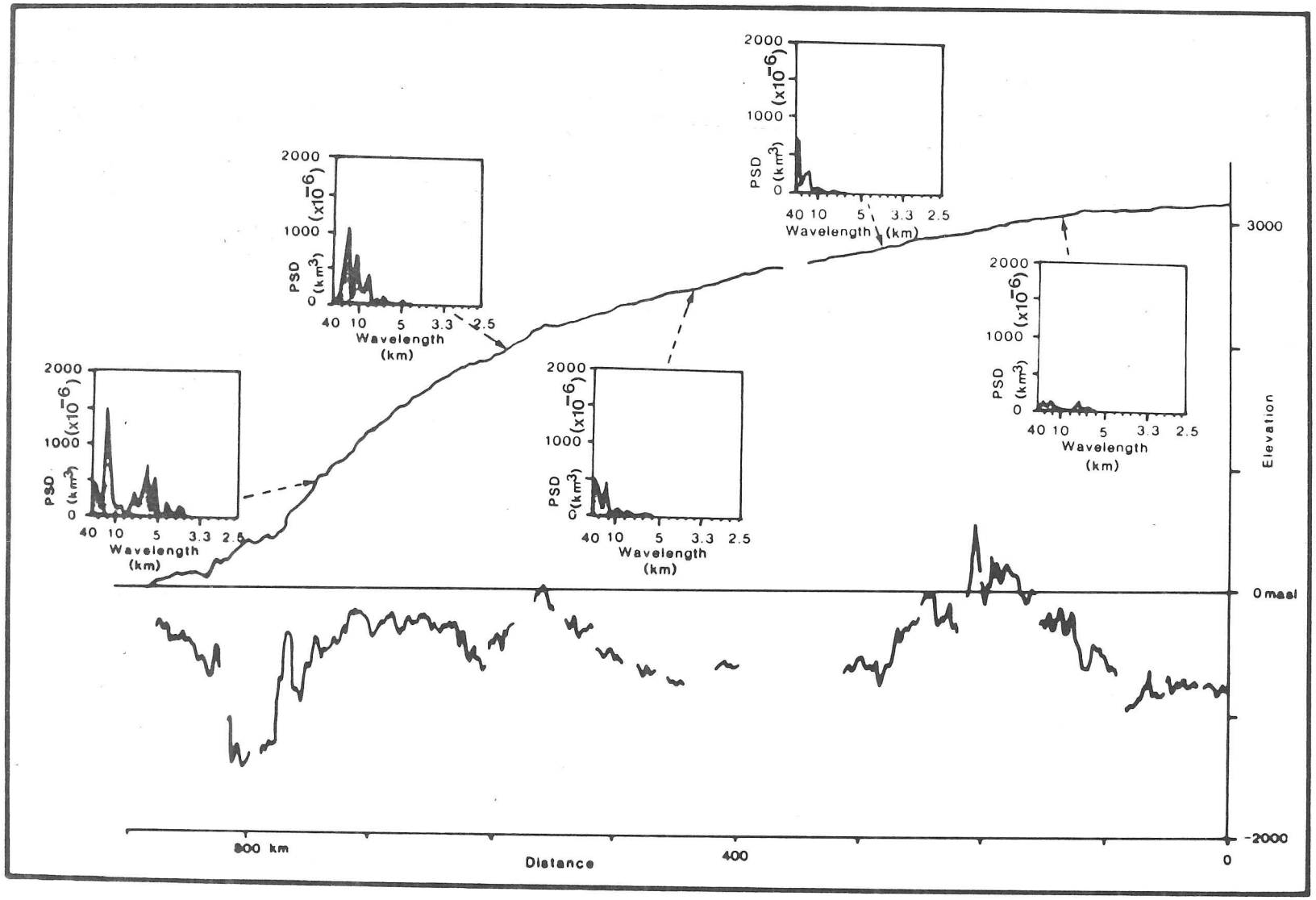

Figure 4.8: Profiles from two flights down flowlines from Dome C to the Wilkes Land coast at 120°E with surface spectra. Bedrock profile from radio echo sounding and surface profile from aircraft altimetry.

in the surface profile itself. Two particular points should be noted. First, there is a marked increase in the energy contained in each as one approaches the coast. The rms deviation of the surface, the square root of the zeroth moment of each spectrum, increases from 2.6 to 12.2 m. Second, the relative importance of wavelengths changes. Near the divide, minor spectral peaks occur at several wavelengths but, as velocities increase downslope, the contributions from wavelengths, typically greater than 25 km, become increasingly dominant. In the coastal region, while long wavelengths occur, the dominant peak is at 12 km; considerable amounts of energy also exist at shorter periods. These two patterns of increasing topographic roughness and increasing dominance of shorter wavelengths as one approaches the thinner ice near the coast are typical of much of East Antarctica which conforms to Vialov's (1958) predicted ice sheet form. Clearly, local effects are associated with variations in subglacial relief, ice velocity and viscosity which distort the regular alteration of surface topography across the ice sheet.

Figure 4.9 shows eight surface profiles which have been bandpass filtered and which further illustrate the trends noted in figure 4.8. They are presented purely to give a visual indication of the surface roughness which is treated statistically in terms of gradients in figure 4.10. Moving from the ice divide towards the thinner, coastal ice (figure 4.10.A to F) the slope distributions become more dispersed. Absolute gradients increase from less than 0.5% to almost 10% in extreme cases. Such deviations are superimposed on a variable mean slope which is approximately zero at the divides and reaches nearly 2% near the margin, representing the theoretically predicted form of the ice sheet (section 1.3). Near the divides, the close correlation of data with the Gaussian curve (added in figures 4.10 and 4.11 for comparative purposes) indicates that the gradients are well approximated by a normal distribution. In the marginal parts of the ice sheet, however, the observed distribution is severely negatively skewed and leptokurtic. Some statistics from these distributions are given in table 4.3 part 1.

in the surface profile itself. Two particular points should be noted. First, there is a marked increase in the energy contained in each as one approaches the coast. The rms deviation of the surface, the square root of the zeroth moment of each spectrum, increases from 2.6 to 12.2 m. Second, the relative importance of wavelengths changes. Near the divide, minor spectral peaks occur at several wavelengths but, as velocities increase downslope, the contributions from wavelengths, typically greater than 25 km, become increasingly dominant. In the coastal region, while long wavelengths occur, the dominant peak is at 12 km; considerable amounts of energy also exist at shorter periods. These two patterns of increasing topographic roughness and increasing dominance of shorter wavelengths as one approaches the thinner ice near the coast are typical of much of East Antarctica which conforms to Vialov's (1958) predicted ice sheet form. Clearly, local effects are associated with variations in subglacial relief, ice velocity and viscosity which distort the regular alteration of surface topography across the ice sheet.

Figure 4.9 shows eight surface profiles which have been bandpass filtered and which further illustrate the trends noted in figure 4.8. They are presented purely to give a visual indication of the surface roughness which is treated statistically in terms of gradients in figure 4.10. Moving from the ice divide towards the thinner, coastal ice (figure 4.10.A to F) the slope distributions become more dispersed. Absolute gradients increase from less than 0.5% to almost 10% in extreme cases. Such deviations are superimposed on a variable mean slope which is approximately zero at the divides and reaches nearly 2% near the margin, representing the theoretically predicted form of the ice sheet (section 1.3). Near the divides, the close correlation of data with the Gaussian curve (added in figures 4.10 and 4.11 for comparative purposes) indicates that the gradients are well approximated by a normal distribution. In the marginal parts of the ice sheet, however, the observed distribution is severely negatively skewed and leptokurtic. Some statistics from these distributions are given in table 4.3 part 1.

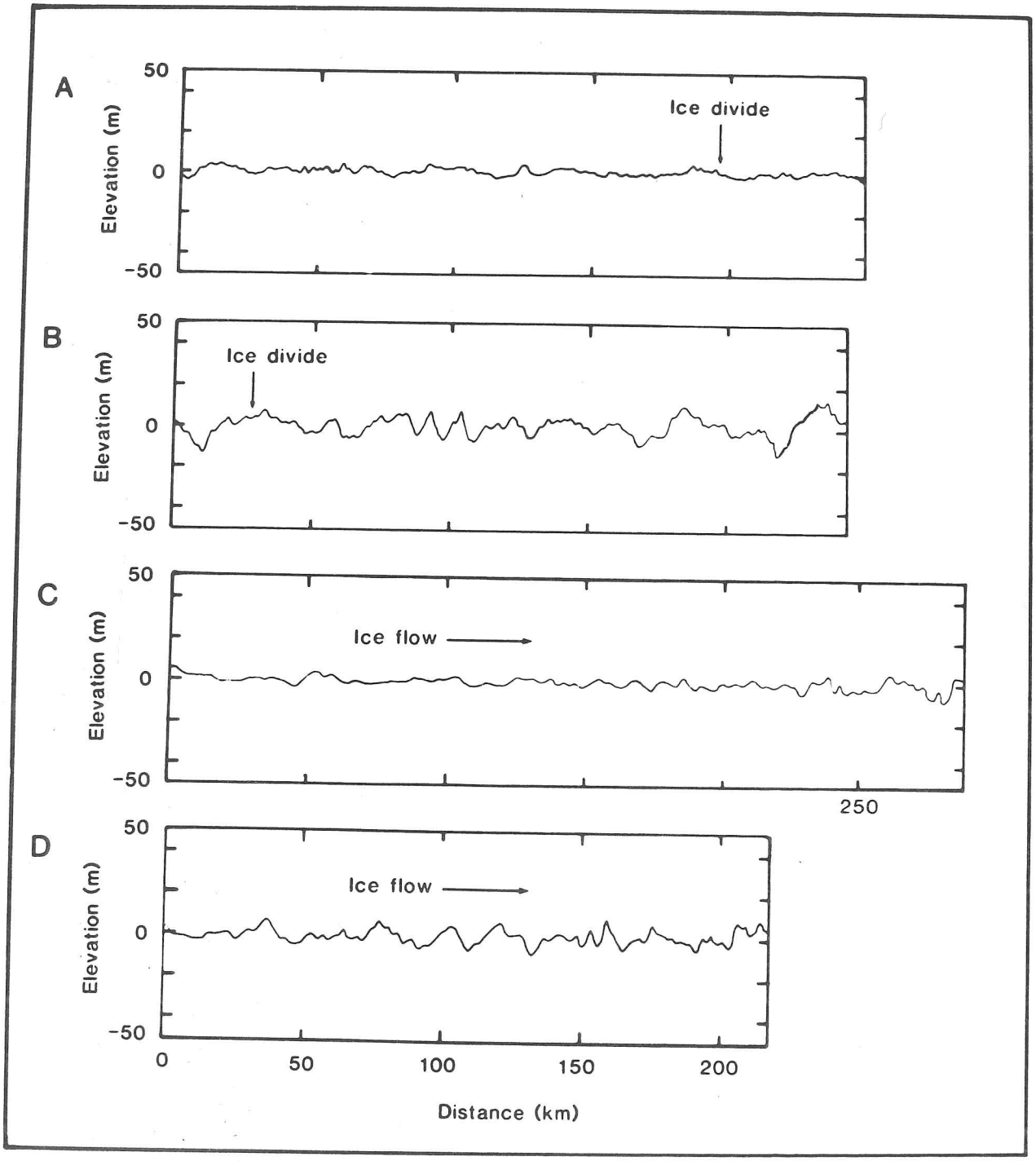

Figure 4.9: Surface profiles of the ice sheet derived from aircraft altimetry and bandpass filtered with cuttoff wavelengths of 500 m and 50 km to show details of the surface topography. All profiles are parallel to flowlines. A: Ridge B towards Vostok; B: across the West Antarctic ice divide (80°S 92°W). C: mid ice sheet (85°S 152°E) between the polar plateau and Lennox King Glacier. D: between Dome C and the Wilkes Land coast. E: polar plateau between the Pole and Foundation Ice Stream. F: Wilkes Land coast at 120°E. G: Thwaites Glacier. H: Institute Ice Stream.

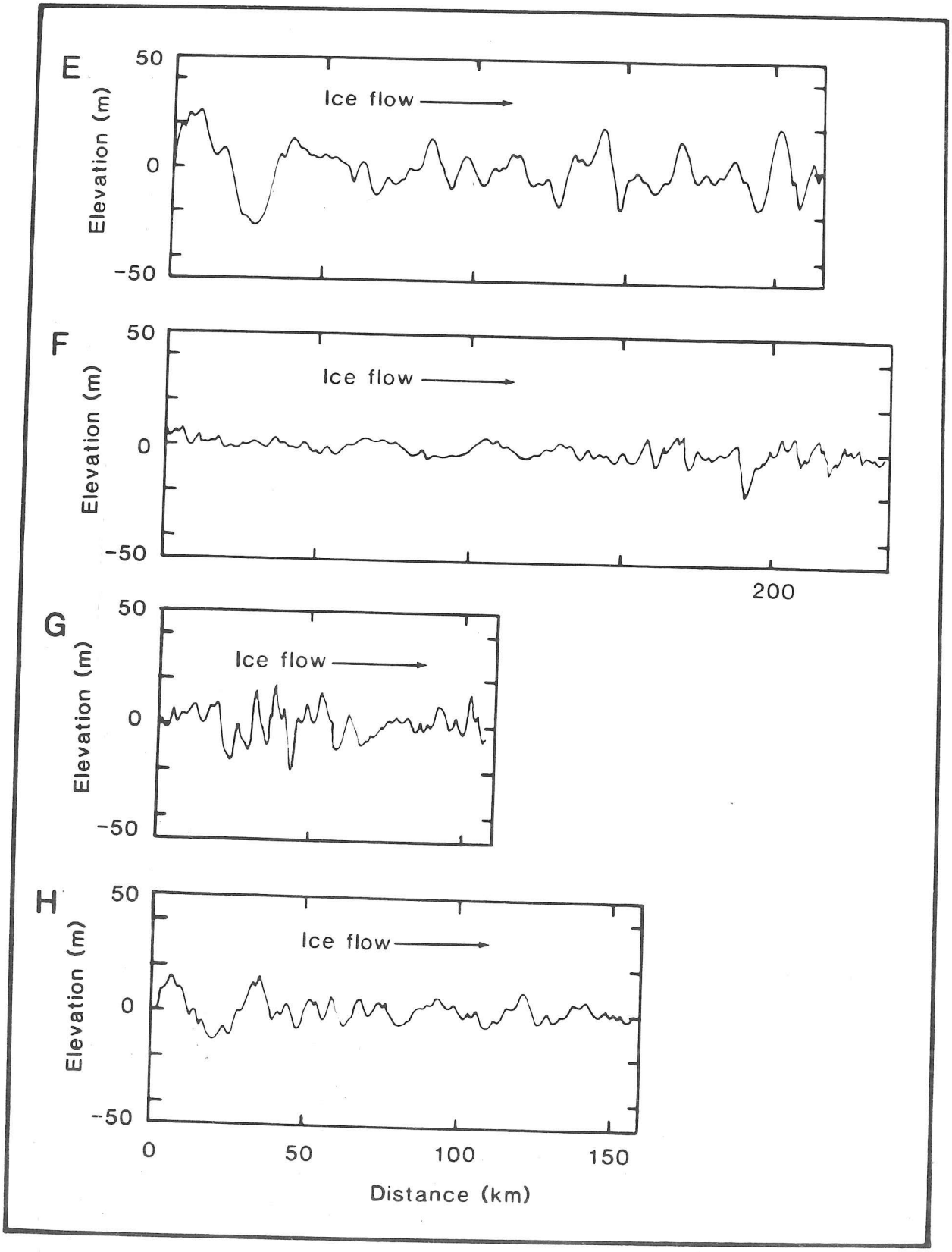

Figure 4.9 continued.

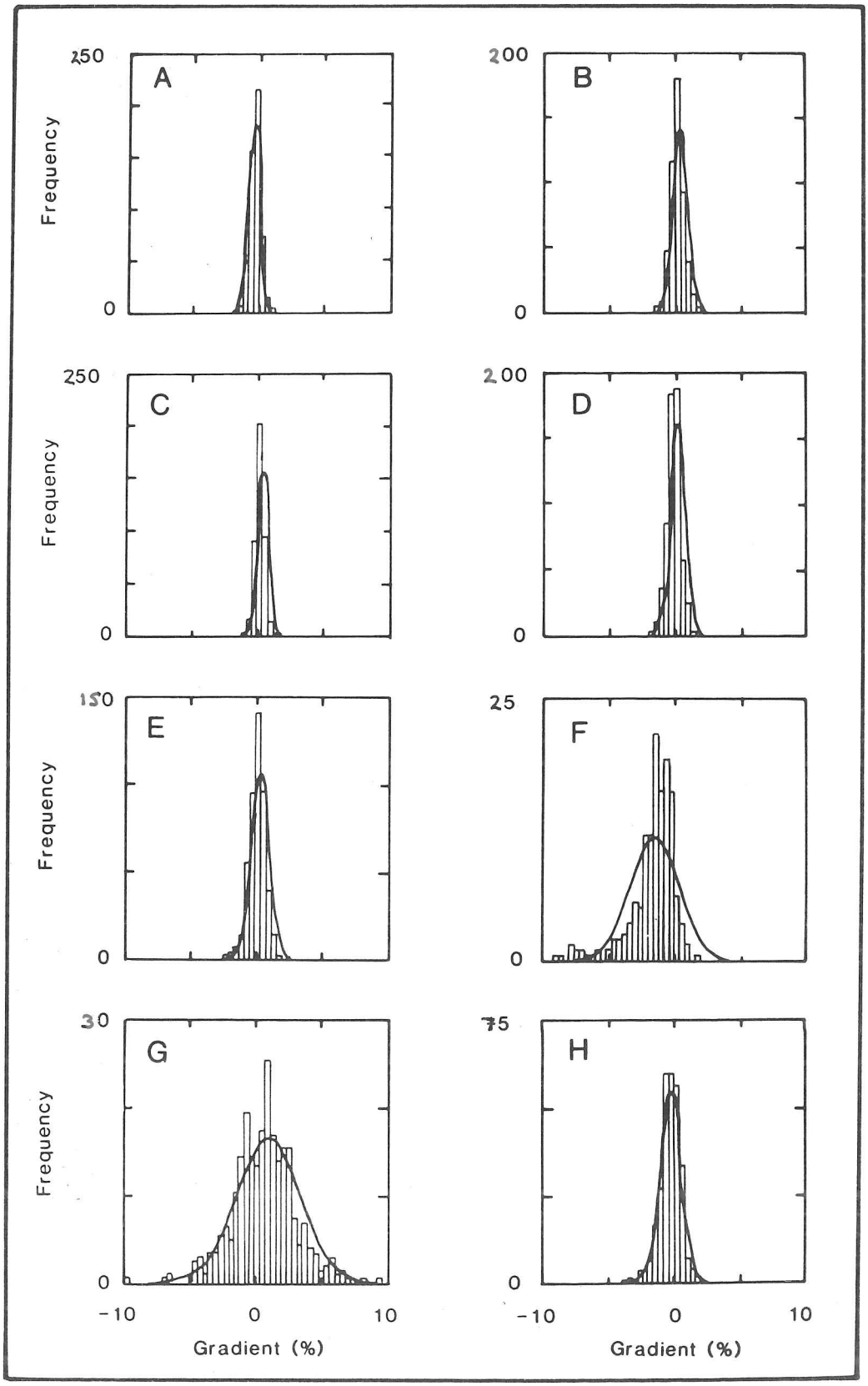

Figure 4.10: Frequency histograms of gradients of 1 km slope segments calculated by fitting a linear regression to derived profiles of the ice sheet surface. Histograms A to H were derived from the profiles in figure 4.9.A to H respectively before they were bandpass filtered. Locations are given in the caption to figure 4.9.

Table 4.3: Gradients derived from fitting 1 km regression lines to ARDS profiles. Statistics relate to histograms in figures 4.9 and 4.10. N is the sample size and coefficients of skewness (m_3) and kurtosis (m_4) are defined by equations (4.2) and (4.3) respectively. μ is the mean and σ_{sd} is the standard deviation of the distribution. Letters refer to figures 4.9 and 4.10.

	Region	μ (%)	σ_{sd} (%)	N	Minimum value (%)	Maximum value (%)	m_3	m_4
	Part 1							
A	Ridge B	-0.162	0.144	497	-0.562	0.307	-0.176	0.171
B	W. Antarctic divide	-0.019	0.275	487	-1.068	0.999	-0.396	1.812
C	Mid E. Antarctic ice sheet	-0.064	0.301	431	-1.055	0.825	-0.100	0.374
D	Dome C - Wilkes Land	-0.298	0.378	572	-1.898	1.213	-0.049	1.900
E	Polar plateau	-0.069	0.638	456	-5.185	2.297	-1.332	10.359
F	Coastal Wilkes Land	-1.973	1.703	115	-8.884	0.318	-1.929	4.393
	Part 2							
	Ice Stream D*	-0.404	0.313	214	-0.868	0.886	-0.055	0.318
	Ice Stream D**	0.015	0.322	198	-0.769	0.913	0.150	-0.266
	Wilkes Land*	-0.320	0.461	164	-2.303	1.428	-0.017	0.635
	Wilkes Land**	0.032	0.548	139	-2.100	1.694	-0.470	1.798
	Part 3							
H	Institute Ice Stream	-0.321	0.580	261	-1.983	1.113	-0.601	-0.107
G	Thwaites Glacier	-0.749	1.450	228	-7.424	2.907	-1.060	3.340

* Down flowline. Minimum and maximum gradients have been normalised by subtraction on the mean.

**Across flowline.

The progression to rougher terrain in thinner, faster-flowing, coastal ice mirrors the development in internal reflecting layers as identified by radio echo sounding (Millar, 1981a). Near centres of outflow, layering extends almost to bedrock and is notably uniform, suggesting only very slow deformation of the ice mass. However, the observed absence of echoes in a proportionately large basal layer (the basal echo-free zone which, where system performance permits, may be up to 50% of the ice thickness) in areas of higher velocities or rough subglacial topography, indicates more severe distortion of ice in three dimensions in response to changing stress fields produced by varying bedrock slopes.

The intersection of ARDS flight lines enables a check on the symmetry of surface undulations (figure 4.11). In both Marie Byrd Land and Wilkes Land, after allowing for the displacement due to a mean downslope gradient, distributions of slopes normal and parallel to flowlines are of similar form and the gradients are closely matched in magnitude. Table 4.3 part 2 lists the statistics for the four distributions; minimum and maximum gradients for both downslope segments have been adjusted for comparison with the cross-profiles by the subtraction of the mean gradient. In the West Antarctic case, the standard deviation of the gradients match very closely and there is a good correlation between the respective minimum and maximum values. The relationship between profiles across and down slopes in Wilkes Land is slightly less clear, there being a 20% difference in the comparative statistics. The small decrease in isotropy in coastal regions is a reflection of the thinner ice and the manner in which flow in three dimensions at the surface is closely controlled by the subglacial terrain, there being less damping of the relief by ice thickness, velocity and viscosity. The fact that ice flow over subglacial peaks appears to produce similar stress gradients in longitudinal and transverse directions, even in coastal regions, indicates the importance of considering ice sheet mechanics in three dimensions. This is discussed further in section 6.3 where ice sheet surface slopes are derived from stress gradients, following the analysis of Robin (1967).

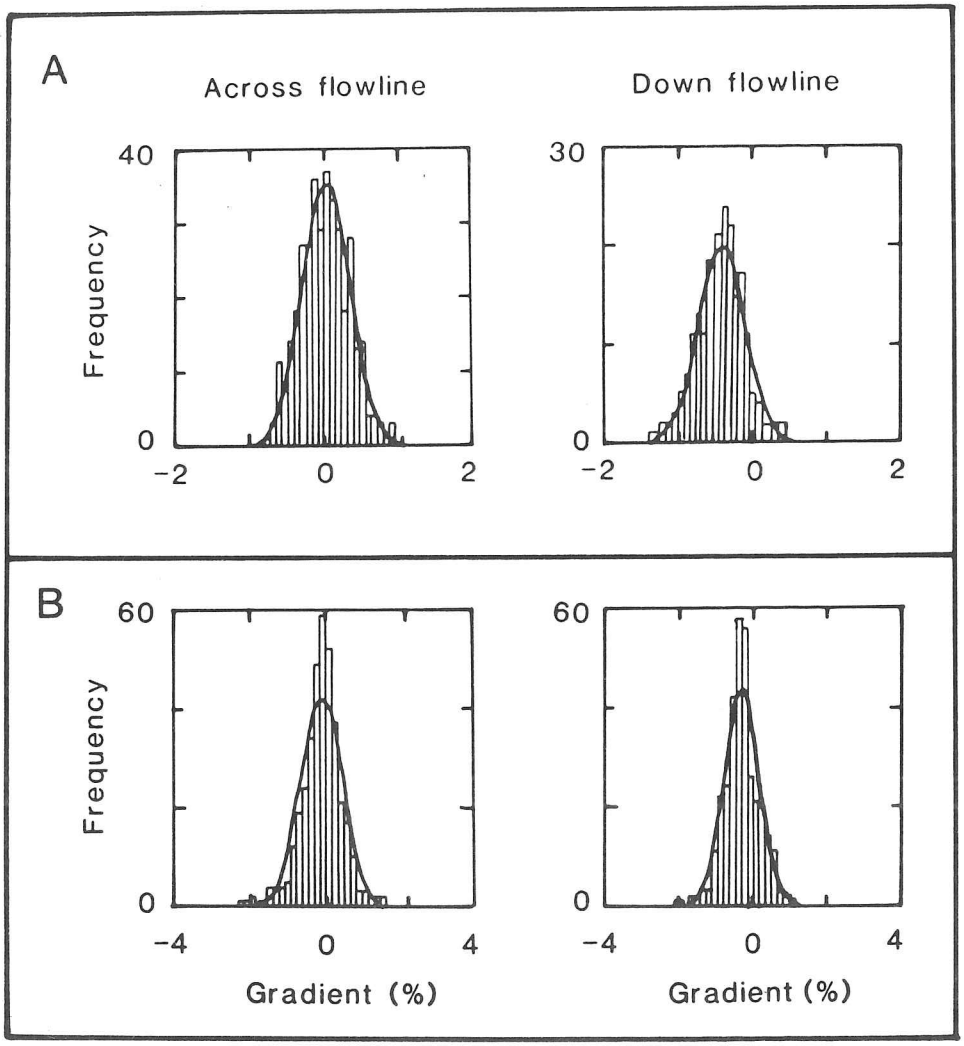

Figure 4.11: Histograms of ice sheet surface gradients from intersecting ARDS profiles giving results down flowlines and along contours. A: head of Ice Stream D, Marie Byrd Land. B: 40 km inland of the Wilkes Land coast at 120°E.

Table 4.4 summarizes some of the broad trends in the surface topography of the ice sheet which have been noted so far.

4.3.4 Exceptions

The preceding characterization of surface topography is based on an ice sheet profile such as that in figure 4.8 which is representative of much of East Antarctica. We will now consider exceptions to the pattern.

First, the general form suggested by Vialov (1958) (equation [1.4]) is not a good approximation in some parts of the ice sheet, particularly in drainage basins which are fringed by large ice shelves, such as those in West Antarctica (Hughes, 1973). Ice Streams C and D, flowing into the Ross Ice Shelf (figure 1.5.C), display markedly concave profiles with low slopes in their seaward portions. Surfaces are notably rougher inland of such areas; West Antarctica (figures 4.9.B and 4.10.B) displays virtually none of the smooth terrain found in central East Antarctica (figures 4.9.A and 4.10.A), its only occurrence being in narrow strips across part of the divide.

Second, less obvious but significant departures from Vialov's (1958) profile frequently occur inland of outlet glaciers and ice streams. They take the form of embayments in the otherwise steeply sloping coastal ice, such as that around Dibble Glacier (figure 4.1). These localized concavities of slope in the ice sheet margin are usually separated by domes, often only tens of kilometres across, which contrast with them by having smoother and more regular topography. The margin of East and West Antarctica is therefore punctuated by a series of valleys and basins which differ from intervening saddles and domes in terms of topography, ice rheology and glaciological regime. The differences are attributed to variations in basal topography, ice temperature and velocity and whether motion is dominated by internal deformation or basal sliding.

Figures 4.10.G and 4.10.H present histograms of gradients from Thwaites Glacier and Institute Ice Stream; bandpass filtered profiles are shown in figures 4.9.G and 4.9.H. They approximate Gaussian distributions more

Table 4.4: General trends identified in the topography of the surface of the Antarctic ice sheet from analyses of aircraft altimetry, Landsat imagery, Seasat altimetry and radio echo sounding data.

	Ice sheet divide	Mid ice sheet	Ice sheet margin
Topography	planar	sinusoidal	irregular
Undulation wavelength	long		short
Undulation amplitude	low		high
Radius of curvature	large		small
Slope distribution			
a) down flowline	normal		negatively skewed and leptokurtic
b) across flowline	normal		non-Gaussian

closely than the other coastal flight section (figure 4.10.F) but both are also notably negatively skewed and leptokurtic. The gradients along Institute Ice Stream are markedly less than those of both Thwaites Glacier and the Wilkes Land coast and may be attributed to very thick ice and to basal lubrication by a water layer which is thought to occur under ice streams. Statistics of these frequency distributions are given in table 4.3 part 3.

Third, there are areas of irregular terrain such as the polar plateau (figure 4.9.E), in central East Antarctica (figure 4.5) and the West Antarctic ice divide (figure 4.9.B) which do not conform to the above model. Such deviations are the result of regionally severe subglacial topography and thin ice, but the effects of velocity and viscosity differences may also be apparent.

4.4 Results from Seasat

A limited amount of altimetry data recorded by Seasat in the Antarctic was available for the present study. Figure 4.12 shows surface elevations in Wilkes Land compiled from over 27 000 Seasat data points and contoured at a 25 m interval (Brooks, 1983). Gaps in the coastal margin indicate an absence of data because of losses of lock. Results in such quantity and of such quality enable the construction of maps superior to those of ice sheets which already exist. It is possible for the first time to identify details of the surface topography rather than the regional trends of contours.

The most striking feature of the contour map is the gently sloping ridge which extends coastwards between 134°E and 139°E. There is an abrupt change of slope at 68°30'S to the more characteristically steeply sloping ice sheet margin found elsewhere. This feature is a local ice divide splitting the catchment area of Frost Glacier from those to the east. On a smaller scale, one may identify many undulations, ridges and other irregularities in the surface which are particularly clear inland of Porpoise Bay. The contour interval enables clear identification of

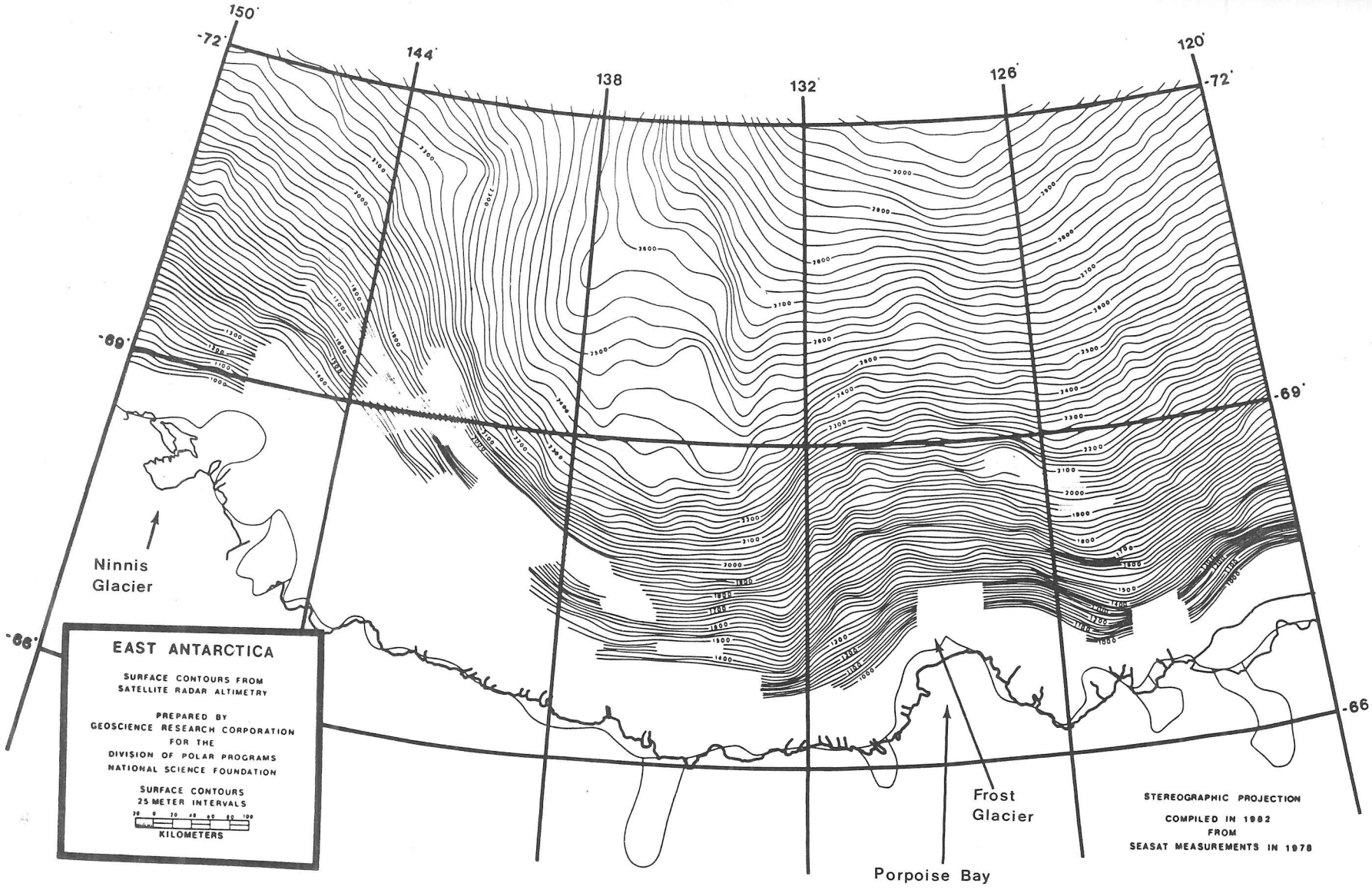

Figure 4.12: Map of surface elevations in Wilkes Land derived from over 27 000 measurements made during 37 passes of Seasat. Contoured at 25 m. (From Brooks, 1983.)

features spaced at approximately 50 km. For a more precise description of such surface features, reference is made to figures 4.9.F and 4.10.F which are taken from a flight line parallel to, but 10 km west of, the 120°E meridian.

Although limited to a narrow, peripheral belt of the ice sheet which does not cover the last, and probably most severe, 100 km of terrain, figure 4.12 does illustrate the coastwards development of surface features. Superimposed on the steepening slopes towards the coast are increasingly large deviations, the gradients of which vary by a factor of two or three over distances of 20 km.

As a source of altimetric profiling with a relative accuracy of up to 2 m (Brenner and Martin, 1982), Seasat data should be suitable for the same type of analysis as was used for the results from the ARDS (section 4.3). However, because of the coarse sampling interval, poor continuity, limited spatial coverage and non-alignment with flow directions (section 2.4), the discussion has to be restricted to a qualitative commentary and will involve data at variable angles to flow. Figure 4.13 shows Seasat surface profiles from Princess Elizabeth and Enderby Lands. Profile A is a 245 km section at the margin of Ridge B which is at angles of between 25° and 55° to the direction of flow. Near the crest there are marked undulations with wavelengths of 8 to 15 km and amplitudes of up to 10 m. The surface topography is more subdued 200 km downslope with longer wavelengths dominating the profile. Given the difficulty of deriving precise topographic profiles from Seasat altimetry in regions of severe terrain (section 3.5), these observations should be treated with caution. In the section from Enderby Land (B) which transects the end of a major ice divide and is approximately normal to flow, the ice divide is uncharacteristically rough, the crest being dominated by relief of up to 20 m. This is a region of many outcrops and nunataks and the effects of rough subglacial terrain and thin ice locally less than 500 to 1000 m thick are evidently reflected in the ice sheet surface.

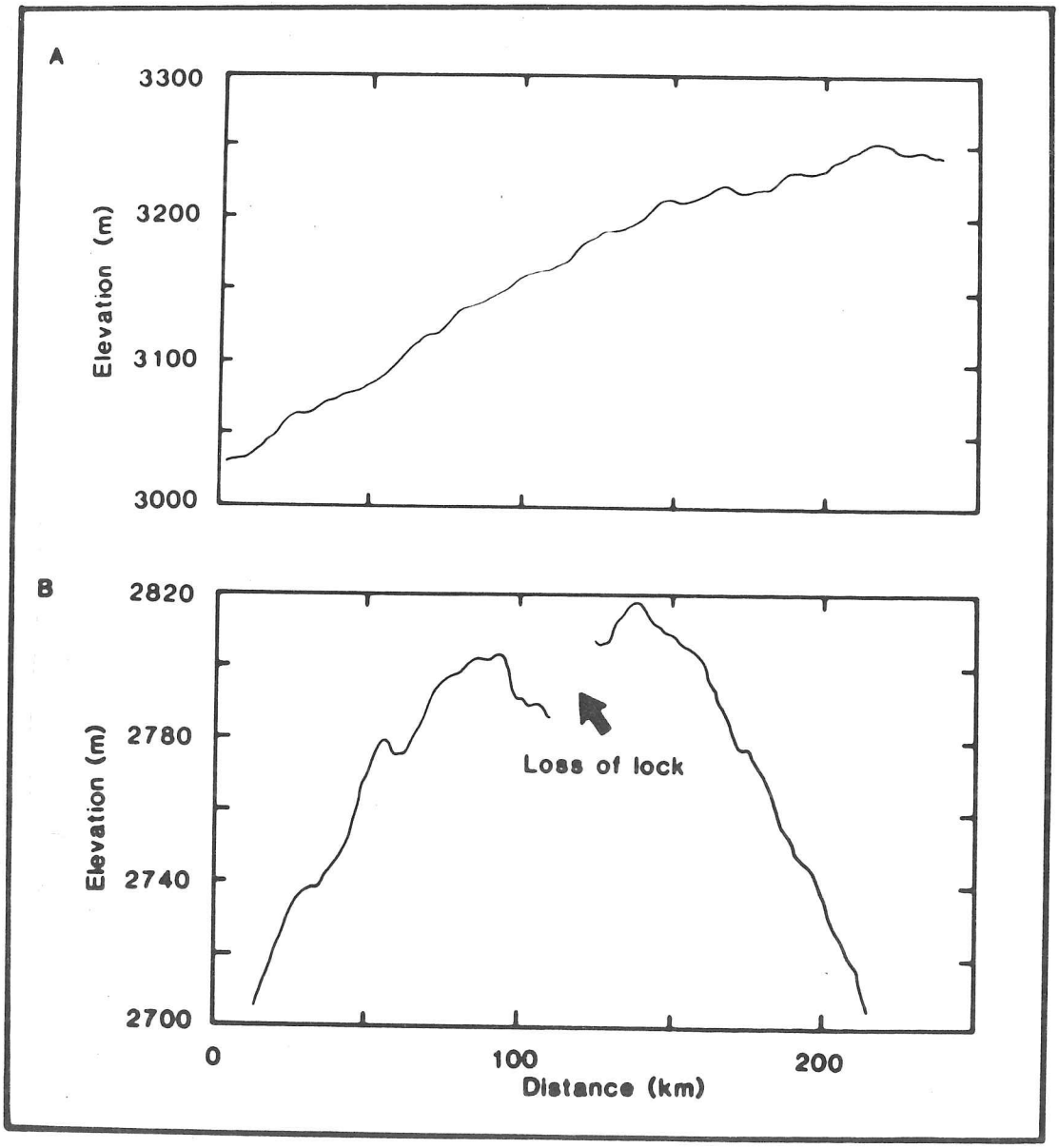

Figure 4.13: Seasat surface profiles from Princess Elizabeth and Enderby Lands where few other elevation observations are available.

4.5 A classification of topography

A knowledge of the distribution of topographic types is of glaciological interest in that it reflects variations in the factors controlling surface roughness which were introduced in section 1.4 and which will be discussed in chapter 5. It is also of value as an input to modelling, a base-line for the interpretation of remote sensing data and, as discussed in section 4.6, is necessary for the design specifications of remote sensing instruments such as radar altimeters.

4.5.1 Classes of topographic variability

The application of classificatory techniques to areal data presents problems, such as the arbitrary definition of classes which form part of a continuum. The technique adopted here has been to produce a three-fold division of the most common topographies present on the surface of the Antarctic ice sheet (Drewry and McIntyre, in press), as identified by the analyses in sections 4.2, 4.3 and 4.4. The limited spatial coverage of the altimetry was partially overcome by extrapolating outwards from the ARDS profiles by means of comparison with detail present on Landsat images (section 3.3).

Bandpass profiles seen to be representative of the three classes are given in figure 4.14. Differentiation was made on the basis of rms roughness, mean wavelengths, amplitudes and gradients and the curvature of undulations. Type 1 roughness has no deviations from the mean greater than about 4 m. The dominant wavelength is around 25 km, although undulations are present at a variety of scales. The Type 2 surface displays maximum peak-to-trough amplitudes of up to 15 or 20 m and deviations from the mean are concentrated in wavelengths of 15 to 25 km. The maximum local gradients may reach $\pm 2\%$. The radii of curvature of Type 3 surfaces is significantly less than for the other topographies. Amplitudes of over 60 m combine with wavelengths often less than 15 km to produce a notably rougher terrain which may display local gradients of up to $\pm 5\%$.

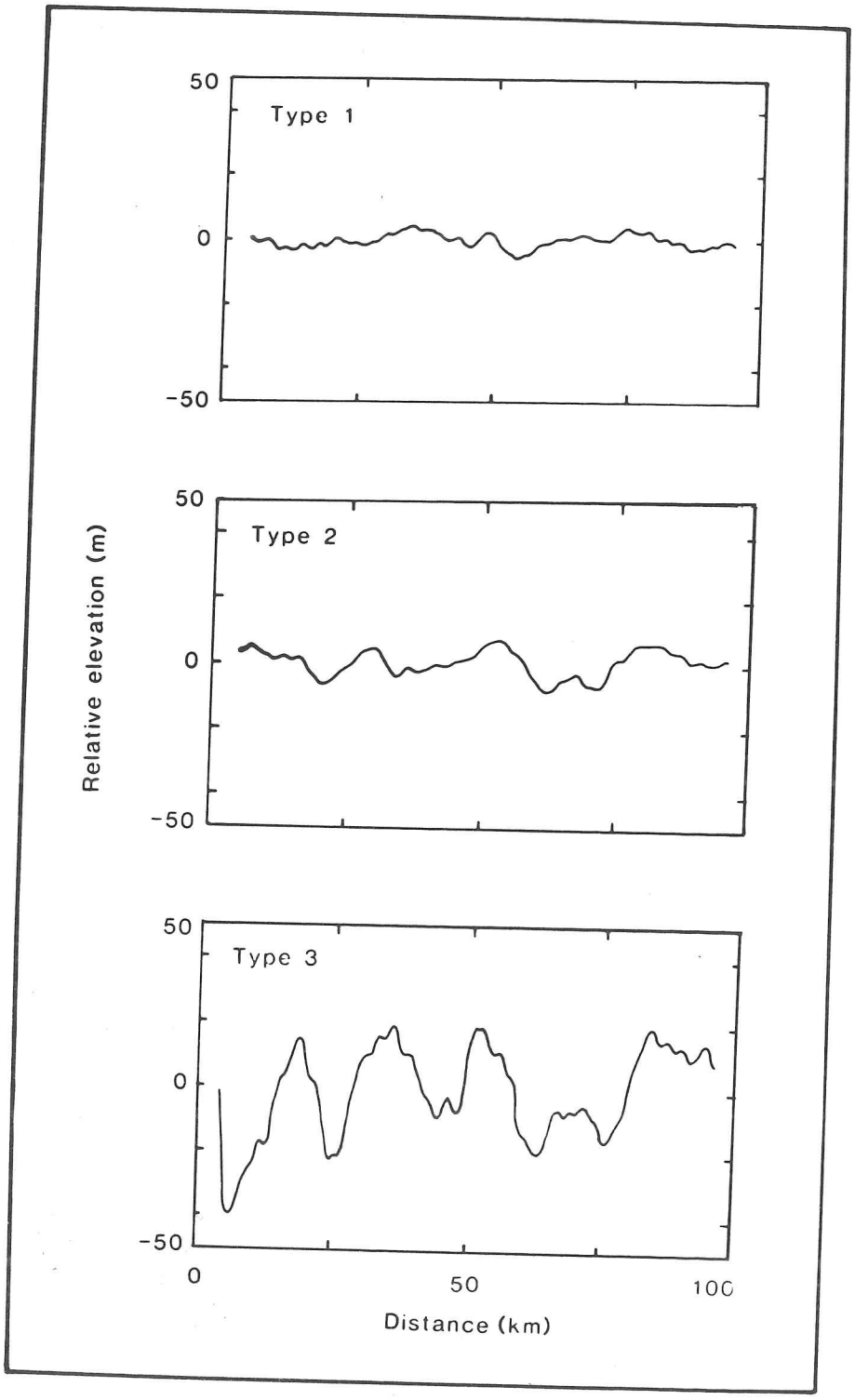

Figure 4.14: Surface profiles representative of the three terrain types chosen to indicate the continuum of surface roughness variation. Data have been bandpass filtered.

4.5.2 Spatial distribution of roughness

The areal distribution of the three topographic types is given in figure 4.15. Mapping of the small scale variations in topography has not been attempted. The significant local deviations and extreme examples which are known to exist within classes have not been taken into account at this scale.

The coastwards transition from smooth to increasingly rough terrain is clearly visible in much of East Antarctica, there being a close relationship between the occurrence of Type 1 terrain and the thick ice of the high, and hence cold, ice divides. Type 2 terrain forms an intermediate zone of variable width and Type 3 topography mirrors the coastal zone in a belt which is several hundred kilometres wide in much of East Antarctica. Further smooth terrain can be identified in Victoria Land, corresponding to the low velocities of two localised centres of outflow. The pattern is very much less clear in West Antarctica where the lower-lying, and hence warmer, ice divide is only picked out by two very narrow strips of the smoothest terrain category; for extensive areas, the centre of outflow is covered by the middle category of roughness reflecting the generally very severe basal topography and warmer ice. A proportionately large part of West Antarctica is covered by Type 3 terrain, generally in the coastal zone. One may clearly identify the heads of the Ross Ice Shelf ice streams and the contributing regions for the Ronne and Filchner Ice Shelves and Thwaites and Pine Island Glaciers. Within these areas, very severe topography occurs locally such as the profile down Thwaites Glacier (figure 4.9.G). One may also identify rough terrain near individual outlet glaciers and ice streams where converging ice flow produces high velocities; David and Slessor Glaciers and Ice Stream F are notable. Two large areas of Type 3 topography associated with thin ice and severe topography are well depicted. The subglacial Gamburtsev Mountains extend the roughest category of terrain of the Lambert Glacier region to within a few hundred kilometres of the ice divide at Ridge B (see figure 1.1); that part of the polar plateau feeding the Ronne and Filchner Ice Shelves is rougher than glaciologically comparable parts of East Antarctica.

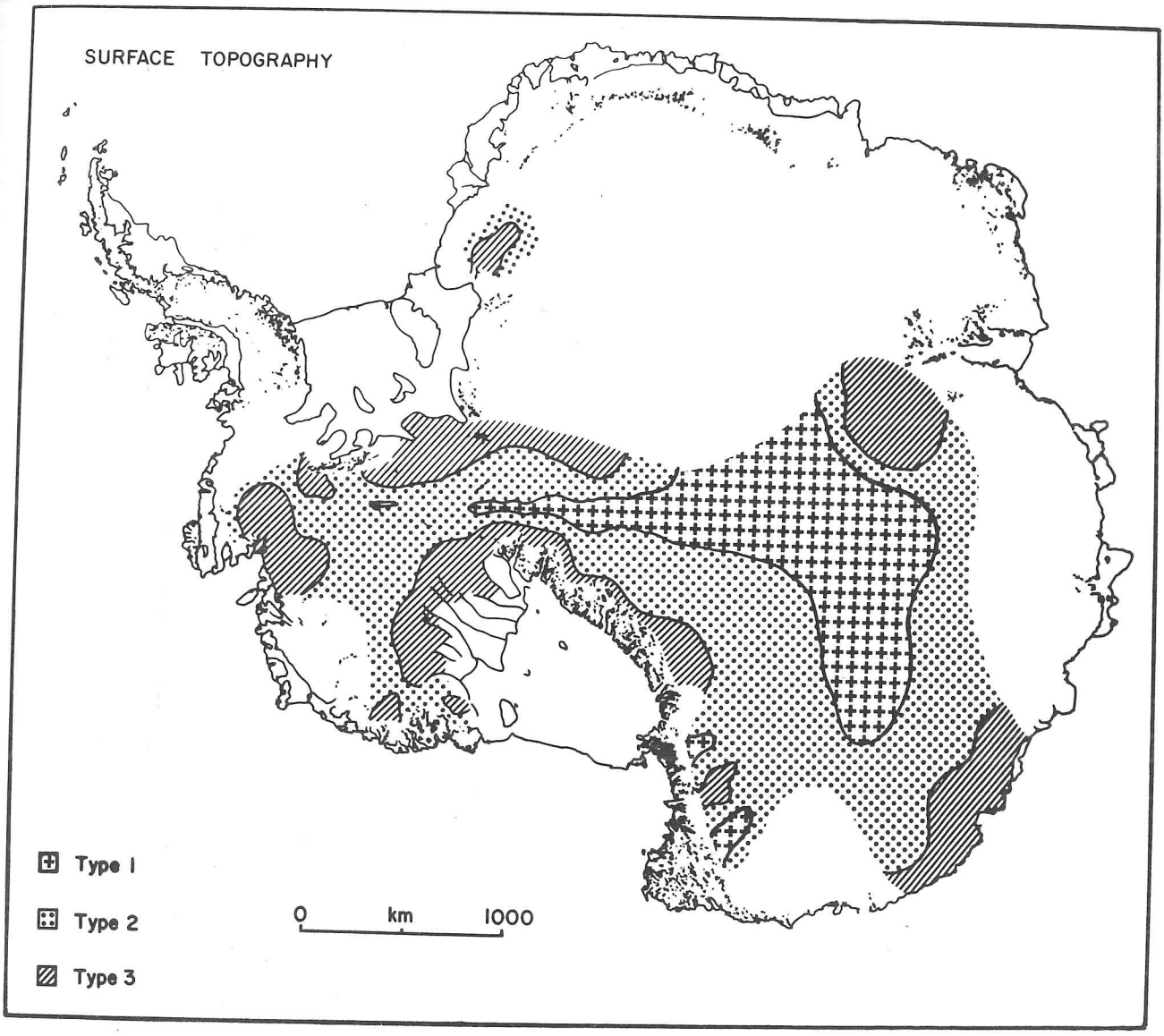

Figure 4.15: The areal distribution of the three types of terrain roughness which indicate the continuum of variations in surface roughness. Class boundaries have been defined from aircraft altimetry and Landsat. Significant local variability may occur within classes.

The above classification covers approximately 4.71 M km^2, that is 39.1% of the grounded ice sheet. The area of Type 1 terrain is 1.19 M km^2 (25.3% of the area of the classification), that of Type 2 is 2.49 M km^2 (52.9%), while the figure for Type 3 terrain is 1.03 M km^2 (21.8%). An accurate estimate of the likely figures for the whole continent is subject to the uncertainties involved in the extrapolation. However, using the patterns identified in that part of the continent already mapped, it seems likely that the proportions would be approximately 20%, 50% and 30% for topographies of Type 1, Type 2 and Type 3 respectively.

4.6 A surface model for satellite altimeter studies

4.6.1 Previous model

It is clear that remote sensing of the Antarctic ice sheet from space can offer the possibility of gathering much critical data needed for observational and theoretical developments concerning ice masses. Robin and others (1983) have listed the contributions that satellite techniques can make towards collecting the key glaciological parameters. To improve the ability of future satellite-borne sensors, in particular radar altimeters, to acquire accurate information from ice sheets, it is necessary to base their design specifications on realistic surface characteristics. The simulation of various tracker algorithms over such surfaces is also an important precursor to the interpretation of real data. Much of the analysis of Seasat data (Martin and others, 1983; Zwally and others, 1983; Brenner and others, 1983) was based on simulations using the three-dimensional model of Zwally and others (1981) which was generated on the basis of data from Greenland and the Antarctic. Undulations and sastrugi, superimposed on a parabolic surface, were expressed by:

$$\Delta z = \sum_{i=1}^{2} s_i \sin \frac{2\pi}{\lambda_i}(x/3+y) + \sum_{i=3}^{4} s_i \sin \frac{2\pi}{\lambda_i}(x+y/3) + \sum_{i=5}^{6} \left(\tfrac{5}{6} s_i + \frac{s_i}{2} \sin \frac{2\pi x}{10^5}\right) \sin \frac{2\pi}{\lambda_i}(x+y/3) \qquad [4.4]$$

where undulation wavelengths, λ_{1-6}, were 5 and 8 m, 0.7, 1, 7 and 12 km respectively and undulation amplitudes, s_{1-6}, were 0.1, 0.1, 0.2, 0.2, 5.0 and 4.0 m respectively. The uniform periodicities were acknowledged to be artificial. Figure 4.16 presents the overall form of the ice sheet with profiles in the x- and y-direction for both sastrugi and dynamic undulations.

4.6.2 A new model

Although the model of Zwally and others (1981) was intended for the modelling of Seasat radar altimeter returns rather than an accurate depiction of the exact surface of an ice sheet, it is apparent from sections 4.2 to 4.5 that there are a number of inaccuracies which should be taken into account. On this basis, a new ice sheet model was constructed (affecting the form of the previous one on several scales, largely to assist with development of the radar altimeter to be flown in the European Space Agency's ERS-1 satellite (Rapley and others, 1983; Drewry and McIntyre, in press).

Based on equation [1.4], which has been shown to be a good approximation of a general ice sheet profile, we take account of ice streams in the marginal parts of the ice sheet. Embayments are produced by adding a sinusoid in the cross-flow direction whose amplitude (A_x) varies down the flow direction. The overall equation for the geometry of the ice sheet is given by

$$z = Z(1-P_x^{1.3})^{1/2.7} - \frac{A_x(\cos 2\pi P_y - 1)}{2} \qquad [4.5]$$

where L is the half-width of ice sheet, Z is the maximum height of ice sheet, A_x is the amplitude of across flow sinusoid at distance x, W_y is the wavelength of across flow sinusoid, $P_x = x/L$ and $P_y = y/W_y$. A three dimensional representation is given in figure 4.17.A which shows four ice streams. This also includes a fringing ice shelf with a width of 5% of the maximum length of the ice sheet. Its height varies from 100 m at the inland

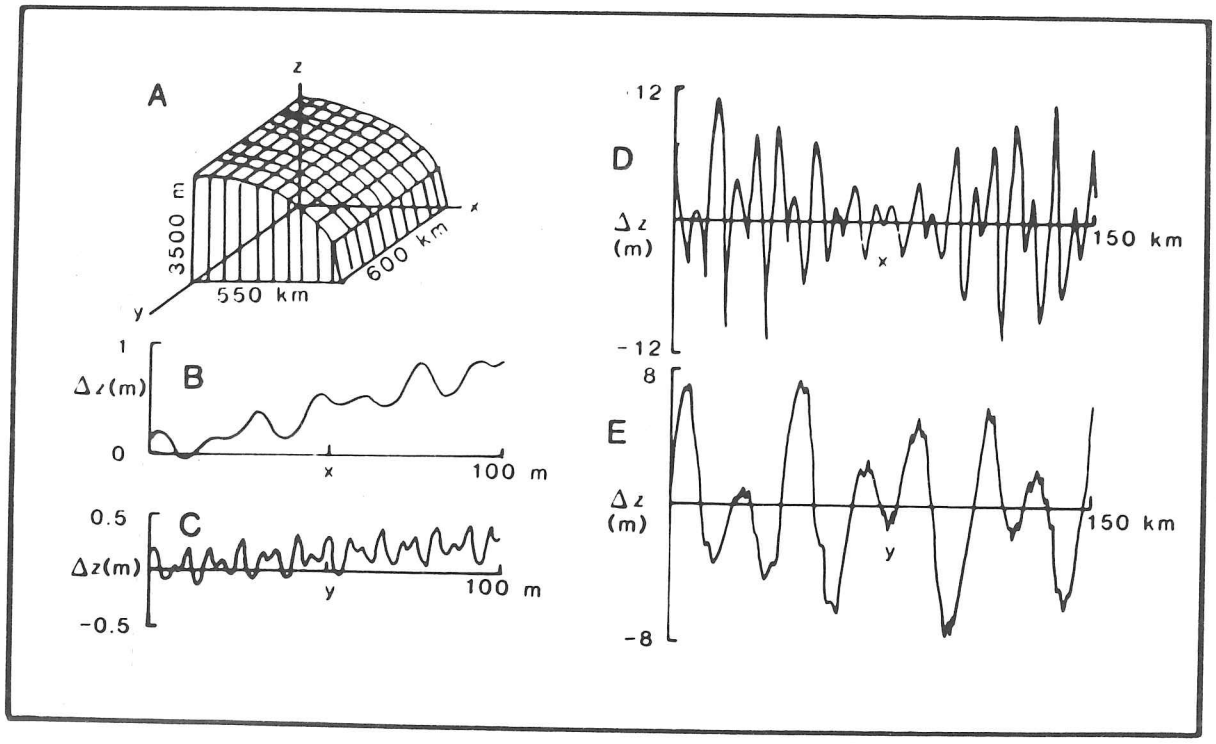

Figure 4.16: The three-dimensional model of Zwally and others (1981) used as the basis for the simulation of Seasat radar altimeter pulses (Martin and others, 1983; Brenner and others, 1983). A: overall form of the ice sheet on which undulations are superimposed. B and C: variations of elevations in x and y dimensions representing sastrugi and other snow features. D and E: variations in x and y dimensions representing ice flow features.

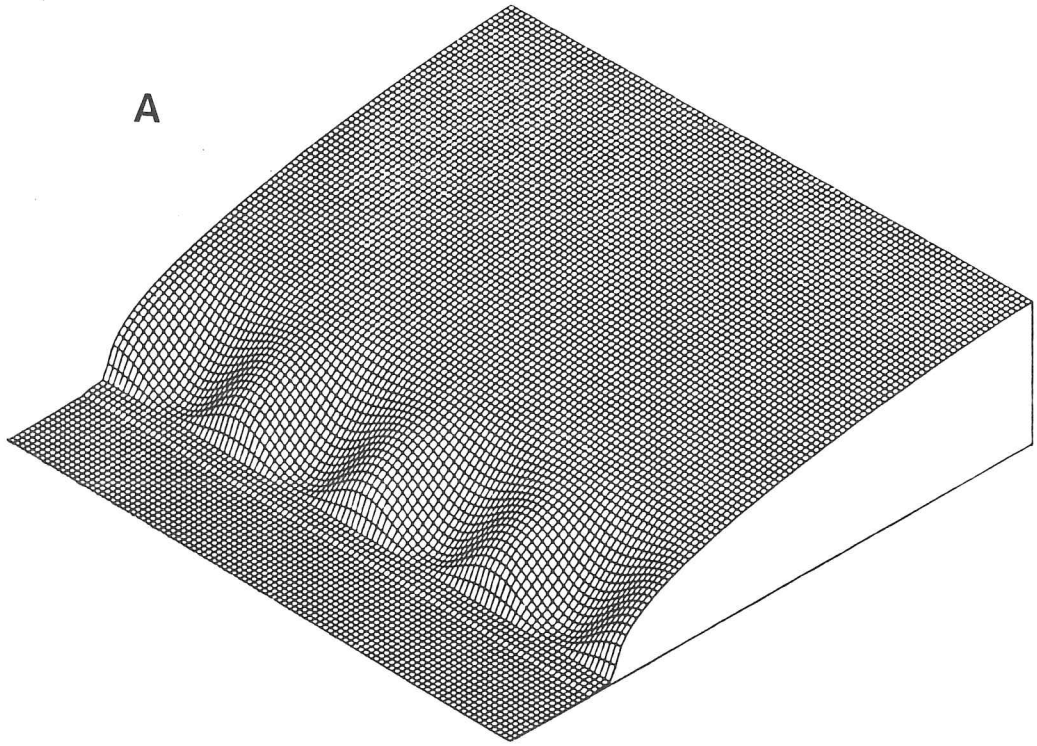

Figure 4.17: Improved statistical model of an ice sheet surface representing variations on a variety of scales. A: isometric view of the ice sheet with coastal embayments representing ice streams and with fringing ice shelf. 1000 km square with a maximum elevation of 3.5 km. B, C and D: isometric views surface topography resulting from ice flow variation from the ice divide, mid ice sheet and coastal region respectively. D also shows a fringing ice shelf with a peripheral cliff of up to 50 m. All are 100 km square with maximum elevations of 5, 20 and 50 m respectively. E: isometric view of tent-shaped variations which represent the continuum of sizes and shapes of sastrugi and other snow features. 100 m square with a maximum elevation of 3 m.

edge to 50 m at its seaward margin where it ends in a vertical cliff.

Another important modification of the model of Zwally and others (1981) is that we introduce amplitude variations in the x-direction of undulations. Thus, ice flow undulations are modelled by bell-shaped mounds offset by a Gaussian-controlled random amount from the centre of each grid cell. The equation for the height of a single undulation is:

$$\Delta z = \exp((-8\ x_{off}^2 + y_{off}^2)/G_s) \qquad [4.6]$$

where x_{off} and y_{off} are the x- and y-offsets from the centre of the undulation respectively and G_s is the grid spacing. The amplitude of each set of mounds, of which there are four, varies from the ice divide to the ice sheet margin. They have been chosen as representative of the data presented in this chapter. First, there is a 25 km grid whose amplitude increases linearly from zero to 20 m at the mid-point of the profile and then decreases to 5 m by the margin. Second, we add a 12.5 km grid whose amplitude rises from zero to 30 m at the margin as a function of x^3. Third, there is a 7.5 km grid which rises from zero to 15 m as a function of x^2 and, fourth, a 4 km grid, the amplitude of which ranges from 1 to 4 m linearly with x. On the fringing ice shelf, only one grid is used, with a spacing of 10 km and an amplitude of 3 m. The superimposition of these grids produces the coastwards development of shortening wavelengths and increasing amplitudes seen over a large proportion of the Antarctic ice sheet. Three isometric views of topography at the ice divide, in mid-ice sheet and in the coastal zone are shown in figures 4.17.B to D, illustrating the irregularity contributed by the four wavelengths and the random offset.

At the smallest scale, we allow for sastrugi and other snow features which are equivalent to the first two terms in equation [4.4]. Two sizes of feature have been chosen as representative of this continuum of features (E. Novotny, personal communication) which occurs naturally in the form of waves, ridges, ripples and hummocks and which reflects the prevailing direction and maximum strength of the wind. These are represented by tent-shaped mounds with wavelengths of 6 and 30 m and amplitudes of 1.2 and 2 m.

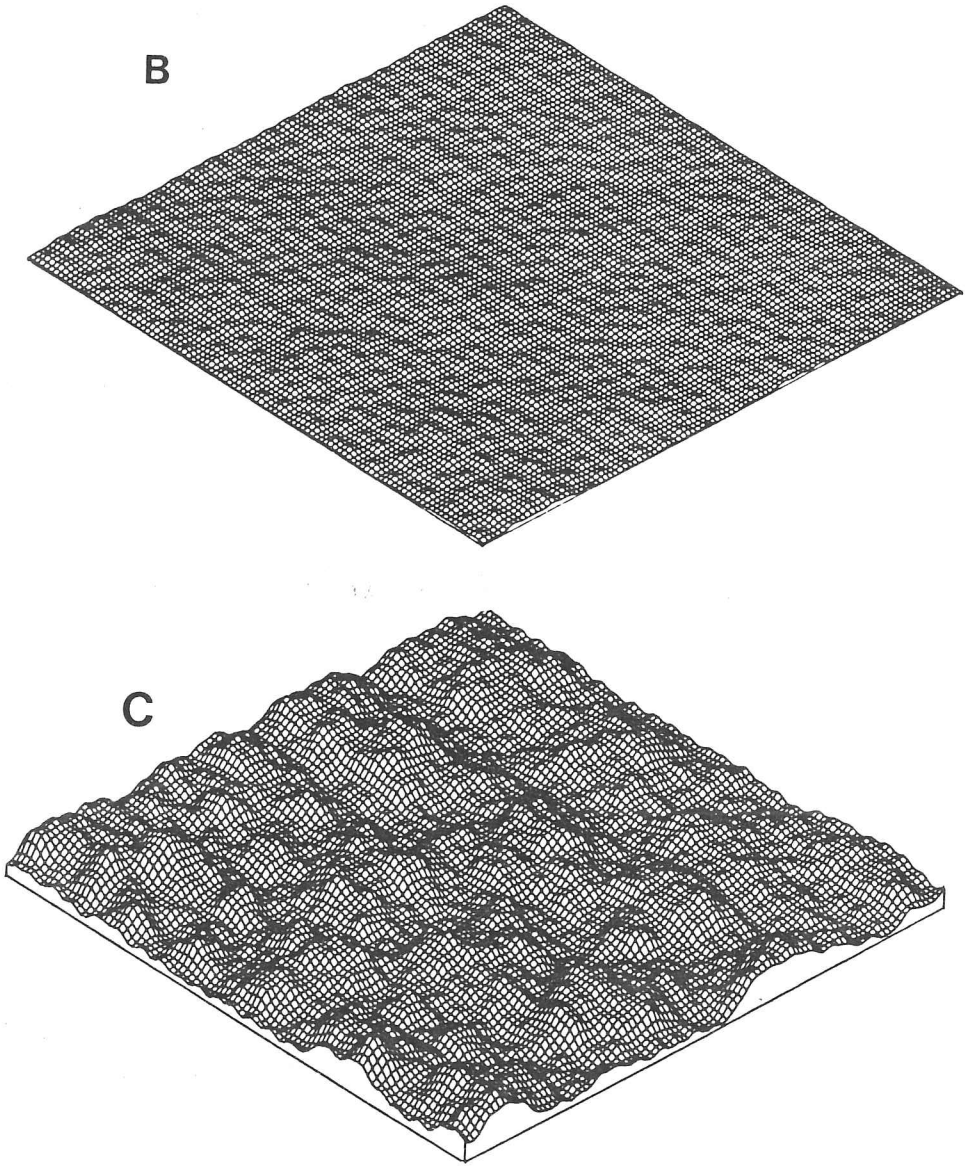

Figure 4.17 continued.

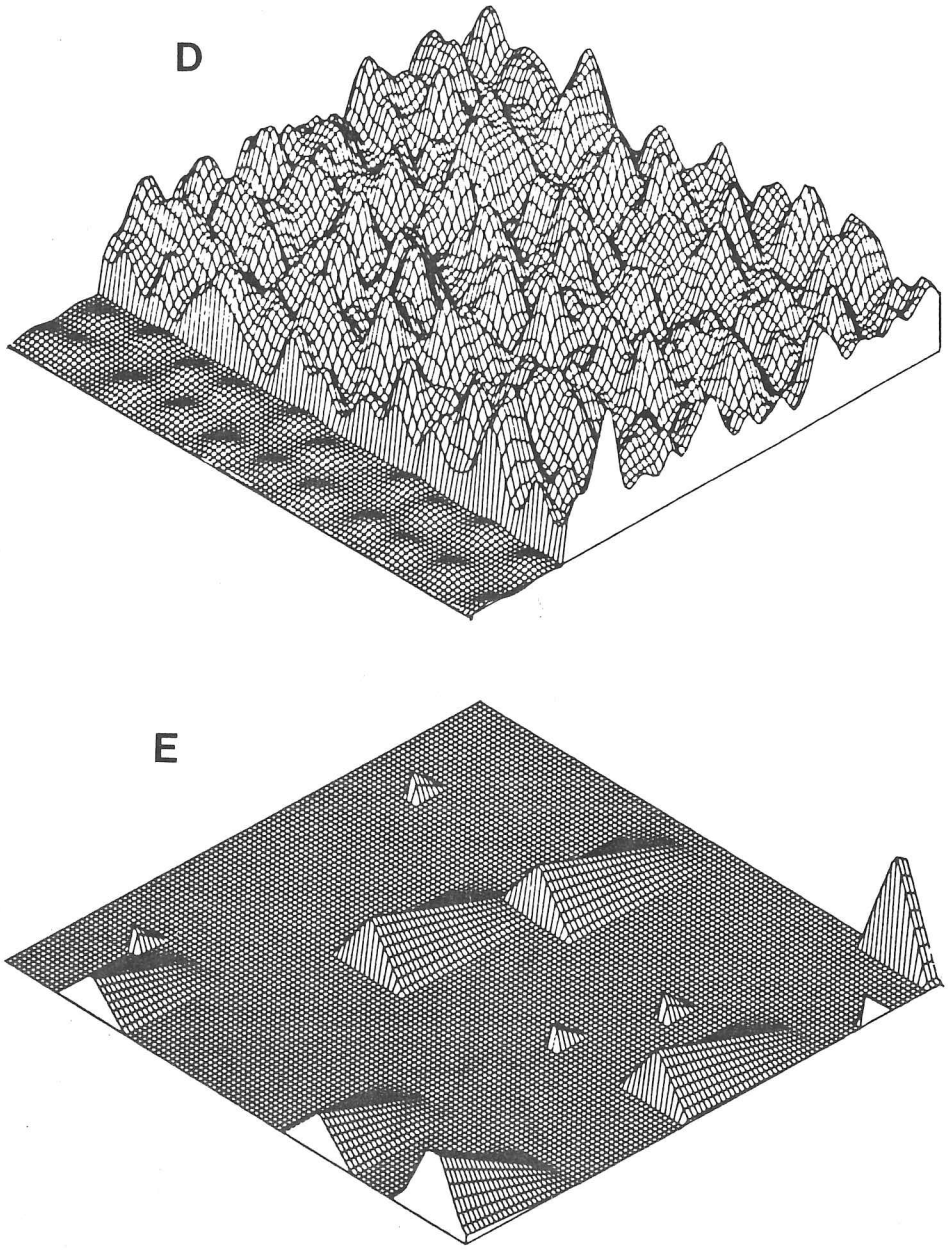

Figure 4.17 continued.

An isometric view is given in figure 4.17.E.

4.7 Summary

The combination of Landsat imagery and aircraft and Seasat altimetry has shown that there is typically a coastwards development in the surface topography of the Antarctic ice sheet with undulation wavelengths decreasing while amplitudes increase. Undulation isotropy indicates the similarity of stresses in longitudinal and transverse directions as ice flows over bedrock irregularities. The coastal region is punctuated by topographic embayments of severe terrain formed by converging ice flow which feeds ice streams and outlet glaciers. Ice streams and flowlines may display distinct, crevassed margins and, in cases, can be traced several hundred kilometres into the ice sheet. The pattern of coastwards development in topography may be significantly distorted by regional variations in ice thickness, temperature and velocity.

This topographic variability has been summarized in a three-fold classification of surface roughness representative of regional terrain differences. It is estimated that over half of the Antarctic ice sheet is covered by the intermediate topographic class. A statistical representation of these variations has been developed as a basis for the simulation of satellite radar altimeter returns over ice sheets. This differs from previous models in that it incorporates coastal embayments representing ice streams, a fringing ice shelf with a peripheral cliff and a random component in the location of undulations which are represented by a series of isotropic mounds of varying dimensions.

CHAPTER 5

FACTORS AFFECTING SURFACE TOPOGRAPHY

5.1 Introduction

This chapter attempts to bring together new observations from radio echo sounding and altimetry which are relevant to the form and flow of the Antarctic ice sheet. The extensive raw data, largely in the form of upper and lower surfaces of the ice sheet, are used to test existing models of surface-bedrock relationships and to indicate which of these describes observations more accurately. Deductions are made about the importance and variability of other factors involved such as ice thickness, temperature, bedrock roughness and basal water.

5.2 Models of bedrock-surface relationships

The relationship between the surface and bedrock profiles of ice sheets has been demonstrated on the large scale by several authors (Bourgoin, 1956; Hochstein, 1967) using equation [1.4] which relates surface slopes and ice thickness. In particular, it has been noted that the steepest surface slopes tend to occur over the highest points of the bedrock (Robin, 1958; Budd, 1966, 1969; Beitzel, 1970). Typical confirmation from our results is given by mean slopes from surface and bedrock profiles down a flowline to Reedy Glacier (figure 5.1.A). This is illustrated more clearly by a graph of mean surface slopes against mean bedrock slopes calculated over 40 km segments (figure 5.1.B). Assuming surface and bedrock profiles with regular undulations 90° out of phase, that is, with maximum surface slopes above bedrock peaks, the relationship between slopes of the two surfaces will be described by a ellipse. When these surface wavelengths are superimposed on an increasing mean gradient to

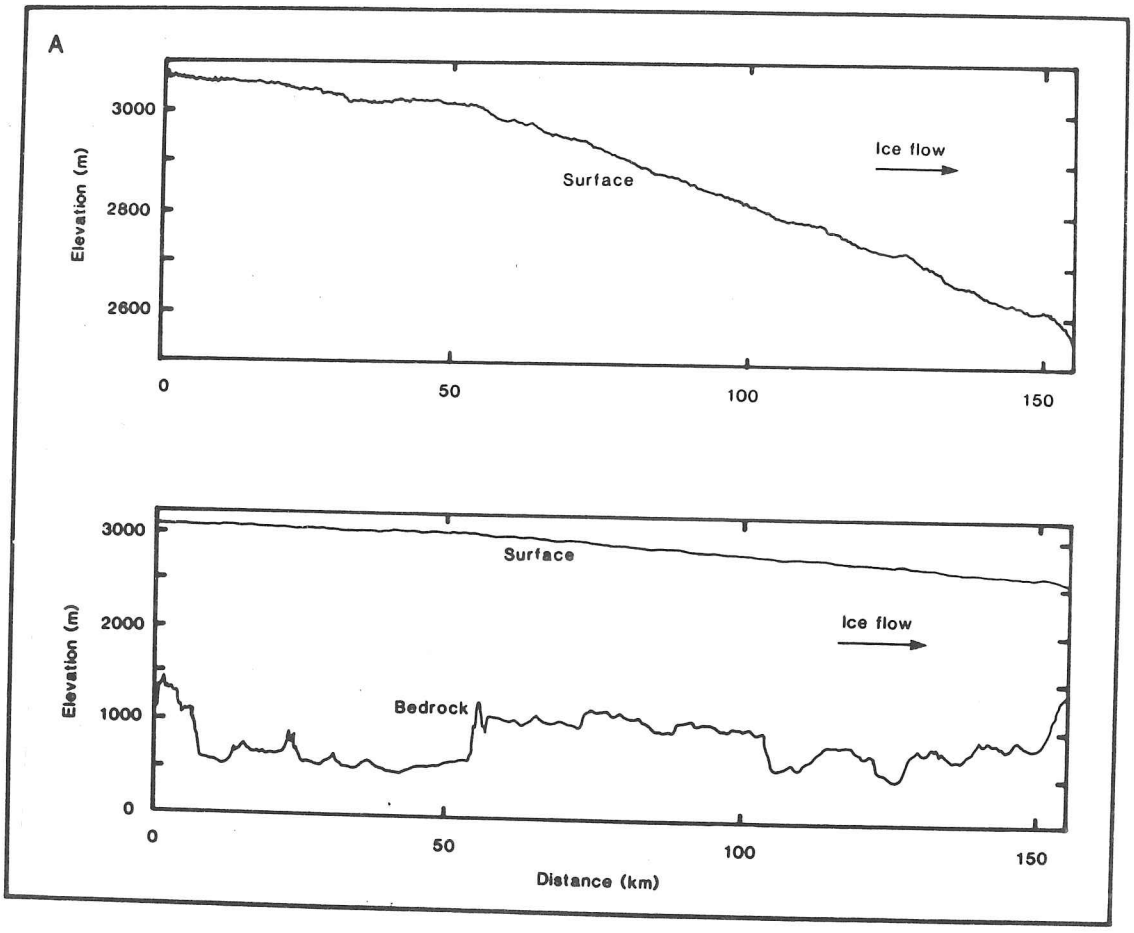

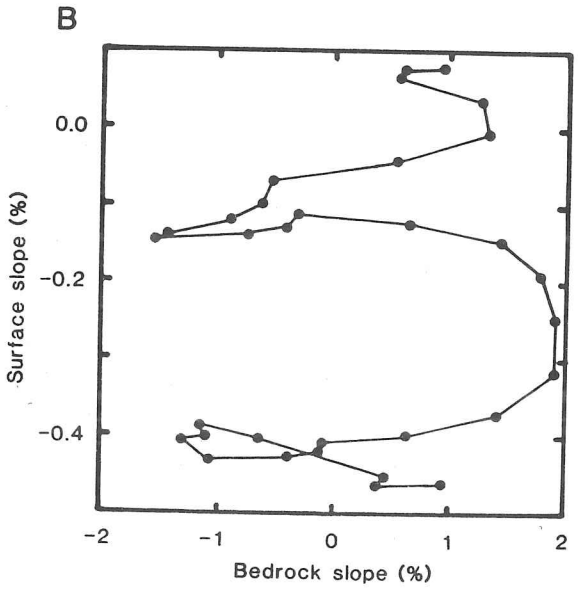

Figure 5.1: A: profiles of the ice sheet down a flowline leading to Reedy Glacier. Lower figure shows bedrock and surface profiles from radio echo sounding and aircraft altimetry respectively. Upper figure shows the surface with an expanded vertical scale. B: the relationship between mean surface and bedrock slopes from the profiles in A calculated over 40 km segments.

account for the regional ice sheet slopes, this should tend towards a cycloid, as shown for Reedy Glacier (figure 5.1.B). Thus, the mean slopes over about 20 times the ice thickness in this profile are approximately described by the form of equation [1.4]. Deviations from the expected relationship may be the result of the departure of the profile from the flowline or the effects of ice flow in three dimensions. More importantly, longitudinal stress gradients (Robin, 1967) may produce local slopes of over 2% on the mean gradient of less than 0.5% and negative slopes. This is discussed further in section 6.3.

A more precise relationship between bedrock and surface amplitudes has been described in terms of ice thickness relative to bedrock wavelengths, mean velocity and viscosity (Budd, 1969, 1970). This transfer function, the damping factor, Ψ, is defined as

$$\Psi = \frac{\rho g z^2}{2\pi\eta u} \quad \frac{(e^{\omega z} - e^{-\omega z})}{(\omega z)^2} \qquad [5.1]$$

where η is the mean viscosity through the ice column, λ is the undulation wavelength and $\omega = 2\pi/\lambda$. It predicts the rapid damping of short wavelengths (figure 5.2.A) as a function of $e^{\omega z}$ and that, for a uniform bedrock distribution, surface amplitudes relative to bedrock amplitudes will be greatest for undulation wavelengths about 3.3 times the ice thickness. This was confirmed by Budd and Carter (1971) using data from Greenland and Law Dome, Antarctica, and by Beitzel (1970) with results from Dronning Maud Land. These observations enabled comparison of observations with the theoretical curve over the range 400 m to 100 km, or between 0.5 and 20 times the ice thickness (figure 5.2.A). It should be noted that the three points from Beitzel's data not included by Budd and Carter have been added and that Beitzel himself omitted two further, seemingly anomalous points. The observations agree fairly well with the theory, but a symmetric curve with a broader peak of greater maximum value would also fit the data.

In a more recent analysis, Hutter and others (1981) derived a filter function, F, which defined the fraction of bedrock amplitudes transmitted

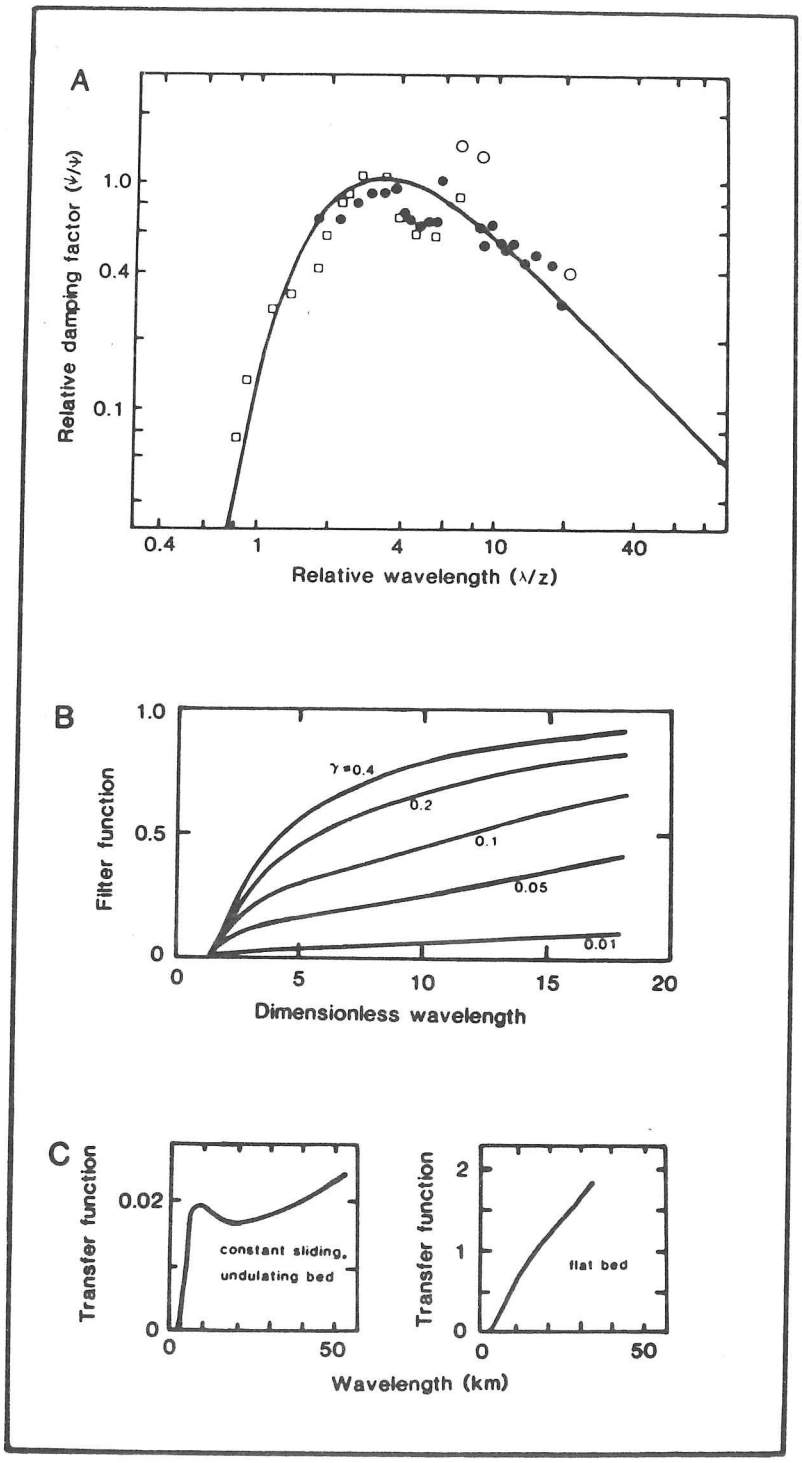

Figure 5.2: Models of the transfer of bedrock undulations to the ice sheet surface. A: relative damping factors against relative wavelengths, redrawn from Budd and Carter (1971). Filled circles from Dronning Maud Land (Beitzel, 1970); squares from Law Dome (Budd and Carter, 1971); open circles are Beitzel's data points omitted by Budd and Carter. B: filter function of Hutter and others (1981) showing the proportionate response of the surface to bedrock undulations of various dimensionless wavelengths, as a function of slope, γ. C: transfer functions of Whillans and Johnsen (1983) which are defined individually for each glaciological regime.

to the ice sheet surface at certain wavelengths. Assuming an ice mass which behaves as a Navier-Stokes fluid,

$$F = \frac{| 4\omega\,\Omega_1 \sin\gamma + 2u\omega^2\Omega_2 |}{\left[(\sin\gamma + u)^2 + (\cos\gamma)\,\Omega_4^2/\omega^4\right]^{1/2}} \qquad [5.2]$$

where $\Omega_1 = \cosh\omega\,/(2\omega\overline{\Delta})$

$\Omega_2 = (\cosh\omega + \omega\sinh\omega)/(2\omega^2\overline{\Delta})$

$\Omega_4 = (\omega - \cosh\omega\,\sinh\omega)/\overline{\Delta}$

$\overline{\Delta} = \cosh^2\omega + \omega^2$

γ = inclination of the ice mass.

Hutter and others concluded that the transfer of bedrock irregularities to the ice sheet surface is proportionate to the undulation's wavelength (figure 5.2.B). There is thus no preferred surface wavelength in relation to the ice thickness. Although applying to bedrock and ice surfaces which are almost parallel and to small bedrock undulations relative to the ice thickness, this model has broader applications in that it encompasses flow by sliding or by internal deformation (cf. Budd, 1970; Hutter and Spring, 1979). The filter function is strongly dependent on the inclination of the ice mass but, as velocity increases, the importance of inclination is reduced. Damping is also increased by vertical temperature gradients within the ice mass. Although the transfer function typically increases monotonically with wavelength, it seems that with basal sliding and certain mean inclinations, the predominant transfer of wavelengths 3 to 5 times the ice thickness may occur; this may also be amplified by temperature differences. Hutter and others (1981) therefore regarded the results of Budd (1970) as a special case.

Whillans and Johnsen (1983) developed a further theory of bedrock-surface relationships in which flow variations were superimposed on an average regime. The approach, mathematically equivalent to that of Hutter and others (1981), involved using measured surface and bedrock profiles to indicate the differences in basal regime that cause the observed ice flow variations. This method has the advantage of not having to first discuss

the physics of basal conditions. Instead, the resulting basal variations were used to infer some features of the dominant physical processes. The model points to the effects of types of motion at the bed; variations in shear stress and sliding along the Byrd Station Strain Network, Antarctica, were found to be of greater direct importance to the resulting surface terrain than was the flow of ice into and out of basal topography. The transfer function, defined differently for separate glaciological regimes but each time giving the proportionate response of the surface to bedrock undulations, showed that ice flow was affected by more extensive basal topography. Two extreme models, believed to bracket the behaviour of real ice masses, are shown in figure 5.2.C. The transfer function is defined for the constant sliding model by the ratio of surface to bedrock amplitudes and, for the flat bed model, as the ratio of surface loading (which is linearly related to surface relief) to the principal component (the sine term) of the basal shear stress variation. Neither model shows an absolute maximum at three ice thicknesses, although there is a minor peak at this wavelength in the constant sliding model. The dominance of these surface wavelengths, as found by Budd and Carter (1971), were attributed by Whillans and Johnsen (1983) to factors such as the dynamics of glacial erosion and deposition or to subglacial water motion.

Vertical variability of ice rheology, thought to be particularly important to the dynamics of polar ice sheets (Robin and Millar, 1982), points to the value of multi-layer models which can incorporate variations in viscosity and velocity with depth. The applicability of this concept was shown by Overgaard and Rasmussen (1979) who found essential agreement with the theory of Johnsen and others (1979); changes of the transfer function along the flowline traversed by the Expeditions Glaciologique International au Groenland (EGIG) were attributed to a varying velocity profile. A more detailed analysis of a similar model has been possible along the International Antarctic Glaciological Project (IAGP) flowline in Wilkes Land using measurements of surface slope, ice thickness and velocity over a 30 km section (Young and others, in press). Given the bedrock topography and large scale flow parameters, the model closely predicted the measured surface profile when the variation of the

the physics of basal conditions. Instead, the resulting basal variations were used to infer some features of the dominant physical processes. The model points to the effects of types of motion at the bed; variations in shear stress and sliding along the Byrd Station Strain Network, Antarctica, were found to be of greater direct importance to the resulting surface terrain than was the flow of ice into and out of basal topography. The transfer function, defined differently for separate glaciological regimes but each time giving the proportionate response of the surface to bedrock undulations, showed that ice flow was affected by more extensive basal topography. Two extreme models, believed to bracket the behaviour of real ice masses, are shown in figure 5.2.C. The transfer function is defined for the constant sliding model by the ratio of surface to bedrock amplitudes and, for the flat bed model, as the ratio of surface loading (which is linearly related to surface relief) to the principal component (the sine term) of the basal shear stress variation. Neither model shows an absolute maximum at three ice thicknesses, although there is a minor peak at this wavelength in the constant sliding model. The dominance of these surface wavelengths, as found by Budd and Carter (1971), were attributed by Whillans and Johnsen (1983) to factors such as the dynamics of glacial erosion and deposition or to subglacial water motion.

Vertical variability of ice rheology, thought to be particularly important to the dynamics of polar ice sheets (Robin and Millar, 1982), points to the value of multi-layer models which can incorporate variations in viscosity and velocity with depth. The applicability of this concept was shown by Overgaard and Rasmussen (1979) who found essential agreement with the theory of Johnsen and others (1979); changes of the transfer function along the flowline traversed by the Expeditions Glaciologique International au Groenland (EGIG) were attributed to a varying velocity profile. A more detailed analysis of a similar model has been possible along the International Antarctic Glaciological Project (IAGP) flowline in Wilkes Land using measurements of surface slope, ice thickness and velocity over a 30 km section (Young and others, in press). Given the bedrock topography and large scale flow parameters, the model closely predicted the measured surface profile when the variation of the

accumulation rate over undulations was also considered. A further step in the development of such models (G.deQ. Robin, personal communication) will be to incorporate data on the dimensions of internal layers as seen by radio echo sounding. This will take account of the transition between shear controlled by bedrock surfaces and shear controlled internally due to mean surface slope which takes place at a relatively sharp boundary around the upper limit of the basal echo-free zone (Robin and Millar, 1982) (section 6.3).

5.3 Ice thickness and bedrock topography

5.3.1 Relationship between surface undulation wavelength and ice thickness

Budd's (1970) treatment of surface-bedrock relationships was based on the dominant transmission of particular bedrock wavelengths relative to the ice thickness. Although his analysis did 'not make clear why ice sheets behave in this way' (Paterson, 1981, p167), observations have confirmed the predictions.

The dominant wavelengths identified in statistical and spectral analyses in chapter 4 and from the traverse data of figure 1.7 are plotted against mean ice thickness in figure 5.3 with data from other sources. A certain amount of scatter is to be expected because of the averaging of ice thickness values and the different errors of each source. There appears to be a relationship between the dominant wavelength and ice thickness, although this connection was not derived from the models of Hutter and other (1981) and Whillans and Johnsen (1983). However, Budd's (1970) linear relationship does not adequately describe the full range of data presented here and a higher-order curve would appear to be more appropriate. The slight grouping of results from each source is a result of the variable bias in each type of observation. For instance, it is difficult to identify undulations on Landsat imagery other than where local and regional slopes are steep compared to the solar elevation. Observations from Landsat will therefore be grouped in the thin ice of coastal regions where amplitudes and

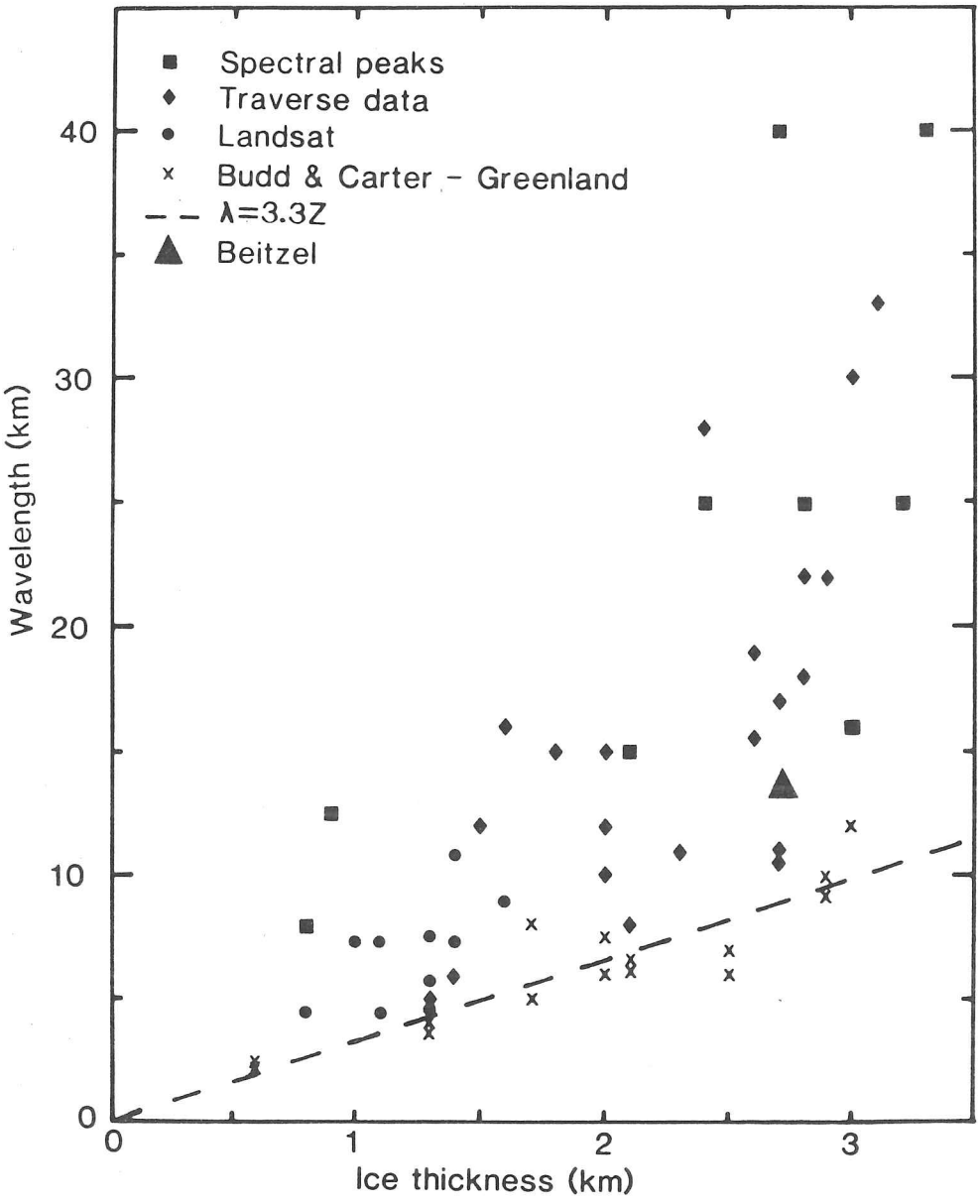

Figure 5.3: Relationship between mean ice thickness and undulation wavelengths. Dashed line is the expected relationship of Budd (1970). Data collected as follows: spectral peaks - section 4.3.3; traverse data - figure 1.7; Landsat - table 4.2; Budd and Carter (1971); Beitzel (1970).

regional slopes are greatest and dominant wavelengths are shortest.

Taking the λ/z ratio from this data, we can determine whether there is a relative wavelength for which damping is at a minimum. The maximum of Budd's Ψ function is broad and ψ is within 90% of its peak for wavelengths of between 2.4 and 4.5 times the ice thickness. The present data, which come from a wide variety of glaciological regimes in the Antarctic, indicate that there is a peak but that it is less clearly defined and of greater magnitude. The mean ratio of wavelength to thickness is 7.5 with a standard deviation of 3.5. The more vaguely phrased conclusion from Budd's (1969) analysis, that 'surface undulations of wavelengths 2 to 10 times the ice thickness may tend to be predominant' (p163), seems to be a more appropriate summary of the relation between ice thickness and surface undulation wavelength. Although 86% of the present data conform to this prediction, the apparent detection of this minimum may be due to the limited range of relative wavelengths being dealt with and more rigorous testing of the above models is necessary.

The lack of agreement between Budd's predictions and observations may result from the breakdown of assumptions. In particular, these include a uniform distribution of bedrock elevations, a uniform ice mass and motion resulting from sliding at the bed. Violations of these may limit the model's usefulness more than those of Hutter and others (1981) and Whillans and Johnsen (1983) which have less stringent restrictions.

5.3.2 Surface and bedrock slope distributions

The nature of the bedrock-surface relationship may be further considered through slope distributions. Figure 5.4 presents distributions of 1 km slope segments down flowlines for the surface and bedrock from a variety of glaciological regimes. It should be noted that in none of the four examples does the bedrock have the uniform distribution assumed by Budd (1970). The closest relationship between surface and bedrock slopes (plot B), as seen by the similar shapes of their distributions, suggests a linear response of the surface to the bedrock in areas of low basal relief and thick, cold ice. A similar regime over severe subglacial terrain

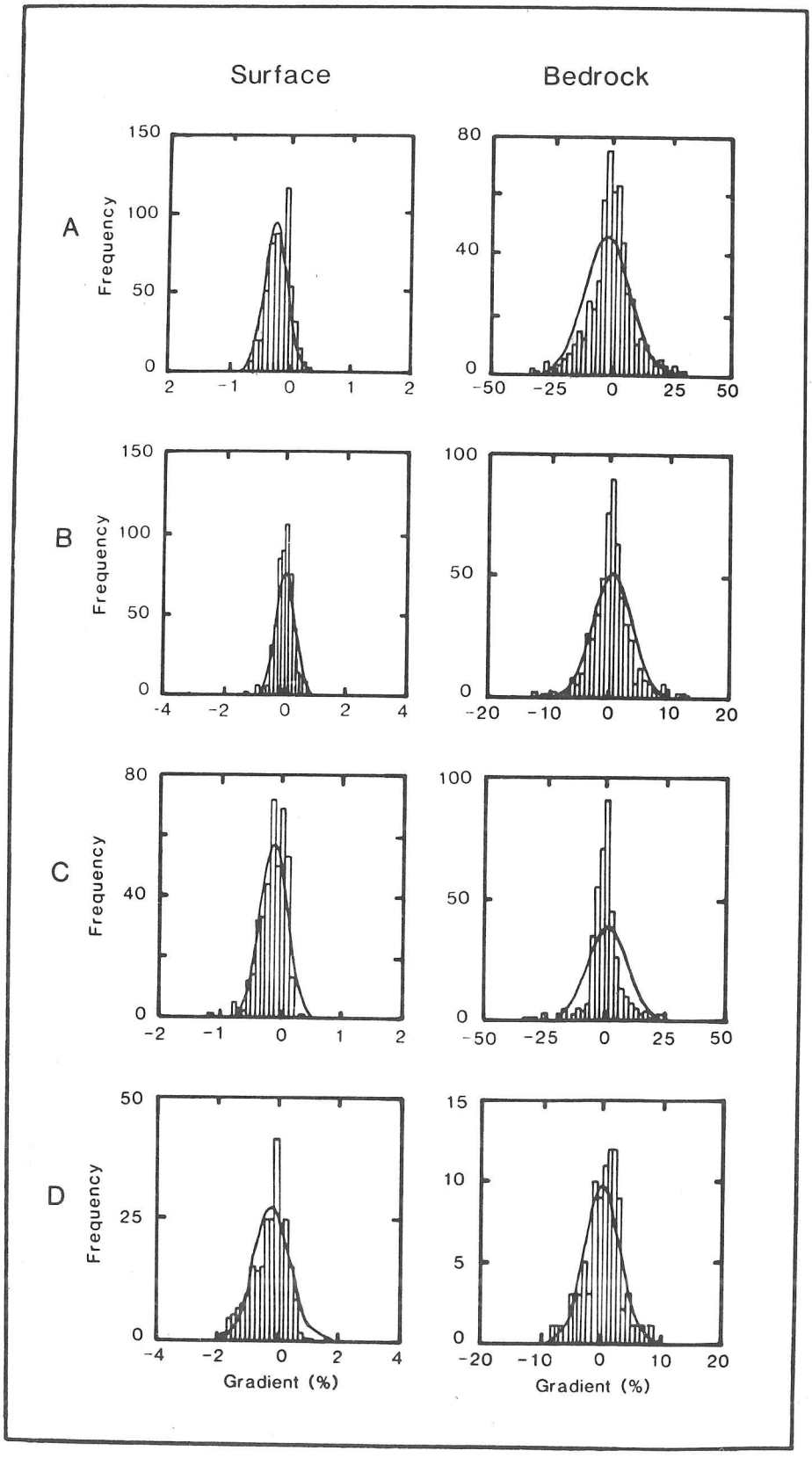

Figure 5.4: Histograms of slopes from surface and bedrock profiles down flowlines. Gaussian functions have been added to aid comparison. A: down flowline from Ridge B; B: mid East Antarctic Ice Sheet (80°S 150°E); C: down flowline leading to Reedy Glacier; D: Thwaites Glacier.

(plot A) indicates less response of the surface to the steepest bedrock slopes. This may be due to intense, horizontal shear zones within the ice (Gow and Williamson, 1976) produced by substantially unbalanced longitudinal and vertical stresses in severe topography; these create a false bottom below which ice is less active (Colbeck and others, 1978), and hence a smoother effective bed. This effect may also be seen in the severe terrain upstream of Reedy Glacier (plot C) where the steepest bedrock slopes are not reflected at the surface. The substantial non-linear damping in this thin ice may also be the result of the high mean viscosity of the ice column (discussed below in section 5.3.3) which inhibits the transfer of basally derived stresses to the surface (Hutter and others, 1981; Whillans and Johnsen, 1983). Plot D, which descends to the grounding line of Thwaites Glacier, has an asymmetric surface distribution due to the high regional slope. Strong bedrock reflections from radio echo sounding records suggest motion is by basal sliding due to water lubrication. The comparative similarity of this bedrock-surface relationship to the others illustrated (for instance, plot B) supports the suggestion of Hutter and others (1981) that the distinction between motion due to basal sliding and internal deformation is not a primary influence of the transfer function.

5.3.3 Surface response to bedrock undulations

Spectral analysis has been used by several authors (Beitzel, 1970; Ishida, 1970; Budd and Carter, 1971) to investigate relationships between surface and bedrock amplitudes and in order to estimate mean flow parameters. The main limitation for the present data involves incomplete migration of the profile (section 2.1). Layering within the ice mass with amplitudes often several hundred metres greater than those of the bedrock suggest that the true basal profile has not been produced by deconvolution and that echoes from valleys are still partly obscured by hyperbolae from adjacent peaks.

Spectral and cross-spectral analyses were carried out on bandpass filtered data of surface and bedrock (and, where possible, the lowest

layer) and frequency response functions were calculated. These are presented as non-dimensional gain factors which indicate the proportionate magnitude in output (profiles of surface and lowest layer) for a unit change in input (profiles of lowest layer and bedrock) at any given frequency (Bennett, 1979). They are therefore directly equivalent to the transfer functions of Hutter and others (1981) and of Whillans and Johnsen (1983). Results from three profiles are shown in figure 5.5 and physical parameters relevant to the models of Budd (1970), Hutter and others (1981) and Whillans and Johnsen (1983) are given in table 5.1. It should be noted that the application of cross-spectral analysis to ice sheet surface and bedrock profiles where ice moves entirely by sliding was not possible since this mode of movement is typically associated with heavy crevassing which prevents the detection of bedrock echoes as a result of scattering. Also, radio echo sounding cannot detect features in the bedrock profile less than a critical wavelength, λ_c, such that the radius of curvature at the bottom of the hollow equals the ice thickness (Budd, 1969). Thus

$$\lambda_c = 2\pi (b z)^{1/2} \qquad [5.3]$$

where b is the bedrock amplitude. This defines the minimum valid wavelength which can be derived from radio echo sounding records. Thus, the minimum detectable wavelength for bedrock undulations with amplitudes of 50 m under 1500 m of ice is 1720 m.

Gain factors for the three bedrock-surface cross-spectra in figure 5.5 show general trends of increasing response with undulation wavelength. This was predicted by Hutter and others (1981) and, in certain circumstances, by Whillans and Johnsen (1983). The three plots (particularly D and G) show peaks at several wavelengths and this is also consistent with the conclusion of Hutter and others. In none of the bedrock-surface plots, however, is there a maximum at about three ice thicknesses as suggested by Budd (1970). This is held to be a more rigorous test of Budd's concepts than the use of individual λ/z ratios described above; it indicates that the present data support the use of the

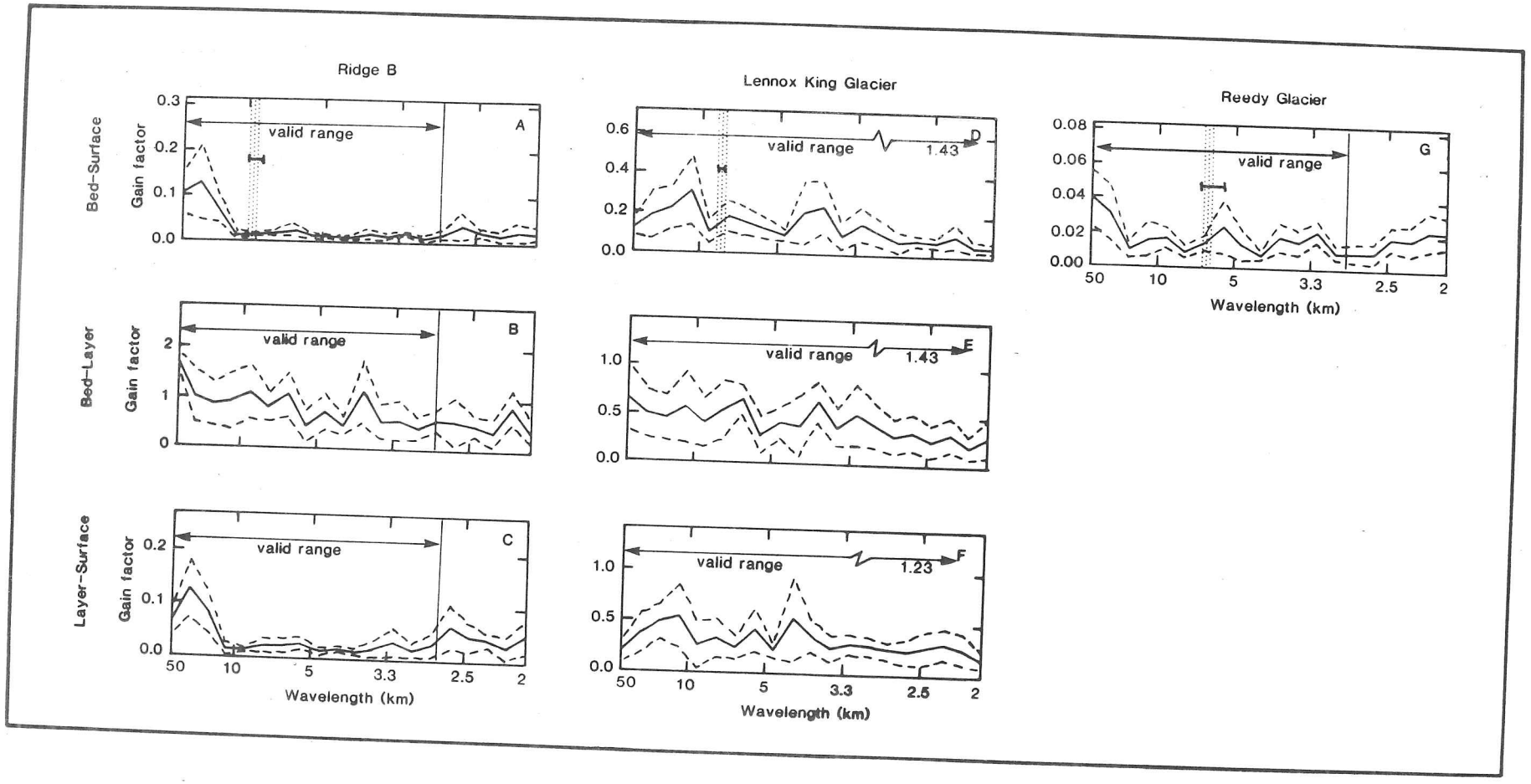

Figure 5.5: Frequency response functions of profiles of bedrock, lowest layer and ice sheet surface down flowlines expressed as non-dimensional gain factors against undulation wavelengths. Valid ranges are defined by equation (5.3). Vertical dotted lines show the expected maximum response of the surface to bedrock of 3.3 ice thicknesses as predicted by Budd (1970) with a range of ±10%. Dashed lines show 95% confidence limits.

model of Hutter and others (1981).

Where the valid range of wavelengths permits (plot D), there is relatively little response of the surface at wavelengths less than the ice thickness of 2450 m. The bedrock-layer gain factors (plot E) show that the shortest wavelengths are damped out in the basal zone while longer wavelengths are transmitted with less attenuation. The generally high response of the layer to the bedrock confirms that the basal ice appears to be a zone of low viscosity (table 5.1) which reacts sensitively to the bedrock profile. However, as the upper body of the ice mass reacts more as a rigid slab to basally generated stresses, increasingly long wavelengths are filtered out. This is most clearly seen in plot C where the surface response of the cold, thick ice at Ridge B is virtually devoid of wavelengths less than about 20 km. Thus, where the greatest proportion of shear occurs near the bed (as is expected at ice divides such as Ridge B (Millar, 1981b) with relatively small basal echo-free zones), the major stress variations through the ice are governed primarily by the higher and more uniform viscosity and velocity of the upper layers. These different responses indicate the importance of rheological and temperature variations in the vertical plane on the flow of the ice sheet and its resulting topography.

The surface response of Reedy Glacier (with maximum gain factors of only 0.04) is particularly low compared with the other profiles in figure 5.5. Its very severe basal topography, steep surface slope, relatively thin ice and high velocity (table 5.1) would suggest a higher surface gain than in the Ridge B and Lennox King Glacier profiles. However, the response is dominated by the high basal temperatures and the resultant low viscosities which severely attenuate the transfer of stresses to the surface. This is predicted to an extent by the models of Budd, Hutter and others and Whillans and Johnsen. Intense horizontal shear zones separating less active ice in topographic lows may also contribute to the very low gain of the profile. The ratio of velocity to thickness (table 5.1), proportionate to the mean shear strain rate through the ice column (Budd and Radok, 1971), shows there to be a very much higher concentration of

Table 5.1: Physical parameters relevant to the three profiles to which cross-spectral analysis has been applied (figure 5.5). Most measured values are from Drewry (1983a). Basal and internal temperatures have been derived using the model of Budd (1969).

Mean values	Ridge B	Lennox King Glacier	Reedy Glacier
Length (km)	271	285	235
Thickness (m)	2700	2450	1800
Depth to lowest layer (%)	90	85	75
RMS bedrock amplitude (m)	150	45	355
Accumulation rate (m a^{-1})	0.04	0.08	0.11
Balance velocity (m a^{-1})	1	2	6
Velocity/thickness ($a^{-1} \times 10^{-3}$)	0.37	0.82	3.33
Driving stress (kPa)	20	30	100
Annual surface temperature (°C)	-59	-55	-36
Basal temperature (°C)	-24	-18	-2
Average temperature in column (°C)	-45	-36	-20
Surface inclination (%)	-0.11	-0.16	-0.56
Bedrock inclination (%)	-0.20	0.26	0.51

shear in this profile than in the other two. The distinct basal echo-free zone seen on radio echo sounding records suggests that this may be between layers of different viscosity and velocity.

5.4 Basal water

5.4.1 Introduction

Knowledge of the presence of basal water conditions is important because of its influence on flow dynamics through the degree of coupling to the bed and and because of implications for temperatures and hence the creep properties of ice (Duval, 1975). Many theories have attempted to predict sliding velocities (Weertman, 1964; Lliboutry, 1968; Kamb, 1970; Morland, 1976a, 1976b), typically on the basis of basal shear stress and bedrock roughness. However, observations indicate that these are not the only important factors (Meier, 1968; Haefeli, 1970). Current theory suggests that pressurized water may play a particularly active role in basal sliding (Weertman, 1964; Lliboutry, 1970; Bindschadler, 1983). The presence of water also influences the creep of ice through its relationship with temperature. The influence of the latter on ice rheology, and hence reaction to varying stress regimes, may dominate certain flow conditions (section 5.3; Hutter and others, 1981; Whillans and Johnsen, 1983).

5.4.2 Subglacial lakes

Subglacial lakes are the most readily identified form of water beneath the Antarctic ice sheet and are indicated by anomalously strong and uniform echoes (Robin and others, 1970) often at depths of several thousand metres. These smooth water surfaces, with high reflection coefficients and lateral extent of several kilometres, are common in parts of East Antarctica (Oswald and Robin, 1973). They tend to be concentrated in rock basins in areas of low surface slope and low ice velocity (for instance, ice domes and divides); this is in agreement with the requirement of low rates of debris deposition (Robin and others, 1977). Previous

inspections of radio echo sounding records from the NSF-SPRI-TUD programme have shown that lakes are typically of the order of one ice thickness in lateral extent and tend to be grouped beneath Ridge B, Dome C and Talos Dome in northern Victoria Land (Oswald and Robin, 1973; Steed, 1980). A very much larger lake, about 50 by 185 km and with a few areas of grounding, was identified 150 km NNW of Vostok (Robin and others, 1977). The ice thickness there is about 3950 m.

A further inspection of the most recent radio echo sounding records has shown 23 more lakes which conform roughly with the previously noted distribution (figure 5.6). Six of these newly discovered lakes are near the West Antarctic ice divide and the Ellsworth and Pensacola Mountains, regions where none has been reported previously. Like most of their East Antarctic counterparts, they occur in the vicinity of centres of outflow. Of the 57 lakes, 68% are in the region of Ridge B and Dome C indicating that basal ice must be close to pressure melting point over considerable areas.

The removal of basal friction over such areas should have an effect on the flow of ice and hence surface topography. Robin and others (1977) reported a mean surface slope of 1 in 2000 over the large Vostok lake compared with a regional value of 1 in 700. Indeed, a shallow depression in the surface, of the sort known by pilots as 'lakes' (Robinson, 1960), has been shown to correspond well with the subglacial water although this has only been confirmed visually (Robin and others, 1977). In the immediate vicinity of Vostok, layering was noted to be depressed locally in association with a lake of intermediate size (Robin and others, 1970). The lake is about 20 km long and has a few areas of grounding; the ice thickness is 4050 m. The area was overflown again in 1977 and so radio echo sounding of bedrock and layers may be compared with the high accuracy surface altimetry collected during that season. The bedrock and four layers are presented with the surface profile in figure 5.7. The layers are clearly depressed in the region of the lake and there is therefore a variable vertical strain rate despite the basal shear stress of zero. However, this appears to be more in accordance with basal topography than

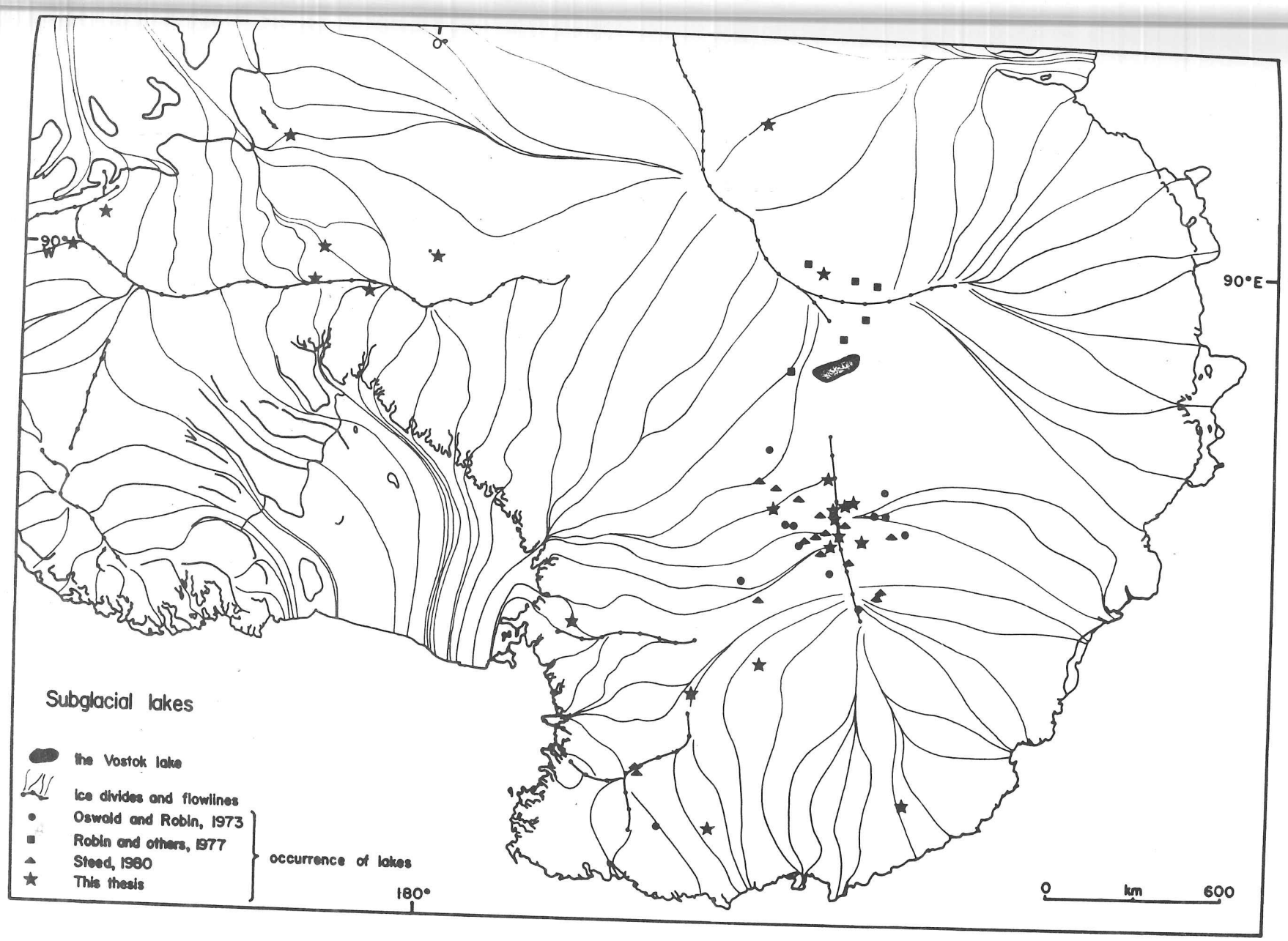

Figure 5.6: Locations of subglacial lakes as identified by radio echo sounding records from the NSF-SPRI-TUD programme.

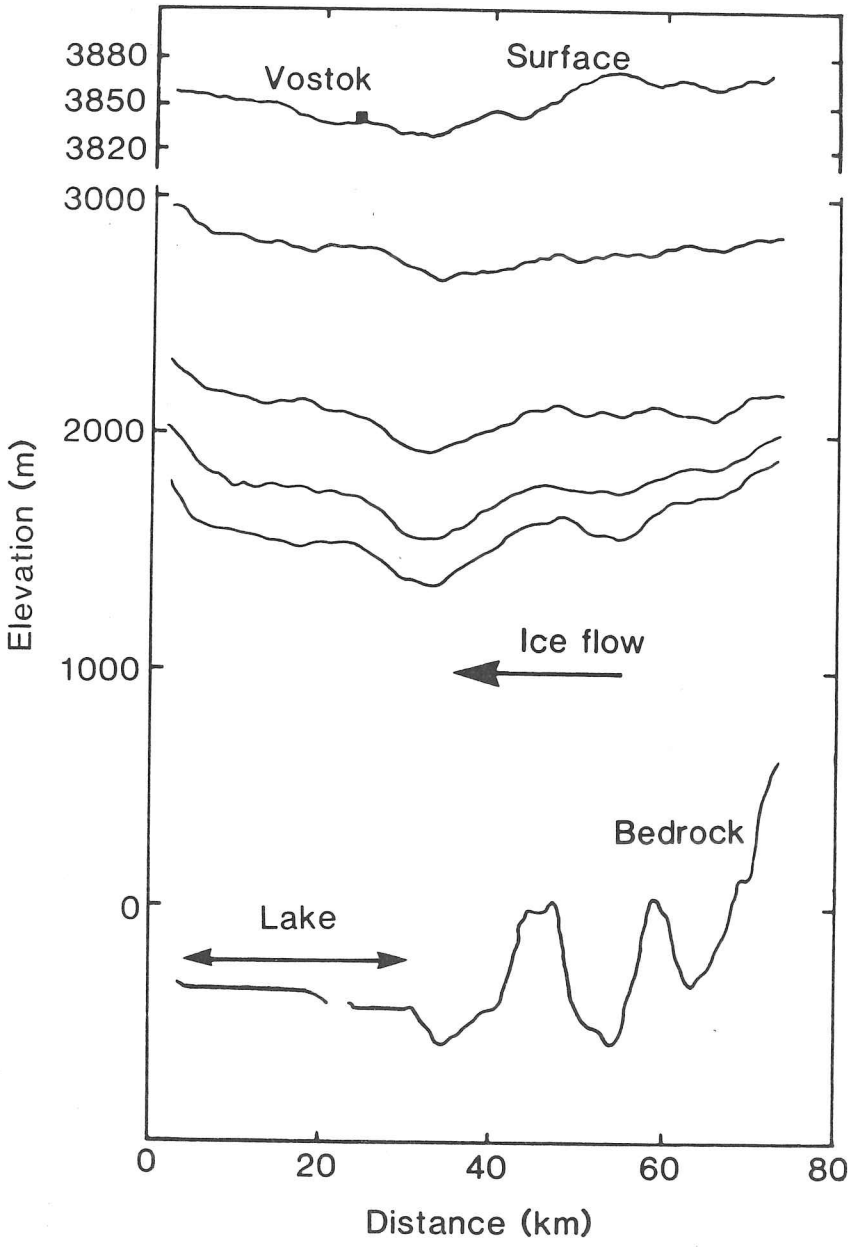

Figure 5.7: Profiles of ice sheet surface, internal layers and bedrock down a flowline to the medium-sized subglacial lake at Vostok. Surface profile from aircraft altimetry, all others from radio echo sounding.

with the presence of the lake. The vertical variability of the layers is not notably different over the lake compared to that above adjacent basal terrain. Indeed, surface elevations down the flowline rise by approximately 25 m over the lake, an effect which must be due to the transmission of significant longitudinal or lateral stresses produced by ice flow over basal relief. It is not possible to distinguish any surface topography due to the lake which is distinct from the regional slope and local topography. The inability to detect the lake's presence in the surface is attributed to the grounding points which effectively halve the lake's dimensions and to the lateral transmission of stress due to flow in three dimensions.

The other lakes identified in the Antarctic are all smaller than the two in the Vostok region and so their presence is unlikely to be indicated directly in the surface topography. Given that they typically occur in fairly rough terrain and under thick ice which is usually relatively cold and of low velocity, the absence of basal friction, even in areas with high concentrations of lakes, is unlikely to be indicated unambiguously at the ice sheet surface.

5.4.3 Water layers

The presence of substantial areas where basal ice is at pressure melting point, but where topographic and other conditions are unsuitable for the formation of lakes, has been discussed by Oswald (1975). Echo strengths in the Dome C region, for instance, remain high well outside the centre of outflow where the lakes occur; similar fading patterns can be found in much of West Antarctica (Drewry and Meldrum, 1978; Jankowski and Drewry, 1981). Seismic evidence (Bentley and Clough, 1971; Dewart, 1976) has also suggested a wet layer under the West Antarctic ice sheet and upwelling of water in the Byrd borehole (Gow, 1970) has been interpreted as indicating a water film of the order of 0.1 mm thick (Weertman, 1970). This may be partly attributed to the anomalously high regional geothermal heat flux associated with volcanism beneath most of the West Antarctic ice sheet (Benson, 1982).

The effects of decoupling of ice from bedrock and the partial submergence of obstacles controlling sliding velocities (Weertman, 1966) are best seen in ice streams where water flowing at the ice sheet bed will be concentrated by the effective pressure gradient (Weertman and Birchfield, 1982). The low surface slopes are thus a logical consequence of the reduced basal shear stress and high velocity (Drewry, 1983b). As will be shown in section 6.2, the absence of agreement between mass balance considerations and predictions based on internal deformation points to the importance of water lubrication. Positive feedback between fast sliding and the production of meltwater (Budd, 1975) has provided satisfactory explanation of observations.

The significance of variable sliding velocities and shear stresses (Whillans and Johnsen, 1983) and of variations in the temperature and viscosity of the ice (Budd, 1970; Hutter and others, 1981) have been considered in section 5.2 and will not be dealt with further here. The importance of basal water in relation to driving stress is considered in section 6.2 and the flow of ice streams and outlet glaciers in response to lubrication is discussed in section 7.2.

5.5 Summary

Consideration of the ice sheet surface topography in relation to bedrock profiles has supported the observed coincidence of surface slopes and bedrock peaks but not the conclusion of Budd (1970) that there is a dominant bedrock wavelength of about three times the ice thickness which is preferentially transmitted to the surface. Agreement was found with the model of Hutter and others (1981) which predicted generally increasing surface response for longer bedrock wavelengths. The significance of a non-isotropic ice mass for these relationships was demonstrated, thereby suggesting that multi-layer modelling is a promising approach.

Ice viscosity and temperature variations appear to have a dominant effect on the transfer of bedrock-induced stresses to the surface. Typically, surface wavelengths less than one ice thickness were not

produced by ice flow over bedrock irregularities and this figure increased as a larger proportion of the ice mass behaved as a rigid slab. Intermediate shear zones also seem to produce significant results by inducing a smoother effective bedrock. The mean ice thickness was noted to be proportional to some power of the wavelength of surface undulations, although previous models had predicted a linear relationship. The distinction between motion due to basal sliding and internal deformation was not found to be a primary influence on surface topography. Only the very largest subglacial lakes are likely to result in distinctive ice sheet terrain through inhibition of the transmission of longitudinal and lateral stresses. The effects of basal water through substantial decoupling under ice streams and as an influence on ice temperature and viscosity will be dealt with in chapters 6 and 7.

CHAPTER 6

STRESS DISTRIBUTIONS

6.1 Introduction

Previous chapters have examined the form of the ice sheet surface and factors controlling its morphology and topography. In particular, attention was focused on the manner in which the surface and bedrock are related. In this chapter, we discuss dynamic rather than static aspects of the ice sheet and hence the physical processes, especially those operating at the bedrock, which cause some of the features noted previously. We consider driving stresses and link the patterns observed to physical variables such as ice thickness, velocity and basal water. Then, in a re-analysis of the work of Robin (1967), we use calculated strain rates to predict surface slopes.

6.2 Driving stresses

6.2.1 Introduction

The basal shear stress of an ice mass is an important parameter because of its relationship to ice flow and hence its effect on topography. Basal drag variations of only 8 kPa (about 10%) may cause surface features with 2 m amplitudes along the Byrd Station Strain Network (Whillans and Johnsen, 1983).

The term 'driving stress' is used here rather than basal shear stress to indicate that we are dealing with the mean stresses in balance with basal shear stresses and longitudinal stress gradients. Robin (1967) and Budd (1968) suggested that the effects of the latter would be largely eliminated if data were averaged over 10 to 20 times the ice thickness but

Cooper, McIntyre and Robin (1982) and Young and others (in press) suggested that a smoothing over about 30 ice thicknesses is necessary in the Antarctic ice sheet.

Sufficient data from radio echo sounding, balloon altimetry and oversnow traverses exist to map driving stresses over about 50% of the Antarctic ice sheet. This was done (Cooper, McIntyre and Robin, 1982; McIntyre and Cooper, 1983) by determining mean values of surface slopes and ice thickness over grid squares of 1^{o} latitude (111 km) as inputs to equation [1.4]. Values were plotted by computer and this was followed by minor hand smoothing (figure 6.1). A consequence of the grid size is that detail was lost in some regions, for instance, near the West Antarctic ice streams and that plotted data stops 50 km from the coast. Errors are largely the result of uncertainties about surface elevations, for example, those due to frequent changes in aircraft altitude in northern Victoria Land. However, flow directions produced while defining the maximum slope of grid squares enabled a rough check to be maintained on consistency and the error is thought to be typically less than 10 kPa.

6.2.2 Patterns

Several patterns may be identified in figure 6.1 which enable more detailed testing of theoretical concepts than earlier studies of driving stress (Budd and others, 1971; Rose, 1979). The clearest trend is the increase in driving stress from ice divides and centres of outflow (less than 20 kPa) to the coast (often over 120 kPa) except when bordered by major ice shelves. This trend occurs in both East and West Antarctica but these regions differ in two important respects. First, the rate of increase is greater in West Antarctica than East Antarctica. Assuming driving stress to be related to velocity (as shown below), this is a consequence of West Antarctica's higher accumulation rates which result in a more rapid increase in velocity with distance from the ice divide. Second, the highest values in West Antarctica are consistently less than those in the East. Since ice thicknesses are roughly comparable in these areas, the difference in maximum values must be the result of the lower slopes in the

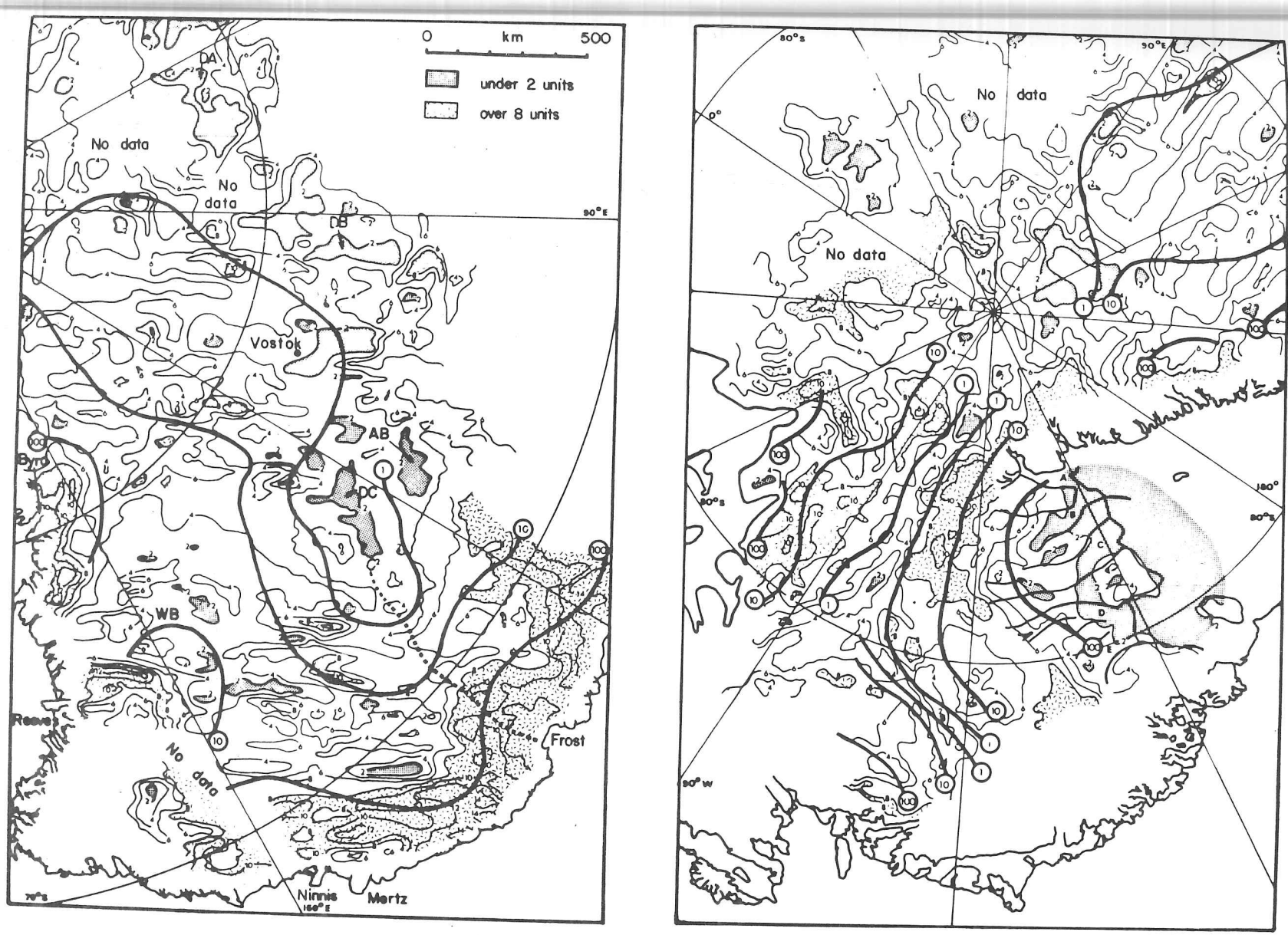

Figure 6.1: Driving stresses (thin contours) and calculated steady state values of mean shear strain rates (thick contours) in East (A) and West (B) Antarctica. Units are 10 kPa and 1.0×10^{-4} a^{-1} respectively. Driving stresses less than 20 kPa are stippled and those over 80 kPa are hatched. DA Dome A; DB Dome B; DC Dome C; WB Wilkes Basin; AB Aurora Basin; A, B, C, D and E are ice streams flowing into the Ross Ice Shelf. (From Cooper, McIntyre and Robin, 1982).

former. These are thought to be due to basal water causing the partial submergence of obstacles and the reduction of basal friction.

The observed increase in driving stress down flowlines may be compared with that from the theoretical profile of an ice sheet on flat bedrock moving only by internal deformation. The resulting surface form (Vialov, 1958) is described by equation [1.7]. Both driving stress profiles are shown in figure 6.2 and it can be seen that the predicted curve provides a rough approximation of the data between Dome C and the Wilkes Land coast. However, even though it is not a region of severe subglacial topography, bedrock irregularities of a few tens of kilometres in extent produce long wavelength variations in driving stress.

At a smaller scale, it is possible to associate characteristic values with certain glaciological circumstances. Thus, low driving stresses (typically less than 20 kPa) are found in four situations: first, at centres of outflow, such as Domes A and C, Ridge B and Talos Dome in East Antarctica and the West Antarctic ice divide (figure 6.1). Although slopes and velocities may be negligible, the scale of smoothing has eliminated zero values. Second, low values occur in association with subglacial lakes (Oswald and Robin, 1973) of large extent. Third, they occur at the seaward end of major ice streams (figure 6.3.B; McIntyre and Cooper 1983 for more detail) and, fourth, where longitudinal stress gradients have not been entirely eliminated, as discussed below.

High driving stresses (greater than 100 kPa) of limited extent are found mainly in two situations: first, in areas of great convergence of flow, such as at the heads of outlet glaciers. This can be seen for Byrd and Frost Glaciers and inland of the West Antarctic ice streams; here the proximity of their catchment areas has caused the coalescence of these crescentic zones of high stress. Second, we find isolated patches of high stress. The occurrence of alternate bands of high and low stress oriented across the direction of ice flow between 130°E and 150°E, north of 75°S (figure 6.1.A), suggests that longitudinal stress gradients have not been fully smoothed by the averaging process. It is possible that such stresses can be transmitted over distances of 50 to 100 km, a distance somewhat

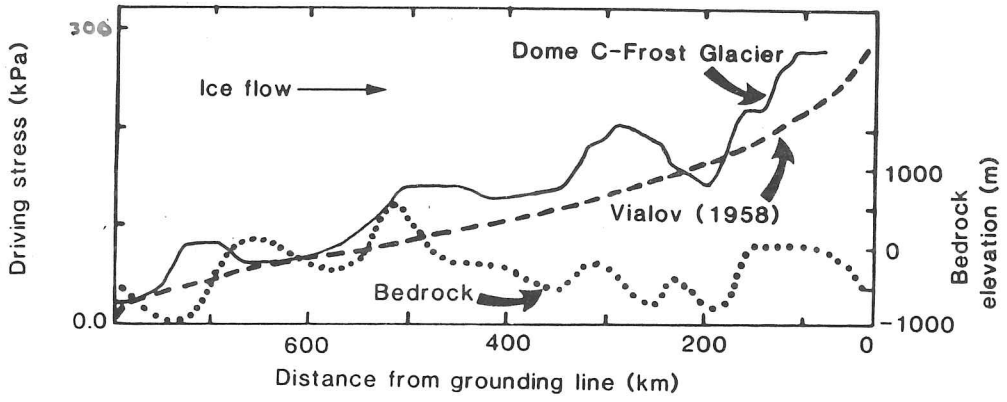

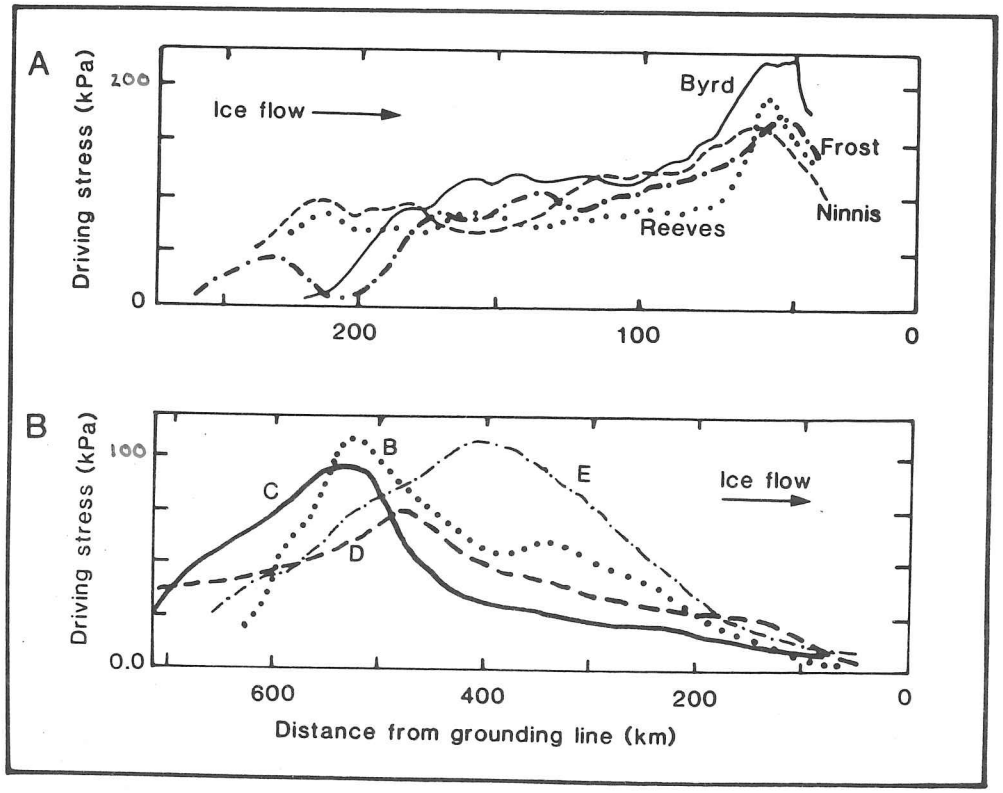

Figure 6.2: Calculated and theoretical (Vialov, 1958) profiles of driving stress between Dome C and Frost Glacier. Bedrock elevations are also given. (Redrawn from Cooper, McIntyre and Robin, 1982).

Figure 6.3: Profiles of driving stress down outlet glaciers (A) and ice streams (B). Data have been averaged over a 50 km window. (Redrawn from Cooper, McIntyre and Robin, 1982).

greater than suggested above.

The pattern of driving stresses down flowlines to outlet glaciers and ice streams may be investigated along individual radio echo sounding flight lines. Data have been averaged using a 50 km window and the resulting profiles may be divided into two types. Most outlet glaciers show increasing driving stresses to about 100 km from the grounding line (figure 6.3.A). At this point, there is a further increase to a peak usually greater than 150 kPa. The driving stress then falls rapidly to zero over the next 50 km before going afloat. Glaciers showing this pattern include Reeves, Byrd, Ninnis and Frost. This is very similar to that found down the IAGP flowline in Wilkes Land (Budd and Young, 1979). Ice entering the West Antarctic ice streams, however, shows swiftly increasing driving stresses with distance until a broader peak of about 100 kPa is reached some 400 to 500 km from the grounding line (figure 6.3.B). Values then fall more gradually than in East Antarctica until the ice is completely decoupled from its bed. These patterns are discussed further in section 7.2.

6.2.3 Effects of ice velocity and thickness

The most important parameters influencing the patterns of driving stress appear to be velocity and ice thickness (Nye, 1957; Weertman, 1957; Budd and Jenssen, 1975; Budd and Smith, 1981; Young, 1981). In the absence of appreciable basal sliding and if longitudinal stress gradients have been effectively smoothed out, we expect surface velocities to be proportional to some power of the driving stress and to thickness (Budd and Radok, 1971). Thus

$$u = kz\tau_b^{\,n} \qquad [6.1]$$

and hence

$$u/z = k\tau_b^{\,n} \qquad [6.2]$$

where k and n are constants. The ratio u/z is proportional to the mean shear strain rate through the ice column. Figure 6.1 shows, in addition to driving stress, contours of u/z derived from balance velocities and

thickness calculated from data given in Drewry (1983a). The pattern of increase in u/z is broadly similar to some power of the driving stress. The 0.0001 a^{-1} contour encircles the low driving stresses of the ice divides where velocities are also at their lowest. The 0.01 a^{-1} contour is generally associated with driving stresses over 80 kPa and with zones of flow convergence around the heads of outlet glaciers.

The relationship may be considered more precisely by plotting derived values of u/z against driving stress for data from both East and West Antarctica (figure 6.4). This allows an extension from reported values down to 0.0001 a^{-1}. Previously noted values for n and k in equation [6.2] are 3.45 and 0.02225 (Budd and Smith, 1981) and 2.50 and 0.08555 (Budd and Jenssen, 1975) respectively. Values from our data are 2.51 and 0.00850 and, although the scatter of our results is greater, they seem sufficiently consistent with other sources to draw the following conclusions. First, the agreement between our steady state values of u/z with the observed relationship for equation [6.2] of Budd and Smith (1981) indicates that our balance velocities are correct to a first approximation. This compares with balance velocities which were calculated to be 80 to 90% of measured velocities (Whillans, 1977; Young, 1979). Second, like Budd and Smith (1981), we find that driving stress is more closely related to u/z than to u. From this we conclude that the major part of surface motion is due to internal shear within the ice mass and not to sliding at the bed. The more scattered points in figure 6.3.A may indicate where this does not apply. Third, the above agreement indicates that driving stresses are not closely related to ice temperatures over much of the ice sheet. It seems from studies of temperature variations with depth that many parts of the ice sheet with basal ice below the pressure melting point still conform to the relationship between driving stress and u/z. This apparent inconsistency could be due to the development of an ice fabric favouring easy glide which compensates for the cold temperatures that would otherwise require greater driving stresses.

It should be noted that points on the flowline between Dome C and Byrd Glacier in figure 6.4.A have higher driving stresses than predicted by the

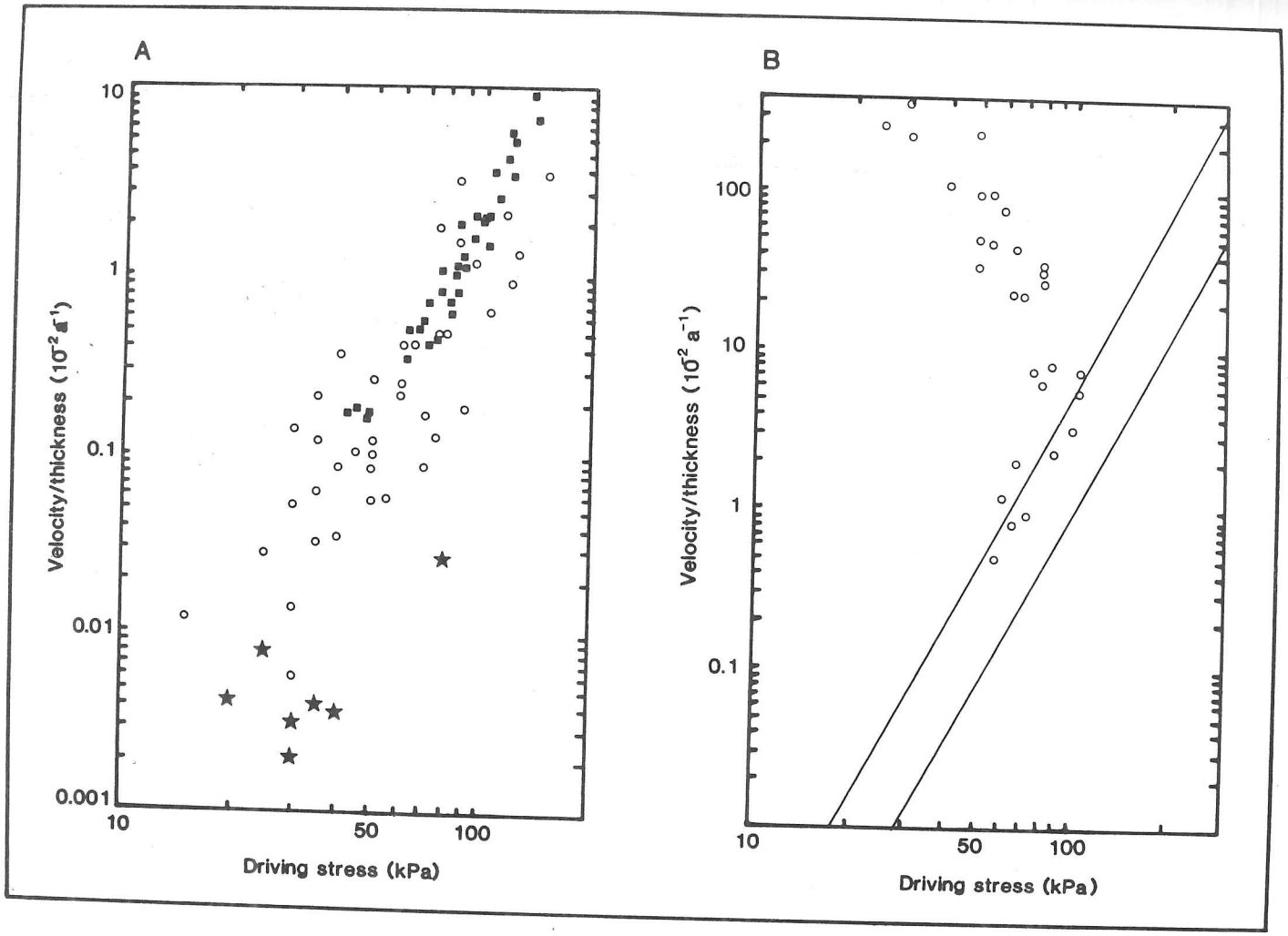

Figure 6.4: Variations of mean shear strain rate (u/z) with driving stress in East (A) and West (B) Antarctica (open circles). Solid squares are from Budd and Smith (1981) and stars are from a profile between Dome B and Byrd Glacier. Envelope in B represents data from polar ice (Budd and Smith, 1981). (A is redrawn from Cooper, McIntyre and Robin, 1982).

regression line. Values of driving stress near Dome A (figure 6.1.A) suggest that the effect may be more marked there. In these regions basal, as well as surface, temperatures may be low at many points and so require high driving stresses. Also, near centres of outflow, crystal fabrics favouring easy glide may not be fully developed. Finally, the topographic isolation of less active pockets of ice below zones with high concentrations of shear may result in an effectively thinner ice mass and hence the over-estimation of driving stresses and the under-estimation of mean shear strain rates.

Values of driving stress and u/z are plotted in figure 6.4.B along with an envelope covering data from polar ice (Budd and Smith, 1981). Low strain rates near the ice divide agree with driving stress values as predicted by equation [6.2], suggesting that motion is largely by internal deformation, as found by Drewry (1983b) with data from Siple Dome. As strain rates increase above 0.1 a^{-1}, however, there is a decline in the driving stress, as would be expected from basal sliding in the presence of cavitation (Lliboutry, 1968; Fowler, 1979), giving a multi-valued sliding law. The assumption of motion by internal deformation in equation [6.2] is therefore violated as movement within the Marie Byrd Land ice streams is increasingly dominated by the effects of pressurized subglacial water (Bindschadler, 1983). This is in keeping with the notably concave seaward ends of the ice streams' profiles (figure 1.5.C; Hughes, 1973, 1975; Denton and Hughes, 1981). We now have the possibility that the proportion of motion due to basal sliding may be derived from figure 6.4.B by noting the increase in the mean shear strain rate (u/z) from that solely due to internal deformation.

6.2.4 Effects of basal water

The presence of a significant thickness of water at the ice sheet bed causing extensive decoupling of the ice streams from their beds can result in this multi-valued sliding relationship (Lliboutry, 1968, 1971; Barnes and others, 1971). Similarly, the inflection of curves in figures 6.3.B and 6.4.B is attributed to the onset of basal separation. The fall in driving

stresses after the peak in figure 6.3.A may also be the result of basal sliding and this is discussed further in section 7.2. As the grounding line is approached, subglacial water submerges increasingly large obstacles to flow, thereby further reducing the generation of longitudinal stress gradients and driving stresses. This can be seen in the declining density of surface undulations towards the grounding line in Landsat images (figure 4.6). Budd (1975) suggested a positive feedback between the fast sliding of ice streams and the production of basal water by the mechanical dissipation of heat during sliding. Drewry (1983b) has shown that taking account of Budd's lubrication factor provides a satisfactory explanation of the behaviour of ice streams where there is major decoupling. The low surface slopes may therefore be a logical consequence of the high velocity and low driving stress values.

The importance of subglacial water to the flow of West Antarctic ice streams is probably increased by the depth of their beds below sea level. Hydrostatic pressure is greater than elsewhere and so bottom drag is further reduced by pressurized water which carries a high proportion of the weight of the overlying ice (Weertman, 1964; Lliboutry, 1979; Bindschadler, 1983). The progressive decoupling of ice streams thus causes their behaviour to tend towards that of ice shelves which deform on an almost frictionless surface under their own weight (Thomas, 1979b). As noted in section 5.4, only the largest subglacial lakes, such as that NNW of Vostok (77.5°S 104°E) identified in figure 6.1.A by values less than 20 kPa, are likely to significantly affect regional driving stress patterns.

6.2.5 Other factors

Bedrock roughness appears to have little effect on driving stress at most scales, presumably because most of the deformation in the ice mass takes place above the level of bedrock relief (Colbeck and others, 1978; Robin and Millar, 1982). On the smaller scale, bedrock-induced longitudinal and basal shear stress gradients may have significant effects on surface slopes in the flow direction, although not on ice

velocity (Young and others, in press). The anomalously low driving stresses noted by Cooper, McIntyre and Robin (1982) to be associated with subglacial basins may be attributed to local centres of outflow which have become apparent with the completion of detailed maps of surface topography (Drewry, 1983a). The values of less than 20 kPa in the region of the Wilkes Basin are therefore likely to be the result of the low mass flux of ice from Talos Dome rather than exceptionally smooth bedrock.

6.3 Longitudinal stresses

6.3.1 Previous modelling

It has long been recognized that longitudinal stress gradients produced by ice flow over bedrock irregularities have significant effects on the surface topography of ice sheets (Robin, 1967; Budd, 1968; section 1.4). Analysing the relationship between surface and bedrock topography down a flowline south of Camp Century in NW Greenland, Robin found that accounting for longitudinal stress gradients (equation [1.9]) enabled qualitative predictions of observed slope fluctuations. Beitzel (1970) confirmed this with data from Dronning Maud Land. Budd (1968) suggested that, when data are averaged over less than about four times the ice thickness, it is also necessary to consider variations in the basal shear stress, T (equation [1.11]). However, since it is not possible to calculate this from observations (Paterson, 1981, p100), we shall deal in this section with longitudinal stresses only.

The calculation of the longitudinal strain rate at the surface (Robin, 1967) involved three principal assumptions. These were

1. $\bar{\sigma}_x' \frac{dz}{dx} \ll z \frac{d\bar{\sigma}_x'}{dx}$
2. $\tau_{xz} \ll \bar{\sigma}_x'$
3. $\dot{\epsilon}_x$ does not vary with depth.

Measurements of borehole tilt in Athabasca Glacier (Paterson and

Savage, 1963) have shown that the third assumption is not always valid. Other evidence for significant variations of the longitudinal strain rate with depth have been found by Shreve and Sharp (1970), Raymond (1971), Hooke (1973), Harrison (1975) and Paterson (1976). A flow model taking account of such variations (Dansgaard and Johnsen, 1969) was found to be necessary to provide correct dating for the Camp Century core. The horizontal velocity was assumed to be constant from the surface down to 400 m above the bedrock but below this level it decreased uniformly. This model gave a significantly better explanation of the temperature-depth profile at Camp Century than previous theory (Nye, 1963) in which shear strain rates were concentrated in a thin basal layer. Support for the flow model of Dansgaard and Johnsen comes from a study of ice fabrics from a core in Law Dome (Russell-Head and Budd, 1979) which showed that shear strain rates decreased towards the bed after reaching a maximum at 66% of the depth in a zone with a high concentration of near-vertical c-axes. Similarly, Robin and Millar (1982) suggested, on the basis of the deformation of internal layering, that a transition in shear strain rates takes place at a boundary around the upper limit of the basal echo-free zone. At this level, changes in the ice fabric would explain strain rate changes without involving any discontinuity in the variations of shear stress with depth.

These developments raise the possibility that the results of Robin (1967) may be improved by calculating strain rates from ice thickness values calculated to the top of the basal echo-free zone rather than to bedrock. This may increase the validity of the third assumption listed above and, if the first one also applies, the altered value for the ice thickness will not have a major effect on the calculation of the longitudinal stress gradient. Although more recent analyses of ice flow over bedrock undulations have been undertaken which deal with longitudinal stresses (Hutter and others, 1981; Whillans and Johnsen, 1983), they will not be considered in this section. This is principally because the treatment is carried out in the frequency domain. The resulting inability to compare the phase relationships of surface and bedrock profiles is, as will be seen below, an important omission when

considering rheological and flow variations in the ice mass. The analysis of Robin (1967) was therefore seen as more appropriate.

6.3.2 Analysis

Despite approximately 55 000 km of radio echo sounding profiles with corresponding high accuracy surface altimetry, very few sections exist which combine all the requirements for repeating Robin's (1967) analysis. These include being down a flowline, continuous profiling of bedrock and the lowest layer and continuous surface altimetry. Of the four profiles available, two descend from Ridge B and Dome A where accumulation rates are less than 0.03 m a^{-1} and hence velocities and longitudinal strain rates are low. In both cases, predicted slopes are very much less than observed ones; maximum values are smaller by a factor of 3 to 5 while the wavelength of variation is typically an order of magnitude shorter. Being near the centre of the ice sheet where surface slopes and basal shear stresses tend to zero, these profiles are in a region where steady state ice sheet profiles, for instance equations [1.5] and [1.7], may not be applicable (Paterson, 1980). These two examples may therefore contravene assumptions 1 and 2 listed above and so the analysis of Robin (1967) may not be relevant. They are not discussed further here.

The third profile is 300 km upstream from Lennox King Glacier in the Transantarctic Mountains and velocities are higher, reaching 5 to 10 m a^{-1}. However, the bedrock profile is particularly regular and smooth; internal reflecting layers deform only gradually and closely mirror the form of the bedrock suggesting that ice flow is virtually laminar. Variations in surface slope are therefore unlikely to be significantly affected by assuming that longitudinal strain rates are uniform down to the lowest layer rather than to bedrock. This is supported by the analysis which shows that both assumptions give reasonable predictions of the observed surface slopes; there is generally a good phase agreement but predicted amplitudes are uniformly greater when assuming constant longitudinal strain rates only down to the lowest layer. As discussed below, this may be attributed to the incorrect estimation of the ice's

rheological properties. This example, although supporting the use of the model of Robin (1967), is not seen as a sufficient test of the non-uniformity of longitudinal strain rates because of the small and regular variations in ice thickness. It is not discussed further here.

A fourth profile is available which is down a flowline from the West Antarctic ice divide (80°S 92°W) towards the Ronne Ice Shelf. This combines rougher bedrock with a higher accumulation rate and temperatures and we may expect longitudinal strain rates to have a more significant effect on surface topography. Since measured values were not available, ice temperatures at the bed and the lowest layer were calculated using the model of Budd (1969). Values of -13 and -24°C gave the flow law constants, A, of 3.66×10^{-9} and 1.75×10^{-9} kPa^{-3} a^{-1} for ice thickness to the bed and to the lowest layer from the compilation of Paterson (1981, p39) for n=3. Balance velocities, calculated on the basis of an accumulation rate of 0.22 m a^{-1} (Drewry, 1983a), increased from zero at the ice divide to 4 m a^{-1}. Having obtained values of the longitudinal strain rate from equation [1.8], equation [1.9] was used to calculate local slope variations.

6.3.3 Results

Using a power law with the exponent n=3 was found to give slope variations very much smaller than the observed data. Although this value is often used for the general modelling of ice masses (Hooke, 1981; Paterson and Budd, 1982), lower values have been considered appropriate for modelling ice deformation at low temperatures and strain rates. Beitzel (1970) found that a linear flow law gave the best results for an analysis of surface slopes in Dronning Maud Land but used n=4 for calculations further down the flowline where strain rates were higher. Consequently, the present data were re-analysed using values of n ranging from 1.6 to 2.5. Figure 6.5 shows the initial profile data (A), the strain rates calculated from depths to bedrock and to the lowest layer (B) and the derived local slopes (C) selected from the values of n which gave the best fit to observed slopes. Figure 6.6 shows the full profiles of

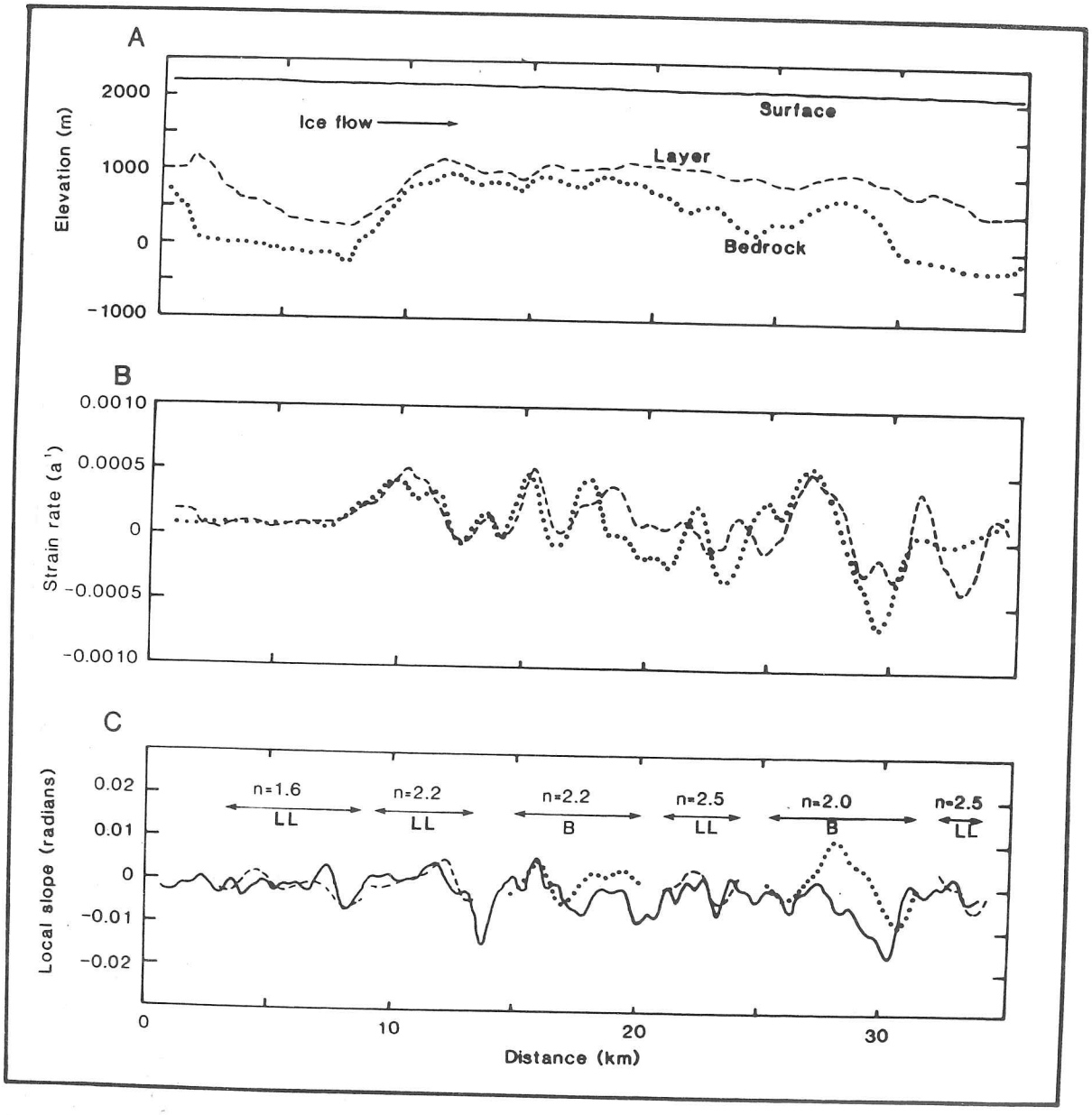

Figure 6.5: A: profile of the Antarctic ice sheet down a flowline from the West Antarctic ice divide (80°S 92°W) showing surface, lowest reflecting layer and bedrock. B: estimated strain rates along the flowline calculated from equation (1.8) using ice thickness as the depth to the layer (dashed line) and to bedrock (dotted line). C: comparison of observed surface slopes derived from aircraft altimetry (solid line) with calculated slopes using depth to lowest layer (dashed line) and to bedrock (dotted line). For each section of calculated slope variation, the value of the exponent in the flow law which was used is shown as well as whether the data were derived from the lowest layer (LL) or from bedrock (B).

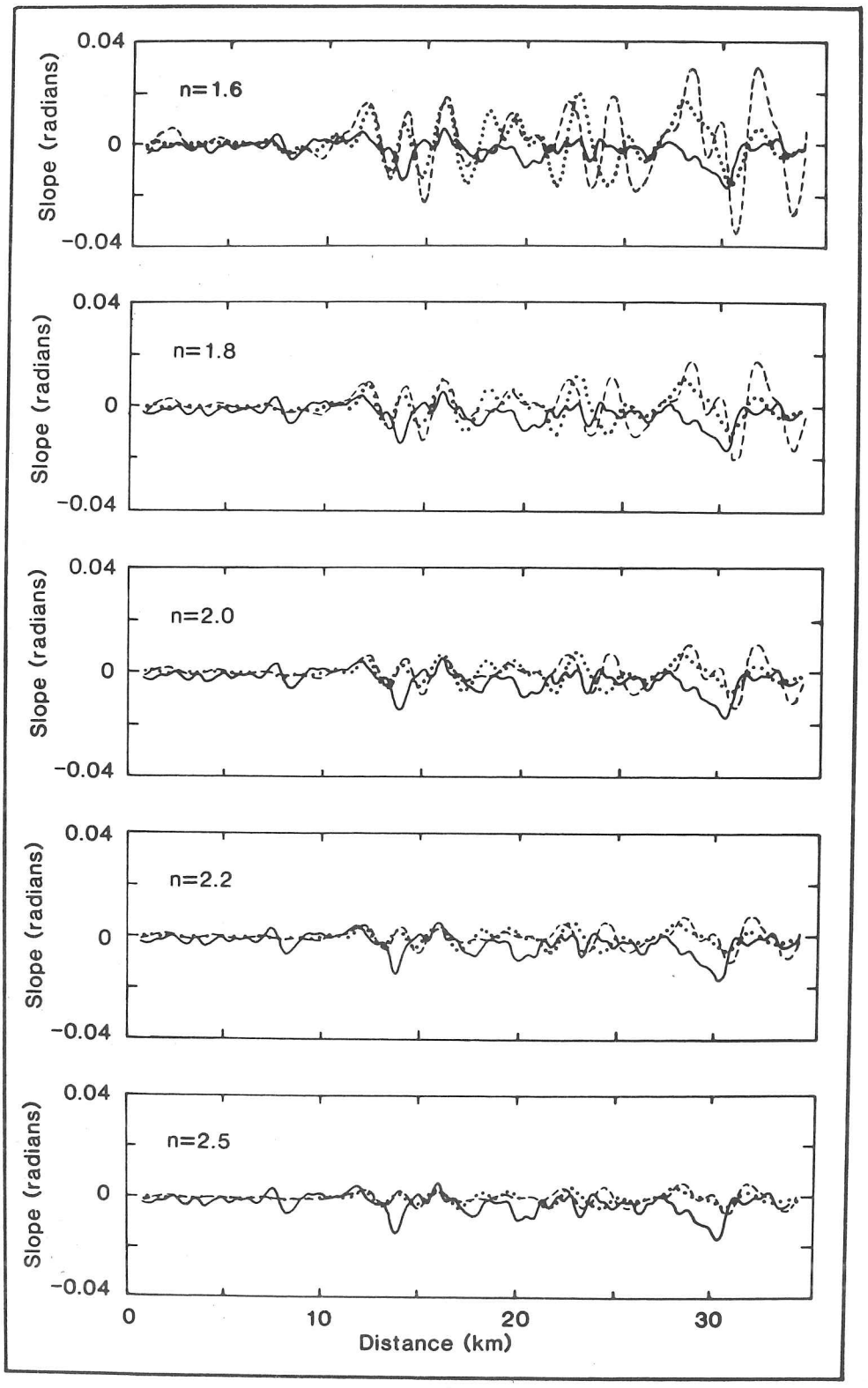

Figure 6.6: Calculated surface slopes as described for figure 6.5.C. The full profile for each exponent used is shown with results from depth to the lowest layer (dashed line) and to bedrock (dotted line).

calculated slopes for the range of values of n.

The amplitudes of calculated slope variations are the product of the constants in the flow law and hence the rheological properties of the ice. The prediction of internal and basal temperatures is dependent on several assumptions (such as the correct estimation of the geothermal heat flux) and so these flow constants are likely to be, at best, rough estimates (Paterson, 1981). The downslope change of n suggests the presence of a progressively changing mechanism which affects the rheological properties of the ice; for instance, this may be through the effects of interstitial water (Duval, 1975), temperature (Robin, 1955), ice fabric (Whillans, 1979) or changing stress fields (Budd, 1968). The regular increase in n shown in figure 6.5.C (with one exception between 25 and 31 km) is consistent with the

idea that the flow law changes from a linear relationship to a higher-order power law as strain rates increase with velocity down the flowline (Budd, 1968; Beitzel, 1970). It is also consistent with the model of ice flow along the Byrd Station Strain Network (Whillans, 1979) in which internal shear was regarded as dependent for the most part on shear stress, ice temperature and the preferential alignment of ice crystals. Since surface slopes, and hence shear stresses, were constant over distances of about 10 ice thicknesses (Whillans, 1975) and since temperature profiles change little along the first 200 km of flowlines in large ice sheets (Budd and others, 1971), the main cause of variations in the rate of internal shear was thought to be the progressive development of ice fabric from the ice divide. This was taken as being proportional to surface velocity which increased as a linear function of distance from the ice divide. The validity of this model (Whillans, 1979) was supported by agreement between the calculated bed profile and that measured by radio echo sounding and between calculated and measured rates of ice sheet thinning. The lack of development of ice fabric favouring faster ice flow near ice divides has also been indicated by the anomalous relationship between the mean shear strain rate and driving stress (Cooper, McIntyre and Robin, 1982), for instance, as was found near Ridge B (figure 6.4.A).

While a value of n=1.6 in figure 6.6 gives slope variations of the correct order ($\pm$0.002 radians) near the ice divide, a flow law with this exponent is clearly inappropriate further down the profile; amplitudes of $\pm$0.01 radians are more precisely predicted with n=2.5. The derived amplitudes could be further adjusted by selecting suitable values for the flow law constant, A, but such modification becomes somewhat arbitrary given the uncertainty involved in calculating these parameters. It should be noted that a further modification of these values could be achieved by adjusting the velocites used to calculate the longitudinal stress gradients as was done by Robin (1967) and Robin and others (1969). An explanation for the need for such corrections may lie in the uncertainties involved in determining these flow law constants, even in the vicinity of a core to bedrock, as was available at Camp Century. Alternatively, they may be due to the fact that the above analysis is two-dimensional. It was noted from Landsat imagery and aircraft altimetry (sections 4.2 and 4.3) that undulations on the ice sheet surface are typically isotropic; even in areas of thin ice and high velocity, form factors did not depart significantly from unity. This approximate isotropy suggests that ice flow over bedrock irregularities results in similar longitudinal and transverse stress gradients and hence that roughly half of the stress gradients involved are absorbed by the lateral displacement of ice. The halving of balance velocities, and hence strain rates and stresses, in order to match the observed magnitude of slope variations (Robin, 1967; Robin and others, 1969) may therefore have compensated for the effects of lateral stress gradients, although this was not recognized at the time. This points to the importance of modelling ice flow in three rather than two dimensions.

For the six sections along the profile for which data are shown in figure 6.5.C, there is a fair correspondence between calculated and observed slopes. The amplitude and phase of slope variations correspond quite well and local slopes, which are up to a factor of six greater than the regional gradient, are predicted to a first approximation by equation [1.9]. A vertical offset is to be expected due to the omission of the term $\tau_b/\rho gz$ from the derived values. However, figure 6.6 shows that the

theory cannot explain all of the observed slope variations; for instance, neither the slopes calculated from the lowest layer nor the bedrock predict the significant depression at 14 km. This is in partial support of the analysis by Bindschadler (1979) which concluded that longitudinal stress gradients did not provide an effective means of improving the calculation of basal shear stresses on Variegated Glacier.

Of the 35 km under consideration, figure 6.5.C shows that 43% of observed slopes are better predicted using the depth to the basal echo-free zone while 31% are explained using the full depth to bedrock. No obvious agreement is apparent for the remaining 26%. Thus, the theory is improved over nearly half of the profile by considering that most shear is concentrated near the lowest reflecting layer. Two examples of this (between 3 and 9 km and 22 and 25 km) occur above distinct bedrock depressions. Down the flowline from each of these, the surface is better explained by a shear zone at, or very close to, the bedrock. We may therefore envisage that the effective bed of the ice mass varies its relative depth in response to topographic and other constraints. The zone of maximum shear strain rates appears to fluctuate between the bedrock and the top of the basal echo-free zone. The basal ice in the two depressions centred at 6 and 23 km may be topographically isolated from, and less active than, that above, as occurs at the margin of the Greenland ice sheet (Colbeck and others, 1978).

Phase differences such as that at about 14 km could also be the result of the treatment of a three dimensional situation by a two dimensional analysis. Direct observations of the movement of ice at glacier beds (Englehardt and others, 1978) and deductions about the flow of ice in three dimensions from the deformation of internal layering (Robin and Millar, 1982) indicate that transverse flow of basal ice may be significant where topography is severe. A further explanation of the poor fit of predicted and observed slopes seen in parts of figure 6.5.C is that basal shear stress variations, as described by the parameter T in equation [1.11] (Budd, 1968), have a significant effect on surface slope variations in some parts of the profile. T is thought to be important

unless data are averaged over horizontal distances of about four ice thicknesses. However, the value of T cannot be calculated from observations (Paterson, 1981, p100) and so we are not able to test the extent of any improvements which it might induce.

The above analysis serves to indicate the variability in rheological properties of ice masses and their flow conditions and points to the difficulties involved in their correct estimation.

6.4 Summary

Sufficient data are available to map driving stresses over half of the Antarctic ice sheet. Superimposed on the general pattern of increasing values towards the coast are zones of high and low driving stresses which may be associated with particular glaciological regimes. Patterns down flowlines to outlet glaciers and to ice streams differ significantly. Variations are clearly dependent on ice thickness and velocity. In much of East Antarctica, driving stresses are closely related to the mean shear strain rate through the ice column, indicating that motion is largely by internal deformation. However, the presence of water under West Antarctic ice streams reduces driving stresses through lubrication and enables significant basal sliding.

Models of longitudinal stress gradients typically assume that ice properties are uniform through the ice column. A re-analysis of the work of Robin (1967) showed that, although appropriate for regions with uniform ice flow and a regular bedrock profile, the model breaks down near ice divides where accumulation rates and longitudinal stress gradients are low. However, down a flowline in West Antarctica where there are notable variations in the thickness of the basal echo-free zone, predictions of surface slope can be improved by assuming that longitudinal strain rates are uniform only down to the lowest continuous reflecting layer. The variability of these results suggests that the zone of maximum shear fluctuates between bedrock and the top of the basal echo-free zone in response to constraints imposed by subglacial topography and variations

in ice temperatures and rheology. The variable flow law exponent used in the calculations indicates the progressive development of an ice fabric favouring faster flow with distance from the ice divide.

CHAPTER 7

THE DYNAMICS OF ICE SHEET OUTLETS

7.1 Introduction

Although only 13% of the Antarctic coastline consists of outlet glaciers and ice streams (Drewry and others, 1982), it has long been recognized that their importance to the dynamic glaciology of the ice sheet is very much greater than this proportion suggests. It has been estimated that 90% of the accumulation falling inland of the coastal zone is discharged through such features (Morgan and others, 1982; Drewry and Robin, 1983). Hughes (1977) identified them as the most 'energetic' elements within an ice sheet and hence the major control on its overall stability. In this chapter we shall draw together evidence on their form and flow in order to better understand their contribution to ice sheet dynamics. The implications of these aspects of ice sheet discharge will be considered with regard to their stability and that of the ice mass as a whole and in relation to the erosion of subglacial landforms.

7.2 Ice flow into outlet glaciers and ice streams

7.2.1 Introduction

On the basis of physical processes, two major components to ice streams and outlet glaciers may be distinguished. They are typified by converging ice flow and by stream flow. An ice sheet outlet may display elements of both but their relative magnitude and importance will vary in response to topographic and glaciological controls.

Sheet flow is thought to be largely the result of motion by internal deformation of the ice mass, as has been shown by the relationship between

driving stresses and mean shear strain rates (section 1.3 and figure 6.4.A; Budd and Jenssen, 1975; Budd and Smith, 1981; Cooper, McIntyre and Robin, 1982). Similarly, the dynamics of the ice mass down the IAGP flowline in Wilkes Land in the region before the deep troughs of Vanderford and Totten Glaciers are explicable by internal deformation (Budd and Young, 1979); even where basal melting occurs, bottom sliding is probably negligible. Ice flow within ice streams, however, is recognized as being due to basal sliding (Rose, 1979; Weertman and Birchfield, 1982). Drewry (1983b) found that data from Marie Byrd Land ice streams were satisfactorily explained by accounting for Budd's (1975) friction lubrication factor, thereby indicating major decoupling of the ice streams by water. This was also seen in section 6.2 where a multi-valued relationship (Lliboutry, 1968) between driving stress and derived shear strain rates was found for West Antarctic data. However, Bindschadler (1983) demonstrated that this is only the case for near-zero water pressures. Where the subglacial water pressure increases, it is this and the resulting stress concentrations in areas where the ice is still in contact with the bed which control the sliding process.

Converging flow is indicated morphologically by basins and broad valleys in the ice sheet surface which terminate in stream flow or the outlet itself. Contour maps of East Antarctica (for instance, Drewry, 1983a) show clear examples inland of Byrd, David, Ninnis and Dibble Glaciers, the first extending over 200 km into the ice sheet. They can also be seen on Landsat imagery where high convergence of flow causes changes in topographic detail as higher velocities reduce the damping of bedrock relief (sections 5.2 and 5.3). The concentration of flow towards Dibble Glacier (figure 4.1) is indicated by an arc of severe topography which is distinct from the smoother domes to either side and the terrain inland. Further illustration is provided by areas of reduced brightness temperatures on passive microwave imagery (Zwally and Gloersen, 1977) which occur up to 500 km inland of major outlet glaciers. Lower values are thought, in this case, to be the result of accumulation controlled by katabatic winds which converge on the basins surrounding outlet glaciers. Support for the presence of strong winds is given by the reduced

concentration of sea ice offshore. Examples include Ninnis, Mertz, Vanderford, Totten and Pine Island Glaciers.

Ice streams are clearly distinguished from adjacent sheet flow by their discrete boundaries which are often curvilinear for several hundred kilometres. Such margins are heavily crevassed shear zones separating the active streams moving at high velocities by basal sliding from the more slowly flowing plateau ice (Rose, 1979). The uniformity of these crevassed zones, seen by aerial photography and Landsat imagery, appears to indicate the relative isolation of the stream from the sheet (section 4.2.3); where the margins are very distinct (for instance, Ice Stream E in figure 4.6), proportionately little lateral feeding is indicated and the boundary is maintained by significantly different velocities. The upper reaches of Pine Island Glacier, however, display curved traces across the boundary which suggest considerable peripheral contributions to the ice stream. This may decrease downstream where the ice streams become progressively isolated from adjacent ice masses as a result of shear decoupling at their sides and the development of glide fabrics (Hughes, 1977; Hughes and Fastook, 1981).

The presence of ice streams is often associated with subglacial terrain which causes flow to be channelled. Valleys in the ice sheet surface have been noted to have corresponding subglacial features (Rose, 1979; Wada and Mae, 1981; Allison and others, 1982; Morgan and others, 1982; Steed and Drewry, 1982; Drewry and Robin, 1983). Lambert Glacier occupies a deeply eroded glacial trough (Morgan and Budd, 1975) which is thought to have reached erosional stability in relation to the present sea level (Drewry and Robin, 1983). Smooth bedrock echoes of uniform intensity upstream of the grounding lines of ice streams in Enderby, Kemp and Mac.Robertson Lands have also been taken to indicate that glacial erosion from high sliding velocities has substantially smoothed the bedrock and contributed to its lowering (Morgan and others, 1982). However, the ice streams of Marie Byrd Land flow in wide and relatively shallow, although smooth, bedrock depressions (Rose, 1979) and Thwaites Glacier shows no distinctive bedrock channel at all (Drewry, 1983b). These subtle landforms in association with

such vigorous ice streams may suggest that the ice flow in these areas is either relatively youthful or transient (Drewry and Robin, 1983).

The transition of regime from converging flow to stream flow, a question of central importance in ice sheet mechanics (Gealy and Weertman, 1983), is thought to occur abruptly in the region of outlet glaciers (Young, 1981). Budd and Young (1979) suggested that, as ice is channelled into deep subglacial troughs, an order of magnitude increase in velocity and an accompanying decrease in shear stress takes place due to the onset of basal sliding. Driving stresses fall from 200 kPa to zero in the 100 km before the grounding line as the ice accelerates. This pattern also occurs within 60 km of the grounding lines of Byrd, Reeves, Ninnis and Frost Glaciers (figure 6.3.A) and in Lambert Glacier (Allison, 1979). Budd and others (1979) found from laboratory experiments that this limiting shear stress was a function of roughness, normal stress and velocity. The subsequent acceleration was thought to be dependent on the reduced effective normal stress (Budd and McInnes, 1978) as the subglacial water layer carried a greater proportion of the weight of the overlying ice.

7.2.2 The topography of the transition from converging to streaming flow

The transition in flow regime may be studied further by consideration of ice sheet topography in the region of outlet glaciers. Landsat imagery shows there to be an abrupt change in surface terrain inland of many outlet glaciers and ice streams, for instance, Thwaites, Frost, Dibble and Byrd Glaciers (figure 7.1). Similar features can be seen around the heads of David Glacier (frontispiece) and Jakobshavn Glacier (figure 3.1). Although irregular in plan form, this transition separates zones of

---

Figure 7.1: Landsat images showing the transition in topography of the ice sheet surface down flowlines to outlet glaciers. Dotted lines separate irregular and smooth terrain types thought to indicate ice flow by internal deformation and basal sliding respectively. Large arrows give flow directions through the outlets. A: Thwaites Glacier (E-1205-14051); B Frost Glacier (E-1466-23272); C: Dibble Glacier (E-1447-23214); D: Byrd Glacier (E-1492-19080). Letters a, x and y refer to points on ARDS profiles in figure 7.2. Flight lines across Thwaites and Frost Glaciers are shown as white lines; that for Byrd Glacier is beyond the latitudinal limit for Landsat.

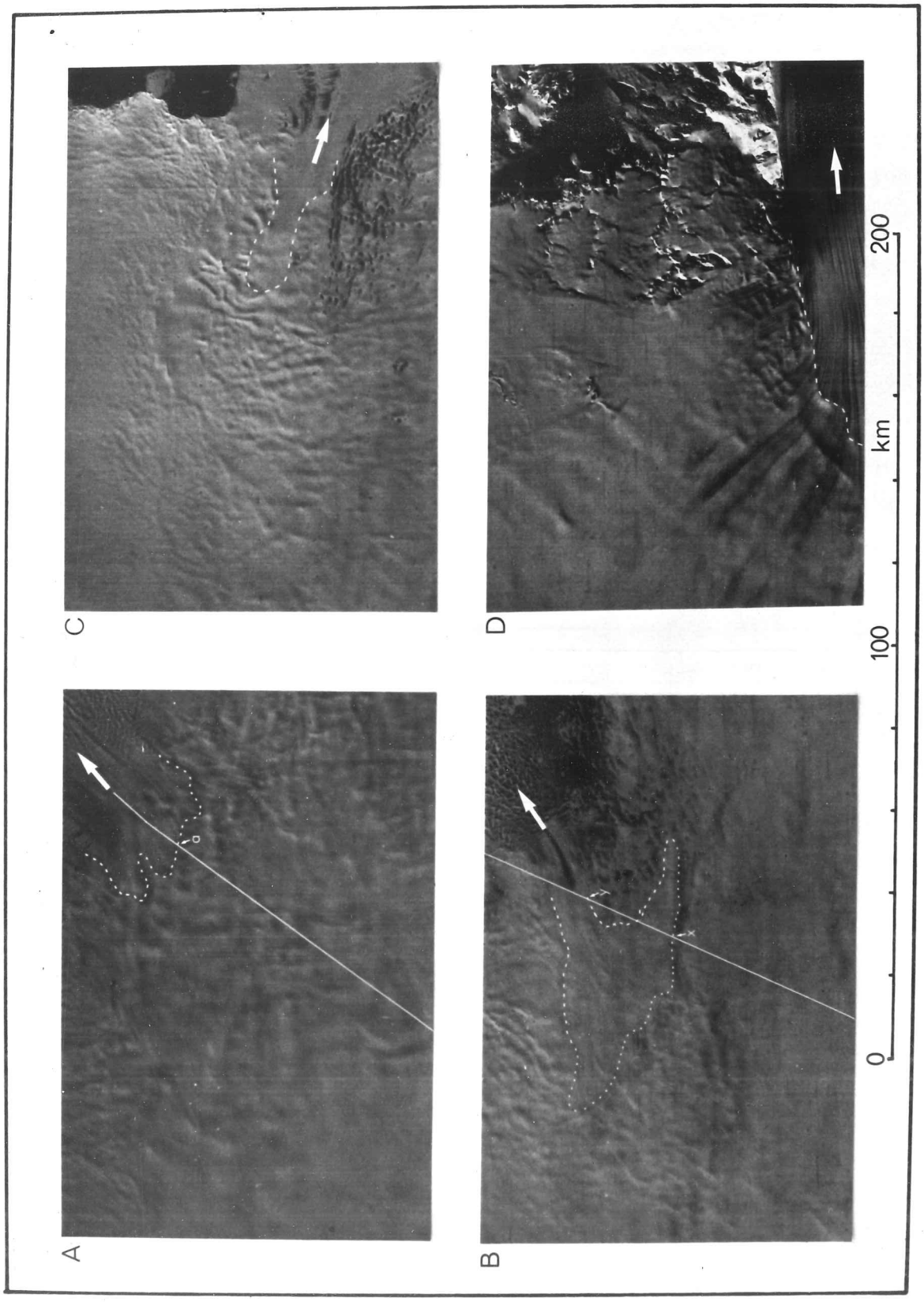

Figure 7.1: caption of previous page.

undulating topography typical of the ice sheet margin from the smoother, relatively featureless terrain feeding the outlet glaciers themselves. The boundary between these areas is, in places, heavily crevassed and often appears to be wind-scoured and free of snow, indicating a scarp-like step. Even when individual crevasses are not visible on Landsat, radio echo sounding shows that consistent cluttering of Z-scope records begins within 2 km of the transition in topography upstream of Frost and Thwaites Glaciers. The imagery shows that other parts of the basins display terrain similar to that of the Marie Byrd Land ice streams; Rose (1979) deduced this to be heavily crevassed ice on the basis of radio echo sounding records and aerial photographs. Similar crevassed basins have been reported inland of many outlet glaciers in Antarctica (Shumskiy, 1970) and in Greenland (Holtzscherer and Bauer, 1954). The observed change in surface topography is indicative of a change in the flow regime (Whillans and Johnsen, 1983) as expected during the transition of motion from internal deformation to basal sliding. The onset of crevassing indicates tensile longitudinal stresses, as would occur with significant basal lubrication.

Details of the form of the ice sheet are available in a few instances along flight lines which intersect basins inland of outlet glaciers (figure 7.2). Derived surface profiles down flowlines to Frost, Thwaites and Byrd Glaciers show distinct features which enable them to be accurately matched with Landsat. In the first two cases studied, the transition between undulating and smooth terrain identified on the imagery corresponds to within 1 km with an abrupt increase in surface gradient. The flight line down Byrd Glacier is beyond the coverage of Landsat. The gradients over these sections are 7.9, 7.7 and 7.2% for Frost, Thwaites and Byrd Glaciers respectively and so are between 6 and 8 times the regional gradients of approximately 1.1, 1.2 and 0.9%. These steep slopes are not associated with changes in aircraft elevation or with the occasional instabilities noted to occur in the pressure altitude signal (section 2.2) and are are over twice as steep as slopes typically associated with surface undulations in these regions. They are clearly the surface expression of the subglacial topography, which is also shown in

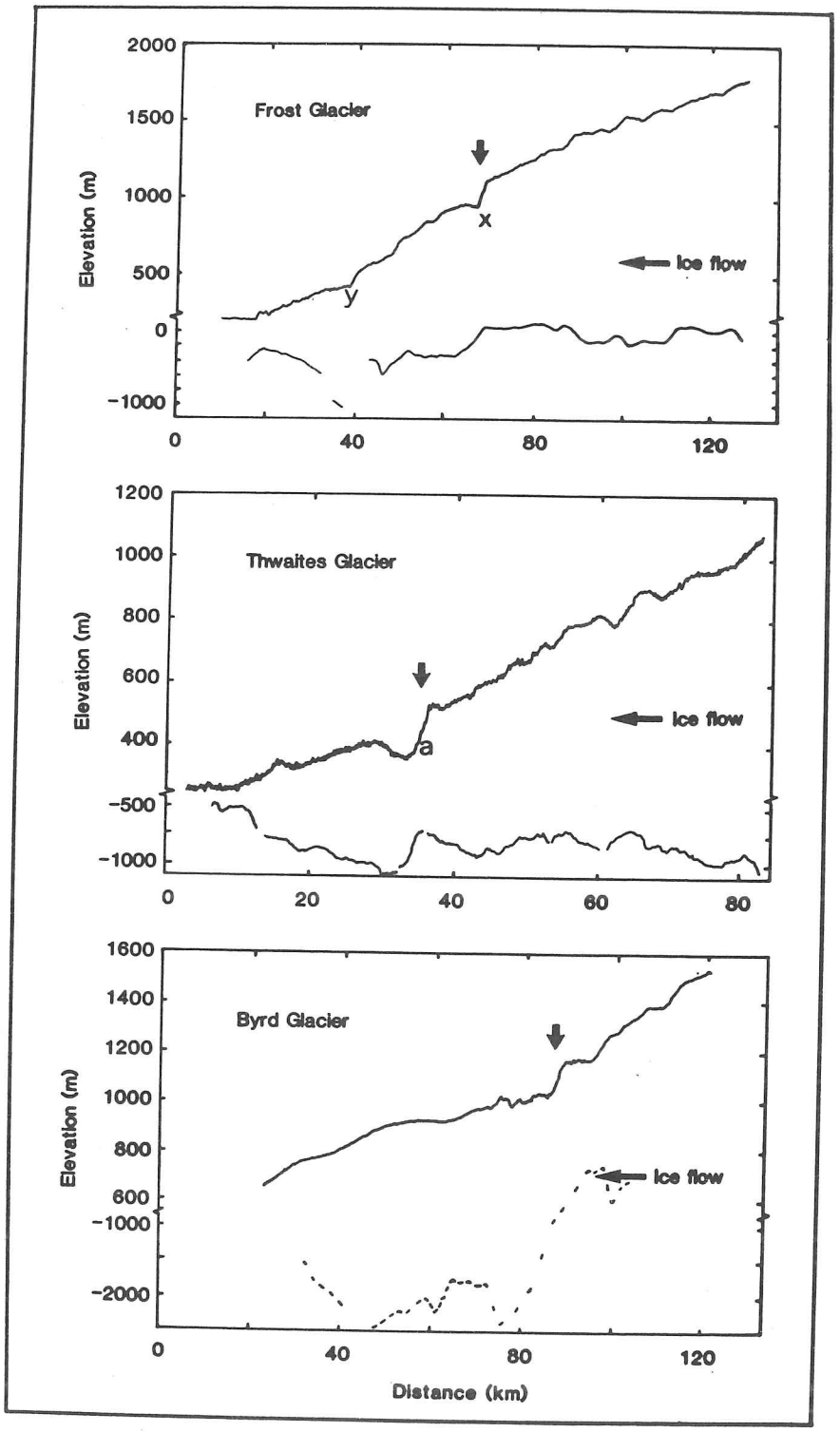

Figure 7.2: Derived surface profiles from aircraft altimetry and bedrock profiles from radio echo sounding down flowlines to Frost (A), Thwaites (B) and Byrd (C) Glaciers showing repetition of steep slopes in association with basal peaks which occur at transition from sheet to stream flow. Bedrock profile for Byrd Glacier is dashed to show sparse data. Note vertical scales for surface and bedrock profiles are different. Points a, x and y refer to locations on Landsat images in figure 7.1.

figure 7.2. Radio echo soundings show there to be bedrock steps of between 400 and 2200 m directly beneath the steep slopes where these are intersected by flight lines. On the basis of Landsat imagery, we may assume that these marked subglacial escarpments surround the heads of the subglacial valleys.

The altimetry profiles of Thwaites, Frost and Byrd Glaciers (figure 7.2) also confirm a trend noted from Landsat; they show a progressive decrease in the occurrence and amplitude of undulations between the zone of maximum slopes and the grounding line. This was reported earlier from Landsat imagery of Ice Stream E (section 4.2.3). The change in topography is again consistent with the progressive decoupling of the ice from its bedrock in association with the onset of basal sliding. As the thickness of the basal water layer builds up, it submerges increasingly large obstacles to flow and is able to bear a greater proportion of the weight of the overlying ice. That the transition to basal sliding begins at the lip of the subglacial valleys feeding these outlet glaciers is supported by the prediction that changes in surface topography, as seen to occur at this point, are largely attributable to variations in flow regime (Whillans and Johnsen, 1983).

7.2.3 Ice dynamics during the transition from converging to steaming flow

Direct measurement of velocities of Antarctic outlet glaciers are generally scarce, particularly inland of the coastal zone in which control points and recognizable features are most common. However, the virtually unlimited number of natural features on the surface of Byrd Glacier enabled Brecher (1982) to make detailed determinations of velocity variations within the fjord walls. Surface velocities of 601 points were calculated photogrammetrically and contours of these in the upper fjord region are shown in figure 7.3 superimposed on a Landsat image. With an expected error of less than 5%, they show good agreement with previous, independently determined velocities (Swithinbank, 1963; Hughes and Fastook, 1981). The relative absence of discernible surface features in the region of converging flow made the calculation of velocities

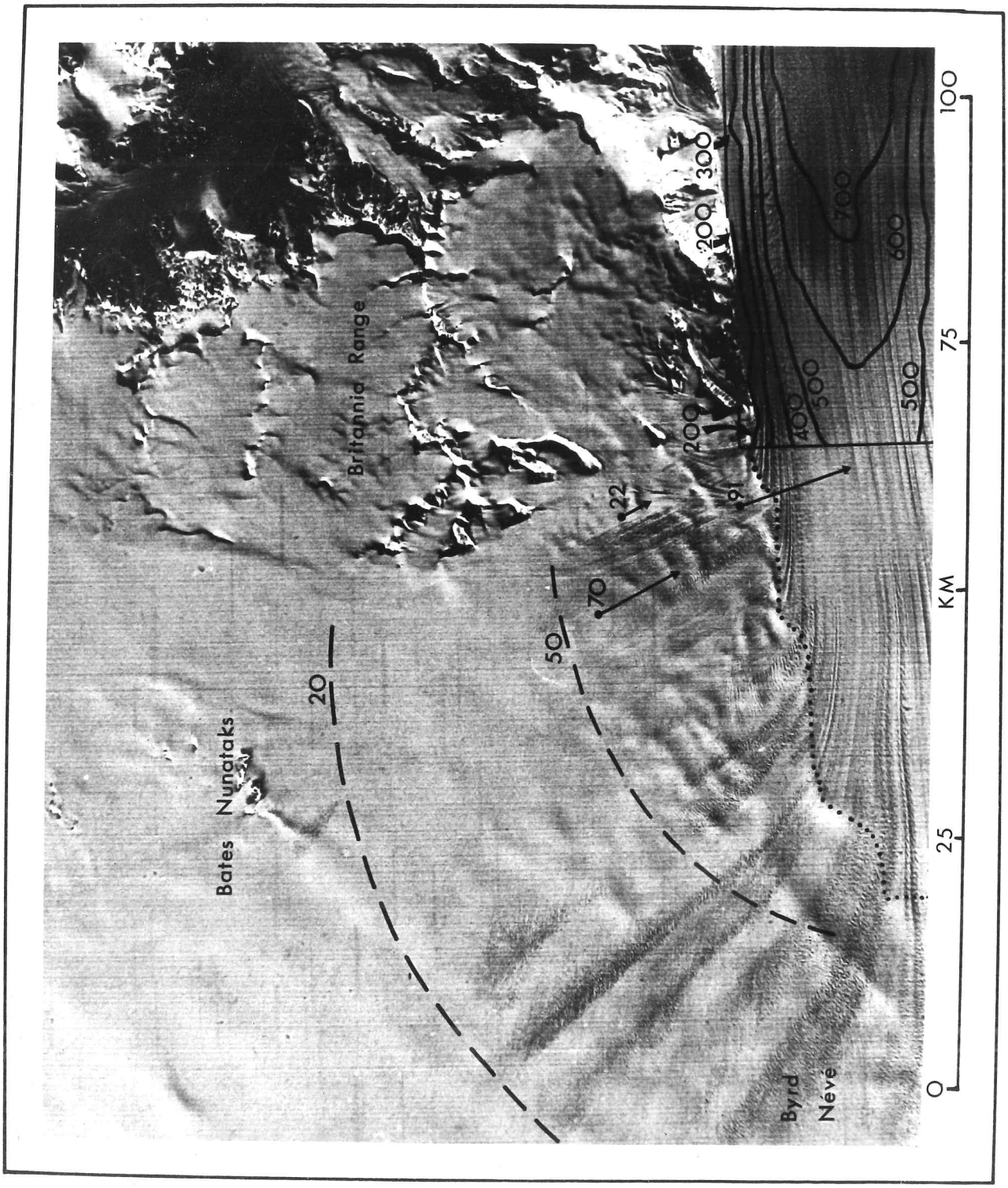

Figure 7.3: Balance and measured velocities in the region of Byrd Glacier. Balance velocities (dashed lines) have been calculated with data from Drewry (1983a). Measured velocities have been calculated photogrammetrically; contoured values (heavy solid lines) are from Brecher (1982) and the three velocity vectors are from Brecher (personal communication).

difficult. However, by placing markers on the glacier surface, three velocity measurements were made (Brecher, written personal communication) and, although of poorer accuracy, provide velocities inland of the observed step in surface topography. Balance velocities have also been calculated for the Byrd Glacier drainage basin (figure 7.3) using data from Drewry (1983a). The good agreement between the measured and calculated values inland of the fjord walls suggests that the latter are accurate to a first approximation.

Figure 7.3 shows there to be a significant change in motion associated with the onset of topography characteristic of streaming flow. Balance velocities increase gradually from the ice divide and are approximately 50 m a^{-1} within 10 to 20 km of the topographic step. The measured velocities show that the ice is still moving at less than 100 m a^{-1} within 2 km of this point. Only 8 km downstream, however, the ice has accelerated to 500 m a^{-1} and reaches a maximum of 875 m a^{-1} within another 55 km. Further, while balance velocities inland show a fairly uniform convergence of flow, ice within the fjord displays very high lateral velocity gradients. This suggests that simple shear occurs in an easy glide fabric along the entire length of the fjord (Hughes and Fastook, 1981). This pattern of velocities is as would be expected during a change to streaming flow where motion is dependent on basal sliding due to water lubrication.

That motion inland of the step is largely due to internal deformation can be seen by comparing values of driving stress with the ratio of velocity to thickness (figure 7.4), which is proportional to the mean shear strain rate through the ice column. As discussed in section 6.2, ice flow dominated by basal lubrication undergoes a transition to low driving stresses while mean shear strain rates increase to very high values (figure 6.4.B). This is not seen for the data in figure 7.4 which are taken from within 10 km of the topographic step in Byrd Glacier. The pattern is similar to that of much of East Antarctica which is thought to move by internal deformation (figure 6.4.A) and there is good agreement with the data of Budd and Smith (1981). Although the scatter of points is quite high, this may be attributed to the use of balance, rather than measured,

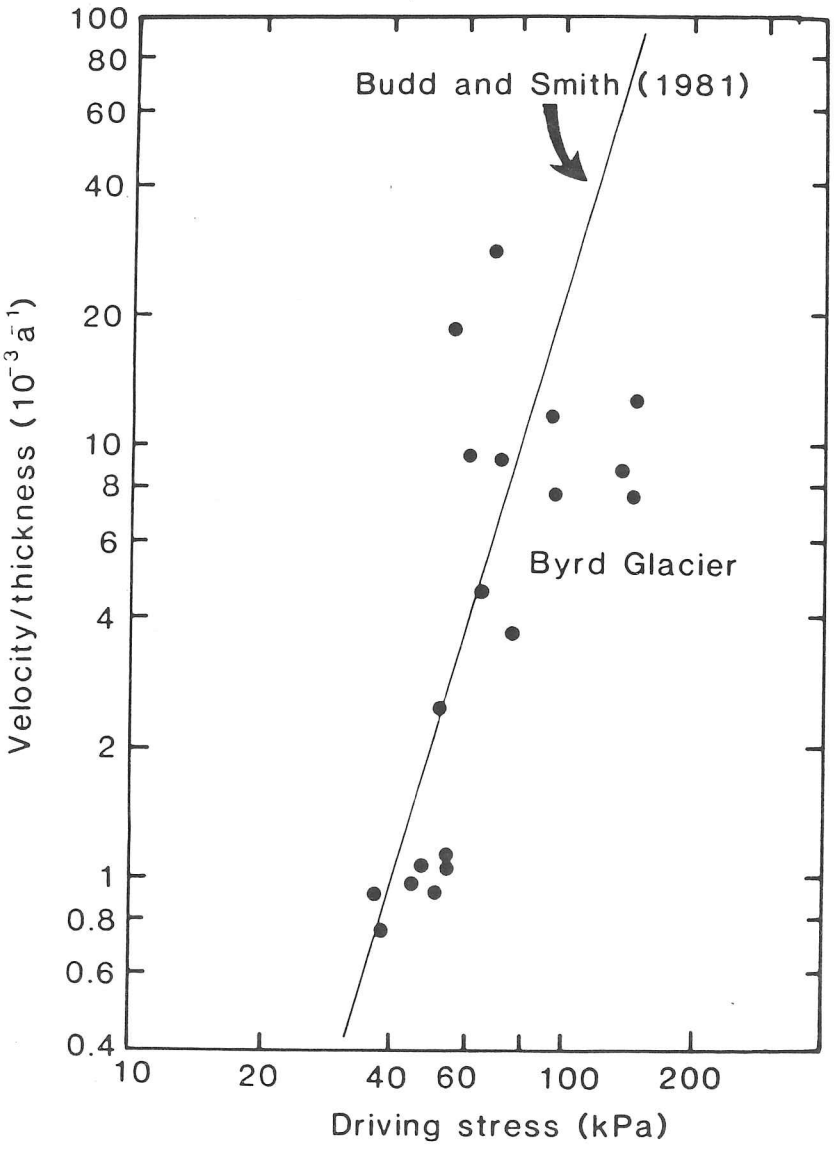

Figure 7.4: Variations of mean shear strain rate (u/z) with driving stress between 10 and 100 km upstream of the step in the Byrd Glacier profile. Regression line is for polar ice which is thought to be moving largely by internal deformation (Budd and Smith, 1981).

velocities and to the small window (20 km) used to calculate driving stresses which is unlikely to have averaged out longitudinal stress gradients (section 6.3).

Direct evidence of basal water, and hence the possibility of basal sliding, downstream of the maximum surface gradient comes from consideration of the strength of returned radio echoes. Figure 7.5 shows bedrock echoes recorded in the ESM mode (section 2.1) down a flowline to Byrd Glacier at points 4.0 km upstream (A), at the mid-point (B) and 3.5 km downstream (C) of the abrupt increase in surface slope. Unfortunately, because this mode of recording was used in only three Antarctic radio echo sounding seasons and because of faults in the recording camera and the changing of film, this is the only outlet glacier for which a complete profile of ESM data is available. Qualitative support for the patterns discussed below may, however, be found in the changing character of bedrock echoes in Z-scope profiles where they are not obscured by heavy crevassing.

Figure 7.5.A shows the great variability in returned peak power which is characteristic of a rough ice-rock interface. The echo consists of many smaller reflections from individual facets; their amplitudes and auto-correlation lengths are related to the distribution of slopes and the auto-correlation length of the reflecting surface (Neal, 1976). Figure 7.5.C, however, shows a very much more uniform level of returned power and is more typical of an interface between ice and ponded water. An intermediate reflecting surface is shown in figure 7.5.B, in which it is actually possible to see the transition from rock to water reflectors over a distance of about 500 m. Contrary to expectations, ESM amplitudes are generally less where the ice is underlain by water (B and C) than by rock (A). This is the result of the rapid increase in ice thickness associated with the step in subglacial topography and hence the greater absorption of the returned power. This pattern of echo strengths confirms previous suggestions that the topographic change seen at the heads of outlet glaciers is associated with a transition in the ice flow regime (Whillans and Johnsen, 1983) and that the head of the subglacial valley marks the

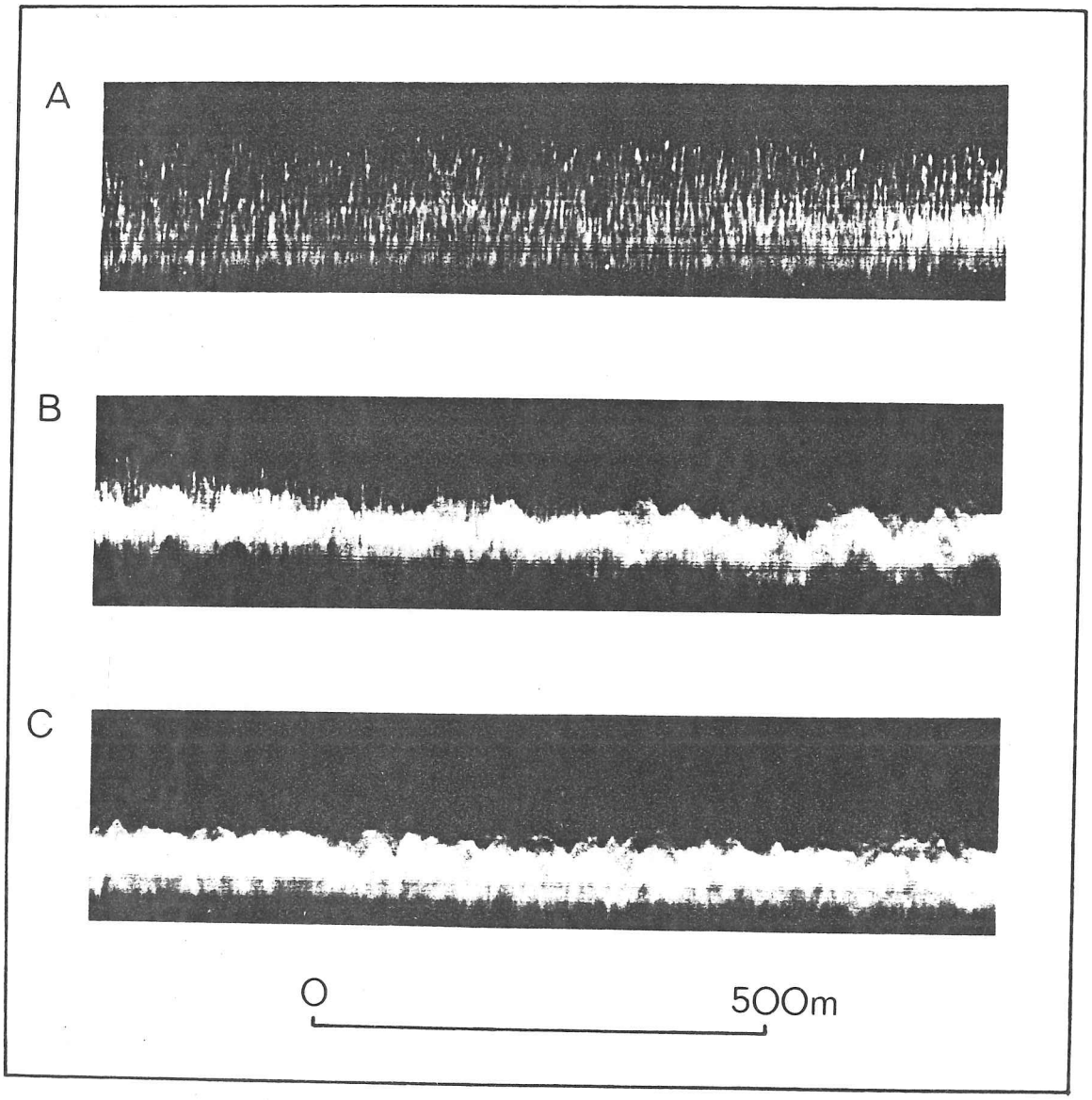

Figure 7.5 ESM records of bedrock echoes down a flowline to Byrd Glacier. A, B and C are 4 km upstream, at and 3.5 km downstream of the step in the surface profile.

point at which basal sliding becomes an important contributor to ice motion.

The location of this transition from slow to fast flowing ice is further confirmed by driving stress patterns. It has been noted that down flowlines to outlet glaciers there is typically a gradual increase to a peak of about 150 kPa within 100 km of the grounding line followed by a rapid decline to zero at the grounding line; this was noted for Byrd, Frost, Reeves, Ninnis, Vanderford and Totten Glaciers (figure 6.3.A; Budd and Young, 1979; Young, 1981; Cooper, McIntyre and Robin, 1982; McIntyre and Cooper, 1983). Similarly, on the basis of ice thicknesses and surface gradients deduced from the elevation and slope of lateral moraine deposits, ice drained through the late Wisconsin fjords of Baffin Island with driving stresses invariably between 20 and 50 kPa (Dowdeswell and Andrews, in press). This pattern is also seen down flowlines to Thwaites and Lennox King Glaciers. Although partially obscured by the relatively long distance over which values are averaged (50 km), the coincidence of the peak in driving stress with the step in the surface profile is consistently within 10 km. That the two are more closely related can be shown by reducing the window size for the calculation of stresses. Despite a considerably distorted pattern due to the effects of longitudinal stress gradients, the peak in driving stress converges on the point of maximum slope. Using mean values over 10 km sections, the maximum driving stresses of 220 and 280 kPa down flowlines to Thwaites and Lennox King Glaciers respectively occur within 2 km of the mid-point of the maximum surface gradient (figure 7.6). This is the case in all of the outlet glaciers studied. The observed rapid decline in driving stresses after this point is clearly the result of basal water, as was indicated by ESM records; this is in agreement with the assumed transition to high velocities, the lower mean gradient downstream, the change in surface topography and the onset of surface crevassing.

The three-dimensional nature of this transition was shown by the arcs of high driving stresses round the heads of ice streams and outlet glaciers (figure 6.1; Cooper, McIntyre and Robin, 1982; McIntyre and

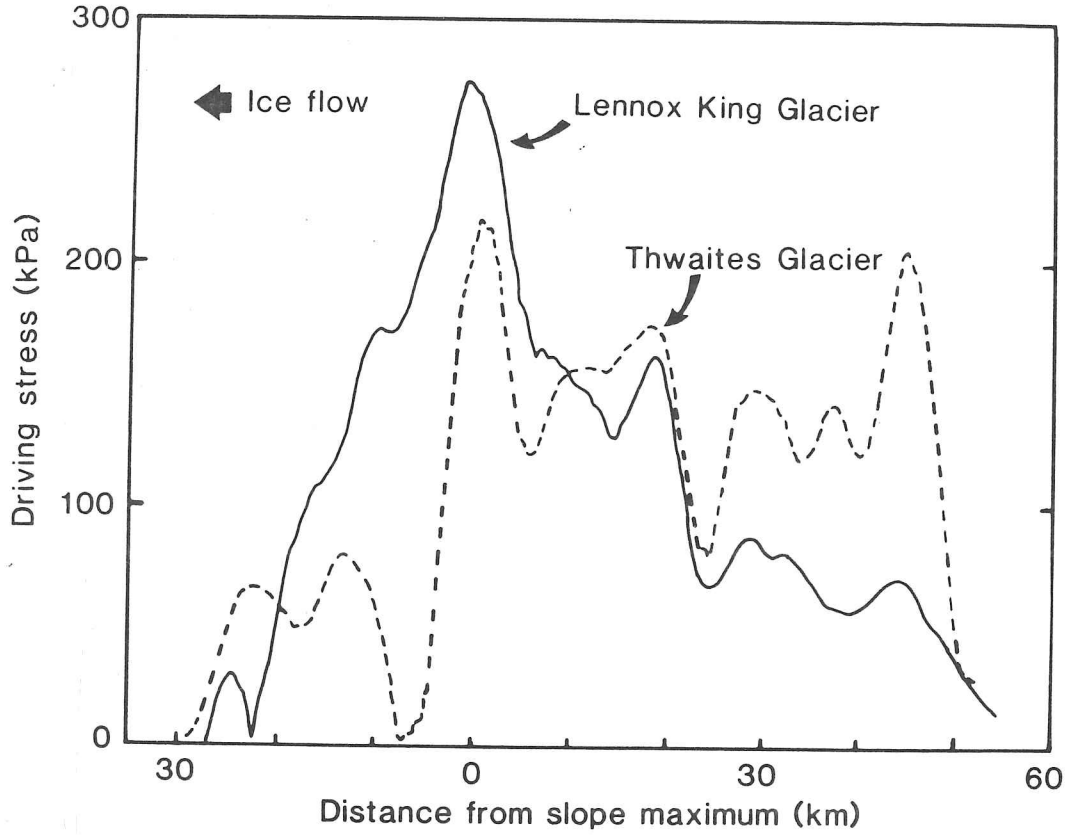

Figure 7.6: Driving stress profiles down flowlines to Thwaites and Lennox King Glaciers calculated over 10 km windows showing the convergence of the peak value on the step in the surface profile as the averaging length is reduced. Compare with figure 6.3.A.

Cooper, 1983). They can now be seen to be associated with the amphitheatre-like basins which mark the change in regime of flow. The subsequent fall to a driving stress of zero at the grounding line, as was found in the two-dimensional analysis, was not reproduced in three dimensions because of the grid size which averaged data over 111 km squares.

It should be noted that a large negative gradient in driving stress downstream of the peak is a mechanism suggested by Robin and Weertman (1973) for the ponding of basal water in what they call the 'trigger zone' of surging glaciers. In the case of outlet glaciers, this process will enhance the acceleration of the ice by retaining subglacial water in the transition zone. Further, since the driving stress pattern is dependent on basal topography, neither it nor the zone of high velocity flow will propagate upstream, as occurs during the surging of temperate glaciers. This is discussed further in section 7.3.1.

Mechanisms for the presence of subglacial water in basins at the head of outlet glaciers, and hence for the onset of basal sliding, are not known with any certainty but two processes have previously been suggested. First, the zone of high convergence of flow, steep slopes and high driving stresses may provide lubrication through mechanical shearing, strain softening and increased water production (Budd and others, 1979). Second, Hughes (1977) suggested that the extensive zones of crevassing in the transition zone may provide suitable conduits for surface meltwater (Pfeffer, 1982) to reach the bed if they remain water-filled, as suggested by Weertman (1973). Differentiation between these mechanisms is not possible given present knowledge of ice sheet dynamics but we may consider the closely related role of basal temperatures in the change in regime.

Weertman (1963), in an analysis of ice flow through a mountain barrier, predicted the profile of the ice sheet and the heat balance at bedrock in the region of outflow. Although he did not allow for the observed concavity in surface form where basal sliding sets in, he recognized that basal ice in immature and very rapidly moving outlet glaciers, and possibly that of mature outlets too, would be at pressure melting point. The coincidence of the zone of maximum stress and the apparent onset of

sliding (Budd and Young, 1979) has been taken to indicate that the acceleration of the ice is induced by frictional heating (Budd and others, 1979), which will also reach a peak at this point. Using the model of Budd (1969), we were able to estimate basal temperatures inland of this zone in Byrd Glacier which occupies a substantial breach in the Transantarctic Mountains. Even assuming a basal temperature gradient of 0.03 $^{o}C\ m^{-1}$ and a balance velocity of 35 m a^{-1}, the basal ice is at pressure melting point 20 km inland of the transition to fast flow in this mature outlet. More realistic values are 0.03 to 0.07 $^{o}C\ m^{-1}$ (Drewry, 1982; Smith and Drewry, in press) and 50 m a^{-1} and so we may assume that the zone of warm basal ice due to frictional heating extends a considerable distance into the ice sheet from the subglacial step. On this basis, the transition to high velocity flow is unlikely to be due to temperature and the importance of a topographic trigger must be assumed.

The preceding evidence linking high velocity flow in outlet glaciers to a characteristic subglacial topographic feature has been largely confined to a few instances for which the necessary sources of data have been available. That the resulting conclusions are more widely applicable, and hence that the association is factual rather than coincidental, can be shown by supporting the discussion with data from other sources. Table 7.1 presents statistics relating to the transition in flow for nine glaciers. Sources used include topographic maps at a scale of 1:250 000 published by the U.S. Geological Survey and radio echo profiles; they are of poorer accuracy than the aircraft altimetry and Landsat imagery but confirm the previously noted details where overlap occurs. The results are consistent and the repetition of certain features should be noted. These are the marked step in the surface profile at the point of transition, the occurrence of a bedrock sill at this point, the lower mean slopes downstream of the step compared with those above, the sharp fall in driving stresses calculated over 10 km sections and the onset of crevassing. All these points support the concept of a topographically initiated transition in flow regime shown by velocity measurements in Byrd Glacier (figure 7.4) and their repetition indicates that it is a consistent feature which controls discharge from the ice sheet.

Table 7.1: Statistics of gradients, driving stresses and sill heights in the region of the transition to high-velocity flow within outlet glaciers.

Glacier	Gradient			Driving stress		Sill	Comments
	above peak	at peak	below peak	peak	below peak		
	(%)	(%)	(%)	(kPa)	(kPa)	(m)	
Frost	1.4	7.9	0.9	160	20	400	
Thwaites	2.0	7.7	1.1	120	30	400	
Byrd	1.3	7.2	0.4	170	40	2200	
Lennox King	1.5	6.2	0.8	160	20	1250	
Mackay	1.7	6.5 8.2	1.6	-	-	-	Two steps in profile close together.
David*	2.0	8.0	0.9	-	-	-	Escarpment round only ¾ of basin.
Scott	0.9	-	0.9	-	-	-	No marked step visible in surface profile.
Scott*	-	7.1	1.6	-	-	-	Escarpment round only ¾ of basin.
Mertz$	-	3.1	1.1	190	40	450	
Ninnis$	1.2	-	0.4	160	30	600 600	Two steps in bedrock profile, 20 and 50 km upstream from driving stress peak. No clear step in surface profile.

* U.S. Geological Survey maps, 1:250,000.

$ S.P.R.I. radio echo sounding profile.

7.2.4 Marie Byrd Land ice streams

The flow regime in West Antarctic ice streams has often been regarded as quite unlike the steady-state flow of outlet glaciers (Hughes, 1973, 1977; Young, 1981). This is partly based on their gradual transition to low driving stresses with increasing shear strain rates between 400 and 600 km upstream of the grounding line (figure 6.3.B) rather than the abrupt decrease in the last 100 km of outlet glaciers (figures 6.3.A and 7.6). Such behaviour does not necessarily indicate instability; the measured velocities of the ice streams have been closely approximated by steady state balance velocities (Rose, 1979; Weertman and Birchfield, 1982). The analysis of gradients in chapter 4 also noted significant differences in the form and topography of Thwaites Glacier and Institute Ice Stream.

West Antarctica differs from East Antarctica in two important respects. First, much of the West Antarctic ice sheet rests below sea level and so the effective normal stress is reduced by hydrostatic pressure. This will be most apparent under the Marie Byrd Land ice streams which flow in bedrock depressions between 500 and 1000 m below sea-level. Second, the West Antarctic ice sheet has higher basal temperatures (section 5.4) and is of lower elevation than East Antarctica and so has higher surface and mean temperatures. Thus, not only is there more water available at the bed, which increases basal decoupling and induces sliding, but the ice's rheological response to stress will be affected. In view of these differences, the transition to basal sliding may be the result of reaching a critical normal stress above buoyancy (Budd and others, 1979) rather than a frictional limit (the product of basal shear stress and sliding velocity) beyond which rapid unstable acceleration is thought to occur in temperate glaciers (Budd, 1975). The repetition of the pattern implies that it may be a stable feature and that the sliding of ice streams under hydrostatic buoyancy differs from that of temperate and fast polar glaciers. This is discussed further in the next section.

7.3 Implications for the flow of the Antarctic ice sheet

7.3.1 Surging of ice sheet outlets

For two decades the question of whether the Antarctic ice sheet undergoes periodic instabilities (Wilson, 1964) has been debated by glaciologists, climatologists and geophysicists. Attention has been particularly keenly focused on the marine West Antarctic ice sheet and its ice streams which are responsible for the majority of its discharge (Robin, 1970; Johnsen and others, 1972; Whillans, 1973, 1976; Weertman, 1974; Hughes, 1975, 1977). The buttressing effect of the Ronne-Filchner and Ross Ice Shelves has been seen to provide a crucial restraint on instabilities (Mercer, 1968; Thomas, 1976; Thomas and Bentley, 1978) and this has led to suggestions that the most likely direction for the collapse of the ice sheet would be into the Amundsen Sea through Pine Island and Thwaites Glaciers (Hughes, 1979a, 1981; Denton and others, 1979; Denton and Hughes, 1981; Lingle and Clark, 1979; Thomas, 1979a; Thomas and others, 1979).

Of central importance to the stability of any part of the ice sheet is the transition from internal deformation to fast flow with basal sliding. Although little is known of the mechanics of this transition, it was shown in section 7.2 that the valley head which typically underlies outlet glaciers initiates fast flow through the acceleration of converging drainage down a steep gradient; it thus acts as a trigger to the higher velocities observed downstream. If this is the case, then the rapid transfer of the transition zone inland, as occurs during the surge of a temperate glacier, seems particularly improbable. With the topographic step controlling the onset of basal sliding, it is likely to induce a form of stability in discharge from the ice sheet since the transition zone will be unable to retreat beyond it. The acceleration of ice through outlet glaciers is therefore pinned to a zone at the head of subglacial valleys by its dependence on topographic initiation. Even with minor fluctuations of the location of the onset of basal sliding due to variations in boundary conditions (such as ice sheet flux, sea level or

climatic regime), the head of the subglacial valley will inhibit propagation of a surge by acting as a sill beyond which grounding line retreat cannot occur (Hughes, 1977; Thomas, 1979a). Thus ice sheets draining through subglacial fjord topography or mountain terrain appear unlikely to undergo instabilities in flow regime. This is an important suggestion with regard to the Greenland ice sheet which drains almost entirely through outlet glaciers. It is interesting to note that no evidence of surge activity has yet been presented for this ice mass.

7.3.2 Types of ice sheet outlet

The development of high velocities in outlet glaciers and the implications of this for the stability of the ice sheet may be further considered through the model of Budd (1975) which recognizes three classes of glacier (ordinary, fast and surging) and two modes of flow. Fast glaciers differ from the ordinary type by having sufficient flux to remain continuously in the fast flow mode with high velocities and low basal stresses. Surging glaciers form an intermediate class and have sufficient flux to reach the fast mode but not to maintain it. They develop a periodically oscillating state between fast and slow modes with gradual build-up and rapid drainage.

An empirical distinction of these flow regimes (Budd, 1975) has been made on the basis of centre-line thickness as a function of surface slope and velocity (figure 7.7). Byrd, Ninnis and Frost Glaciers are all classed as fast polar glaciers by this relationship (figure 7.7). They support the concept of a lubrication factor enabling the development of high velocities after a critical limit of velocity and basal stress has been reached (Budd and Allison, 1975; Budd and Jenssen, 1975). Although Byrd Glacier has previously been cited as having all the traits of a surging glacier (Hughes, 1977), it is consistent with the steady-state assumptions of the model.

The relationship does not hold, however, for the West Antarctic ice streams which drain into the Ross Ice Shelf. Using mean values of thickness and balance velocity for Ice Streams B, C, D and E (Rose, 1979),

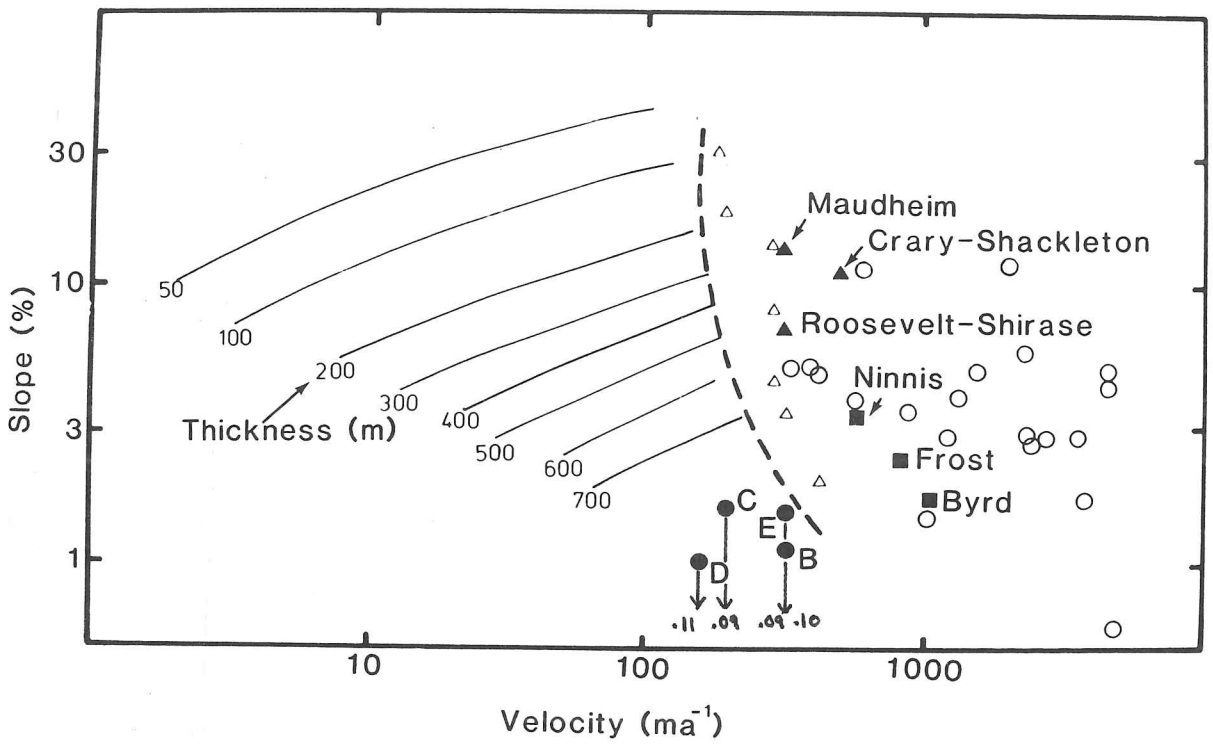

Figure 7.7: Relationship between mean thickness, velocity, slope and flux for ordinary, surging (triangles) and fast flowing (circles) glaciers (from Budd, 1975). Also shown are values for Byrd, Ninnis and Frost Glaciers. Byrd Land ice streams (B, C, D, and E) and three confined ice shelves are indicated only by values of velocity and thickness. Data sources are Swithinbank (1955) Robin (1958, 1975), Rose (1979) and Thomas and others (1982).

we find significant inconsistencies with the expected value of surface slope (figure 7.7). Observed gradients (typically less than 0.1%) are less than predicted by an order of magnitude or more. An error of this size cannot be explained by a difference between calculated and real velocities or by inaccuracies in thickness or slope measurements. That the model does not fit the data suggests the inapplicability of using a lubrication factor to explain their presumed high velocities. This in turn implies that the three-fold classification of Budd (1975) should be modified to conform with the relationship between their form and flow. In support of this, Young (1981) suggested that there is a qualitative difference between these ice sheet outlets and fast polar glaciers. He noted that their distributions of surface slope, flux, ice thickness, stress and velocity were quite unlike those of ordinary and fast-flowing glaciers. This is confirmed by the differences evident in figure 7.7. Also, the rapid transition zone in fast outlet glaciers which separates slow moving ice in the interior from the region of fast flow with low basal shear stress (figure 6.3.A) does not occur in these ice streams. In a recent analysis of the dynamics of Ice Stream B, Bindschadler (1983) concluded that, although double-valued sliding relationships have been used to explain the observed acceleration of ice streams under low slopes (Budd, 1975), the higher velocities were better explained by pressurized subglacial water. High water pressures result in basal separation and stress concentration where the ice is still in contact with the bed. It is these concentrations that control the sliding velocity.

A better understanding of these ice sheet outlets is gained by comparing them with confined ice shelves which, given the results of figure 7.7 and the suggested importance of pressurized water, may be expected to behave in a similar manner. In both cases, it is likely that the walls rather than the bases of the ice streams provide most of the restriction to flow. Indeed, on the basis of localized flat surfaces with ice thicknesses indicating hydrostatic equilibrium, Robin and others (1970) suggested the presence of a series of 'pseudo' ice shelves in this region of Marie Byrd Land. Using data on ice thickness, surface velocity and surface slope for ice shelf segments (approximately 50 km in

width) between ice rises, grounding points and land-based ice, we find a similar disagreement with the model of Budd (1975) (figure 7.7). Surface slopes from Quarisen (Maudheim Ice Shelf) and locations between Roosevelt Island and Shirase Coast and between Crary Ice Rise and Shackleton Glacier in the Transantarctic Mountains are lower than expected by one to two orders of magnitude. It is therefore reasonable to consider the Marie Byrd Land ice streams as more closely related to ice shelves than to terrestrial ice. They appear to represent landward extensions of the ice shelf which penetrate the West Antarctic ice sheet. Their behaviour is consistent with ice which is flowing under the influence of lateral coupling rather than the basal shearing which dominates terrestrial ice flow.

7.3.3 Surging of the ice sheet

Mass balance calculations have been attempted for many drainage basins and sections of the ice sheet (Lorius, 1962; Bogorodsky and others, 1977; Shimizu and others, 1978; Allison, 1979; Young, 1979; Naruse, 1979) but the uncertainties involved, often due to the scarcity of data, make conclusions about the likelihood of past surging somewhat unreliable. The presence of areas of bare ice in Lambert Glacier's drainage basin (section 4.2.2; McIntyre, in preparation) is a case in point. Computer modelling of the surging potential of a section of East Antarctica (Budd and McInnes, 1978) has shown that the form of the ice sheet inland of Mirny is very similar to that which is predicted for the partial build-up following a surge. The build-up is thought to be indicated by the calculated positive mass budget. The reliability of this model must however be questioned because the ice sheet profile used in the analysis is not directly up a flowline from Mirny. By taking transects through an ice sheet at various angles to flow, any number of high order curves may be obtained and so this profile cannot be used for an exact comparison. A further question to be considered is the possibility of a surge occurring at that location. Although ice sheet outlets have been identified as likely locations for the initiation of instabilities (Hughes, 1977; Thomas, 1979a), the discussion in section 7.3.1 suggests that the

width) between ice rises, grounding points and land-based ice, we find a similar disagreement with the model of Budd (1975) (figure 7.7). Surface slopes from Quarisen (Maudheim Ice Shelf) and locations between Roosevelt Island and Shirase Coast and between Crary Ice Rise and Shackleton Glacier in the Transantarctic Mountains are lower than expected by one to two orders of magnitude. It is therefore reasonable to consider the Marie Byrd Land ice streams as more closely related to ice shelves than to terrestrial ice. They appear to represent landward extensions of the ice shelf which penetrate the West Antarctic ice sheet. Their behaviour is consistent with ice which is flowing under the influence of lateral coupling rather than the basal shearing which dominates terrestrial ice flow.

7.3.3 Surging of the ice sheet

Mass balance calculations have been attempted for many drainage basins and sections of the ice sheet (Lorius, 1962; Bogorodsky and others, 1977; Shimizu and others, 1978; Allison, 1979; Young, 1979; Naruse, 1979) but the uncertainties involved, often due to the scarcity of data, make conclusions about the likelihood of past surging somewhat unreliable. The presence of areas of bare ice in Lambert Glacier's drainage basin (section 4.2.2; McIntyre, in preparation) is a case in point. Computer modelling of the surging potential of a section of East Antarctica (Budd and McInnes, 1978) has shown that the form of the ice sheet inland of Mirny is very similar to that which is predicted for the partial build-up following a surge. The build-up is thought to be indicated by the calculated positive mass budget. The reliability of this model must however be questioned because the ice sheet profile used in the analysis is not directly up a flowline from Mirny. By taking transects through an ice sheet at various angles to flow, any number of high order curves may be obtained and so this profile cannot be used for an exact comparison. A further question to be considered is the possibility of a surge occurring at that location. Although ice sheet outlets have been identified as likely locations for the initiation of instabilities (Hughes, 1977; Thomas, 1979a), the discussion in section 7.3.1 suggests that the

transition to high velocity flow is pinned by its dependence on a subglacial trigger. The inland propagation of a surge would be inhibited by the typical bedrock step which underlies these outlets. However, intervening ice sheet margins, such as the coast at Mirny, are characterised by diverging flow. The transition in regional patterns of ice flow and mass balance required for the development of high velocities and unstable behaviour suggest that this is not a probable location for the initiation of a surge.

Consideration should be given to the areas of the ice sheet which will be affected by an instability in its discharge. Evidence from Barnes Ice Cap, North-East Land and Vatnajokull (Liestøl, 1969; Løken, 1969; Holdsworth, 1977; Thorarinsson, 1964, 1969; Schytt, 1969) indicates that surging can occur independently in separate drainage basins within the ice mass. When a surge is initiated, its effects on the ice mass appear to be largely confined to its direct catchment area. In view of the anomalous behaviour of only one of the outlets from Marie Byrd Land, Ice Stream C which Rose (1979) suggested may indicate a post-surge dormancy, it appears that this may apply in the Antarctic ice sheet as well.

This suggestion is particularly important in the light of Landsat imagery and the most recent maps of the surface topography of the Antarctic ice sheet (figure 4.12; Drewry, 1983a; Zwally and others, 1983) which have been compiled from large numbers of accurate results from satellite and aircraft remote sensing. They indicate that the pattern of centres of outflow, ice divides and flow directions is very much more complex than the previous suggestions (Gould, 1940; Budd and others, 1971) even on a smaller scale than suggested by Drewry and Robin (1983). The coastline in particular is punctuated by a complex series of regional and local ice divides, such as that inland of Porpoise Bay (figure 4.12). The influence of these features on the propagation of instabilities is likely to be significant in that they will delimit the areas affected by a surge. The local nature of many such features implies that should a surge occur in an outlet of the Antarctic ice sheet, its influence may be limited spatially and not propagate through the whole ice mass.

7.3.4 Ice stream erosion

The association of ice sheet outlets and subglacial topography has been discussed in section 7.2. The origin of troughs characteristic of glaciated regions has been attributed to many factors of which tectonic movements, pre-existing topography and glacial erosion have frequently been discussed (King, 1959; Embleton and King, 1975; Sugden and John, 1976). The importance of the various factors of origin must vary considerably from one case to another (Flint, 1947) but, once the trough has been initiated, it will tend to concentrate increasing amounts of ice into it and thus enhance its permanence. This will be achieved through the commencement of erosive mechanisms such as abrasion and plucking which operate once ice flow changes to a regime dominated by sliding. Accelerated vertical erosion is most probable in zones of increased ice thickness, higher velocities and existing concave topography (Nye, 1957; King, 1959; Holtedahl, 1967) as occur in a trough underlying an outlet of an ice sheet and, in particular, just beyond the rim of the valley. Thus, feedback will take place between the subglacial topography and glacial erosion; this will involve the onset of sliding as the ice passes over the valley rim, the resulting acceleration in velocity and erosion, accentuation of the trough's topography and hence greater concentration of flow. We may therefore expect that the initial topography which caused the change to basal sliding will be exaggerated and expanded; ice flow will simultaneously accentuate the topography which pins the transition at that point.

This scheme of topographically initiated stream flow is inherent to concepts of the selectivity of glacial erosion within ice sheets. Sugden (1968), quoting results from Greenland and Antarctica (Dansgaard, 1961; Fristrup, 1964; Gow, 1965), concluded that stream flow within ice sheets is a reasonably common occurrence and that under certain conditions, streams are capable of eroding troughs. Similarly, Clayton (1965) stated that erosion is concentrated in valleys while plateau areas may remain largely unaffected by the passage of ice. Our evidence supports this scheme which suggests that ice sheet motion is

dominated by internal deformation until the steep gradients of subglacial valley heads initiate sliding and fast velocities.

Several characteristic topographic components of glacial troughs, among them the steep valley head and associated overdeepened profile, have often presented difficulties to glaciologists and geomorphologists attempting to explain their origin. These occur on many scales in glaciated landscapes. Sognefjord in Norway displays a dramatic headwall which falls 2000 m to sea level in less than 20 km; the deepening continues until a level of more than 1200 m below sea level is reached over 130 km from the coast. The fjord depth at its seaward end is only 100 m below sea level. Skelton Inlet, Antarctica, has been found to have a maximum depth of 1933 m below sea level and, with the water at its mouth nearly 500 m shallower, is the most severely overdeepened fjord yet reported (Crary, 1966).

The mechanisms which produce such features are far from certain. Sugden and John (1976) explained overdeepening by the relative position of the equilibrium line along the trough which usually determines the location of the zone of greatest ice discharge. Here, velocity and ice thickness will tend to be greater than elsewhere, thus favouring higher than normal rates of erosion. Crary (1966) observed that the thickness of floating ice in a fjord increases inland. The motion of ice at the bottom has an upward component and he likened its motion to a chain saw which is normally clear of any contacts. An increase in ice thickness or uplift of the land would bring the bottom material gradually into contact with the moving underside of the ice, allowing direct erosive action to take place. Bathymetry of the valley floor should thus reflect the ice-water boundary at the maximum extent of the ice, showing an increase in depth up the fjord. Multiple basins would result from changes in boundary conditions, such as sea level or ice flux and thickness. The mechanism by which floating ice erodes is thus completely different from that of grounded ice.

The preceding discussion raises the possibility that the development of a steep headwall and subsequent overdeepening may be associated with the onset of basal sliding. Following the commencement of glacial erosion

at the valley rim, the pre-existing topography has a concave form and thickness and velocity increase rapidly downstream. These three aspects have been noted as likely to enhance vertical erosion and therefore produce a means of accentuating initial relief. Erosion will then increase downstream towards a maximum which is determined by the progressive decoupling of the ice from its bed by water. This hydrostatic buoyancy is due to the presence of water from frictional melting, which increases with velocity of the ice stream, and from the sea.* At the grounding line, the ice becomes freely floating and so will have lost its erosive ability until the mechanism suggested by Crary (1966) becomes operative. Thus, the fjord will develop, first, a steep headwall due to the rapid onset of basal sliding, second, an overdeepened inland end as velocity, thickness and topographic concavity increase and, third, a progressively shallower bedrock as hydrostatic decoupling reduces the ice's erosive ability. With the maximum erosive power concentrated at the valley head near the headwall, this feature is likely to retreat upstream as suggested by Souchez (1967). In agreement with this discussion is the observation that the multiple basins of many fjord floors are just downstream of tributary junctions. This suggests that greater vertical erosive power is related to the increase in velocity and thickness and the concentration of ice flow due to the lateral input of ice to the main stream (King, 1959; Holtedahl, 1967).

Assuming that these processes of headwall retreat and inland overdeepening occur, we may return to figure 7.2 and compare the subglacial topography of Byrd and Thwaites Glaciers. The former exhibits a headwall of some 2200 m which is approximately 100 km inland from the seaward flank of the Transantarctic Mountains. If Byrd Glacier has existed for 25 million years either as an outlet for the East Antarctic ice sheet or as a glacier fed by more local mountain ice masses (Smith and Drewry, in press), the headwall retreat through the mountains represents a mean rate of headwall erosion of 4 mm a^{-1}. This may be an underestimate because of the uplift of the mountains. However, given that it occupies a major zone of tectonic weakness, this is not an unrealistic rate of erosion. Thwaites Glacier, on the other hand, shows a vertical step of only 400 m which is

* The presence of subglacial water may also increase the potential abrasion rate which is dependent on ice velocity and effective normal pressure (Boulton, 1974). Hydrostatic forces will reduce the overburden pressure of the ice, thereby changing from a basal regime of till lodgement to one of possible abrasive downwearing.

displaced 10 to 15 km inland of its grounding line. Although it now has velocities of about 3 km a^{-1} compared to a maximum of 875 m a^{-1} for Byrd Glacier and hence presumably a high erosive power, this has been taken to indicate that it is a youthful, or perhaps transient, feature (Drewry and Robin, 1983).

The scheme of changing flow regime outlined above may also help us to reconstruct the glacial periods in areas now free of ice. The well developed fjord terrain of Norway, for instance, is at least in part a relic of the Fennoscandian ice sheet which was centred on the Baltic between 110 and 10 ka BP with its western limit at Norway's Atlantic coast. There are many examples of high inland areas such as Jotunheimen and Rondane which are deeply dissected by hierarchies of fjords. Typically, they have steep headwalls and are often overdeepened inland. We may therefore envisage that much of the discharge from this part of the ice sheet was through ice streams flowing in these subglacial valleys. The fjord heads marked the transition to high velocity flow as basal sliding became dominant and the adjacent areas of overdeepening showed the zone in which vertical erosion, due to the combined effects of velocity, thickness and existing topography, was at its maximum.

Given that the dimensions of ice sheet outlets have been correlated with the size of their drainage basins (Haynes, 1972), we expect the major fjords to be well spaced out along the coastline and so have large areas of the ice sheet contributing to their flux. This can be seen at present in East Antarctica where Byrd, Nimrod, Beardmore, Shackleton, Scott and Reedy Glaciers, at regular intervals of 150 to 300 km, capture most of the discharge through the southern Transantarctic Mountains. This would suggest that outflow from the Fennoscandian ice sheet was dominated by discharge through Hardangerfjord, Sognefjord, Nordfjord and Trondheimsfjord while the smaller intervening outlets drained relatively local areas, for instance, as occurs today inland of McMurdo Sound (Drewry, 1982).

A further consequence of these spatial patterns of flow regime and erosive ability associated with subglacial topography is that we would

expect certain parts of the Antarctic to display fjord terrain following deglaciation. Many of the outlet glaciers in Enderby Land, for instance, are known to be underlain by significant troughs (Allison and others, 1982; Morgan and others, 1982). It is possible that removal of the ice in this area would reveal topography very similar to that of western Norway, British Columbia or southern Chile. We would expect the fjords to penetrate as far inland as is indicated by their zones of streaming flow which, in the cases of Rayner, Beaver, Thyer and Auster Glaciers, is between 50 and 100 km.

7.4 Summary

A comparison of data from aircraft altimetry, Landsat and radio echo sounding has shown there to be characteristic surface topographies associated with sheet and stream flow. The transition between the two is abrupt and is associated with a step in the subglacial topography. This point marks the onset of basal sliding and high velocities due to subglacial water and results in the crevassed amphitheatre-like basins round the heads of outlet glaciers. This is also the zone of maximum driving stress beyond which values decline rapidly as velocities increase. The transition appears to be topographically initiated since basal temperatures are at pressure melting point well inland of the change in regime. The Marie Byrd Land ice streams exhibit qualitative differences to other ice sheet outlets; the change to lower driving stresses is gradual and occurs several hundred kilometres inland. They have particularly low surface slopes and appear in form and flow regime to resemble confined ice shelves rather than grounded ice.

The repeated association of the transition to rapid sliding with a distinct subglacial feature implies a stabilizing effect in discharge from the ice sheet; acceleration of the ice is pinned to a subglacial step and propagation of high velocities inland beyond this feature seems unlikely. Should surging of the ice sheet take place, it is unlikely to occur through existing outlet glaciers.

Rapid ice flow through subglacial trenches may also ensure a permanent association through accentuation of the feature by erosion. This is concentrated towards the heads of outlet glaciers upstream of the region where significant basal decoupling occurs; it is suggested that this may be a mechanism for the overdeepening of fjords at their inland ends and the development of very steep fjord headwalls. This association of ice flow regimes and topography may be of use in the elucidation of the discharge from former ice sheets.

CHAPTER 8

CONCLUSIONS

8.1 Summary of conclusions

In this section, we bring together some of the main conclusions drawn in earlier chapters.

The combination of altimetry, imagery and radio echo sounding collected from aircraft and satellite has provided a more detailed insight in the form and flow of the Antarctic ice sheet than would be gained by using them separately. The aircraft altimetry has been particularly valuable as a source which accurately describes ice surface features over distances of hundreds of metres to hundreds of kilometres. It has also confirmed that much of the detail seen on Landsat imagery represented true topographic variability and has enabled more precise identification of grounding lines and crevasse zones. By comparison, however, Seasat altimetry presented a significantly averaged record of the ice sheet surface. Even after retracking of waveforms and vertical and horizontal corrections to allow for the size of the footprint, Seasat was unable to detect features with vertical dimensions of up to tens of metres and could not maintain lock in the more steeply sloping and irregular terrain of coastal regions.

Statistical and spectral analyses of altimetry has enabled the topographic variability of the ice sheet surface to be determined. Velocity and ice thickness variations result in a gradual increase in the amplitude and decrease in the wavelength of surface undulations with distance from ice divides. Temperature variations have a significant effect on the distribution of surface roughness. The distinct glaciological regimes of ice streams and outlet glaciers result in topographic embayments which are separated by relatively stagnant domes and saddles and are typically ringed by the most severe terrain of the ice

sheet. This variability has been summarized, for the purposes of simulating and interpreting satellite radar altimeter returns, in a new statistical model.

Consideration of the relationship between the top and bottom profiles of the ice sheet has shown that, unlike results from previous analyses, there is no bedrock wavelength which is preferentially transmitted to the ice sheet surface. Rather, there is increasing surface response at longer wavelengths although ice viscosity and temperature were found to have a dominant effect. The non-isotropic and non-isothermal nature of the ice sheet was also found to be very important in determining its response to boundary conditions, suggesting that multi-layer modelling will prove a valuable approach. Only the largest subglacial lakes can be unambiguously detected by inspection of surface detail but the regional decoupling of the ice by thin layers of basal water, for instance as occurs under the West Antarctic ice streams, can result in reduced topographic detail as well as an overall concave morphology.

The mapping of driving stresses over approximately half of the Antarctic ice sheet has shown that, as well as a general pattern of increasing values towards the coast, particular glaciological circumstances may be associated with high or low values. Variations are closely related to ice thickness, velocity and the presence of basal water films. The Marie Byrd Land ice streams appear to be qualitatively different from fast flowing outlet glaciers in that they are dominated hundreds of kilometres inland by substantial basal decoupling and low driving stresses and slopes.

A re-analysis of models of longitudinal stress gradients has shown the importance of recognizing that an ice sheet is a non-isotropic medium in which longitudinal strain rates cannot be assumed to be uniform vertically. In particular, the zone of maximum shear may fluctuate between bedrock and the top of the basal echo-free zone in response to constraints imposed by subglacial topography and variations in ice temperature and rheology. Near ice divides, the upper body of ice tends to behave as a cold, rigid slab. There also appears to be a progressive development with

distance from ice divides of an ice fabric which favours faster flow. The effects of transverse longitudinal stress gradients were found to be important, thereby suggesting the need for modelling ice flow in three dimensions.

The transition in outlet glaciers from slowly converging flow moving by internal deformation to streaming flow due to basal sliding occurs abruptly and is triggered by a bedrock step. That this change in regime occurs at the valley head of subglacial fjords is supported by patterns of surface topography, slopes, crevassing, velocity, subglacial water and driving stresses. The Marie Byrd Land ice streams do not display this rapid transition and appear in form and flow regime to resemble confined ice shelves rather than grounded ice.

Evidence that the onset of fast flow is controlled by subglacial topography indicates a significant stabilizing effect on discharge from the ice sheet; the change in regime is pinned to a subglacial feature and instabilities seem unlikely to propagate inland as occurs in the surging of temperate glaciers. The onset of basal sliding in association with the rapid discharge of ice through subglacial trenches may also provide a mechanism for the production of overdeepened fjords and steep headwalls since this is the point at which concentrated erosion will begin. This association with topography may help in the reconstruction of the dynamics of former ice sheets.

8.2 Developments

This brief section draws together some of the main suggestions of this thesis which could be followed up by further research.

Given the present and future value to glaciology of remotely sensed data, it is important that all aspects of each source are understood so that their full potential may be realized. This should involve further comparison of sources and the collection of ground truth to aid interpretation and resolve ambiguities. In particular, such an approach could be applied with useful results to satellite radar altimetry which is

likely to provide considerable amounts of highly accurate data on the form and topography of ice masses in the near future but has, as yet, not been investigated in great depth.

A significant advance for the modelling of polar ice sheets is likely to be the further development of a multi-layer approach to ice flow and deformation. The restrictions imposed by isothermal and isotropic assumptions are becoming increasingly apparent and, as the theoretical base of the subject becomes more sophisticated, is likely to pose a more serious problem. Such modelling offers the ability to allow for inhomogeneities within the ice mass which, particularly in the vertical dimension, appear to dominate its response to boundary conditions.

While this thesis has addressed some aspects of the abrupt transition to high-velocity flow seen in outlet glaciers, other questions relating to of the discharge of ice from ice sheets present significant problems. For instance, little is known about the behaviour of the West Antarctic ice streams and how they differ from more typical, fast-flowing outlets or about their gradual transition to high velocities several hundreds of kilometres inland. Neither is it known whether flowlines feeding some outlets, such as Lambert and Slessor Glaciers, several hundred kilometres from the coast represent isolated zones of distinct glaciological regimes which are important to the discharge from the ice sheet downstream. The relative stability of ice fronts between ice sheets outlets is also a problem which has received little attention.

Finally, emphasis should be placed on the continuation and development of investigations of the relationship between the form of the ice sheet surface and the physical processes of ice flow within it and at its base. This may prove a useful way of elucidating aspects of flow in three dimensions. This approach is particularly important in view of the expected rapid advances in the study of the surface through satellite remote sensing in the near future. It is essential that this wealth of data be used to support other aspects of glaciology (such as deep coring and temperature measurement) rather than cause an imbalance between elements of the subject.

BIBLIOGRAPHY

Allison, I.F. 1979. The mass budget of the Lambert Glacier drainage basin, Antarctica. Journal of Glaciology, Vol 22, No 87, p223-235.

Allison, I., Frew, R. and Knight, I. 1982. Bedrock and ice surface topography of the coastal regions of Antarctica between 48°E and 68°E. Polar Record, Vol 21, No 132, p241-252.

Arnold, G.C. 1982. An evaluation of the Seasat altimeter's overland profiling in northern Wilkes Land, East Antarctica. Unpublished manuscript.

Bader, H. 1961. The Greenland Ice Sheet. In: Cold Regions Science and Engineering, F.J. Sanger (ed). Part 1, Section B2, p1-18. CRREL, Hanover, New Hampshire, USA.

Ball, F.K. 1960. Winds on the ice slopes of Antarctica. In: Antarctic Meteorology. Pergamon Press, Oxford. p9-16.

Barnes, P., Tabor, D. and Walker, J.F.C. 1971. The friction and creep of polycrystalline ice. Proceedings of the Royal Society of London, Series A, Vol 324, No 1557, p127-155.

Beitzel, J.E. 1970. The relationship of ice thickness and surface slopes in Dronning Maud Land. International Association of Scientific Hydrology, Publication 86, p191-203.

Behrendt, J.C., Wold, R.J. and Dowling, F.L. 1962. Ice surface elevation of central Marie Byrd Land. Journal of Glaciology, Vol 4, No 31, p121-123.

Bennett, R.J. 1979. Spatial Time Series: Analysis-Forecasting-Control. Pion, London. 674pp.

Benson, C.S. 1982. Volcanic heat and the West Antarctic ice sheet. Remarks during general discussion. Annals of Glaciology, Vol 3, p360.

Bentley, C.R. 1964. The structure of Antarctica and its ice cover. In: Research in Geophysics, H. Odishaw (ed), Vol 2, p335-389. MIT Press, Cambridge, Massachusetts, USA.

Bentley, C.R. and Clough, J.W. 1971. Antarctic sub-glacial structure from seismic refraction measurements. In: Antarctic Geology and Geophysics, R.J. Adie (ed), p683-692.

Bindschadler, R. 1979. Longitudinal stress gradients and basal shear stress of a temperate valley glacier (abstract only). Journal of Glaciology, Vol 24, No 90, p507-508.

Bindschadler, R. 1983. The importance of pressurized subglacial water in separation and sliding at the glacier bed. Journal of Glaciology, Vol 29, No 101, p3-19.

Black, H.P. and Budd, W.F. 1964. Accumulation in the region of Wilkes, Wilkes Land, Antarctica. Journal of Glaciology, Vol 5, No 37, p3-16.

Blaiklock, K.V., Stratton, D.G. and Miller, J.H. 1966. Survey. Transantarctic Expedition, 1955-1958, Scientific Reports, No 15, 27pp.

Bogorodsky, B.B., Trepov, G.B. and Sheremetev, A.P. 1977. The use of radio sounding for the measurement of the velocity and thickness of the Antarctic ice cover (in Russian). Physika Zemli, No 1, p95-100.

Bourgoin, J-P. 1956. Quelques caracteres analytiques de la surface et du socle de l'inlandsis groenlandais. Annales de Geophysique, Vol 12, No 1, p75-83.

Brecher, H. 1982. Photogrammetric determination of surface velocities and elevations on Byrd Glacier. Antarctic Journal of the US, 1982 Review, Vol 17, No 5, p79-81.

Brenner, A.C. and Martin, T.V. 1982. Function of Seasat-1 altimeter over ice. EG&G Washington Analytical Services Center, Planetary Sciences Department Report, No 013-82.

Brenner, A.C., Bindschadler, R.A., Thomas, R.H. and Zwally, H.J. 1983. Slope-induced errors in radar altimetry over continental ice sheets. Journal of Geophysical Research, Vol 88, No C3, p1617-1623.

Brooks, R.L. 1983. Scientists use satellite data to map ice sheet contours. Antarctic Journal of the US, Vol 18, No 2, p17-18.

Brooks, R.L., Campbell, W.J., Ramseier, R.D., Stanley, H.R. and Zwally, H.J. 1978. Ice sheet topography by satellite altimetry. Nature, Vol 274, No 5671, p539-543.

Budd, W.F. 1966. The dynamics of the Amery Ice Shelf. Journal of Glaciology, Vol 6, No 45, p335-358.

Budd, W.F. 1968. The longitudinal velocity profile of large ice masses. International Association of Scientific Hydrology, Publication 79, p58-77.

Budd, W.F. 1969. Dynamics of ice masses. ANARE Scientific Reports, Series A (IV), Glaciology. Publication 108. 216pp.

Budd, W.F. 1970. Ice flow over bedrock perturbations. Journal of Glaciology, Vol 9, No 55, p29-48.

Budd, W.F. 1971. Stress variations with ice flow over undulations. Journal of Glaciology, Vol 10, No 59, p177-195.

Budd, W.F. 1975. A first simple model for periodically self-surging glaciers. Journal of Glaciology, Vol 14, No 70, p3-21.

Budd, W.F., Landon-Smith, I.H. and Wishart, E.R. 1967. The Amery Ice Shelf. In: Physics of snow and ice, H. Oura (ed), Vol 1, Part 1, p447-467. Sapporo: Institute of Low temperature Science, Hokkaido University.

Budd, W.F. and Carter, D.B. 1971. An analysis of the relation between the surface and bedrock profiles of ice caps. Journal of Glaciology, Vol 10, No 59, p197-209.

Budd, W.F., Jenssen, D. and Radok, U. 1971. Derived physical characteristics of the Antarctic Ice Sheet. ANARE Interim Report, Series A (IV), Glaciology. No 120. 178pp.

Budd, W.F. and Radok, U. 1971. Glaciers and other large ice masses. Reports on Progress in Physics, Vol 34, No 1, p1-70.

Budd, W.F. and Allison, I.F. 1975. An empirical scheme for estimating the dynamics of unmeasured glaciers. International Association of Scientific Hydrology, Publication 104, p246-256.

Budd, W.F. and Jenssen, D. 1975. Numerical modelling of glacier systems. International Association of Scientific Hydrology, Publication 104, p257-291.

Budd, W.F. and McInnes, B. 1978. Modelling surging glaciers and periodic surging of the Antarctic ice sheet. In: Climatic Change and Variability: A southern perspective, A.B. Pittock, L.A. Frakes, D. Jenssen, J.A. Peterson and J.W. Zillman (eds), p228-234.

Budd, W.F. and Young, N.W. 1979. Results from the IAGP flow-line study inland of Casey, Wilkes Land, Antarctica. Journal of Glaciology, Vol 24, No 90, p89-101.

Budd, W.F., Keage, P.L. and Blundy, N.A. 1979. Empirical studies of ice sliding. Journal of Glaciology, Vol 23, No 89, p157-170.

Budd, W.F. and Smith, N. 1981. The growth and retreat of ice sheets in response to orbital radiation changes. International Association of Scientific Hydrology, Publication 131, p369-409.

Bufton, J.L., Robinson, J.E., Ferniano, M.D. and Flatow, F.S. 1981. Satellite laser altimeter for measurement of ice sheet topography. IEEE Transactions on Geoscience and Remote Sensing, Vol GE-20, No 4, p544-549.

Bull, C.B.B. 1971. Snow accumulation in Antarctica. In: Research in the Antarctic, L. O. Quam (ed), p367-421.

Clayton, K.M. 1965. Glacial erosion in the Finger Lakes region, New York State, USA. Zeitschrift fur Geomorphology, Vol 9, p50-62.

Colbeck, S.C., St. Lawrence, W. and Gow, A.J. 1978. Creep rupture at depth in a cold ice sheet. Nature, Vol 275, No 5682, p733.

Collins, I.F. 1968. On the use of equilibrium equations and flow law relating the surface and bed topography of glaciers and ice sheets. Journal of Glaciology, Vol 7, No 50, p199-204.

Colvill, A.J. 1977. Movement of Antarctic ice fronts measured from satellite imagery. Polar Record, Vol 18, No 115, p390-394.

Cooper, A.P.R., McIntyre, N.F. and Robin, G.deQ. 1982. Driving stresses in the Antarctic ice sheet. Annals of Glaciology, Vol 3, p59-64.

Crabtree, R.D. and Doake, C.S.M. 1980. Flowlines on Antarctic ice shelves. Polar Record, Vol 20, No 124, p31-37.

Crabtree, R.D. and Doake, C.S.M. 1982. Pine Island Glacier and its drainage basin: results from radio echo sounding. Annals of Glaciology, Vol 3, p65-70.

Crary, A.P. 1966. Mechanism of fiord formation indicated by studies of an ice-covered inlet. Geological Society of America, Bulletin, Vol 77, p911-930.

Dansgaard, W. 1961. The isotopic composition of natural waters with special reference to the Greenland ice cap. Meddelelser om Gronland, Vol 165, No 2, p1-120.

Dansgaard, W. and Johnsen, S.J. 1969. A flow model and a time scale for the ice core from Camp Century, Greenland. Journal of Glaciology, Vol 8, No 53, p215-223.

Dater, H.M. 1975. History of Antarctic Exploration and Scientific Exploration. Antarctic Map Folio Series, V.C. Bushnell (ed), Folio 19. American Geographical Society.

Denton, G.H., Hughes, T.J., Fastook, J.L., Schilling, D.H. and Lingle, C.S. 1979. Reconstruction and disintegration of ice sheets from the CLIMAP 18 000 and 125 000 years BP experiments: results (abstract only). Journal of Glaciology, Vol 24, No 90, p495-496.

Denton, G.H. and Hughes, T.J. 1981. The Last Great Ice Sheets. Wiley, New York. 484pp.

Dewart, G. 1976. Seismic evidence of a wet zone under the West Antarctic ice sheet. Journal of Glaciology, Vol 16, No 74, p73-88.

Dowdeswell, E.K. and Andrews, J.T. In press. The fiords of Baffin Island: description and classification. In: Quaternary studies of Baffin Island, Baffin Bay and West Greenland, J.T. Andrews and M. Andrews (eds).

Drewry, D.J. 1973. Sub-ice relief and geology of East Antarctica. PhD thesis, University of Cambridge. 217pp.

Drewry, D.J. 1975. Radio echo sounding map of Antarctica (90°E-180°). Polar Record, Vol 17, No 109, p359-374.

Drewry, D.J. 1982. Ice flow, bedrock and geothermal studies from radio echo sounding inland of McMurdo Sound, Antarctica. In: Antarctic Geoscience, C. Craddock (ed), p977-983. Symposium on Antarctic Geology and Geophysics. Madison, Wisconsin. August 1977.

Drewry, D.J. (ed) 1983a. Antarctica: Glaciological and Geophysical Folio. Scott Polar Research Institute, Cambridge, UK.

Drewry, D.J. 1983b. Antarctic ice sheet: aspects of current configuration and flow. In: Megageomorphology, V. Gardiner and H. Skoging (eds), p18-38. OUP, Oxford.

Drewry, D.J. and Meldrum, D.T. 1978. Antarctic airborne radio echo sounding, 1977-78. Polar Record, Vol 19, No 120, p267-273.

Drewry, D.J., Meldrum, D.T. and Jankowski, E.J. 1980. Radio echo and magnetic sounding of the Antarctic Ice Sheet, 1978-79. Polar Record, Vol 20, No 124, p43-51.

Drewry, D.J., Jordan, S.R. and Jankowski, E.J. 1982. Measured properties of the Antarctic Ice Sheet: surface configuration, ice thickness, volume bedrock characteristics. Annals of Glaciology, Vol 3, p83-91.

Drewry, D.J. and Robin, G.deQ. 1983. Form and flow of the Antarctic ice sheet during the last million years. In: The Climatic Record in Polar Ice Sheets, G.deQ. Robin (ed), p28-38. CUP, Cambridge.

Drewry, D.J. and McIntyre, N.F. In press. The Antarctic ice sheet: a surface model for satellite altimeter studies. In: Models in Geomorphology, M.J. Woldenburg (ed). Allen and Unwin, London.

Duchossois, G. and Plevin, J. 1981. Remote sensing from space: review of future plans and prospects. In: Remote Sensing in Meteorology, Oceanography and Hydrology, A.P. Cracknell (ed), p66-80. Ellis Horwood, Chichester.

Embleton, C. and King, C.A.M. 1975. Glacial Geomorphology. Arnold, London. 583pp.

Endo, Y. and Fujiwara, K. 1973. Characteristics of the snow cover in East Antarctica along the route of the JARE South Pole traverse and factors controlling such characteristics. JARE Scientific Reports, Series C, No 7, 27pp.

Englehardt, H.F., Harrison, W.D. and Kamb, B. 1978. Basal sliding and conditions at the glacier bed as revealed by bore-hole photography.

Journal of Glaciology, Vol 20, No 84, p469-508.

Evans, S. 1963. Radio techniques for the measurement of ice thickness. Polar Record, Vol 11, No 73, p406-410.

Flint, R.F. 1947. Glacial Geology and the Pleistocene Epoch. Wiley, New York. 589pp.

Fristrup, B. 1966. The Greenland Ice Cap. (Translated by B. Stoner) University of Washington Press, Seattle. 312pp.

Fujii, Y. and Kusunoki, K. 1982. The role of sublimation and condensation in the formation of ice sheet surface at Mizuho Station, Antarctica. Journal of Geophysical Research, Vol 87, No C6, p4293-4300.

Gealy, W.J. and Weertman, J. (eds) 1983. Workshop on the Jakobshavn Glacier (Greenland). Northwestern University, Evanston, Illinois. February 1983. Unpublished manuscript.

Giovinetto, M.B. 1964. The drainage system of Antarctica: accumulation. In: Antarctic Snow and Ice Studies, M. Mellor (ed). American Geophysical Union, Washington D.C. Antarctic Research Series, Vol 2, p127-155.

Giovinetto, M.B. 1970. The Antarctic ice sheet and its probable bi-modal response to climate. International Association of Scientific Hydrology, Publication 86, p347-358.

Glen, J.W. 1955. The creep of polycrystalline ice. Proceedings of the Royal Society of Landon, Series A, Vol 228, p519-538.

Gould, L.M. 1940. Antarctic regions. In: Proceedings of the Sixth Pacific Science Congress, (Berkeley, California) 1939, Vol 2, p671-674.

Gow, A.J. 1965. On the accumulation and seasonal stratification of snow at the South Pole. Journal of Glaciology, Vol 5, No 40, p467-477.

Gow, A.J. 1970. Preliminary results of studies of ice cores from the 2164 m deep drill hole, Byrd Station, Antarctica. International Association of Scientific Hydrology, Publication 86, p78-90.

Gow, A.J. and Rowland, R. 1965. On the relationship of snow accumulation to surface topography at 'Byrd Station', Antarctica. Journal of Glaciology, Vol 5, No 42, p843-847.

Gow, A.J. and Williamson, T.C. 1976. Rheological implications of the internal structure and crystal fabrics of the West Antarctic ice sheet as revealed by deep core drilling at Byrd Station. Geological Society of America, Bulletin, Vol 87, No 12, p1665-1677.

Haefeli, R. 1970. Changes in the behaviour of Unteraargletscher in the last 125 years. Journal of Glaciology, Vol 9, No 56, p195-212.

Hamming, R.W. 1977. Digital Filters. Prentice Hall, New Jersey. 226pp.

Harrison, C.H. 1972. Radio propagation effects in glaciers. PhD thesis, University of Cambridge. 193pp.

Harrison, W.D. 1975. A measurement of surface-perpendicular strain-rate in a glacier. Journal of Glaciology, Vol 14, No 70, p31-37.

Haynes, V.M. 1972. The relationship between the drainage areas and sizes of outlet troughs of the Sukkertoppen ice cap, west Greenland. Geografiska Annaler, Vol 54A, No 2, p66-75.

Henry, R.F. and Graefe, P.W.U. 1971. Zero-padding as a means of improving definition of computed spectra. Marine Sciences Branch, Manuscript Report Series, No 20. Department of Energy, Mines and Resources, Ottawa. 10pp.

Hochstein, M.P. 1967. Morphologie der westantarktichen Eiskappe zwichen Mary Byrd und Edith Ronne Land. Polarforschung, Bd 6, Jahrg 35, Ht 1-2, p27-31.

Hoffer, R.M. 1978. Biological and physical considerations of applying computer-aided analysis techniques to remote sensor data. In: Remote Sensing: The Quantitative Approach, P.H. Swain and S.M. Davis (eds), p227-289. McGraw-Hill, New York.

Holdsworth, G. 1977. Surge activity on the Barnes Ice Cap. Nature, Vol 269, No 5629, p588-590.

Holtedahl, H. 1967. Notes on the formation of fjords and fjord valleys. Geografiska Annaler, Vol 49A, No 2-4, p188-203.

Holtzscherer, J-J. and Bauer, A. 1954. Contribution a la connaissance de l'inlandsis du Groenland. International Association of Scientific Hydrology, Publication 39, p244-297.

Hooke, R. LeB. 1973. Structure and flow in the margin of the Barnes Ice Cap, Baffin Island, NWT, Canada. Journal of Glaciology, Vol 12, No 66, p423-438.

Hooke, R. LeB. 1981. Flow law for polycrystalline ice in glaciers: comparison of theoretical predictions, laboratory data and field measurements. Reviews of Geophysics and Space Physics, Vol 19, No 4, p664-672.

Hughes, T.J. 1972. Is the Antarctic ice sheet disintegrating? Scientific justifications. ISCAP Bulletin, No 1, 90pp. Ohio State University.

Hughes, T.J. 1973. Is the West Antarctic ice sheet disintegrating? Journal of Geophysical Research, Vol 78, No 33, p7884-7910.

Hughes, T.J. 1975. The West Antarctic ice sheet: instability, disintegration

and initiation of ice ages. Reviews of Geophysics and Space Physics, Vol 13, No 4, p502-526.

Hughes, T.J. 1977. West Antarctic ice streams. Reviews of Geophysics and Space Physics, Vol 15, No 1, p1-46.

Hughes, T.J. 1979a. Reconstruction and disintegration of ice sheets for the CLIMAP 18 000 and 125 000 years BP experiments: theory (abstract only). Journal of Glaciology, Vol 24, No 90, p493-495.

Hughes, T.J. 1979b. Byrd Glacier. Antarctic Journal of the US, Vol 14, No5, p88-91.

Hughes, T.J. 1981. The weak underbelly of the West Antarctic ice sheet. Journal of Glaciology, Vol 27, No 97, p518-525.

Hughes, T.J. 1983. The Jakobshavn Glacier ice drainage system. In: Workshop on the Jakobshavn Glacier (Greenland), W.J. Gealy and J. Weertman (eds). Northwestern University, Evanston, Illinois. February 1983. Unpublished manuscript.

Hughes, T.J. and Fastook, J.L. 1981. Byrd Glacier: 1978-1979 field results. Antarctic Journal of the US, Vol 16, No 5, p86-89.

Hutter, K., Legerer F. and Spring, U. 1981. First-order stresses and deformations in glaciers and ice sheets. Journal of Glaciology, Vol 27, No 96, p227-271.

Ishida, T. 1970. Glaciological research on the inland traverse of the 8th Japanese Antarctic Research Expedition. International Association of Scientific Hydrology, Publication 86, p130-138.

Jankowski, E.J. 1981. Airborne geophysical investigations of sub-glacial structure of West Antarctica. PhD thesis, University of Cambridge. 293pp.

Jankowski, E.J. and Drewry, D.J. 1981. The structure of West Antarctica from geophysical studies. Nature, Vol 291, No 5810, p17-21.

Johnsen, S.J., Dansgaard, W., Clausen, H.B. and Langway, C.C. 1972. Oxygen isotope profiles through the Antarctic and Greenland ice sheets. Nature, Vol 235, No 5339, p429-434.

Johnsen, S.J., Rasmussen, K., and Reeh, N. 1979. Theory of deformations within ice sheets due to bottom undulations (abstract only). Journal of Glaciology, Vol 24, No 90, p512.

Kamb, B. 1970. Sliding motion of glaciers: theory and observations. Reviews of Geophysics and Space Physics, Vol 8, No 4, p673-728.

King, C.A.M. 1959. Geomorphology in Austerdalen, Norway. Geographical Journal, Vol 125, p357-369.

Kotlyakov, V.M., Barkov, N.I., Loseva, I.A. and Petrov, V.N. 1974. Novaya karta pitaniya lednikovogo pokrova Antarktidy (New map of the accumulation on the Antarctic ice sheet). Materialy Geyatsiologicheskikh Issledovaniy Khronika, Obsuzhdeniya, Vyp 24, p248-255.

Krimmel, R.M. and Meier, M.F. 1975. Glacier applications of ERTS images. Journal of Glaciology, Vol 15, No 73, p391-402.

Landsat Data Users' Handbook, 1979. Revised edition. US Geological Survey.

Liestøl, O. 1969. Glacier surges in West Spitsbergen. Canadian Journal of Earth Sciences, Vol 6, No 4, p895-897.

Lillesand, T.M. and Keifer, R.W. 1979. Remote Sensing and Image Interpretation. Wiley, New York. 612pp.

Lingle, C.S. and Clark, J.A. 1979. Antarctic ice sheet volume at 18 000 BP and Holocene sea level changes at the West Antarctic margin. Journal of Glaciology, Vol 24, No 90, p213-230.

Lister, H. 1959. Contribution to general discussion. Geophysical Journal of the Royal Astronomical Society, Vol 2, p168.

Lliboutry, L. 1968. General theory of subglacial cavitation and sliding of temperate glaciers. Journal of Glaciology, Vol 7, No 49, p21-58.

Lliboutry, L. 1970. Ice flow law from ice sheet dynamics. International Association of Scientific Hydrology, Publication 86, p216-228.

Lliboutry, L. 1979. Local friction laws for glaciers: a critical review and new openings. Journal of Glaciology, Vol 23, No 89, p67-95.

Lorius, C. 1962. Contribution to the knowledge of the Antarctic ice sheet: a synthesis of glaciological measurements in Terre Adelie. Journal of Glaciology, Vol 4, No 31, p79-92.

Løken, O.H. 1969. Evidence of surges on the Barnes Ice Cap, Baffin Island. Canadian Journal of Earth Sciences, Vol 6, No 4, p899-901.

Martin, P.J. 1976. Ridges on Antarctic ice rises. Journal of Glaciology, Vol 17, No 75, p141-144.

Martin, P.J. and Sanderson, T.J.O. 1980. Morphology and dynamics of ice rises. Journal of Glaciology, Vol 25, No 91, p33-45.

Martin, T.V., Zwally, H.J., Brenner, A.C. and Bindschadler, R.A. 1983. Analysis and retracking of continental ice sheet radar altimeter waveforms. Journal of Geophysical Research, Vol 88, No C3, p1608-1616.

McIntyre, N.F. and Cooper, A.P.R. 1983. Driving stresses. In: Antarctica: Glaciological and Geophysical Folio, D.J. Drewry (ed), Sheet 5.

McIntyre, N.F. In prep. The mass balance of the Lambert Glacier drainage basin, Antarctica.

Meier, M.F. 1968. Calculations of slip of Nisqually Glacier on its bed: no simple relation of sliding velocity velocity to shear stress. International Association of Scientific Hydrology, Publication 79, p49-57.

Mellor, M. 1959. Ice flow in Antarctica. Journal of Glaciology, Vol 3, No 25, p377-387.

Mellor, M. 1964. Remarks concerning the Antarctic mass balance. Polarforschung, Bd 5, Jahrg 33, Ht 1-2, p179-180.

Mercer, J.H. 1968. Antarctic ice and Sangamon sea level. International Association of Scientific Hydrology, Publication 79, p217-225.

Millar, D.H.M. 1981a. Radio echo layering in polar ice sheets and past volcanic activity. Nature, Vol 292, No 5822, p441-443.

Millar, D.H.M. 1981b. Radio echo layering in polar ice sheets. PhD thesis, University of Cambridge. 177pp.

Morgan, V.I. and Budd, W.F. 1975. Radio echo sounding of the Lambert Glacier basin. Journal of Glaciology, Vol 15, No 73, p103-112.

Morgan, V.I., Jacka, T.H., Ackerman, G.J. and Clarke, A.L. 1982. Outlet glaciers and mass-budget studies in Enderby, Kemp and Mac.Robertson Land, Antarctica. Annals of Glaciology, Vol 3, p204-211.

Morland, L.W. 1976a. Glacier sliding down an inclined wavy bed. Journal of Glaciology, Vol 17, No 77, p447-462.

Morland, L.W. 1976b. Glacier sliding down an inclined wavy bed with friction. Journal of Glaciology, Vol 17, No 77, p463-477.

Naruse, R. 1979. Thinning of the ice sheet in Mizuho Plateau, East Antarctica. Journal of Glaciology, Vol 24, No 90, p45-52.

Neal, C.S. 1976. Radio echo profiling. Journal of Glaciology, Vol 17, No 77, p527-530.

Nye, J.F. 1957. The distribution of stress and velocity in glaciers and ice sheets. Proceedings of the Royal Society of London, Series A, Vol 239, No 1216, p113-133.

Nye, J.F. 1963. Correction factor for accumulation measured by the thickness of annual layers in an ice sheet. Journal of Glaciology, Vol 4, No 36, p785-788.

Orowan, E. 1949. Remarks at joint meeting of the British Glaciological Society, the British Rheologists Club and the Institute of Metals.

Journal of Glaciology, Vol 1, No 4, p231-236.

Oswald, G.K.A. 1975. Radio echo studies of polar glacier beds. PhD thesis, University of Cambridge. 134pp.

Oswald, G.K.A. and Robin, G.deQ. 1973. Lakes beneath the Antarctic ice sheet. Nature, Vol 245, No 5423, p251-254.

Overgaard, S. and Rasmussen, K. 1979. Study of deformations within ice sheets due to bottom undulations by means of radio echo sounding (abstract only). Journal of Glaciology, Vol 24, No 90, p513.

Paterson, W.S.B. 1976. Vertical strain-rate measurements in an arctic ice cap and deductions from them. Journal of Glaciology, Vol 17, No 75, p3-12.

Paterson, W.S.B. 1980. Ice sheets and ice shelves. In: Dynamics of Snow and Ice Masses, S.C. Colbeck (ed), p1-78. Academic Press, London.

Paterson, W.S.B. 1981. The Physics of Glaciers. Pergamon Press, Oxford. 2nd edition. 380pp.

Paterson, W.S.B. and Savage, J.C. 1963. Measurements on Athabasca Glacier relating to the flow law of ice. Journal of Geophysical Research, Vol 68, No 15, p4537-4543.

Paterson, W.S.B. and Budd, W.F. 1982. Flow parameters for ice sheet modeling. Cold Regions Science and Technology, Vol 6, No 2, p175-177.

Pfeffer, T. 1982. The effect of crevassing on the radiative absorptance of a glacier surface (abstract only). Annals of Glaciology, Vol 3, p353.

Rapley, C.G. Griffiths, H.D., Squire, V.A., Lefebvre, M., Birks, A.R., Brenner, A.C., Brossier, C., Clifford, L.D., Cooper, A.P.R., Cowan, A.M., Drewry, D.J., Gorman, M.R., Huckle, H.E., Lamb, P.A., Martin, T.V., McIntyre, N.F., Milne, K., Novotny, E., Peckham, G.E., Schgounn, C., Scott, R.F., Thomas, R.H. and Vesecky, J.F. 1983. A study of satellite radar altimeter operation over ice-covered surfaces. European Space Agency Contract Report, No 5182/82/F/CG(SC). 224pp.

Raymond, C.F. 1971. Determination of the three-dimensional velocity field in a glacier. Journal of Glaciology, Vol 10, No 58, p39-53.

Robin, G.deQ. 1958. Seismic shooting and related investigations. Norwegian-British-Swedish Antarctic Expedition, 1949-52. Scientific Results, Vol 5, Glaciology 3. Norsk Polarinstitutt, Oslo. 134pp.

Robin, G.deQ. 1966. Mapping the Antarctic ice sheet by satellite altimetry. Canadian Journal of Earth Sciences, Vol 3, No 6, p893-901.

Robin, G.deQ. 1967. Surface topography of ice sheets. Nature, Vol 215, No 5105, p1029-1032.

Robin, G.deQ. 1970. Stability of ice sheets as deduced from deep temperature gradients. International Association of Scientific Hydrology, Publication 86, p141-151.

Robin, G.deQ. 1975. Ice shelves and ice flow. Nature, Vol 253, No 5488, p168-172.

Robin, G.deQ. 1983. Coastal sites, Antarctica. In: The Climatic Record in Polar Ice Sheets, G.deQ. Robin (ed), p118-122. CUP, Cambridge.

Robin, G.deQ., Evans, S. and Bailey, J.T. 1969. Interpretation of radio echo sounding in polar ice sheets. Philosophical Transactions of Royal Society of London, Series B, Vol 265, No 1166, p437-505.

Robin, G.deQ., Swithinbank, C.W.M. and Smith, B.M.E. 1970. Radio exploration of the Antarctic ice sheet. International Association of Scientific Hydrology, Publication 86, p97-115.

Robin, G.deQ. and Weertman, J. 1973. Cyclic surging of glaciers. Journal of Glaciology, Vol 12, No 64, p3-18.

Robin, G.deQ., Drewry, D.J. and Meldrum. D.T. 1977. International studies of ice sheet and bedrock. Philosophical Transactions of Royal Society of London, Series B, Vol 279, p185-196.

Robin, G.deQ. and Millar, D.H.M. 1982. Flow of ice sheets in the vicinity of subglacial peaks. Annals of Glaciology, Vol 3, p290-294.

Robin, G.deQ., Drewry, D.J. and Squire, V.A. 1983. Satellite observations of polar ice fields. Philosophical Transactions of Royal Society of London, Series A, Vol 309, p243-255.

Robinove, C.J. 1982. Computation with physical values from Landsat digital data. Photogrammetric Engineering and Remote Sensing, Vol 48, No 5, p781-784.

Robinson, I.S. 1983. Satellite observations of ocean colour. Philosophical Transactions of Royal Society of London, Series A, Vol 309, p173-190.

Robinson, R.V. 1960. From the practice of visual orientation during Antarctic flights. Information Bulletin of the Soviet Antarctic Expedition, No 18, p28-29.

Rose, K.E. 1978. Radio echo sounding studies of Marie Byrd Land, Antarctica. PhD thesis, University of Cambridge. 204pp.

Rose, K.E. 1979. Characteristics of the ice flow in Marie Byrd Land, Antarctica. Journal of Glaciology, Vol 24, No 90, p63-76.

Rozema, W. 1968. The use of spectral analysis in describing lunar surface roughness. US Geological Survey Interagency Report: Astrogeology, No 12. 34pp.

Russell-Head, D.S. and Budd, W.F. 1979. Ice sheet flow properties from combined borehole shear and ice core studies. Journal of Glaciology, Vol 24, No 90, p117-130.

Schytt, V. 1969. Some comments of glacier surges in eastern Svalbard. Canadian Journal of Earth Sciences, Vol 6, No 4, p867-873.

Shimizu, H., Watanabe, O., Kobayashi, S., Yamada, T., Naruse, R. and Ageta, Y. 1978. Glaciological aspects and mass budget of the ice sheet in Mizuho Plateau. In: Glaciological Studies in Mizuho Plateau, Antarctica, 1969-75, T. Ishida (ed). Memoirs of National Institute of Polar Research, Special Issue No 7, p264-274. NIPR, Tokyo.

Shreve, R.L. and Sharp, R.P. 1970. Internal deformation and thermal anomalies in lower Blue Glacier, Mount Olympus, Washington, USA. Journal of Glaciology, Vol 9, No 55, p65-86.

Shumskiy, P.A. 1970. The Antarctic ice sheet. International Association of Scientific Hydrology, Publication 86, p327-347.

Smith, A.G. and Drewry, D.J. In press. Transantarctic uplift: delayed phase change due to linear heat source? Nature.

Smith, B.P. 1980. Descriptive analyses of January 1978 Antarctic RES mission flown by ARDS-configured LC-130 aircraft. MSc. thesis, Naval Postgraduate School, Monterey, California.

Souchez, R. 1967. Le recult des verrous-gradins et rapports glaciare-periglaciare en Antarctique. Revue Geomorphologie Dynamique, Vol 17, No 2, p49-54.

Steed, R.H.N. 1980. Geophysical investigations of Wilkes Land, Antarctica. PhD thesis, University of Cambridge. 178pp.

Steed, R.H.N. and Drewry, D.J. 1982. Radio echo sounding investigations of Wilkes Land, Antarctica. In: Antarctic Geoscience, C. Craddock (ed), p969-975. Symposium on Antarctic Geology and Geophysics. Madison, Wisconsin. August 1977.

Stephenson, S.J. and Doake, C.S.M. 1982. Dynamic behaviour of Rutford Ice Stream. Annals of Glaciology, Vol 3, p295-299.

Sugden, D.E. 1968. The selectivity of glacial erosion in the Cairngorm Mountains, Scotland. Institute of British Geographers, Transactions, Vol 45, p79-92.

Sugden, D.E. and John, B.S. 1976. Glaciers and Landscape. Arnold, London. 376pp.

Swithinbank, C.W.M. 1955. Ice shelves. Geographical Journal, Vol 121, Part 1, p64-76.

Swithinbank, C.W.M. 1959. The morphology of the inland ice sheet and nunatak areas of western Dronning Maud Land. Norwegian-British-Swedish Antarctic Expedition, 1949-52. Scientific Results, Vol 3, Glaciology 1. Norsk Polarinstitutt, Oslo. 146pp.

Swithinbank, C.W.M. 1963. Ice movement of valley glaciers flowing into the Ross Ice Shelf, Antarctica. Science, Vol 141, No 3580, p523-524.

Swithinbank, C.W.M. 1977. Glaciological research in the Antarctic Peninsula. Proceedings of the Royal Society of London, Series B, Vol 279, p161-183.

Swithinbank, C.W.M., Doake, C.S.M., Wager, A. and Crabtree, R. 1976. Major change in the map of Antarctica. Polar Record, Vol 18, No 114, p295-299.

Swithinbank, C.W.M. and Lane, C. 1977. Antarctic mapping from satellite imagery. Conference of Commonwealth Survey Officers, 1975, ch 11. Ministry of Overseas Development, London.

Thomas, R.H. 1976. Thickening of the Ross Ice Shelf and equilibrium state of the West Antarctic ice sheet. Nature, Vol 259, No 5540, p180-183.

Thomas, R.H. 1979a. The dynamics of marine ice sheets. Journal of Glaciology, Vol 24, No 90, p167-178.

Thomas, R.H. 1979b. Ice shelves: a review. Journal of Glaciology, Vol 24, No 90, p273-286.

Thomas, R.H. and Bentley, C.R. 1978. The equilibrium state of the eastern half of the Ross Ice Shelf. Journal of Glaciology, Vol 20, No 84, p509-514.

Thomas, R.H., Sanderson, T.J.O. and Rose, K.E. 1979. Effect of climatic warming on the West Antarctic ice sheet. Nature, Vol 277, No 5695, p355-358.

Thomas, R.H., MacAyeal, D.R., Eilers, D.H. and Gaylord, D.R. 1982. Glaciological studies of the Ross Ice Shelf, Antarctica, 1973-1978. In: The Ross Ice Shelf: Glaciology and Geophysics, C.R. Bentley and D.E. Hayes (eds). Antarctic Research Series, Vol 40.

Thorarinsson, S. 1964. Sudden advance of Vatnajokull outlet glaciers 1930-1964. Jokull, Vol 14, p76-89.

Thorarinsson, S. 1969. Glacier surges in Iceland, with special reference to the surges of Bruarjokull. Canadian Journal of Earth Sciences, Vol 6, No 4, p875-882.

Verdin, J. 1983. Corrected vs. uncorrected Landsat 4 MSS data. Landsat Data Users' Notes, No 27, p4-8.

Vialov, S.S. 1958. Regularities of glacial shields movement and the theory of plastic viscous flow. International Association of Scientific

Hydrology, Publication 47, p266-275.

Wada, M. and Mae, S. 1981. Airborne radio echo sounding on the Shirase Glacier and its drainage basin, East Antarctica. Antarctic record, No 72, p16-25.

Washburn, A.L. and Bentley, C.R. 1983. Snow and Ice Research: An Assessment. Committee of Glaciology, Polar Research Board, National Research Council. National Academy Press, Washington DC. 126pp.

Weertman, J. 1957. On the sliding of glaciers. Journal of Glaciology, Vol 3, No 21, p33-38.

Weertman, J. 1963. Profile and heat balance at the bottom surface of an ice sheet fringed by mountain ranges. International Association of Scientific Hydrology, Publication 61, p245-252.

Weertman, J. 1964. The theory of glacier sliding. Journal of Glaciology, Vol 5, No 39, p287-303.

Weertman, J. 1966. Effects of a basal water layer on the dimension of ice sheets. Journal of Glaciology, Vol 6, No 44, p191-202.

Weertman, J. 1970. Method for setting a lower limit on the water layer thickness at the bottom of an ice sheet and the time required for upwelling of water into a borehole. International Association of Scientific Hydrology, Publication 86, p69-73.

Weertman, J. 1973. Can a water-filled crevasse reach the bottom surface of a glacier? International Association of Scientific Hydrology, Publication 95, p139-145.

Weertman, J. 1974. Stability of the junction of an ice sheet and an ice shelf. Journal of Glaciology, Vol 13, No 67, p3-11.

Weertman, J. and Birchfield. G.E. 1982. Subglacial water flow under ice streams and West Antarctic ice sheet stability. Annals of Glaciology, Vol 3, p316-320.

Whillans, I.M. 1973. State of equilibrium of the West Antarctic inland ice sheet. Science, Vol 182, No 4111, p476-479.

Whillans, I.M. 1975. Effect of inversion winds on topographic detail and mass balance on inland ice sheets. Journal of Glaciology, Vol 14, No 70, p85-90.

Whillans, I.M. 1976. Radio echo layers and the recent stability of the West Antarctic ice sheet. Nature, Vol 264, No 5582, p152-155.

Whillans, I.M. 1977. The equation of continuity and its application to the ice sheet near 'Byrd Station', Antarctica. Journal of Glaciology, Vol 18, No 80, p359-371.

Whillans, I.M. 1978. Surface mass-balance near 'Byrd Station', Antarctica, and its importance to ice core stratigraphy. Journal of Glaciology, Vol 20, No 83, p301-310.

Whillans, I.M. 1979. Ice flow along Byrd Station Strain Network, Antarctica. Journal of Glaciology, Vol 24, No 90, p15-28.

Whillans, I.M. and Johnsen, S.J. 1983. Longitudinal variations in glacial flow: theory and test using data from Byrd Station Strain Network, Antarctica. Journal of Glaciology, Vol 29, No 101, p78-98.

Williams, R.S., Thorarinsson, S., Bjornsson, H. and Gudmundsen, B. 1979. Dynamics of Iceland ice caps and outlet glaciers (abstract only). Journal of Glaciology, Vol 24, No 90, p505-507.

Williams, R.S., Meunier, T.K. and Ferrigno, J.G. 1983. Blue ice, meteorites and satellite imagery in Antarctica. Polar Record, Vol 21, No 134, p493-496.

Wilson, A.T. 1964. Origin of ice ages: an ice shelf theory for Pleistocene glaciation. Nature, Vol 201, No 4915, p147-149.

Yokoyama, K. 1978. Distribution of surface structures od the ice sheet in Mizuho Plateau. In: Glaciological studies in Mizuho Plateau, East Antarctica, 1969-75, T. Ishida (ed). Memoirs of National Institute of Polar Research, Special Issue No 7, p26-37. NIPR, Tokyo.

Young, N.W. 1979. Measured velocities of interior East Antarctica and the state of mass balance within the IAGP area. Journal of Glaciology, Vol 24, No 90, p77-87.

Young, N.W. 1981. Responses of ice sheets to environmental changes. International Association of Scientific Hydrology, Publication 131, p331-360.

Young, N.W., Sheehy, D. and Hamley, T. In press. Ice flow along an IAGP flowline, Wilkes Land, Antarctica. Submitted to Journal of Glaciology.

Zumberge, J.H. and Swithinbank, C.W.M. 1962. The dynamics of ice shelves. In: Antarctic Research. American Geophysical Union, Geophysical Monograph No 7, p197-208.

Zwally, H.J. and Gloersen, P. 1977. Passive microwave images of the polar regions and research applications. Polar Record, Vol 18, No 116, p431-450.

Zwally, H.J., Thomas, R.H. and Bindschadler, R.A. 1981. Ice sheet dynamics by satellite laser altimetry. NASA Technical Memorandum, No 82128.

Zwally, H.J., Bindschadler, R.A., Brenner, A.C., Martin, T.V. and Thomas, R.H. 1983. Surface elevation contours of Greenland and Antarctic ice sheets. Journal of Geophysical Research, Vol 88, No C3, p1589-1596.

Addendum

Boulton, G.S. 1974. Processes and patterns of glacial erosion. In: Glacial Geomorphology, D.R. Coates (ed), p41-87. Publications in Geomorphology, State University of New York, Binghampton, New York.

Duval, P. 1975. The role of the water content on the creep rate of polycrystalline ice. International Association of Scientific Hydrology, Publication 118, p29-33.

Fowler, A.C.1979. A mathematical approach to the theory of glacier sliding. Journal of Glaciology, Vol 23, No 89, p131-141.

Robin, G.deQ. 1955. Ice movement and temperature distribution in glaciers and ice sheets. Journal of Glaciology, Vol 2, No 18, p523-532.

Warren, S.G. 1982. Optical properties of snow. Reviews of Geophysics and Space Physics, Vol 20, No 1, p67-89.

UNIVERSITY
LIBRARY
CAMBRIDGE